Université de Montréal

Caractérisation de la vulnérabilité sélective des neurones dopaminergiques dans le contexte de la maladie de Parkinson

par Nicolas Giguère

Département de Neurosciences
Faculté de Médecine

Thèse présentée
en vue de l'obtention du grade de Philosophiae Doctor (Ph. D.)
en Sciences Neurologiques

Octobre 2018

Résumé

La maladie de Parkinson (MP) est une maladie neurodégénérative dont les symptômes moteurs caractéristiques sont causés par la mort des neurones dopaminergiques de la substance noire compacte (SNc) dans le mésencéphale. Dans environs 15% des cas, des mutations dans des gènes encodant des protéines telles que Parkin, Pink1, DJ-1, α-synucléine, LRRK2 ou GBA, sont responsable de l'apparition de la maladie. Ces gènes sont impliqués dans des processus physiologiques comme la mitophagie, la fonction lysosomiale, la réponse au stress oxydatif, la présentation antigénique mitochondriale ou le transport axonal. De manière intéressante, ces processus ont tous un impact direct ou indirect sur la capacité des neurones à produire l'énergie nécessaire à leur survie, ainsi que sur leur niveau basal de stress oxydatif. Une des questions centrales dans l'étude de la MP est de savoir pourquoi des altérations dans des processus aussi généraux mènent à la mort sélective de petits groupes de neurones dans le cerveau, tels que les neurones dopaminergiques de la SNc. La comparaison de ces neurones à leurs voisins de l'aire tegmentaire ventrale (VTA) qui sont eux aussi dopaminergiques, mais bien moins affectés dans la MP, est un des exemples les plus flagrants de cette vulnérabilité sélective.

Une hypothèse récente suggère que certaines caractéristiques propres aux neurones dopaminergiques de la SNc mettraient une immense pression sur leurs capacités bioénergétiques, ce qui les rendrait sélectivement vulnérables à tout stress supplémentaire. Par exemple, ces neurones auraient tendance à former des dérivés toxiques de la dopamine dans des conditions de stress, ce qui impacterait négativement leur capacité à produire efficacement leur énergie. Ils auraient aussi un patron de décharge de type « pacemaker » impliquant des courants calciques très énergivores. Finalement, ils posséderaient une arborisation axonale particulièrement élaborée, nécessitant une quantité phénoménale d'énergie pour y propager les potentiels d'action et y induire la relâche de neurotransmetteurs. Une de nos hypothèses est que ces caractéristiques rendent les neurones dopaminergiques de la SNc particulièrement actifs au niveau bioénergétique et les poussent à la limite de leurs capacités énergétiques. Tout stress cellulaire supplémentaire, tel que ceux associés aux altérations génétiques énoncées

précédemment, à l'exposition à des toxines environnementales ou tout simplement au vieillissement, pourrait alors mener à leur mort.

De manière intéressante, il semble que l'élaboration d'un axone à l'arborisation ultra-complexe soit une caractéristique commune aux populations neuronales affectées dans la MP, telles que les neurones dopaminergiques de la SNc, les neurones cholinergiques du noyau pédonculopontin ou les neurones noradrénergiques du locus coeruleus, contrairement à la présence de dopamine ou de courants calciques liés à une décharge ou de type « pacemaker ». Il est donc plus probable que cette caractéristique soit centrale dans la vulnérabilité sélective des populations neuronales dans la MP. Malheureusement, aucune comparaison directe de la taille de l'arborisation axonale de ces neurones avec des populations neuronales épargnées n'est à ce jour disponible, tout comme l'impact de la modulation de la taille de cette arborisation sur les besoins énergétiques et la vulnérabilité des neurones.

Pour commencer à évaluer cette possibilité, nous avons comparé, par culture cellulaire, les neurones dopaminergiques de la SNc à ceux de la VTA et montré qu'ils sont particulièrement actifs au point de vue bioénergétique, avec peu de capacité de réserve, et qu'ils possèdent une arborisation axonale de taille bien plus importante. À l'aide de la sémaphorine 7A, un facteur de guidage axonal, nous avons réduit la taille de cette arborisation et réduit du même coup les besoins énergétiques et la vulnérabilité de ces neurones. Dans un deuxième temps, nous avons évalué ces mêmes paramètres chez des neurones de souris KO pour Parkin, Pink1 ou DJ-1 et montré que les neurones de la SNc KO pour Parkin sont plus vulnérables aux conditions de culture et sont moins efficaces pour produire leur énergie. Dans un dernier temps, nous avons démontré, *in vivo* cette fois, que les neurones dopaminergiques de la SNc ont une arborisation axonale de taille plus importante que ceux de la VTA et avons utilisé le KO conditionnel du récepteur D2 pour augmenter encore plus l'étendue de cette arborisation axonale. Dans ce modèle, nous avons montré que les neurones de la SNc sont plus vulnérables aux lésions à la 6-OHDA, mais pas à la surexpression d'α-synucléine.

Dans son ensemble, cette thèse amène pour la première fois des preuves directes que la taille de l'arborisation axonale est un facteur majeur dans la vulnérabilité sélective des neurones dopaminergiques de la SNc dans le contexte de la MP.

Mots-clés : Maladie de Parkinson, Neurones Dopaminergiques, Arborization Axonale, Mitochondrie, Parkin, Vulnérabilité Sélective.

Abstract

Parkinson's disease (PD) is a neurodegenerative disease whose characteristic motor symptoms are caused by the death of midbrain dopaminergic neurons of the subtantia nigra pars compacta (SNc). In about 15% of cases, mutations in gene products such as Parkin, Pink1, DJ-1, α-synuclein, LRRK2 or GBA are responsible for the onset of the disease. These genes are involved in physiological processes such as mitophagy, lysosomal function, oxidative stress response, mitochondrial antigen presentation or axonal transport. Interestingly, these processes are all directly or indirectly related to the ability of neurons to produce the energy they need for survival and to their level of basal oxidative stress. One of the central questions in the study of PD is why alterations in such ubiquitous processes lead to the selective death of small groups of neurons in the brain, such as the dopaminergic neurons of the SNc. The comparison of these neurons with their neighbours of the ventral tegmental area (VTA), which are also dopaminergic but much less affected in PD, is one of the most striking examples of this selective vulnerability.

One recent hypothesis suggests that certain characteristics specific to SNc dopaminergic neurons induce a tremendous pressure on their bioenergetic capacities and increase basal oxidative stress, which could make them selectively vulnerable to any additional stress. For example, these neurons are thought to form toxic derivatives of dopamine under stress conditions, which could negatively impact their ability to efficiently produce their energy. They also have a pacemaking firing pattern implicating energy intensive calcium currents. Finally, they are thought to have a particularly elaborated axonal arborization, requiring a phenomenal amount of energy to propagate the action potentials and induce release of neurotransmitters. One of our hypotheses is that these characteristics make SNc dopaminergic neurons particularly active bioenergetically and push them to the limit of their energetic capacities. Any subsequent cellular stress, such as those associated with the previously mentioned genetic alterations, exposure to environmental toxins or simply aging, could then lead to their death.

Interestingly, the development of an ultra-complex axonal arborization is a potentially shared feature of neuronal populations affected in PD, including dopaminergic neurons of the SNc, cholinergic neurons of the pedunculopontine nucleus or noradrenergic neurons of the locus coeruleus. It is therefore possible that this characteristic is central to the selective vulnerability of certain neuronal populations in PD. Unfortunately, no direct comparison of the axonal arborization size of these neurons with spared neuronal populations is currently available, neither is the impact of the modulation of the axonal arborization size on energy requirements and neuronal vulnerability.

To begin to evaluate this possibility, we compared the dopaminergic neurons of the SNc to those of the VTA in culture and showed that they are particularly bioenergetically active, with little spare capacity, and have a much larger axonal arborization size. Using semaphorin 7A, an axon guidance factor, we reduced the size of this axon and at the same time reduced the energy requirements and vulnerability of these neurons. In a second step, we evaluated these same parameters in SNc neurons from Parkin, Pink1 or DJ-1 KO mice and showed that SNc neurons from Parkin KO mice are more vulnerable to culture conditions and are less efficient in producing their energy. Lastly, we demonstrated, *in vivo* this time, that dopaminergic neurons of the SNc have a larger axonal arborization than those of the VTA and used the conditional KO of the D2 receptor to further increase the size of this axon. In this model, SNc neurons were more vulnerable to 6-OHDA lesions, but not to overexpression of α-synuclein.

Overall, this thesis provides for the first-time direct evidence that axonal arborization size is a major factor in the selective vulnerability of dopaminergic neurons of the SNc in the context of Parkinson's disease.

Keywords : Parkinson's Disease, Dopaminergic Neurons, Axonal Arborization, Mitochondria, Parkin, Selective Vulnerability.

Table des matières

Liste des tableaux

Introduction

Article I

Liste des figures

Introduction

Article I

Article II

Article III

Article IV

Discussion

Annexes

Liste des abréviations

5-HT : Sérotonine
6-OHDA : 6-hydroxydopamine
ARIH1 : « Ariadne-1 homologue »
ATP : Adénosine triphosphate
BCL2-L-13 : « B-cell lymphoma 2 like 13 »
BDNF : Facteur neurotrophique issu du cerveau, « Brain-Derived Neurotrophic Factor »
CAV : Canaux calciques voltage-dépendent de type L
DCC : « Deleted in colorectal cancer»
DKK1 : Dickkopf 1
DJ-1 : Protéine déglycase DJ-1
EBF1 : « Early B-Cell Factor 1 »
EN1 : Engrailed-1
EN2 : Engrailed-2
FGF : Facteur de croissance issu des fibroblastes
FKBP8 : « FK506-binding protein 8 »
GBA1 : Glucocérébrosidase 1
GDNF : Facteur de croissance issu des cellules gliales
GPe : Globus Pallidus externe
GPi : Globus Pallidus interne
HHARI : « Human Homologue of Drosophila Ariadne »
KO : Knock-out
LC3 : « Microtubule-associated protein 1A/1B-light chain 3 »
LMX1a : « LIM homeobox transcription factor 1, alpha »
LMX1b : « LIM homeobox transcription factor 1, beta »
LRRK2 : « Leucine-rich repeat kinase 2 »
MAO : Monoamine oxidase
March5 : « Membrane Associated Ring-CH-Type Finger 5 »
MP : Maladie de Parkinson
MPP+ : 1-methyl-4-phenylpyridinium
MPPP : Desmethylprodine
MPTP : 1-méthyl-4-phényl-1,2,3,6-tétrahydropyridine
NADH : Nicotinamide adénine dinucléotide
NET : Transporteur de la norépinephrine
NURR1 : « Nuclear receptor related-1 protein »
OTX2 : « Orthodenticle homeobox 2 »
PARKIN : E3 ubiquitin ligase Parkin
Pink1 : «PTEN-induced putative kinase 1»
PITX3 : « Pituitary homeobox 3 »
TH : Tyrosine Hydroxylase
TNF : Facteur de nécrose tumorale
ROS : Espèces réactives à l'oxygène
RRF : Aire rétrorubrale
SEMA7A : Sémaphorine 7A
SNc : Substantia nigra pars compacta
SNCA : α-synucléine
SNr : Substantia nigra pars reticulata
STN : Noyau sous-thalamique
VGLUT2 : Transporteur vésiculaire du glutamate de type 2
VMAT2 : Transporteur vésiculaire des monoamines de type 2
VPS35 : « Vacuolar protein sorting-associated protein 35 »
VTA : Aire tegmentaire ventrale
WNT1 : « Proto-oncogene protein Wnt-1 »
WT : Type sauvage, « Wildtype »

À mes parents et mon frère

Remerciements

En rétrospective, les années passées à la préparation de cette thèse ont été particulièrement formatrices, autant du côté académique que personnel et professionnel. Les moments heureux comme les plus difficiles ont été d'autant plus mémorables, car partagés avec des personnes extraordinaires. Famille, collègues, mentors et amis ont rendu ce périple précieux et unique.

Pour commencer, j'aimerais remercier mon directeur de recherche et mentor Louis-Éric Trudeau pour son support, sa confiance et sa passion inspirante. Un merci particulier à Marie-Josée Bourque pour ses exploits techniques et humains, ainsi que pour son écoute.

Merci aussi à mes parrains, Richard Robitaille et Adriana DiPolo, aux membres du jury de thèse, Rajeshwar Awatramani, Elvire Vaucher et Ann-Noël Samaha, ainsi qu'à tous les collègues, stagiaires et collaborateurs, plus particulièrement Dominic Thibault, Consiglia Pacelli, Martin Levesque, Ruth S. Slack, David Park et Daniel Levesque.

Finalement un merci tout spécial aux membres de ma famille qui ont su croire en moi et qui m'ont supporté durant toutes ces années, mais surtout merci à ma meilleure amie et conjointe, Dre Janic Bergeron, qui rend chaque jour un peu plus unique.

«I seem to have been only like a boy playing on the seashore, and diverting myself in now and then finding a smoother pebble or a prettier shell than ordinary, whilst the great ocean of truth lay all undiscovered before me. »

- Isaac Newton

De « Brewster, Memoirs of Newton (1855) »

Avant-Propos

Cette thèse se présente dans un contexte où les dernières décennies ont vu de grandes avancées dans la compréhension des divers mécanismes impliqués dans la maladie de Parkinson (MP); que ce soit par l'utilisation de toxines perturbant plusieurs fonctions cellulaires ou par l'étude de mutations génétiques répliquant en partie certaines facettes de la maladie. Toutefois, bien qu'il soit établi depuis plus de 50 ans que les symptômes moteurs typiques de la maladie soient causés majoritairement par la mort des neurones dopaminergiques de la substance noire compacte (SNc), peu est connu sur les raisons pour lesquelles cette petite population neuronale est sélectivement vulnérable.

À travers cette thèse, nous tenterons d'éclaircir ce point d'ombre. Après un bref historique des points tournants dans l'étude de la dopamine, suivi d'une description sommaire de la MP et des différentes hypothèses de vulnérabilité sélective existantes, nous tenterons de démontrer que les neurones dopaminergiques de la SNc sont spécifiquement vulnérables puisqu'ils se trouvent dans une situation particulièrement délicate au niveau bioénergétique, en grande partie causée par leur arborisation axonale massive. Nous explorerons aussi l'influence de certaines mutations impliquées dans les formes familiales de la maladie sur cette vulnérabilité sélective.

Chapitre 1 : Introduction

1.1 Notes historiques sur la dopamine

Que ce soit par son rôle majeur dans les phénomènes de dépendance ou par son implication dans la MP, la dopamine occupe une place de choix dans la culture populaire comme molécule de la motivation et du plaisir. Toutefois, ses débuts ont été bien plus modestes.

1.1.1 Découverte et premiers mécanismes

Synthétisée en 1910 par George Barger et James Ewens, la dopamine fut initialement décrite par Henry Dale (Prix Nobel de Physiologie ou Médecine de 1938 avec Otto Loewi), comme un analogue de l'adrénaline à l'activité sympathomimétique faible. Dès lors, on ne lui attribua aucune signification physiologique et elle sombra dans l'oubli pendant près de 30 ans.

Elle refit surface en 1938, quand Peter Holtz en Allemagne découvrit la dopa décarboxylase dans des homogénats de tissus de mammifères (plus particulièrement dans les reins), l'enzyme responsable de la transformation de la L-DOPA en dopamine. Puis en 1939, Holtz et Hermann Blaschko décrivirent indépendamment la voie de synthèse des catécholamines [1, 2] (Figure 1). Brièvement, pour produire de la dopamine, la tyrosine doit être hydroxylée en L-DOPA par la tyrosine hydroxylase (TH) [3], étape limitante dans cette synthèse. Puis la L-DOPA doit être décarboxylée en dopamine par la DOPA décarboxylase. Elle peut ensuite être transformée en noradrénaline puis en adrénaline par deux réactions enzymatiques subséquentes supplémentaires.

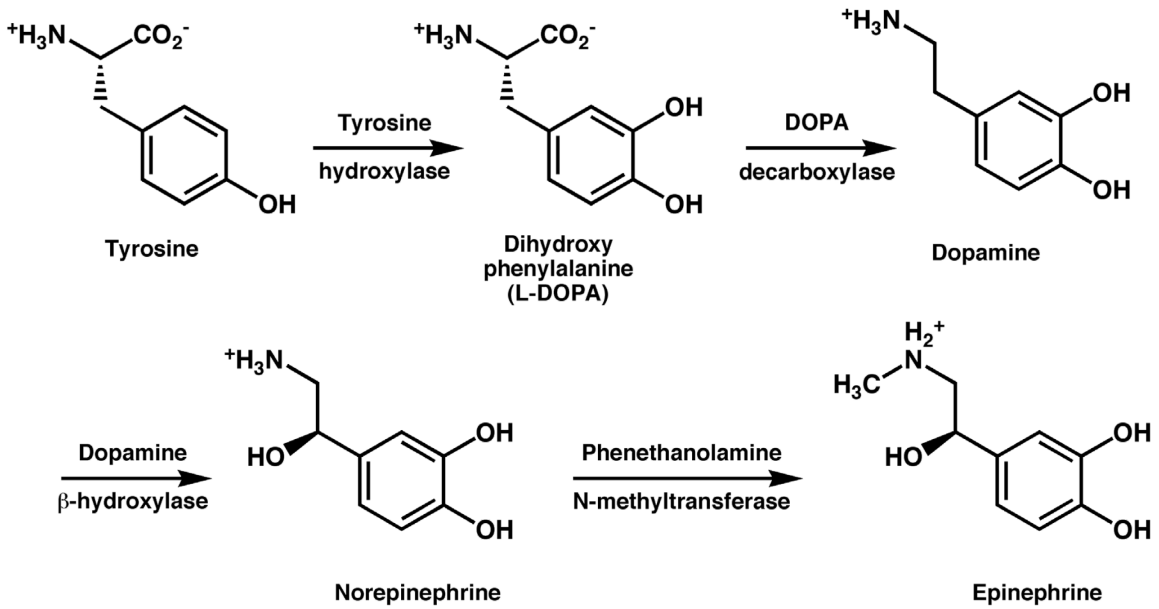

Figure 1. Voies de synthèse des catécholamines.

Source : http://fr.academic.ru/pictures/frwiki/84/Tyrosine_metabolism.png

Dans les années 40, la dopamine était toujours considérée comme un simple intermédiaire dans la synthèse de la noradrénaline n'ayant aucune fonction physiologique spécifique. Ce n'est qu'en 1956 que Blaschko suggéra, dans une conférence pour la « Swiss Society of Physiology, Biochemistry and Pharmacology », qu'elle pourrait avoir un rôle biologique unique. Son postulat fut en partie confirmé deux ans plus tard par Oleh Hornykiewicz [4] qui potentialisa l'effet vaso-dépresseur de la dopamine en inhibant sa dégradation et en administrant son précurseur, la L-DOPA.

À peu près au même moment à la fin des années 50, la présence de la dopamine fut confirmée dans le cerveau [5], plus précisément dans le striatum [6, 7], et des travaux chez le lapin par Arvid Carlsson et son équipe montrèrent que l'effet tranquillisant de la réserpine, un hypotenseur, était dû à la déplétion du cerveau en dopamine (mais aussi en noradrénaline et en sérotonine)[8]. Ses effets étaient du même coup réduits par l'administration concomitante de L-DOPA. Cette découverte ouvrit le pas à une série d'autres qui permirent à Carlsson de recevoir

en 2000 le Prix Nobel de Physiologie ou Médecine avec Paul Greengard et Eric Kandel. Dans les mêmes années, la présence de la monoamine-oxydase (MAO) fut décrite dans le cerveau comme enzyme responsable de la dégradation des monoamines telles que la sérotonine (5-HT) et la dopamine [9–11]. Ces travaux montrèrent aussi que l'utilisation d'inhibiteurs de cette enzyme augmente les niveaux cérébraux de monoamine et potentialise l'effet de la L-DOPA. Ces inhibiteurs furent les premiers médicaments à être utilisés dans le traitement de la dépression. Toutefois, ils furent majoritairement remplacés plus tard par des inhibiteurs sélectifs de la recapture des monoamines pour leurs effets secondaires moins importants. Malgré ces découvertes, les fonctions spécifiques de la dopamine dans le cerveau restaient source de débat à cause de l'incapacité des techniques du temps à révéler la présence de neurones dopaminergiques ou de voies de projections spécifiques.

1.1.2 Anatomie des voies dopaminergiques

Dans les années 60, Hillarp & Falck développèrent une nouvelle méthode d'histochimie fluorescente qui permit pour la première fois de visualiser l'anatomie des systèmes catécholaminergiques et indoleaminergiques [12]. C'est en 1965, à l'aide de cette méthode, que les voies de projections des neurones dopaminergiques furent découvertes [13–15] (Figure 2). Chez le mammifère, ces neurones sont distribués dans 9 noyaux (A8 à A16), mais sont majoritairement présents dans le noyau A9 (SNc), A10 (aire tegmentaire ventrale, VTA) et en plus faible nombre dans le noyau A8 (aire rétrorubrale, RRF). Brièvement, leurs projections furent catégorisées en 3 voies dopaminergiques. Les projections mésolimbiques et mésocorticales qui ont pour origine la VTA (mais aussi la SNc et la RRF) et qui font respectivement contact avec le striatum ventral, aussi appelé noyau accumbens (mais aussi à l'amygdale, au septum, au tubercule olfactif et à l'hippocampe) et avec le cortex préfrontal (mais aussi le cortex cingulaire et périrhinal). Les projections mésostriées proviennent quant à elles en grande majorité de la SNc (mais aussi la VTA et la RRF) et contactent le striatum dorsal; divisé en noyau caudé et putamen chez les primates [16]. D'autres voies de projections dopaminergiques ont aussi plus tard été décrites; soit la voie tuberoinfundibulaire émanant du noyau arqué de l'hypothalamus et

contactant le lobe intermédiaire de l'hypophyse et de l'éminence médiane, mais aussi une voie descendante secondaire provenant de la SNc et qui contacte le noyau pédonculopontin et le noyau cunéiforme [17]. Des travaux tirant avantage d'approches génétiques intersectionnelles ont récemment permis de décrire encore plus précisément ces voies de projections en quantifiant les projections de sous populations dopaminergiques à l'intérieur même de la SNc et de la VTA [18].

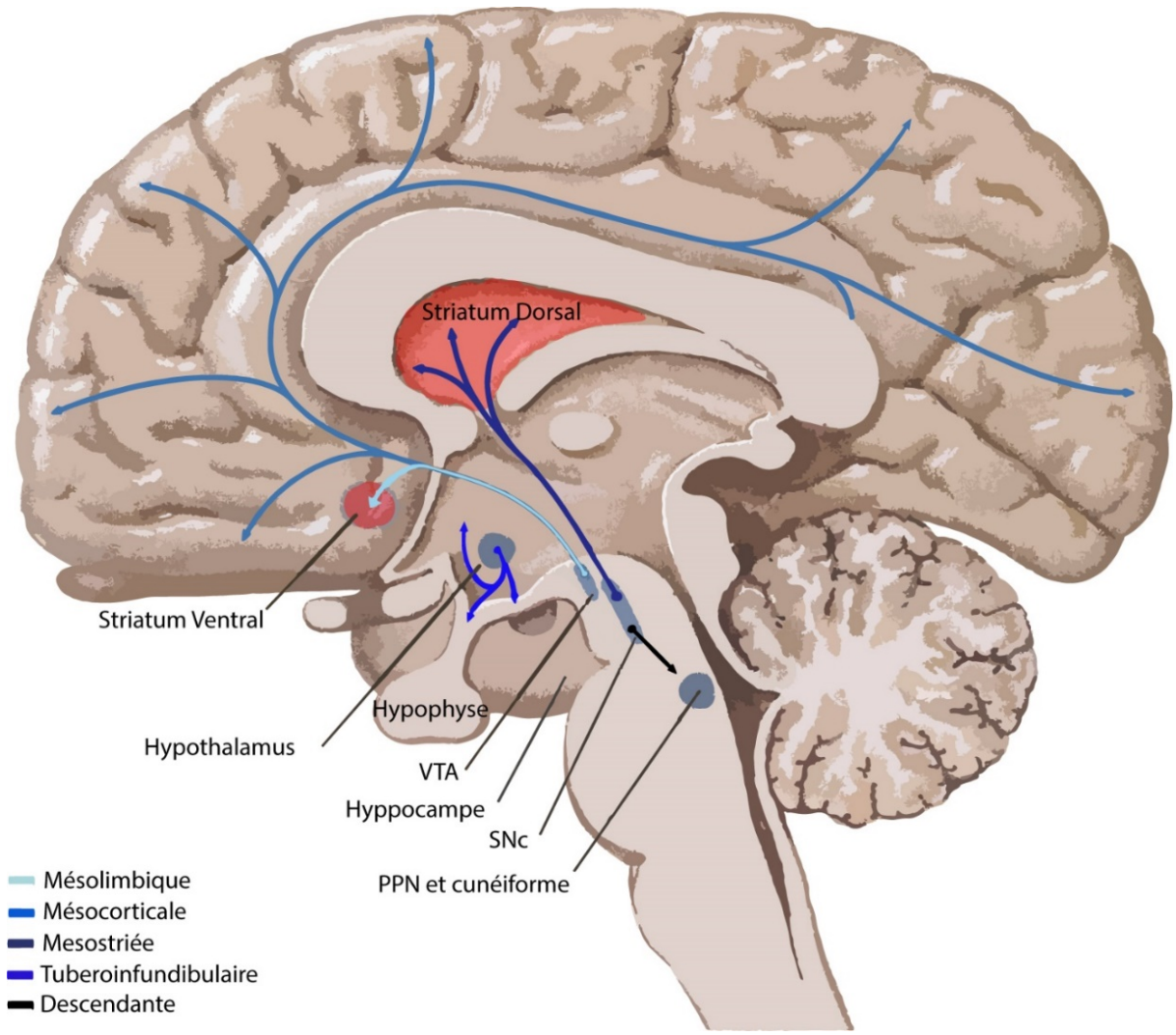

Figure 2. Voies de projections du système dopaminergique mésencéphalique. En rouge, régions du cerveau particulièrement dense en fibres dopaminergiques. Adaptation de Scarr et al,. 2013 [19]. Reproduction avec permission.

Bien que le système dopaminergique soit conservé à travers différentes espèces, le nombre de neurones et de connexions dopaminergiques varie grandement. Par exemple, dans la SNc de rat, on compte en moyenne 12 000 neurones qui font chacun 100 000 à 250 000 contacts dans le striatum. Chez l'humain, on parle plutôt de 382 000 neurones formant chacun plus d'un million de terminaisons [19].

L'établissement de ce nombre particulièrement important de terminaisons sur un large territoire et à grande distance des corps cellulaires nécessite, durant le développement du système dopaminergique, l'apport de plusieurs facteurs de croissance et de guidage axonal. Brièvement, l'élaboration des premiers segments axonaux quittant le mésencéphale autour de E11 se fait sous l'influence de plusieurs gradients de molécules établis par l'organisateur du mésencéphale-rhombencéphale, tels que les Wnts et les FGFs [20]. Par exemple, la sécrétion de FGF8 induit l'expression de sémaphorine 3F dans le mésencéphale, ce qui le rend non-permissif à la croissance locale des prolongements dopaminergiques. Les prolongements axonaux dopaminergiques détectent alors cette sémaphorine par l'entremise du récepteur neuropiline 2, dont la voie signalisation mène à la déstabilisation de la dynamique de l'actine et à l'effondrement du cône de croissance axonal [21, 20]. Du côté des Wnts, Wnt5 est fortement exprimé dans la partie plus caudale du mésencéphale et lui aussi repousse les prolongements dopaminergiques, par l'entremise du récepteur Frizzeled3. Au contraire Wnt7b est exprimé selon un gradient opposé à Wnt5 et attire les prolongements dopaminergiques vers leur sortie du mésencéphale [22, 20]. Ces prolongements joignent alors le faisceau médian du télencéphale et se dirigent vers le striatum. Au cours de ce trajet, à partir de E12,5, la répulsion induite par la sémaphorine 3F reste importante, mais plusieurs autres éléments tels que les Netrines et DCC, les Slits et les Robos sont nécessaires à certains sous-ensembles d'axones dopaminergiques [20].

À l'entrée du striatum, vers E13,5, ces mêmes éléments, en plus d'une multitude d'éphrines et d'autres sémaphorines, sont nécessaires à l'élaboration adéquate de l'innervation dopaminergique striatale [20]. Par exemple, il semble que la Netrine1 soit particulièrement importante pour la séparation des prolongements provenant de la SNc et de la VTA qui

innerveront respectivement le striatum dorsal et ventral. En effet, les prolongements de la SNc sont attirés par de plus faibles concentrations de Netrine1 que ceux de la VTA et sont insensibles à de fortes concentrations de ce facteur. C'est donc la présence d'un gradient de Netrine1, plus concentré dans le striatum ventral, qui permettrait la séparation des prolongements de provenances différentes [23]. Pour plus de détails sur les multiples facteurs guidant la croissance des axones dopaminergiques, voir Van den Heuvel et al., 2008 et Prestoz et al., 2012 [24, 25].

De manière intéressante, plusieurs de ces facteurs sont toujours exprimés chez l'adulte et, bien que nos connaissances sur leurs fonctions exactes à ce stade restent limitées, ils semblent être importants pour le maintien de l'innervation dopaminergique [25, 26]. De façon similaire, certains facteurs de croissance, tels que le GDNF, le BDNF et le FGF, sont aussi exprimés dans le striatum adulte et procurent d'importants signaux rétrogrades prosurvie aux neurones dopaminergiques [27–32].

1.1.3 Récepteurs et transporteurs

Malgré les découvertes initiales des voies de projections dopaminergiques, le débat faisait toujours rage dans les années 60 sur le statut de neurotransmetteur de la dopamine. Il fut résolu dans les années 70 avec la découverte des récepteurs de la dopamine.

Les premières données sur ce sujet remontent à 1972, lorsque Paul Greengard démontra que l'application de dopamine dans le noyau accumbens de rat activait l'adenylate cyclase [33]. Il proposa alors l'existence d'un récepteur à la dopamine. Puis en 1976, Philip Seeman identifia un site pouvant être marqué à la fois par la dopamine et l'halopéridol, dans le cadre de sa quête d'un récepteur spécifique aux antipsychotiques. Il nomma alors ce site le « neuroleptic/dopamine receptor » [34]. Plus tard, ce récepteur fut renommé récepteur dopaminergique D2 dans le cadre d'une étude du couplage des récepteurs dopaminergiques à

l'adénylate cyclase [35]. On y identifia alors deux récepteurs; le D2, couplé négativement par la protéine $G\alpha_{i/o}$ et le D1, couplée positivement par la protéine $G\alpha_{s/olf}$ [36].

Le développement de la biologie moléculaire dans les années 80 a par la suite permis d'identifier par clonage 5 sous-types de récepteurs, 2 ayant un couplage de type D1 (D1 et D5) et 3 ayant un couplage de type D2 (D2, D3 et D4). Une des particularités intéressantes du récepteur D2 est qu'il peut se retrouver au niveau présynaptique en tant qu'autorécepteur et du fait même réguler la relâche de dopamine [37]. Il peut aussi être désensibilisé [38] et s'internaliser [39, 40] lorsqu'activé chroniquement. Finalement, une autre particularité des récepteurs dopaminergiques est qu'ils peuvent s'associer entre eux [41] pour former des hétéromères.

Vers la fin des années 80, l'étude de l'action de ces récepteurs au niveau du striatum permis de décrire les deux voies de projections des ganglions de la base vers le thalamus nécessaires pour déclencher/réguler le mouvement; soit la voie directe (D1) et la voie indirecte (D2) [42–45](Figure 3A). Brièvement, la voie directe implique les neurones GABAergiques striataux qui expriment le récepteur D1 et la voie indirecte ceux qui expriment le récepteur D2 (environ 50% d'entre eux pour chaque voie). Ces neurones reçoivent des afférences excitatrices corticales et thalamiques et ont une action inhibitrice sur différentes structures des ganglions de la base, principalement le globus pallidus et la substance noire réticulée (SNr). La SNr ainsi que la partie externe du globus pallidus (GPe) sont considérées comme des noyaux de sortie, car leur activité est la résultante des boucles d'activation/inhibition présentes dans les voies directes et indirectes des ganglions de la base. Ces noyaux de sortie étant constitués de cellules inhibitrices connectées au thalamus, leur activation induit une inhibition thalamique et donc une inhibition du contrôle du mouvement. La voie directe est nommée ainsi, car son activation va mener à l'inhibition directe des noyaux de sortie, permettant le mouvement en désinhibant le thalamus. La présence de dopamine va accentuer cet effet puisque l'activation du récepteur D1 a un effet modulateur positif sur les neurones striataux de cette voie. Pour ce qui est de la voie indirecte, son action sur les noyaux de sortie passe indirectement par la levée de l'inhibition du noyau sous-thalamique (STN) qui lui active normalement de façon tonique les noyaux de sortie. Cette activation permet le maintien de l'inhibition de l'activité thalamique. En présence de

dopamine, les neurones striataux de la voie indirecte vont être inhibés par l'effet modulateur négatif du récepteur D2 et le mouvement sera permis.

Dans un contexte pathologique où il y a absence de dopamine (Figure 3B), la voie indirecte n'est plus réprimée et donc freine l'activité thalamique et la voie directe n'est plus activée et donc ne promeut plus cette même activité. On obtient alors une inhibition globale du thalamus et donc des troubles moteurs tels qu'observés dans la MP (voir section 1.2 pour plus de détails).

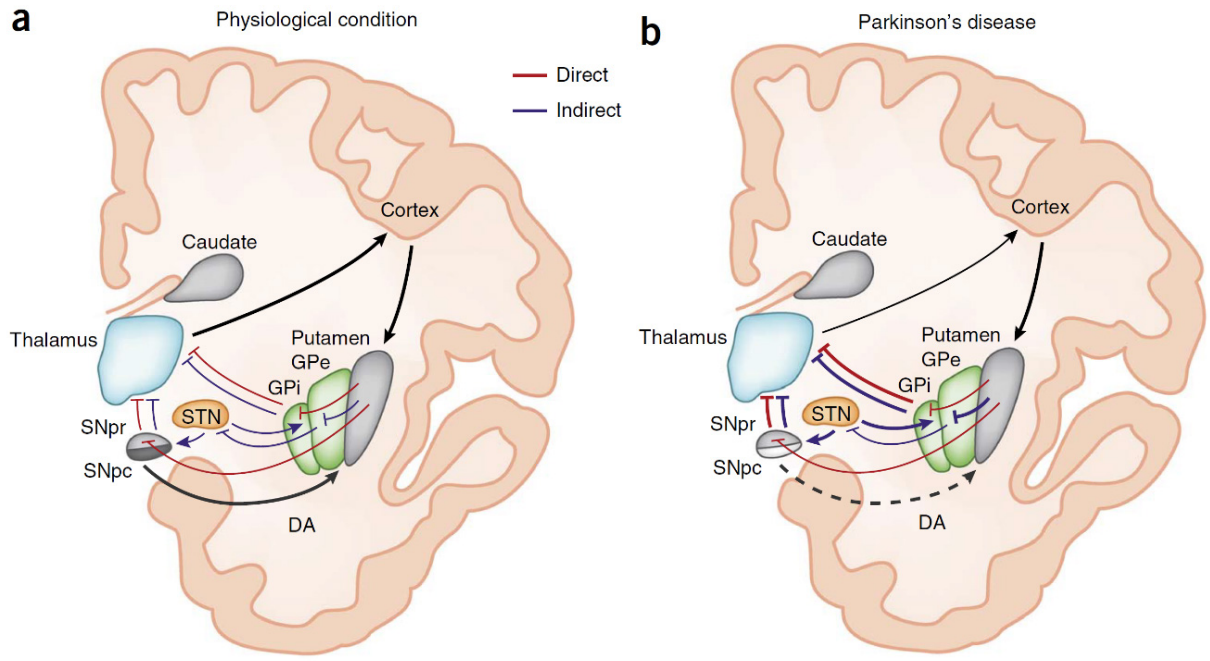

Figure 3. Schématisation classique des voies directes et indirectes des ganglions de la base dans des conditions physiologiques et dans la MP [46]. Reproduction avec permission.

Finalement, dans les années 90, le clonage des transporteurs vésiculaires des monoamines (VMATs) et du transporteur de la dopamine (DAT) permit de mieux comprendre de quelle façon certaines drogues, telles que la cocaïne et de l'amphétamine, augmentent les niveaux cérébraux de dopamine [47–52]. Brièvement, chez les neurones dopaminergiques, le

VMAT2 a pour fonction d'emmagasiner la dopamine dans des vésicules servant à la relâche de la dopamine au niveau synaptique et le DAT a pour fonction la recapture de la dopamine libérée au niveau des sites de libération. La cocaïne a pour effet de bloquer cette recapture et donc de maintenir les niveaux extracellulaires de dopamine élevée. De son côté l'amphétamine inverse l'action du DAT et y est échangée contre une molécule de dopamine pour entrer dans la cellule. Une fois en contact avec le VMAT2, l'amphétamine va pénétrer dans les vésicules et induire un efflux de dopamine. Il en résulte encore une fois des niveaux extracellulaires de dopamine très élevés [53].

1.1.4 Hétérogénéité des populations dopaminergiques

Les années 90 et 2000 ont aussi amené leur lot de découvertes quant à la diversité des sous-populations dopaminergiques et leurs propriétés. La comparaison entre les neurones dopaminergiques de la SNc et de la VTA est particulièrement intéressante puisqu'ils ont été longtemps considérés comme formant une population plutôt homogène, même si leurs voies de projections diffèrent. Il est maintenant reconnu que plusieurs caractéristiques les différentient. Par exemple, les neurones de la VTA expriment en plus grande proportion le transporteur vésiculaire du glutamate de type 2 (VGlut2), leur permettant de co-libérer la dopamine et le glutamate [54]. Peu de neurones de la SNc ont cette capacité. Aussi, bien que les deux populations présentent une activité électrique de type « pacemaker », la décharge des neurones de la SNc s'accompagne de lentes oscillations calciques causées par l'ouverture à la membrane plasmique de canaux calciques voltage dépendant de type L, CAV1.1 et 1.3 [55, 56]. De leur côté, les neurones de la VTA présentent une faible expression de ce canal, mais paradoxalement, expriment une plus grande quantité de protéines qui permettent de tamponner le calcium telles que la calbindine [57, 58]. Ils expriment aussi de plus faibles niveaux du DAT [48, 59] et du récepteur D2 [60] et auraient un compartiment axonal de taille plus modeste [19, 61, 62], bien qu'aucune mesure comparative directe n'ait été effectuée avant les travaux de cette thèse.

Les afferences et la circuiterie locale de la SNc et de la VTA sont aussi en partie différentes. Les neurones dopaminergiques des deux régions reçoivent des afférences provenant du cortex, du striatum, du pallidum, de l'amygdale, de l'hypothalamus, du thalamus et de plusieurs noyaux du mésencéphale, tels que la SNr, le raphé et le noyau pedonculopontin [63]. Cependant, les neurones de la SNc reçoivent préférentiellement des afférences GABAergiques du striatum dorsal, du globus pallidus et de la SNr et des afférences glutamatergiques des noyaux sous-thalamique et pedonculopontin [63, 64]. En ce qui concerne les neurones de la VTA, ils reçoivent préférentiellement des afférences GABAergiques du striatum ventral, du pallidum ventral, de la substance grise périaqueducale et de l'hypothalamus latéral, des afférences glutamatergiques du noyau parasousbthalamique, en plus de projections de la RRF et du raphé dorsal [63, 65, 66]. Une particularité supplémentaire de la VTA est la présence locale de multiples neurones purement glutamatergiques et GABAergiques, en plus des neurones dopaminergiques, contrairement à la SNc qui ne possède majoritairement que des neurones dopaminergiques. Par ces différences dans leurs afférences, leurs efferences et leur circuiterie locale, les deux régions sont préférentiellement impliquées dans des fonctions biologiques distinctes. Par exemple, la VTA est très importante pour les phénomènes de dépendance, de prise de décision et d'aversion, tandis que la SNc est principalement impliquée dans le contrôle des fonctions motrices [67].

Une autre différence importante entre les neurones dopaminergiques de la SNc et de la VTA se trouve dans les différents facteurs de transcriptions, facteurs de croissance et récepteurs nécessaires à leur différentiation et maturation normale au cours du développement [68]. Plusieurs d'entre eux tels que Nurr1, Wnt1, EN1 et 2, LMX1a et b, DKK1, Ebf1 et DCC sont nécessaires aux deux populations neuronales. Toutefois, l'ablation de certains de ces gènes induit des altérations spécifiques à une ou l'autre des populations. Par exemple, l'expression de OTX2 semble cruciale pour les neurones de la VTA et l'expression de PITX3 primordiale pour les neurones de la SNc [68]. De plus, certains de ces facteurs, tels que LMX1a et b, sont aussi exprimés chez l'adulte et sont nécessaires à la survie des neurones dopaminergiques après leur maturation [69]. De manière intéressante, l'expression de plusieurs de ces facteurs semble liée entre eux. Par exemple, l'absence de LMX1b chez le modèle KO pour ce gène induit une perte de l'expression de PITX3 chez les neurones dopaminergiques durant leur développement, ainsi

que leur mort éventuelle [70]. Cette dégénérescence est induite par la perte d'expression du BDNF [71] et de l'acide rétinoïque (via l'aldéhyde déhydrogénase 1A1)[72].

1.2 Maladies associées; emphase sur la maladie de Parkinson

Le système dopaminergique, par son réseau complexe et ses effets importants sur le comportement et le mouvement, régule de nombreux processus neurophysiologiques tels que la motivation, l'attention, la mémoire et les mouvements volontaires [73]. Plusieurs maladies découlent donc d'altérations dans les fonctions de ce système telles que la schizophrénie, la dépendance aux drogues d'abus, les troubles de l'attention, la maladie de Huntington et la MP.

1.2.1 La Schizophrénie

Brièvement, la schizophrénie est une maladie psychiatrique neurodéveloppementale caractérisée par des symptômes dits positifs tels que des distorsions de la réalité et des troubles de la pensée, des symptômes négatifs tels qu'une expression réduite des émotions et la présence d'avolition et des symptômes cognitifs tels que des troubles du fonctionnement exécutif et des troubles de l'attention [74]. L'hypothèse générale neurodéveloppementale de la schizophrénie suggère que des perturbations dans le développement normal du cerveau aboutiraient à des changements moléculaires qui rendraient l'individu affecté plus sensible à développer la maladie au début de l'âge adulte. En ce qui concerne le système dopaminergique, la schizophrénie serait caractérisée par des niveaux excessifs de dopamine striatale et des concentrations réduites au niveau cortical [75]. Le traitement pharmacologique actuel se fait à l'aide d'antagonistes du récepteur D2 appelés antipsychotiques qui sont efficaces à réduire les symptômes positifs. Il est aussi suggéré que les systèmes glutamatergiques et GABAergiques sont impliqués dans la maladie [74–76].

1.2.2 La dépendance aux drogues d'abus

La dépendance aux drogues d'abus est caractérisée par un désir compulsif d'utiliser de façon récurrente des drogues telles que les psychostimulants. Ces drogues, incluant la cocaïne et les amphétamines, ont pour effet d'augmenter temporairement les niveaux de dopamine cérébraux, créant une sensation de bien-être. Les mécanismes d'action de certaines de ces substances ont été décrits brièvement dans la section 1.1.3 et impliquent plus spécifiquement les neurones dopaminergiques de la VTA et leurs projections au striatum ventral. Les traitements actuels, très limités et non curatifs, incluent des thérapies de substitution pour certaines substances, un sevrage et du soutien psychologique et médical pour pallier aux symptômes de sevrage et éviter la rechute [77, 78].

1.2.3 Les troubles de l'attention

Les troubles de l'attention sont caractérisés par des niveaux d'inattention inappropriés pour le stade développemental et sont souvent accompagnés de problèmes d'hyperactivité ou d'impulsivité. L'hypothèse actuelle sur la pathogenèse de la maladie suggère qu'une maturation retardée des circuits ganglions de la base, qui se résorbe souvent à l'âge adulte, serait en cause. Le système dopaminergique est considéré central dans la maladie puisque des mutations dans plusieurs gènes qui y sont reliés, telles que dans le DAT et dans plusieurs récepteurs dopaminergiques, sont associées à la maladie. De plus, les traitements pharmacologiques les plus efficaces pour les troubles de l'attention sont à base de psychostimulants qui augmentent les niveaux de dopamine dans le cerveau [79]. L'utilisation de ces molécules est toutefois maintenant remise en question [80].

1.2.4 La maladie d'Huntington

La maladie d'Huntington est une maladie neurodégénérative causée par une mutation génétique dans le gène huntingtin induisant une expansion des répétitions glutamine présentes dans le gène [81]. Elle est caractérisée par des mouvements involontaires brusques et irréguliers causés par une perte des neurones de projection striataux et corticaux [82, 83]. Elle est accompagnée par une augmentation initiale des niveaux de dopamine cérébraux, ainsi que d'une réduction de l'expression des récepteurs dopaminergiques [84]. Cependant, on observe plutôt une diminution des niveaux de dopamine dans les stades tardifs de la maladie. Des changements dans la transmission glutamatergique sont aussi observés. Les traitements actuels sont purement symptomatiques et visent à réduire les mouvements involontaires à l'aide de neuroleptiques et de benzodiazépines [84].

1.2.5 La maladie de Parkinson

Pour ce qui est de la MP, elle est principalement caractérisée par des symptômes moteurs, causés par la dégénérescence graduelle des neurones dopaminergiques de la SNc. Les sections suivantes décriront en détail plusieurs aspects de la maladie.

1.2.5.1 Épidémiologie et étiologie

La MP est la maladie neurodégénérative la plus commune après la maladie d'Alzheimer. Elle affecte 0,2% des Canadiens, 5% de ceux qui résident en établissement de soin, et 79% des patients atteints ont plus de 65 ans. L'âge moyen de l'apparition des premiers symptômes moteurs est de 64 ans avec un diagnostic en moyenne 2 ans plus tard [85]. Deux fois plus d'hommes que de femmes sont atteints.

Bien que plus de 70% des cas soient considérés idiopathiques, il existe plusieurs facteurs de risques environnementaux et génétiques [86]. De rares formes familiales de la maladie sont observées dans 10-15% des patients et comprennent des mutations dans des gènes comme SNCA (α-synucléine), LRRK2, VPS35, GBA1, Pink1, DJ-1 et Parkin. Ces gènes sont impliqués dans des processus comme la mitophagie [87], le transport vésiculaire [88], la réponse antioxydante [89, 90] ou la fonction lysosomiale [91, 92]. Du côté environnemental, plusieurs éléments ont été associés à un risque accru de développer la maladie, tels que la consommation de produits laitiers, l'exposition aux pesticides, l'abus d'amphétamines et de méthamphétamines, la contraction de mélanomes, les traumas cérébraux et le diabète de type 2 [86]. Les facteurs potentiellement protecteurs sont la consommation de tabac/nicotine, de caféine et/ou de thé, une concentration élevée d'urée sanguine (antioxydant), l'activité physique et l'utilisation chronique d'ibuprofène (anti-inflammatoire non-stéroïdien) ou de bloqueurs des canaux calciques (pour le traitement de la haute pression) [86].

1.2.5.2 Découverte, symptômes et traitements

La MP a été initialement décrite par James Parkinson en 1817 comme suit :

« *Involuntary tremulous motion, with lessened muscular power, in parts not in action and even when supported; with a propensity to bend the trunk forward, and to pass from a walking to a running pace: the senses and intellects being uninjured* [93]. »

Les critères diagnostiques ont quelque peu évolué depuis. Selon l'« International Parkinson and Movement Disorder Society », le diagnostic peut être émis lorsque le patient présente un état clair de parkinsonisme (bradykinésie, tremblement au repos et/ou rigidité), en excluant les autres causes potentielles, telles que par exemple des anormalités cérébelleuses, une paralysie supranucléaire, une démence frontotemporale ou une aphasie primaire progressive. La présence de critères secondaires peut aussi appuyer le diagnostic, tels qu'une dysfonction olfactive ou une dénervation sympathique cardiaque [94].

Au niveau anatomique, ce n'est qu'en 1925 qu'Édouard Brissaud proposa que la maladie soit caractérisée par des dommages à la SNc, sans toutefois savoir que ce noyau était dopaminergique. Le lien entre la MP et le système dopaminergique fut seulement suggéré vers la fin des années 50. Sachant que la L-DOPA est le précurseur naturel de la dopamine, le Dr André Barbeau et le Dr Walter Birkmayer furent les premiers à initier indépendamment des essais cliniques en l'administrant à leurs patients en 1961. L'effet antiakinetic observé par Birkmayer fut publié comme suit :

« *Bed-ridden patients who were unable to sit up, patients who could not stand up when seated, and patients who when standing could not start walking performed all these activities with ease after L-DOPA. They walked around with normal associated movements and they could even run and jump. The voiceless, aphonic speech, blurred by pallilalia and unclear articulation, became forceful and clear as in a normal person* [95]. »

Puis, en 1967, Hoehn and Yahr ont introduit le premier système de classification de l'avancement de la maladie encore aujourd'hui reconnu internationalement [96]. Bien qu'il n'existe toujours aucun traitement curatif, la L-DOPA reste le traitement de choix pour atténuer les symptômes de la maladie. Malheureusement, un problème majeur avec ce traitement est l'induction de dyskinésies après quelques années de traitement. L'occurrence après 5 ans de traitement est de 16% chez les individus dont la maladie s'est déclarée après 70 ans et de 50% chez les individus dont la maladie s'est déclarée avant 60 ans. Le facteur de risque associé le plus important est la dose de L-DOPA administrée [97]. Pour cette raison, plusieurs agents visant à potentialiser l'effet de la L-DOPA et donc à réduire les doses nécessaires pour observer un effet bénéfique sont utilisés, tels que des agonistes dopaminergiques ou des bloqueurs de la dégradation de la dopamine.

1.2.5.3 Signes pathologiques et modèles associés

En plus de la mort des neurones dopaminergiques de la SNc, un des marqueurs spécifiques de la maladie est la présence de corps de Lewy dans le tronc cérébral et le cortex

(Figure 4). Ces agrégats protéiques anormaux ont été découverts en 1912 par Fritz Heinrich Lewy, mais leur présence dans la SNc et leur nom caractéristique est attribué respectivement à Konstantin Nikolaevich Trétiakoff et à Gonzalo Rodríguez Lafora qui les nomma ainsi en 1913 [98]. Ils sont composés majoritairement d'α-synucléine, une protéine synaptique dont la forme tronquée en c-terminal est particulièrement pathologique chez les neurones, par son agrégation et ses interactions avec plusieurs protéines telles que la tubuline et Parkin. De manière surprenante, il a aussi été proposé que l'α-synucléine aurait la capacité d'être transportée d'une cellule à l'autre et donc de propager la maladie entre les zones cérébrales synaptiquement connectées [99].

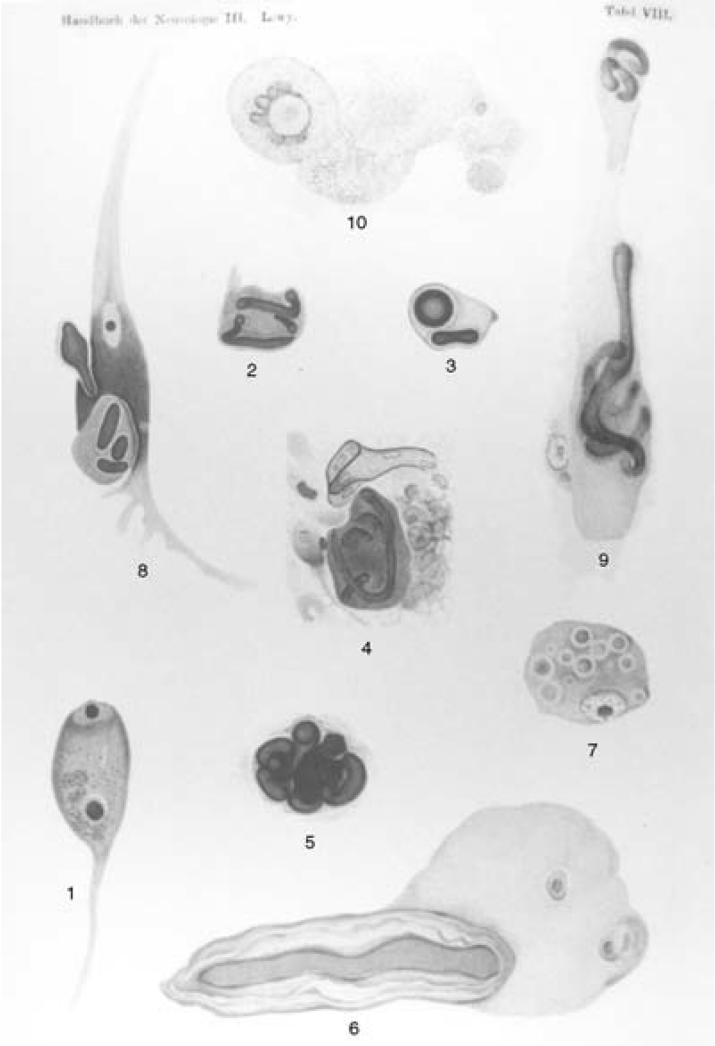

Figure 4. Premières illustrations décrivant les corps de Lewy dans la MP par Friedrich Heinrich Lewy en 1912 [101]. Reproduction avec permission.

Cette observation a mené au début des années 2000 à la publication par Heiko Braak d'un nouveau système de classification pathologique de la maladie basé sur la présence de corps de Lewy dans différentes régions du cerveau (Tableau I) [100]. Brièvement, les lésions apparaîtraient initialement dans le noyau moteur dorsal IX/X et/ou dans la zone intermédiaire réticulaire. Elles progresseraient ensuite vers le raphé caudal, le locus coeruleus et le noyau réticulaire gigantocellulaire pour atteindre la SNc au troisième stade. La pathologie progresserait ensuite dans le cortex temporal et allocortex au stade 4, puis au néocortex au stade 5, pour finalement atteindre le cortex prémoteur au stade 6. Puisque ces corps de Lewy sont majoritairement formés d'α-synucléine, la surexpression de formes sauvages ou mutées de celle-ci ou l'injection de fibrilles (forme agrégée de la protéine) ont grandement été utilisées ces dernières années pour créer de meilleurs modèles de la maladie.

Stages in the evolution of PD-related pathology

Stage 1 $N = 21$; medulla oblongata	Lesions in the dorsal IX/X motor nucleus and/or intermediate reticular zone
Stage 2 $N = 13$; medulla oblongata and pontine tegmentum	Pathology of stage 1 plus lesions in caudal raphe nuclei, gigantocellular reticular nucleus, and coeruleus–subcoeruleus complex
Stage 3 $N = 24$; midbrain	Pathology of stage 2 plus midbrain lesions, in particular in the pars compacta of the substantia nigra
Stage 4 $N = 24$; basal prosencephalon and mesocortex	Pathology of stage 3 plus prosencephalic lesions. Cortical involvement is confined to the temporal mesocortex (transentorhinal region) and allocortex (CA2-plexus). The neocortex is unaffected
Stage 5 $N = 17$; neocortex	Pathology of stage 4 plus lesions in high order sensory association areas of the neocortex and prefrontal neocortex
Stage 6 $N = 11$; neocortex	Pathology of stage 5 plus lesions in first order sensory association areas of the neocortex and premotor areas, occasionally mild changes in primary sensory areas and the primary motor field

Tableau I. Stades de l'évolution de la pathologie dans la MP tels que publiés initialement par le Dr. Heiko Braak [100]. Reproduction avec permission.

Un autre modèle aujourd'hui incontournable dans l'étude de la MP provient d'un mystérieux, mais maintenant célèbre, cas clinique décrit par le docteur William Langston dans les années 80 [101]. L'histoire commença en fait en 1947 avec Albert Ziering qui synthétisa pour la première fois le Desmethylprodine 1,3-Dimethyl-4-phenyl-4-propionoxypiperidine (MPPP), un opioïde synthétique. Puis dans les années 70, Barry Kidston tenta de reproduire ces

travaux et s'injecta la substance. Il produisit toutefois un mélange de MPPP et de 1-methyl-4-phenyl-1,2,3,6-tetrahydropyridine (MPTP). Après quelques jours, il devint complètement paralysé et ne pouvait plus parler. Après des mois de thérapies électroconvulsives pour traiter un diagnostic initial erroné de schizophrénie catatonique, il fut traité à la L-DOPA ce qui réduisit grandement ses symptômes et permit de diagnostiquer chez lui la MP.

À l'été 1982, 7 individus avec historique d'abus de substances furent hospitalisés dans différents hôpitaux de Californie avec des symptômes similaires à ceux de Kidston. William Langston recensa alors ces cas et découvrit qu'un chimiste collégial avait subtilisé l'article d'Albert Ziering sur la synthèse du MPPP de la bibliothèque de Standford et avait fait une erreur similaire à celle de Barry Kidston lors de la synthèse. Le problème était qu'il avait vendu sa mixture comme de l'héroïne aux 7 individus maintenant parkinsoniens. Une fois traités à la L-DOPA, tous virent une réduction majeure de leurs symptômes et, après leur décès plusieurs années plus tard, leur diagnostic fut confirmé par l'observation d'une mort importante des neurones de leur SNc lors de l'autopsie.

L'effet du MPTP est dû à sa transformation par les cellules gliales en 1-méthyl-4-phényl pyridinium (MPP+), une toxine qui altère le fonctionnement du complexe I mitochondrial. Il en résulte alors une production importante de réactifs à l'oxygène (ROS) et des dommages oxydatifs qui mènent à la mort des cellules qui l'ont assimilé. Le MPP+ est toutefois sélectif aux neurones dopaminergiques puisqu'il entre dans la cellule par le transporteur DAT [101]. Depuis, plusieurs autres toxines affectant la fonction mitochondriale, telles que la roténone (inhibiteur du complexe I) et la 6-Hydroxydopamine (6-OHDA, production de ROS, inhibiteur du complexe I et IV) ont été utilisées pour modéliser la MP [102, 103]. Tout comme le MPP+, la 6-OHDA est sélective aux neurones dopaminergiques, car elle entre dans la cellule par le transporteur DAT. Elle a toutefois aussi une affinité pour le transporteur de la norépinephrine (NET) et donc un inhibiteur de ce transporteur est habituellement administré lors d'injection de 6-OHDA comme modèle de la MP, pour assurer une lésion spécifique des neurones dopaminergiques. L'utilisation de ces toxines a permis de comprendre que la fonction mitochondriale est assurément impliquée dans les perturbations observées dans la MP.

1.2.5.4 Implications de la fonction mitochondriale

Brièvement, la mitochondrie a plusieurs fonctions dans la cellule, autant dans le stockage des réserves de calcium que dans les mécanismes d'apoptose, mais surtout dans la production d'énergie sous forme d'ATP (Figure 5). Dans les cellules eucaryotes, l'ATP est principalement produite par deux processus; soit la glycolyse ayant lieu dans le cytosol et la phosphorylation oxydative ayant lieu dans la mitochondrie. Au cours de la glycolyse, le glucose est métabolisé en pyruvate pour produire 2 molécules d'ATP. Le pyruvate entre alors dans la mitochondrie et participe au cycle de l'acide citrique. C'est à travers ce cycle que les coenzymes nécessaires à la production d'énergie par phosphorylation oxydative sont produites (NADH et $FADH_2$). Contrairement à la glycolyse qui ne produit que 2 molécules d'ATP, la phosphorylation oxydative est bien plus efficace et produit de 30 à 36 molécules d'ATP par molécule de glucose. Les neurones étant de grand consommateur d'énergie, ils se fient principalement à la phosphorylation oxydative pour leur production d'ATP [104]. Cette importante production d'énergie implique toutefois plusieurs complexes protéiques mitochondriaux et donc ne peut se produire qu'à l'intérieur de la mitochondrie.

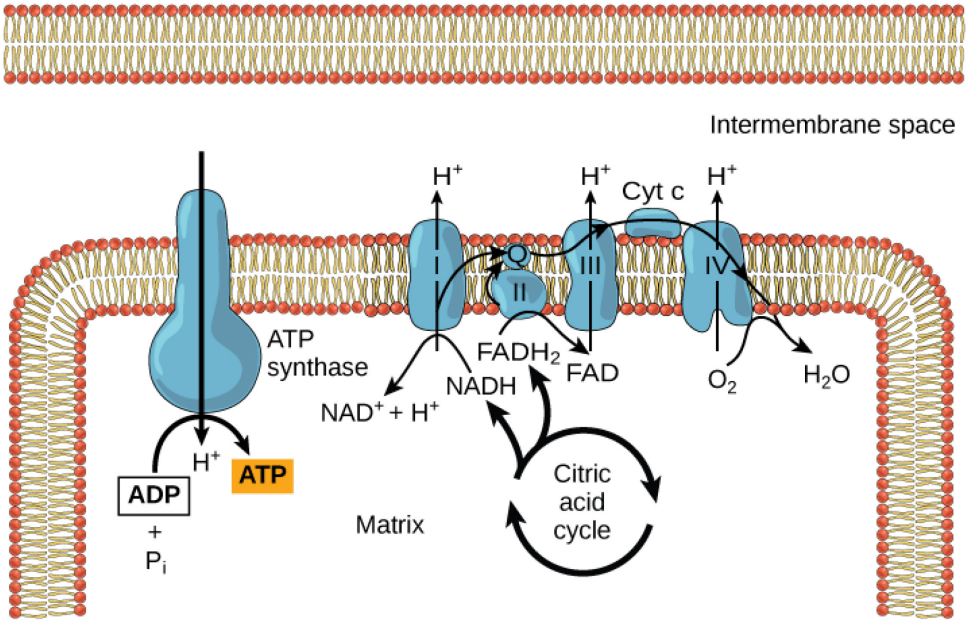

Figure 5. Schématisation de la production d'ATP dans la mitochondrie par l'ATP synthase à l'aide du gradient de proton créé par la chaîne de transport d'électrons.
Reproduction avec permission.
Source :https://courses.lumenlearning.com/wm-biology1/chapter/reading-electron-transport-chain/

La mitochondrie est un organite intracellulaire contenant une membrane externe et interne. C'est dans cette membrane interne que l'on retrouve l'ATP synthase qui phosphoryle l'ADP en ATP en utilisant un gradient de protons dont la concentration est plus élevée dans l'espace intermembranaire que dans la matrice. Ce gradient de protons est formé par la chaîne de transport d'électrons, une structure protéique comprenant 4 complexes qui sont responsables de l'induction d'une différence de potentiel membranaire de part et d'autre de la membrane interne. Les électrons de la chaîne de transport nécessaires à la création de ce gradient de protons sont fournis par les coenzymes cités ci-haut et sont acceptés par l'oxygène (O_2) à la fin de leur transport, produisant deux molécules d'eau (H_2O). À cause de la nature fortement oxydative de l'oxygène, la phosphorylation oxydative peut aussi produire des intermédiaires bien plus réactifs que l'eau, tels que des ions superoxyde et peroxyde, et induire un certain niveau de stress oxydatif. Ces ions sont produits lorsque des électrons s'échappent prématurément de la chaîne de transport d'électrons, dans des conditions où le potentiel membranaire mitochondrial est altéré. La régulation de l'efficacité de la fonction mitochondriale est donc cruciale à la survie neuronale [105]. Le potentiel de membrane mitochondrial régule aussi l'entrée de calcium dans la mitochondrie, qui tamponne les niveaux cytosoliques et sert de réserve calcique. Ce calcium pourra alors être relâché lors de différents processus physiologiques, tels que la relâche de neurotransmetteurs, mais aussi dans les processus apoptotiques [105]. Pour plus de détails sur la fonction mitochondriale, voir Osellame et al., 2012 [106].

Tel que mentionné dans la section précédente, plusieurs toxines maintenant utilisées pour modéliser la MP ont pour principal effet de bloquer le complexe I mitochondrial, empêchant l'entrée d'électrons dans la chaîne de transport d'électrons et déstabilisant le gradient de protons nécessaire à la production d'énergie, ainsi que la régulation des niveaux de calcium. Il en résulte une production massive de ROS qui perturbe une multitude de fonctions cellulaires et mène à la mort des neurones [107].

1.2.5.5 Déterminants de la mort neuronale

Historiquement, deux grands types de morts cellulaires ont été décrits, soit la nécrose, où la rupture des membranes cellulaires induit un déversement du contenu cellulaire dans

l'espace intercellulaire, et l'apoptose, où la présence de signaux internes ou externes induit la mort programmée par la formation de corps apoptotiques sans déversement du contenu cellulaire. Depuis, plusieurs autres types de morts cellulaires ont été décrits [108], tels que la mort par autophagie; un dérèglement des processus normaux de dégradation du contenu cellulaire. Dans la MP, il est maintenant reconnu que la plupart des neurones dopaminergiques de la SNc meurent par des mécanismes de mort programmée; plus précisément par apoptose et/ou par mort par autophagie [109]. L'apoptose est un type de mort programmée qui peut être déclenché de façon extrinsèque ou intrinsèque [110]. La voie extrinsèque est enclenchée lors de l'activation de récepteurs de mort cellulaire membranaires de type TNF par des signaux externes, tels que l'inflammation. S'en suit alors l'activation des caspases 8 et 10 et le déclenchement de l'apoptose par l'activation de caspases effectrices qui vont dégrader les protéines intracellulaires [109]. La voie intrinsèque est quant à elle déclenchée par n'importe quel stress cellulaire, tel que l'augmentation des niveaux ROS, des dommages génétiques ou la perte de supports trophiques. Cette voie, dite mitochondriale, est activée lorsque les mitochondries perdent leur potentiel de membrane, libèrent leur réserve de calcium et deviennent perméables. S'en suit alors la relâche du cytochrome C, un donneur d'électron normalement impliqué dans la chaîne de transport d'électrons. Une fois dans le cytosol, ce cytochrome va activer la caspase 9, qui elle va activer des caspases effectrices, initiant la dégradation protéique [109].

Ces phénomènes d'apoptose sont souvent précédés et même accompagnés de mécanismes d'autophagie, procédés par lesquels des éléments cytoplasmiques sont isolés dans des vésicules qui sont par la suite fusionnées aux lysosomes, formant des autophagosomes où leur contenu sera dégradé [111]. Dans la MP, il est même maintenant suggéré que la mort de certains neurones pourrait se produire exclusivement par autophagie (en l'absence d'apoptose) [109]. L'autophagie est aussi impliquée dans la perte importante des fibres dopaminergiques striatale, phénomène apparaissant bien avant la perte neuronale. Cette observation a mené à l'hypothèse de mort rétrograde (dying-back) durant laquelle la perte des fibres dopaminergiques est accompagnée d'une accumulation d'α-synucleine qui altère les mécanismes d'autophagie, de transport axonal et même la fonction mitochondriale [112].

1.2.5.6 Facteurs génétiques

Bien qu'assez rares, plusieurs formes familiales de la MP sont induites par des mutations dans des gènes ayant une grande influence sur la fonction mitochondriale. La diversité de ces mutations et leurs implications dans une multitude de mécanismes impliquant la mitochondrie sont au cœur de l'hypothèse de dysfonction mitochondriale dans la MP. Par souci de synthèse, seules les mutations les plus fréquentes, ou celles pour lesquelles un lien direct avec la fonction mitochondriale a été établi, seront présentées ici. Pour plus de détails sur les autres mutations liées à l'hypothèse mitochondriale dans la MP, voir Larsen et al. 2018 [105].

Ce lien direct est particulièrement établi pour des mutations menant à la perte de fonction de trois protéines, soit Parkin, Pink1 et DJ-1, trois formes autosomales récessives menant au développement précoce de la MP. Par exemple, Parkin est une ubiquitine ligase qui est recrutée par Pink1 aux mitochondries dépolarisées pour induire leur élimination par mitophagie, une forme spécifique d'autophagie [87]. Lorsque la fonction mitochondriale est optimale, Pink1 est importée à la membrane interne mitochondriale où elle est clivée et inactivée [113]. Lorsque la mitochondrie est dépolarisée ou lorsqu'il y a accumulation de ROS, cette importation est altérée et Pink1 reste à la membrane externe mitochondriale, où elle s'accumule et s'active par autophosphorylation. Pink1 activée peut alors recruter Parkin et l'activer par phosphorylation [114]. Parkin activée va alors ubiquitiner plusieurs protéines membranaires mitochondriales, déclenchant l'importation de la mitochondrie dans l'autophagosome [115]. Plus récemment, il a aussi été démontré que la dégradation des protéines mitochondriale peut se faire par la création de vésicules mitochondriales, qui seront directement fusionnées aux lysosomes, sans impliquer les mécanismes de phagocytose [116]. Parkin et Pink1 seraient aussi impliqués dans ce mécanisme [117], en plus d'être aussi importants pour la fusion/fission mitochondriale [118, 119] et pour la répression de la présentation antigénique mitochondriale [120]. De son côté, DJ-1 semble réguler la production de ROS mitochondriaux et donc protéger les cellules du stress oxydatif par son action antioxydante, bien que les mécanismes exacts induisant ces effets restent mal définis [89, 90]. La perte de fonction de ces protéines dans la MP mènerait donc à l'accumulation de mitochondries dépolarisées, libérant de grandes quantités de ROS, et à la mort neuronale. Pour plus de détails sur les fonctions de ces trois protéines, voir Trempe et Fon, 2013

[121]. Au cours des dernières années, ces mutations ont été utilisées chez la souris pour tenter de créer de meilleurs modèles de la MP. Malheureusement, elles ne semblent pas suffisantes pour induire un phénotype parkinsonien ni même la mort des neurones dopaminergiques de la SNc [122–126]. Cet échec reste un des grands mystères dans la modélisation de la MP.

D'autres mutations sont plutôt considérées comme des facteurs de risque importants pour la MP, puisque leur pénétrante est beaucoup plus faible. Par exemple, les individus porteurs de mutations dans l'enzyme lysosomal glucocerebrosidase (GBA1) ont jusqu'à 20 fois plus de chances de développer la maladie [127] et ces mutations sont retrouvées dans plus de 5% des formes sporadiques de la MP. Cette enzyme, dont la fonction est d'hydrolyser le glucosylceramide en glucose et céramide, jouerait aussi un rôle important dans la dégradation de l'α-synucléine [128], protéine dont l'accumulation est source de pathologie dans la MP. La perte de fonction de cette enzyme mènerait aussi à une dépolarisation mitochondriale, à une réduction de la production d'ATP et à une augmentation du stress oxydatif, par une diminution de l'efficacité de dégradation des protéines mitochondriales dans le contexte des processus mitophagiques [105].

En lien avec cette accumulation pathologique de protéines dans la MP, des mutations autosomales dominantes, ainsi que des duplications et triplications dans le gène encodant l'α-synucléine, sont maintenant reconnues comme responsables de certaines formes rares et précoces de la MP. D'autres mutations plus fréquentes dans ce gène ont aussi été identifiées comme facteur de risque pour la maladie [129]. Dans la plupart des cas, c'est l'augmentation des niveaux d'α-synucléine causée par ces mutations qui est responsable de la pathologie. L'importance relative des mécanismes de toxicité de l'α-synucléine reste source de débat [130], que ce soit par ses effets sur l'expression de certains gènes, sur le transport axonal, sur les fonctions lysosomales ou sur la fonction synaptique. Il est toutefois intéressant de noter que cette protéine influence aussi grandement la fonction mitochondriale et les mécanismes d'autophagie. Son accumulation dans des conditions pathologiques aurait pour effet d'augmenter la fission mitochondriale et les niveaux de ROS, tout en diminuant la production

d'ATP. Elle aurait aussi tendance à s'accumuler dans les lysosomes, réduisant la capacité des neurones à dégrader toutes protéines ou organites défectueux. Toutefois, il a aussi été suggéré que des dysfonctions mitochondriales pourraient précéder et même déclencher l'accumulation d'α-synucléine dans la MP. Par exemple, l'agrégation de cette protéine à été observée suite à l'exposition à des toxines mitochondriales comme la roténone, le paraquat et le MPTP dans des modèles de la MP [131, 132]. Pour plus de détails sur les mécanismes de toxicité de l' α-synucléine, voir Wong et al., 2017 [130].

Finalement, les causes les plus fréquentes des formes autosomales dominantes de la MP sont causées par des mutations dans le gène encodant une kinase nommée LRRK2 [133]. D'autres mutations dans ce gène sont aussi considérées comme des facteurs de risque important au développement de la maladie. Cette kinase est potentiellement impliquée dans une multitude de processus physiologiques, comme le trafic vésiculaire, l'autophagie et la fonction mitochondriale, mais sa fonction spécifique reste source de débats [134]. Le fait que certaines de mutations étudiées induisent une augmentation de l'activité de la kinase, tandis que d'autres ont plutôt pour effet de la diminuer, ajoute un niveau de complexité supplémentaire à l'étude des fonctions de LRRK2. Dans des conditions physiologiques, LRRK2 serait important pour le transport de vésicules axonales [135] et certaines de ces mutations induiraient une diminution de la relâche de neurotransmetteurs par des altérations dans la dynamique des vésicules synaptiques [136]. Certaines mutations de LRRK2 inhiberaient aussi certains processus autophagiques, augmentant l'accumulation d'α-synucléine et diminuant la capacité des neurones de recycler les mitochondries dépolarisées [137]. S'en suivraient une diminution de la production d'ATP et une augmentation des niveaux de ROS qui accélérerait la mort neuronale. Pour plus de détails sur l'implication de LRRK2 dans la MP, voir Singh et al., 2019 [137].

Grâce à l'étude des multiples mutations responsables du développement précoce de la MP, il est maintenant indéniable que la fonction mitochondriale est au cœur des processus physiopathologiques de la MP.

Chapitre 2 : Maladie de Parkinson et vulnérabilité sélective (Article I)

Une des questions non résolues dans l'étude de la MP est que, bien que présentes dans toutes les cellules, les mutations des formes familiales de la maladie induisent des dysfonctions cellulaires suffisantes à mener à la mort cellulaire de seulement quelques populations neuronales spécifiques, dont les plus étudiés sont les neurones dopaminergiques de la SNc. De plus, il existe une vulnérabilité plus importante de certaines sous-populations à l'intérieur même de la SNc. Par exemple, dans la MP et dans plusieurs de ses modèles, le tiers ventral de la SNc est plus vulnérable que le tiers dorsal. Plusieurs éléments pourraient expliquer cette différence tels que l'expression différentielle de plusieurs protéines, récepteurs ou canaux. Par exemple, il semble que l'expression de l'ALDH1A1 soit neuroprotectrice pour les neurones du tiers ventral et que la perte de son expression dans la MP participe à leur dégénérescence préférentielle [138, 139]. Les neurones du tiers ventral expriment aussi peu la calbindine [140, 141], une protéine qui tamponne le calcium. Pour plus de détails sur les différences potentielles entre le tiers ventral et dorsal de la SNc, voir Double K.L. et al,. 2010 [142].

L'article qui suit passe en revue la qualité des données décrivant la mort neuronale dans la MP dans différentes régions du cerveau humain et tente de mettre en évidence les différentes caractéristiques qui rendent les neurones dopaminergiques de la SNc particulièrement vulnérables, ainsi que la possibilité que ces caractéristiques soient partagées entre l'ensemble des populations affectées. Il résume du fait même une partie des résultats de cette thèse.

Contributions des auteurs

Nicolas Giguère : Révision de la littérature et écriture du manuscrit.

Samuel Burke Nanni : Révision de la littérature et écriture du manuscrit.

Louis-Éric Trudeau : Écriture du manuscrit.

*Nicolas Giguère et Samuel Burke Nanni sont co-premiers auteurs.

On cell loss and selective vulnerability of neuronal populations in Parkinson's disease

Nicolas Giguère*, Samuel Burke Nanni*, and Louis-Eric Trudeau

Department of pharmacology and physiology, Department of neurosciences, CNS Research Group, Faculty of Medicine, Université de Montréal

Author contribution: *These authors are co-first authors

Publié dans la revue « Frontiers in Neurology » le 19 juin 2018.
https://doi.org/10.3389/fneur.2018.00455

2.1 Abstract

Significant advances have been made uncovering the factors that render neurons vulnerable in Parkinson's disease (PD). However, the critical pathogenic events leading to cell loss remain poorly understood, complicating the development of disease-modifying interventions. Given that the cardinal motor symptoms and pathology of PD involve the loss of dopamine (DA) neurons of the substantia nigra pars compacta (SNc), a majority of the work in the PD field has focused on this specific neuronal population. PD however, is not a disease of DA neurons exclusively: pathology, most notably in the form of Lewy bodies and neurites, has been reported in multiple regions of the central and peripheral nervous system, including for example the locus coeruleus, the dorsal raphe nucleus and the dorsal motor nucleus of the vagus. Cell and/or terminal loss of these additional nuclei is likely to contribute to some of the other symptoms of PD and, most notably to the non-motor features. However, exactly what regions show actual, well-documented, cell loss is presently unclear. In this review we will first examine the strength of the evidence describing the regions of cell loss in idiopathic PD, as well as the order in which this loss occurs. Secondly, we will discuss the neurochemical, morphological and physiological characteristics that render SNc DA neurons vulnerable, and will examine the evidence for these characteristics being shared across PD-affected neuronal populations. Some of the insights raised by focusing on the underpinnings of the selective vulnerability of neurons in PD might be helpful to facilitate the development of new disease-modifying strategies and improve animal models of the disease.

2.2 Introduction

Parkinson's disease (PD) was first described two centuries ago in *An essay on the shaking palsy* (3). Since then, great strides have been made in understanding the disease basics. However – as with many other neurodegenerative disorders – there is still no disease modifying treatment for PD. Unfortunately, progress has been slow, and a thorough understanding of the pathological processes has been elusive.

PD as a clinical diagnosis is characterized by the detection of significant motor deficits (including bradykinesia, resting tremor and rigidity) due, in large part, to a loss of dopamine (DA)-containing neurons of the substantia nigra pars compacta (SNc). The SNc is a neuronal population projecting to the caudate and putamen and is critical for regulation of basal ganglia circuitry. At clinical presentation, it has been estimated that 40 to 60% of SNc DA neurons have already degenerated (4, 5). The clinical features of the disease are diverse and include substantial non-motor features including, autonomic and olfactory dysfunction, constipation, sleep disturbances, depression, and anxiety (7-9).

The diagnostic criteria for PD have been recently re-defined by the International Parkinson and Movement Disorder Society (MDS), with the MDS Clinical Diagnostic Criteria for Parkinson's disease (MDS-PD Criteria (6)). A diagnosis is made when there is documented parkinsonism (defined as bradykinesia, with tremor at rest and/or rigidity), followed by the exclusion of other possible causes of parkinsonism, and with additional supporting criteria, including olfactory dysfunction or cardiac sympathetic denervation (See (6)). The recent nature of this re-evaluation illustrates both the heterogeneity of PD expression, and the difficulties encountered in defining it.

In ~70% of the 'clinically typical PD cases', the hallmark pathological finding is the presence of Lewy pathology (LP) in the SNc (7, 8) – however, LP is also found across the central, peripheral, and enteric nervous system (CNS, PNS, and ENS) (9). This includes both Lewy bodies and Lewy neurites: both similar cellular inclusions, formed predominantly of

aggregated α-synuclein, but also including a large number of different molecules, proteins and organelles, such as ubiquitin, tubulin, neurofilaments, lipids, and mitochondria (10).

In considering the broad localization of LP and the origins of the various symptoms of PD, a critical point to consider is the dysfunction and loss of neurons in regions of the CNS and PNS, other than the SNc. There have been, indeed, many studies concluding that cholinergic neurons in the pedunculopontine nucleus (PPN), noradrenergic neurons of the locus coeruleus (LC), cholinergic neurons of the nucleus basalis of Meynert (NBM) and of the dorsal motor nucleus of the vagus (DMV), and serotonergic neurons of the raphe nuclei (RN) are lost in PD. The strength of the evidence for actual neuronal cell body loss in these regions is highly variable and one of the questions addressed in the present review. The fact that the diagnostic criteria for PD have over time been refined adds another layer of complexity to the task of identifying the origin of the diverse symptoms of PD. Presently, PD is classified into either primary or secondary subtypes. Primary parkinsonism includes genetic and idiopathic forms of the disease and secondary parkinsonism includes forms induced by drugs, infections, toxins, vascular defects, brain trauma or tumors or metabolic dysfunctions. This second subtype of PD is also sometimes called atypical parkinsonism when concomitant to progressive supranuclear palsy, multiple system atrophy or corticobasal degeneration, for example.

Since pathology is likely to emerge through different processes depending of PD subtypes, and since modern classification was non-existent when a substantial part of the research literature was produced, attempting to reach clear general vision of various pathophysiological markers and their link to the disease progression for each sub-type of PD presents a significant challenge. This review will primarily focus on idiopathic PD, since this category represents the large majority of cases and is likely to represent most of the subjects examined in studies where PD type was not provided.

Another main hurdle in PD research is that the chain of events that leads to the death of neurons is still not clear. The fact that pathology is thought to begin years/decades before the appearance of symptoms might, in part, explain this lack of progress.

PD has been considered to exist as either a strictly monogenetic or environmentally-triggered disease, as well as a mixture of the two. The pathological mechanisms at the core of each form have been proposed to converge in causing cellular stress secondary to mitochondrial dysfunction, perturbed proteostasis and elevated oxidative stress. A major conundrum is that at first glance, these factors alone fail to explain why PD pathology is restricted to very limited subsets of brain nuclei. Therefore, a key question is what do these PD sensitive neurons have in common and what is it about them that renders them more vulnerable compared to neurons from other brain regions?

A better understanding of the fundamental nature of cell loss and cellular dysfunction in the parkinsonian brain is required to develop critically needed, novel, therapeutic strategies. In this review, we aim to re-evaluate the evidence for cell loss in PD, then to highlight the common characteristics that could explain their selective vulnerability.

2.3 Physiopathology of Parkinson's Disease

The focus on SNc DA neurons has brought significant advances in our understanding of PD pathophysiology, as well as of the signaling pathways that lead to DA neuron death. Studies using DA neuron selective toxins such as 6-OHDA and MPTP, as well as investigations of gene products mutated in familial forms of the disease (including α-synuclein, Parkin, Pink1, LRRK2, DJ-1 and GBA1), have been instrumental to better understand some of the key dysfunctional processes implicated in the disease. These include protein clearance (11-13), mitochondrial turnover (14-16), ROS management and inflammation (17, 18). Perturbations of these processes have been proposed to underlie distinct physiological dysfunctions in PD-vulnerable neurons (19). Nonetheless, since the first introduction of Levodopa in the 1950s and the development of deep-brain stimulation in the 1990s, increased understanding of PD pathophysiology has not yet permitted the discovery of disease-modifying therapies.

As stated previously, PD is more than just a disease of DA and the SNc. Non-motor symptoms – including a reduced sense of smell, constipation, orthostatic hypotension, sleep disturbances, depression, and anxiety – are likely to be due to impaired function and/or loss of non-DA neurons. (20) There has thus been a growing interest in better understanding the implications of other regions of the CNS and PNS in the progression of PD pathology. In the early 2000s, pioneering work by Braak and colleagues defined stages in PD based on the appearance of LP in various regions of the nervous system, correlating their findings to the symptomatic progression of the disease (2, 21, 22). Most notably, LP was detected in the dorsal IX/X motor nuclei, the intermediate reticular zone, the medulla oblongata, the pontine tegmentum, the caudal RN, the gigantocellular reticular nucleus, the coeruleus–subcoeruleus complex, the pars compacta of the substantia nigra, the basal prosencephalon, the mesocortex and the neocortex. However, multiple lines of evidence suggest that LP is not systematically seen in the PD brain and LP is also documented in healthy individuals (23). Also, in some cases of PD, and most notably in early-onset genetic forms, loss of SNc DA neurons has been reported to occur in the absence of detectable LP (24-26).

Although the role of LP in the pathogenesis of PD has been the subject of much debate (27), the detection of LP has remained central in investigations of the key brain regions and circuits underlying PD pathophysiology. In this context, it may be useful to focus attention on brain and PNS regions that show documented cell death and/or axonal degeneration, irrespective of the presence or absence of LP. This could perhaps provide new perspectives on the actual, more proximate, causes of the major symptoms of the disease and their progression. Relevant to the present point, in their most recent and insightful work, Braak and Tredici write, “We ascribed the same weight to axonopathy and nerve cell dysfunction (presumably attributable, but not limited, to the presence of Lewy pathology) as to neuronal death because the development of pathology together with neurotransmitter loss, axonal, and somatodendritic dysfunction in multiple neuronal populations could prove to be more stressful for involved neurons over time than premature cell death within a select neuronal population” (9).

2.4 Where and when does neuronal loss appear in PD?

Loss of neurons in the brain is thought to occur in the context of normal ageing. For example, there have been multiple publications reporting significant age-dependent decline in neuron number in the SNc (28-36), as well as in regions such as the PPN (37) and LC (38, 39). Above and beyond such cell loss associated with normal ageing, a key question is where in the brain can one find substantial neuronal loss in PD?

Although numerous publications have referred to cell loss occurring in many CNS and PNS regions in the context of PD, we believed it germane to re-evaluate the published scientific literature addressing this question.

To do so, we took great care to find work concentrating on neuronal loss and not only denervation (as is common for the heart, for example (40-42)). We found 90 primary research articles reporting PD-specific cell loss in the following regions (**Table 1**): the SNc, VTA, amygdala, cortex, DMV, hypothalamus, laterodorsal tegmental nucleus, LC, NBM, OB, oral pontine reticular nucleus, PPN, pre-supplementary motor cortex, RN, supraoptic nucleus, sympathetic/parasympathetic ganglia, and thalamus. These original articles span from 1953 to 2015. The techniques used to quantify cell loss varied, and we have classified them accordingly. Across all regions examined, 14 of the examinations were defined as *observational*, 39 as implicating *manual* counting, 18 used *computer-assisted* counting, and 26 used *stereological* counting methods. While informative, the value of observational studies can be considered limited given their lack of precision and the fact that they are greatly influenced by the observer. Lack of bias is also difficult to assure in studies involving manual counting. This technique is also unable to assure that a cell is not being counted twice if present in two subsequent sections. Other techniques such as computer-assisted counting were developed to improve on these aforementioned methods, however, these are also limited in that they often lack rigorous systematic sampling, are sensitive to tissue shrinkage, and are often unable to account for local tissue thickness, or for cells damaged on slice edges. These issues are systematically addressed using modern stereological counting techniques. Another issue to consider is that many of the

studies included in this review, including those employing stereology, either did not use age-matched controls or did not state whether counting was conducted blind to diagnosis. Yet another apparent feature of this literature is the diversity of method iterations used, the varying number of brain regions assessed in each study and, importantly, the stage or type of PD studied (and how this was defined). Here, we will discuss the evidence of cell loss (if not otherwise stated, relative to healthy control cases), ordering the regions in subsections according to the strength of the evidence (**Table 1**).

2.4.1 Substantia nigra pars compacta

Loss of SNc DA neurons in PD is indisputable. Here we found 38 studies addressing this directly with a total of 612 brains. However, if we consider the methods used, we found that 10 of these studies were observational, 8 involved manual counting methods, 8 used computer-assisted methods, and 12 used stereology. Considering stereological methods as best practice for unbiased evaluation of cell number, 181 brains were quantified as such for SNc: still a large number. The average cell loss reported for studies involving stereological methods is ~ 68%. The definition and clinical stage of PD in most studies varied greatly, especially in reporting. For example, for the 12 studies using stereological methods, three papers (43-45) staged each case according to the Braak staging (to be expected given that Braak staging only came about in the early 2000s). In the same 12 studies, the age 'since disease onset' varied between 1 to 27 years when stated, the Hoehn and Yahr ratings (H&Y, used to describe the progression severity of PD symptoms) varied between 2 to 5 and the UPDSR score (that includes H&Y rating, symptoms and quality-of-life scores) was also on occasion provided. A correlation with disease duration/severity was found in 10 studies. It is relevant here to mention that some authors, including Gibb et al. (46) have discussed the selective vulnerability of restricted sub-regions within the SNc. These data are important and relevant to the progression of the field; however, we found this distinction absent in the majority of the work we examined.

2.4.2 Pedunculopontine nucleus and Locus coeruleus

The evidence for cell loss for both the PPN (11 studies), containing cholinergic neurons and the LC (18 studies), containing noradrenergic neurons, is also relatively strong. For the PPN, four studies used stereological methods. In these four studies, the average loss of cholinergic PPN neurons was 41% and the range of PD stages amongst the subjects evaluated was broad. For example, in Rinne, 2008 (47), the PD cases ranged from a H&Y rating of 2.5 to 5; in Karachi, 2010 (48), UDPRS score was used, and in both Hepp, 2013 (49) and Pienaar, 2013 (50), the PD cases were between Braak stages 4 and 6 and between 2 and 4, respectively. Although sample sizes were relatively small in these two studies, nine and eight, respectively, it is somewhat surprising that in the most advanced PD group, loss of cholinergic PPN neurons was not higher than for less advanced PD subjects, contrarily to the report by Rinne, 2008 (47).

Methodology and scales of PD progression
We searched the scientific literature using the search engines and databases of PubMed, Google Scholar and ScienceDirect. The following search terms were used: 'PD', and 'cell loss', 'cell death' or 'reduced cell/neuron number'. Furthermore, these terms were used in combination with brain structure keywords: 'SNc', 'VTA', 'LC', 'Raphe', 'DMV', 'PPN', 'NBM' and 'enteric system' ('ENS'), and 'gut'. Review and original article abstracts were screened, then, where appropriate, read. Where any direct or indirect claim for cell loss was found (rather than only the presence of LP), the claim was followed to its original source. The Hoehn and Yahr scale (H&Y) is a widely used clinical rating scale, which defines broad categories of motor function in PD (where 1 is the least severe, and 5, most severe symptoms) (1). Braak staging is a method of classifying the progression of PD pathology and symptoms based on the presence of lewy pathology (where 1 represents initial pathology in the brain stem, and 6, severe pathology including the neocortex) (2).

Surprisingly, we found no study quantifying loss of LC neurons using stereological counting methods. For the LC, 221 brains were studied, with cell loss ranging from 'some' to

94%. Five of the studies were based on observational quantifications, 4 on manual counting and 9 used computer-assisted counting. In these 18 papers, when stated, the H&Y score was between 3 and 5, and disease duration was between 1 and 31 years. A correlation of the extent of cell loss with disease duration was found in two of these studies (51, 52).

2.4.3 Dorsal motor nucleus of the vagus, Raphe nuclei, nucleus basalis of Meynert and ventral tegmental area

Substantial cell loss has been documented in the DMV, containing cholinergic neurons, with 7 studies evaluating this loss in 49 cases. Of these, only one study (53) used stereology, where they reported 55% neuronal loss in eight PD cases, ranging from 5 to 24 years post diagnosis and reported correlation with disease duration/severity.

The importance of re-evaluating cell loss is PD is apparent when considering the serotoninergic RN. For these nuclei, which are considered by many authors to be lost in PD, we found 7 papers describing neuronal loss varying between 0 to 90%. Cheshire et al. however, using stereology in 44 late-stage PD subjects, found no cell loss in the dorsal raphe nucleus (54). In the NBM, containing cholinergic neurons, we found 13 papers, 12 using manual counting methods and one observational, which estimated an average neuronal loss of between ‘some’ to 72%. No correlation with disease duration was reported. The high prevalence of concomitant PD and Alzheimer's disease (AD) might explain why cell loss varied so much for this region. Surprisingly, only 8 studies directly evaluated neuronal loss in the VTA, a dopaminergic region often considered to be only modestly affected in PD. Of these, one study used stereology (55) to evaluate the loss of neurons in 3 cases of PD (or 6 including PD with a secondary diagnosis) that were between 1- and 27-years post diagnosis and reported an average neuronal loss of 31%. One paper reported correlation of the extent of cell loss with disease duration (56).

2.4.5 Thalamus, hypothalamus, olfactory bulb

Four studies reported neuronal loss in thalamic nuclei, with 2 using stereology (57, 58). In Henderson, 2000, 9 subjects with H&Y disease ratings between 2 and 5 statistically significant loss of 30 to 40% was reported in the centromedian-parafasicular complex. However, no loss was found in the motor thalamus in 9 subjects with similar H&Y disease ratings in the work of Halliday, 2005. Neuronal loss has also sometimes been reported in the hypothalamus (9 studies), with one using stereology; Thannickal et al. (59) reported a 50% cell loss in 10 PD cases, with increased loss with disease severity. Olfactory dysfunction is now well established as an early symptom of PD. Four studies evaluating cell loss in the olfactory bulb were reported. One of these (60) described a 57% decrease in neuronal number (identified as cells with "a prominent nucleolus surrounded by Nissl substance"), while the others (61-63), using stereology, reported a 100% increase in the number of TH-positive neurons.

2.4.5 Peripheral nervous system, spinal cord and other brain regions

Though there is substantial evidence for LP occurring in the ENS (64), we did not find any study reporting direct – quantitative evidence – for neuronal loss in the gut. Though it has been inferred that ENS glial cell loss is occurring (65), there is evidence that neuronal loss in the gut is not associated with PD (66). Of note, a publication often cited in support of neuronal loss in the ENS (67) shows, in fact, neuronal loss in the DMV. With regards to the spinal cord, published evidence is also scarce; of the studies most relevant here, Wakabayashi et al. (68), using manual counting methods, described a loss of 31% and 43% respectively in the 2nd and 9th thoracic segments of the intermediolateral of the spinal cord. For the amygdala, the pre-supplementary motor cortex, several other cortical regions, the laterodorsal tegmental nucleus and the oral pontine reticular nucleus, we found only single studies supporting loss, with stereology used for the amygdala (30% loss) (69) and cortex (10% loss) (69) (see Table 1).

2.4.6 Regional order of cell loss?

In summary, it seems clear that there is some level of cell loss in PD in restricted regions including the SNc, LC, NBM, PPN, DMV, VTA and probably the RN. However – because of the lack of data for some regions, the variety of techniques used to count neurons, potentially numerous unintentional sources of bias, and because of the inconsistency in criteria used for subject sampling – firm conclusions are somewhat limited. In particular, it is difficult to conclude on the relative extent and temporal order of cell loss in these different brain regions as a function of disease progression, information that would be critical to advance the field. Indeed, a direct comparison of the extent of neuronal loss in different regions examined in different studies is hazardous, even if stereological studies were to be selected. Interestingly, of the 38 studies we identified evaluating cell loss in the SNc, only 5 of these also looked at the VTA, and of these only 1 used stereology. Given the importance of the difference in vulnerability of these two nuclei, a systematic evaluation of the extent of loss of these neurons in PD would be very informative. But even if as a technique, stereology mitigates for most of the classic biases, it is still unable to account for the variation in subject sampling, i.e. variation in disease duration, sex and age, unless these criteria were considered in a similar way for each study. Unfortunately, this has not, thus far, been the case. In conclusion, it seems clear that stereological studies comparing multiple regions in the same subjects and these regions in subject at different stages of PD are critically needed to advance the field.

2.5 What are the common features shared by neurons affected in PD?

Although, as mentioned previously, the evidence for the extent of cell loss in regions other than the SNc in the PD brain is not always sufficiently documented, it is clear that some level of cell loss occurs in a limited subset of regions beyond the SNc (Figure 1A), or, to the least, that neuronal functions including neurotransmission are perturbed in multiple neuronal circuits. It is therefore of great interest to identify some of the biological features that distinguish

neuronal subgroups in terms of their basal vulnerability to some of the cellular stresses that are invoked to trigger PD, including altered proteostasis (due to lysosomal and/or proteosomal impairment), mitochondrial dysfunction and sustained oxidant stress (including from highly reactive DA metabolites).

Several groups have been tackling this question by interrogating the characteristics that render neurons, starting with those of the SNc, particularly vulnerable to degeneration / cell death (76-78). It is likely that some shared functional or structural properties are responsible for selective vulnerability of affected nuclei, as opposed to features truly unique to SNc DA neurons. The causative characteristic(s) should be present in all affected neurons, but also be absent in neurons that do not degenerate or that degenerate much later in the disease. Four main converging hypotheses on selective vulnerability in PD have been gaining attention lately (Figure 1B), related to DA toxicity, iron-content, autonomous pacemaking and axonal arborization size. The next section will explore the likelihood that these hypotheses can explain why select neuronal populations are particularly vulnerable in PD.

2.5.1 Dopamine toxicity

Firstly, it has been suggested that DA neurons in general are most at risk because they produce DA as a neurotransmitter, a molecule that can be toxic in certain conditions through the generation of reactive quinones during its oxidation (79). This oxidation has been proposed to be implicated in the production of neuromelanin in SNc DA neurons. These DA quinones have been shown to interact with and negatively impact the function of mitochondrial protein complexes I, III and V (80) and of other proteins such as tyrosine hydroxylase, the DA transporter and α-synuclein (81, 82). Such reactive by-products can promote mitochondrial dysfunction, pathological aggregation of proteins such as α-synuclein and oxidative stress (83). Increasing the vesicular packaging of DA accordingly reduces the vulnerability of DA neurons, while down-regulating vesicular packaging has the opposite effect (84-87). Although highly relevant, this phenomenon alone does not readily explain the differential vulnerability of different dopaminergic neuron subgroups (such as SNc vs VTA) and cannot contribute to the potential vulnerability of non-dopaminergic neurons in PD. Also, in the context of DA-induced

toxicity, it is puzzling that levodopa therapy, acting to increase DA synthesis, does not appear to accelerate cell loss (88, 89). For these reasons, even if DA toxicity most certainly contributes to degeneration of SNc DA neurons, it is certainly not the sole factor driving neuronal death in PD.

2.5.2 Iron content

Secondly, iron content is thought to also be an important contributor to the selective vulnerability of SNc DA neurons. Iron is known to be able to generate ROS by the Fenton reaction and has been shown to accumulate with age in SNc (90-92). Since the mitochondrial electron transport chain relies on iron sulphur clusters for its function and since it is believed that SNc neurons have particularly high bioenergetic demands (76, 78, 93), elevated iron content could in part underlie elevated and sustained mitochondrial activity. Another interesting feature of iron in SNc DA neurons is that it can be chelated by neuromelanin, which renders it unavailable for mitochondrial function. Even if the affinity of iron for neuromelanin is much lower than for other iron binding proteins such as ferritin, it is possible that accumulation of neuromelanin and loss of ferritin concentration with age impacts gradually mitochondrial function, which could eventually promote cell death. However, data about potential iron content and iron-binding protein concentration changes in PD is still a matter of debate (94, 95). In addition, data is lacking on iron levels in other brain regions presenting cell death in PD. In fact, the only other region studied in this context has been the LC, which did not show high iron relative to the SNc (96-99).

2.5.3 Autonomous pacemaking

A third highly attractive hypothesis to explain the vulnerability of SNc DA neurons has its origins in the fact that these neurons demonstrate autonomous pacemaking. Many receptors/channels can potentially modulate the excitability and survival of DA neurons (100). The fact that pacemaking activity in SNc DA neurons is accompanied by slow oscillations in intracellular calcium concentrations, caused by the opening of voltage-dependent Cav1 plasma membrane calcium channels (Cav1.1 and 1.3) has recently renewed interest to this topic. In the

Cav1 family, Cav1.3 has been suggested to be of particular interest because its voltage-sensitivity and inactivation properties allow a subset of the calcium channels to always stay open during pacemaking, causing extensive calcium entry (77). These oscillations have a positive contribution to cell physiology because they help maintain pacemaking and directly promote mitochondrial oxidative phosphorylation (OXPHOS) (101). However, by doing so, they have been proposed to also promote chronically high levels of ROS production (102, 103). Along with a reduction in mitochondrial function with age, chronically elevated oxidative stress has been proposed to be a causative factor in the decline of neuronal survival (104). Interestingly, CaV currents and autonomous pacemaking are also a feature of LC and DMV neurons (102, 103), and have been hypothesized to be involved in their vulnerability. The fact that other neuronal populations also expressing Cav1.3 such as hippocampal neurons (105) and striatal spiny projection neurons (106) do not degenerate in PD highlights the possibility that the particular vulnerability of SNc DA neurons is due to a combination of physiological phenotypes and not only intracellular calcium oscillations. Intriguingly, recent post-mortem studies showed that there was no decrease in Cav1.3 mRNA level in early or late stage PD in human SNc compared to controls (106, 107), despite significant loss of SNc neurons. Finally, in addition to CaV channels, ATP sensitive potassium channels (K-ATP) have also been reported to regulate the excitability and vulnerability of SNc DA neurons (108).

2.5.4 Axonal arborization size

A fourth hypothesis proposes that neurons such as those of the SNc are particularly vulnerable because of the massive scale of their axonal arborization, leading to very high numbers of axon terminals, elevated energetic requirements and chronically high oxidant stress. Indeed, it has been shown that SNc DA neurons have an exuberant and highly arborized axonal arborization with estimates upwards of a million neurotransmitter release sites per SNc DA neuron in humans (76, 109): this would make them some of the most highly arborized neurons in the nervous system. This characteristic has the potential to place a very large bioenergetic burden on these cells, leaving little margin for additional bioenergetic stress (76, 78, 93). Related to this, it has been calculated that the ATP requirement for propagation of one action potential grows exponentially with the level of branching (110). In a recent publication (78), we

demonstrated *in vitro* that reducing the axonal arbor size of SNc DA neurons to a size more similar to that of VTA DA neurons using the axonal guidance factor Semaphorin 7A, was sufficient to greatly reduce basal OXPHOS and reduce their vulnerability to toxins including MPP+ and rotenone. Although as previously discussed, the extent of neuronal loss is still unclear for many neuronal populations, it does seem likely that most neuronal nuclei affected in PD include neurons that are relatively few in number, but all possess long and profuse unmyelinated axonal arbors and a large number of axonal terminals (111-116). However, comparative data evaluating axonal arbor size amongst these populations and in populations of neurons that do not degenerate in PD is presently lacking. An interesting possible exception to this hypothesis could be striatal cholinergic interneurons, which were previously estimated in rats to present 500 000 axonal varicosities (117, 118), but have not been reported to degenerate in PD. This estimate was obtained by dividing the estimated number of terminals by the estimated number of cholinergic interneurons in the striatum, which was based on the total number of striatal neurons and the proportion of cholinergic interneurons. Considering recent stereological counting of the number of neurons in the rat striatum, it is possible that the total number of terminals estimated for striatal cholinergic neurons may have been overestimated by a factor of six (119). Based on this report, axonal arborization size of striatal cholinergic interneurons would be less than half of that of SNc neurons. Careful quantitative and comparative studies are clearly needed.

2.6 A global bioenergetic failure hypothesis

One commonality between these four hypotheses is that they all suggest that vulnerable neurons are under intense mitochondrial / bioenergetic demand. This could alter the oxidative stress response by depleting antioxidants like glutathione (GSH), as previously suggested to occur in the PD brain (120-122). This stress could also, at a certain point, place the cells in a situation in which the rate of OXPHOS required to sustain neurotransmitter release and cellular excitability leaves too little of the cell's resources to sustain other key cellular functions such as degradation of damaged or misfolded proteins (77). This could lead to preferential dysregulation

of axon terminals, triggering a dying back cascade culminating later in cell death (5, 123, 124). Approximately half of the oxygen consumed by mitochondria in SNc DA neurons appears to be used by activity-dependent cellular processes such as firing and neurotransmitter release (78). In this context, axon terminal degeneration seen early in the disease, prior to cell death, could be in part an attempt by stressed neurons to adapt to such excessively high metabolic needs. Such a dying back process could also lead to increased amounts of damaged axonal proteins to manage, potentially promoting their accumulation in intracellular inclusions. Since α-synuclein is highly concentrated in axon terminals, it is possible that retraction of axonal processes in a cell where protein degradation systems are overwhelmed promotes creation of pathological aggregates of this protein, thus accelerating cell death. Interestingly, lysosomal defects secondary to GBA1 gene mutations are present in up to 10% of PD patients. This gene encodes a glucocerebrosidase responsible for breaking down lysosomal glucolipid. When GBA1 is mutated, the level of glucolipid and of misfolded proteins increases in neurons. This is likely to represent a particular challenge for highly arborized neurons such as those of the SNc, perhaps explaining why such mutations are now considered the greatest genetic risk factor for PD (125-131). Similarly, mutations in gene products implicated in mitophagy and mitochondrial antigen presentation (PARK2, Pink1) (132, 133), oxidative stress response (PARK7) (134, 135) or vesicular trafficking (LRRK2) (136, 137) are present in familial forms of PD and their detrimental impact on cellular functions could represent larger challenges for highly arborized and energetically ambitious neurons.

2.7 Towards better treatments of PD

In the context of the hypotheses discussed here regarding the origin of the selective vulnerability of neurons in PD, novel strategies to promote survival and preservation of cellular functions amongst challenged neuronal populations could possibly come from approaches that aim to reduce mitochondrial burden by either reducing neuronal metabolic needs or optimizing mitochondrial function. As an example, the CaV1.3 channel inhibitor isradipine is presently in phase 3 clinical trial and could possibly reduce the calcium- and activity-related metabolic stress

of SNc DA neurons leading to neuroprotection (138). Other promising molecules could come from the repurposing of drugs used to treat diabetes and other metabolic diseases. One example is exenatide, a glucagon-like-peptide-1 agonist that has the property to increase glucose-induced insulin secretion, to prevent the rise of ROS and prevent decreases of mitochondrial function in diet-induced obese mice (139). This agonist was found to reduce the loss of DA neurons in the MPTP mouse model (140) and a recent clinical trial has shown improved motor function after 60 days of administration to PD patients (141). Overexpression of the mitochondrial deacetylase SIRT3 has also recently been shown in two studies to reduce basal OXPHOS by DA neurons and to protect SNc neurons in rodent models of PD (142, 143). With further discoveries of the underlying causes of the intrinsic vulnerability of neurons in the PD brain and PNS, multiple other strategies may soon be devised to address some of the specific challenges faced by energetically challenged neurons.

In conclusion, although the presently available data strongly argue that multiple populations of neurons are affected in PD and degenerate to varying extents, new work is needed to provide a more systematic, comparative, and time-dependent quantification of neuronal loss in this disease. More comprehensive and convincing data on cell death and axon terminal dysfunction in PD will likely provide additional impetus for new work aiming to solve the long-awaited challenge of identifying disease-modifying therapeutic approaches for this incapacitating and ill-treated disorder.

2.8 Acknowledgements

This work was supported by a grant from the Brain Canada and Krembil Foundations, as well as by the Canadian Institutes of Health Research. We would like to express our gratitude to Ms. Sarah Ouellet for her help preparing the illustrations and to Drs. Edward Fon, Michael Schlossmacher and Birgit Liss who graciously provided feedback on an earlier version of this manuscript. We also thank Dr. Heiko Braak for helping us identify some key literature.

2.9 References

1. Hoehn MM, Yahr MD. Parkinsonism: onset, progression and mortality. Neurology. 1967;17(5):427-42.

2. Braak H, Del Tredici K, Rub U, de Vos RA, Jansen Steur EN, Braak E. Staging of brain pathology related to sporadic Parkinson's disease. Neurobiology of aging. 2002;24(2):197-211.

3. Parkinson J. An essay on the shaking palsy. 1817. J Neuropsychiatry Clin Neurosci. 2002;14(2):223-36; discussion 2.

4. Cheng HC, Ulane CM, Burke RE. Clinical progression in Parkinson disease and the neurobiology of axons. Ann Neurol. 2010;67(6):715-25.

5. Burke RE, O'Malley K. Axon degeneration in Parkinson's disease. Exp Neurol. 2013;246:72-83.

6. Postuma RB, Berg D, Stern M, Poewe W, Olanow CW, Oertel W, et al. MDS clinical diagnostic criteria for Parkinson's disease. Movement disorders. 2015;30(12):1591-601.

7. Lewy, F.H. (1912) Paralysis agitans. I. Pathologische Anatomie. Handbuch der Neurologie (ed. Lewandowsky, M.). Vol. 3, Springer, Berlin, pp. 920–958.

8. Tretiakoff C. Contribution à l'étude de l'anatomie pathologique du locus niger de Soemmering avec quelques deductions relatives à la pathologenie des troubles du tonus musculaire de la maladie de Parkinson. Thèse, Paris. 1919.

9. Braak H, Del Tredici K. Neuropathological staging of brain pathology in sporadic Parkinson's disease: Separating the wheat from the chaff. J Parkinsons Dis. 2017;7(s1):S73-S87.

10. Shults CW. Lewy bodies. Proc Natl Acad Sci U S A. 2006;103(6):1661-8.

11. Vilchez D, Saez I, Dillin A. The role of protein clearance mechanisms in organismal ageing and age-related diseases. Nat Commun. 2014;5:5659.

12. Mercado G, Castillo V, Soto P, Sidhu A. ER stress and Parkinson's disease: Pathological inputs that converge into the secretory pathway. Brain Res. 2016;1648(Pt B):626-32.

13. Cai Y, Arikkath J, Yang L, Guo ML, Periyasamy P, Buch S. Interplay of endoplasmic reticulum stress and autophagy in neurodegenerative disorders. Autophagy. 2016;12(2):225-44.

14. Truban D, Hou X, Caulfield TR, Fiesel FC, Springer W. Pink1, Parkin, and mitochondrial quality control: What can we learn about Parkinson's disease pathobiology? J Parkinsons Dis. 2017;7(1):13-29.

15. Giannoccaro MP, La Morgia C, Rizzo G, Carelli V. Mitochondrial DNA and primary mitochondrial dysfunction in Parkinson's disease. Movement disorders. 2017;32(3):346-63.

16. Bose A, Beal MF. Mitochondrial dysfunction in Parkinson's disease. J Neurochem. 2016;139 Suppl 1:216-31.

17. Tiwari PC, Pal R. The potential role of neuroinflammation and transcription factors in Parkinson disease. Dialogues in clinical neuroscience. 2017;19(1):71-80.

18. Joshi N, Singh S. Updates on immunity and inflammation in Parkinson disease pathology. Journal of neuroscience research. 2017.

19. Duda J, Potschke C, Liss B. Converging roles of ion channels, calcium, metabolic stress, and activity pattern of Substantia nigra dopaminergic neurons in health and Parkinson's disease. J Neurochem. 2016;139 Suppl 1:156-78.

20. Pfeiffer RF. Non-motor symptoms in Parkinson's disease. Parkinsonism Relat Disord. 2016;22 Suppl 1:S119-22.

21. Braak H, Del Tredici K, Bratzke H, Hamm-Clement J, Sandmann-Keil D, Rüb U. Staging of the intracerebral inclusion body pathology associated with idiopathic Parkinson's disease (preclinical and clinical stages). Journal of Neurology. 2002;249(0):1-.

22. Braak H, Ghebremedhin E, Rub U, Bratzke H, Del Tredici K. Stages in the development of Parkinson's disease-related pathology. Cell Tissue Res. 2004;318(1):121-34.

23. Markesbery WR, Jicha GA, Liu H, Schmitt FA. Lewy body pathology in normal elderly subjects. J Neuropathol Exp Neurol. 2009;68(7):816-22.

24. Sasaki S, Shirata A, Yamane K, Iwata M. Parkin-positive autosomal recessive juvenile Parkinsonism with alpha-synuclein-positive inclusions. Neurology. 2004;63(4):678-82.

25. Hayashi S, Wakabayashi K, Ishikawa A, Nagai H, Saito M, Maruyama M, et al. An autopsy case of autosomal-recessive juvenile parkinsonism with a homozygous exon 4 deletion in the parkin gene. Movement disorders. 2000;15(5):884-8.

26. Schneider SA, Alcalay RN. Neuropathology of genetic synucleinopathies with parkinsonism: Review of the literature. Movement disorders. 2017;32(11):1504-23.

27. Surmeier DJ, Obeso JA, Halliday GM. Selective neuronal vulnerability in Parkinson disease. Nat Rev Neurosci. 2017;18(2):101-13.

28. Buchman AS, Shulman JM, Nag S, Leurgans SE, Arnold SE, Morris MC, et al. Nigral pathology and parkinsonian signs in elders without Parkinson disease. Ann Neurol. 2012;71(2):258-66.

29. Cabello CR, Thune JJ, Pakkenberg H, Pakkenberg B. Ageing of substantia nigra in humans: cell loss may be compensated by hypertrophy. Neuropathol Appl Neurobiol. 2002;28(4):283-91.

30. Fearnley JM, Lees AJ. Ageing and Parkinson's disease: substantia nigra regional selectivity. Brain. 1991;114 (Pt 5):2283-301.

31. Fedorow H, Tribl F, Halliday G, Gerlach M, Riederer P, Double KL. Neuromelanin in human dopamine neurons: comparison with peripheral melanins and relevance to Parkinson's disease. Prog Neurobiol. 2005;75(2):109-24.

32. Ma SY, Roytt M, Collan Y, Rinne JO. Unbiased morphometrical measurements show loss of pigmented nigral neurones with ageing. Neuropathol Appl Neurobiol. 1999;25(5):394-9.

33. Naoi M, Maruyama W. Cell death of dopamine neurons in aging and Parkinson's disease. Mech Ageing Dev. 1999;111(2-3):175-88.

34. Rudow G, O'Brien R, Savonenko AV, Resnick SM, Zonderman AB, Pletnikova O, et al. Morphometry of the human substantia nigra in ageing and Parkinson's disease. Acta neuropathologica. 2008;115(4):461-70.

35. Stark AK, Pakkenberg B. Histological changes of the dopaminergic nigrostriatal system in aging. Cell Tissue Res. 2004;318(1):81-92.

36. Thiessen B, Rajput AH, Laverty W, Desai H. Age, environments, and the number of substantia nigra neurons. Adv Neurol. 1990;53:201-6.

37. Ransmayr G, Faucheux B, Nowakowski C, Kubis N, Federspiel S, Kaufmann W, et al. Age-related changes of neuronal counts in the human pedunculopontine nucleus. Neuroscience Letters. 2000;288(3):195-8.

38. Lohr JB, Jeste DV. Locus ceruleus morphometry in aging and schizophrenia. Acta Psychiatr Scand. 1988;77(6):689-97.

39. Shibata E, Sasaki M, Tohyama K, Kanbara Y, Otsuka K, Ehara S, et al. Age-related changes in locus ceruleus on neuromelanin magnetic resonance imaging at 3 Tesla. Magn Reson Med Sci. 2006;5(4):197-200.

40. Goldstein DS. Cardiac denervation in patients with Parkinson disease. Cleveland Clinic journal of medicine. 2007;74 Suppl 1:S91-4.

41. Wong KK, Raffel DM, Koeppe RA, Frey KA, Bohnen NI, Gilman S. Pattern of cardiac sympathetic denervation in idiopathic Parkinson disease studied with 11C hydroxyephedrine PET. Radiology. 2012;265(1):240-7.

42. Orimo S, Oka T, Miura H, Tsuchiya K, Mori F, Wakabayashi K, et al. Sympathetic cardiac denervation in Parkinson's disease and pure autonomic failure but not in multiple system atrophy. J Neurol Neurosurg Psychiatry. 2002;73(6):776-7.

43. Dijkstra AA, Voorn P, Berendse HW, Groenewegen HJ, Netherlands Brain B, Rozemuller AJ, et al. Stage-dependent nigral neuronal loss in incidental Lewy body and Parkinson's disease. Movement disorders. 2014;29(10):1244-51.

44. Iacono D, Geraci-Erck M, Rabin ML, Adler CH, Serrano G, Beach TG, et al. Parkinson disease and incidental Lewy body disease: Just a question of time? Neurology. 2015;85(19):1670-9.

45. Milber JM, Noorigian JV, Morley JF, Petrovitch H, White L, Ross GW, et al. Lewy pathology is not the first sign of degeneration in vulnerable neurons in Parkinson disease. Neurology. 2012;79(24):2307-14.

46. Gibb WR, Fearnley JM, Lees AJ. The anatomy and pigmentation of the human substantia nigra in relation to selective neuronal vulnerability. Adv Neurol. 1990;53:31-4.

47. Rinne JO, Ma SY, Lee MS, Collan Y, Roytta M. Loss of cholinergic neurons in the pedunculopontine nucleus in Parkinson's disease is related to disability of the patients. Parkinsonism & Related Disorders. 2008;14(7):553-7.

48. Karachi C, Grabli D, Bernard FA, Tande D, Wattiez N, Belaid H, et al. Cholinergic mesencephalic neurons are involved in gait and postural disorders in Parkinson disease. J Clin Invest. 2010;120(8):2745-54.

49. Hepp DH, Ruiter AM, Galis Y, Voorn P, Rozemuller AJM, Berendse HW, et al. Pedunculopontine cholinergic cell loss in hallucinating Parkinson disease patients but not in dementia with Lewy bodies patients. Journal of Neuropathology and Experimental Neurology. 2013;72(12):1162-70.

50. Pienaar IS, Elson JL, Racca C, Nelson G, Turnbull DM, Morris CM. Mitochondrial abnormality associates with type-specific neuronal loss and cell morphology changes in the pedunculopontine nucleus in Parkinson disease. Am J Pathol. 2013;183(6):1826-40.

51. Gai WP, Halliday GM, Blumbergs PC, Geffen LB, Blessing WW. Substance P-containing neurons in the mesopontine tegmentum are severely affected in Parkinson's disease. Brain. 1991;114 (Pt 5):2253-67.

52. Bertrand E, Lechowicz W, Szpak GM, Dymecki J. Qualitative and quantitative analysis of locus coeruleus neurons in Parkinson's disease. Folia neuropathologica. 1997;35(2):80-6.

53. Gai WP, Blumbergs PC, Geffen LB, Blessing WW. Age-related loss of dorsal vagal neurons in Parkinson's disease. Neurology. 1992;42(11):2106-11.

54. Cheshire P, Ayton S, Bertram KL, Ling H, Li A, McLean C, et al. Serotonergic markers in Parkinson's disease and levodopa-induced dyskinesias. Movement disorders. 2015;30(6):796-804.

55. McRitchie DA, Cartwright HR, Halliday GM. Specific A10 dopaminergic nuclei in the midbrain degenerate in Parkinson's disease. Exp Neurol. 1997;144(1):202-13.

56. Damier P, Hirsch EC, Agid Y, Graybiel AM. The substantia nigra of the human brain. II. Patterns of loss of dopamine-containing neurons in Parkinson's disease. Brain. 1999;122 (Pt 8):1437-48.

57. Henderson JM, Carpenter K, Cartwright H, Halliday GM. Degeneration of the centre median-parafascicular complex in Parkinson's disease. Ann Neurol. 2000;47(3):345-52.

58. Halliday GM, Macdonald V, Henderson JM. A comparison of degeneration in motor thalamus and cortex between progressive supranuclear palsy and Parkinson's disease. Brain. 2005;128(Pt 10):2272-80.

59. Thannickal TC, Lai YY, Siegel JM. Hypocretin (orexin) cell loss in Parkinson's disease. Brain. 2007;130(Pt 6):1586-95.

60. Pearce RK, Hawkes CH, Daniel SE. The anterior olfactory nucleus in Parkinson's disease. Movement disorders. 1995;10(3):283-7.

61. Huisman E, Uylings HB, Hoogland PV. A 100% increase of dopaminergic cells in the olfactory bulb may explain hyposmia in Parkinson's disease. Mov Disord. 2004;19(6):687-92.

62. Huisman E, Uylings HB, Hoogland PV. Gender-related changes in increase of dopaminergic neurons in the olfactory bulb of Parkinson's disease patients. Movement disorders. 2008;23(10):1407-13.

63. Mundinano IC, Caballero MC, Ordonez C, Hernandez M, DiCaudo C, Marcilla I, et al. Increased dopaminergic cells and protein aggregates in the olfactory bulb of patients with neurodegenerative disorders. Acta neuropathologica. 2011;122(1):61-74.

64. Klingelhoefer L, Reichmann H. Pathogenesis of Parkinson disease--the gut-brain axis and environmental factors. Nat Rev Neurol. 2015;11(11):625-36.

65. Singaram C, Ashraf W, Gaumnitz EA, Torbey C, Sengupta A, Pfeiffer R, et al. Dopaminergic defect of enteric nervous system in Parkinson's disease patients with chronic constipation. Lancet. 1995;346(8979):861-4.

66. Annerino DM, Arshad S, Taylor GM, Adler CH, Beach TG, Greene JG. Parkinson's disease is not associated with gastrointestinal myenteric ganglion neuron loss. Acta neuropathologica. 2012;124(5):665-80.

67. Benarroch EE, Schmeichel AM, Sandroni P, Low PA, Parisi JE. Involvement of vagal autonomic nuclei in multiple system atrophy and Lewy body disease. Neurology. 2006;66(3):378-83.

68. Wakabayashi K, Takahashi H. Neuropathology of autonomic nervous system in Parkinson's disease. Eur Neurol. 1997;38 Suppl 2:2-7.

69. Harding AJ, Stimson E, Henderson JM, Halliday GM. Clinical correlates of selective pathology in the amygdala of patients with Parkinson's disease. Brain. 2002;125(Pt 11):2431-45.

70. Hirsch E, Graybiel AM, Agid YA. Melanized dopaminergic neurons are differentially susceptible to degeneration in Parkinson's disease. Nature. 1988;334(6180):345-8.

71. German DC, Manaye K, Smith WK, Woodward DJ, Saper CB. Midbrain dopaminergic cell loss in Parkinson's disease: computer visualization. Ann Neurol. 1989;26(4):507-14.

72. Halliday GM, Li YW, Blumbergs PC, Joh TH, Cotton RG, Howe PR, et al. Neuropathology of immunohistochemically identified brainstem neurons in Parkinson's disease. Ann Neurol. 1990;27(4):373-85.

73. Paulus W, Jellinger K. The neuropathologic basis of different clinical subgroups of Parkinson's disease. J Neuropathol Exp Neurol. 1991;50(6):743-55.

74. Zarrow C, Lyness SA, Mortimer JA, Chui HC. Neuronal loss is greater in the locus coeruleus than nucleus basalis and substantia nigra in Alzheimer and Parkinson diseases. Arch Neurol. 2003;60:337-41.

75. Halliday GM, Blumbergs PC, Cotton RG, Blessing WW, Geffen LB. Loss of brainstem serotonin- and substance P-containing neurons in Parkinson's disease. Brain Res. 1990;510(1):104-7.

76. Bolam JP, Pissadaki EK. Living on the edge with too many mouths to feed: Why dopamine neurons die. Movement disorders. 2012;27(12):1478-83.

77. Surmeier DJ, Schumacker PT, Guzman JD, Ilijic E, Yang B, Zampese E. Calcium and Parkinson's disease. Biochem Biophys Res Commun. 2017;483(4):1013-9.

78. Pacelli C, Giguere N, Bourque MJ, Levesque M, Slack RS, Trudeau LE. Elevated mitochondrial bioenergetics and axonal arborization size are key contributors to the vulnerability of dopamine neurons. Curr Biol. 2015;25(18):2349-60.

79. Segura-Aguilar J, Paris I, Munoz P, Ferrari E, Zecca L, Zucca FA. Protective and toxic roles of dopamine in Parkinson's disease. J Neurochem. 2014;129(6):898-915.

80. Van Laar VS, Mishizen AJ, Cascio M, Hastings TG. Proteomic identification of dopamine-conjugated proteins from isolated rat brain mitochondria and SH-SY5Y cells. Neurobiol Dis. 2009;34(3):487-500.

81. Xu Y, Stokes AH, Roskoski R, Jr., Vrana KE. Dopamine, in the presence of tyrosinase, covalently modifies and inactivates tyrosine hydroxylase. Journal of neuroscience research. 1998;54(5):691-7.

82. Whitehead RE, Ferrer JV, Javitch JA, Justice JB. Reaction of oxidized dopamine with endogenous cysteine residues in the human dopamine transporter. J Neurochem. 2001;76(4):1242-51.

83. Mosharov EV, Larsen KE, Kanter E, Phillips KA, Wilson K, Schmitz Y, et al. Interplay between cytosolic dopamine, calcium, and alpha-synuclein causes selective death of substantia nigra neurons. Neuron. 2009;62(2):218-29.

84. Lohr KM, Bernstein AI, Stout KA, Dunn AR, Lazo CR, Alter SP, et al. Increased vesicular monoamine transporter enhances dopamine release and opposes Parkinson disease-related neurodegeneration in vivo. Proc Natl Acad Sci U S A. 2014;111(27):9977-82.

85. Pifl C, Rajput A, Reither H, Blesa J, Cavada C, Obeso JA, et al. Is Parkinson's disease a vesicular dopamine storage disorder? Evidence from a study in isolated synaptic vesicles of human and nonhuman primate striatum. J Neurosci. 2014;34(24):8210-8.

86. Caudle WM, Richardson JR, Wang MZ, Taylor TN, Guillot TS, McCormack AL, et al. Reduced vesicular storage of dopamine causes progressive nigrostriatal neurodegeneration. J Neurosci. 2007;27(30):8138-48.

87. Guillot TS, Miller GW. Protective actions of the vesicular monoamine transporter 2 (VMAT2) in monoaminergic neurons. Mol Neurobiol. 2009;39(2):149-70.

88. Fahn S. Does levodopa slow or hasten the rate of progression of Parkinson's disease? J Neurol. 2005;252 Suppl 4:Iv37-iv42.

89. Lipski J, Nistico R, Berretta N, Guatteo E, Bernardi G, Mercuri NB. L-DOPA: a scapegoat for accelerated neurodegeneration in Parkinson's disease? Prog Neurobiol. 2011;94(4):389-407.

90. Haacke EM, Miao Y, Liu M, Habib CA, Katkuri Y, Liu T, et al. Correlation of putative iron content as represented by changes in R2* and phase with age in deep gray matter of healthy adults. J Magn Reson Imaging. 2010;32(3):561-76.

91. Daugherty A, Raz N. Age-related differences in iron content of subcortical nuclei observed in vivo: a meta-analysis. Neuroimage. 2013;70:113-21.

92. Bilgic B, Pfefferbaum A, Rohlfing T, Sullivan EV, Adalsteinsson E. MRI estimates of brain iron concentration in normal aging using quantitative susceptibility mapping. Neuroimage. 2012;59(3):2625-35.

93. Ren Y, Liu W, Jiang H, Jiang Q, Feng J. Selective vulnerability of dopaminergic neurons to microtubule depolymerization. J Biol Chem. 2005;280(40):34105-12.

94. Friedman A, Galazka-Friedman J, Bauminger ER. Iron as a trigger of neurodegeneration in Parkinson's disease. Handb Clin Neurol. 2007;83:493-505.

95. Sian-Hulsmann J, Mandel S, Youdim MB, Riederer P. The relevance of iron in the pathogenesis of Parkinson's disease. J Neurochem. 2011;118(6):939-57.

96. Kosta P, Argyropoulou MI, Markoula S, Konitsiotis S. MRI evaluation of the basal ganglia size and iron content in patients with Parkinson's disease. J Neurol. 2006;253(1):26-32.

97. Zecca L, Shima T, Stroppolo A, Goj C, Battiston GA, Gerbasi R, et al. Interaction of neuromelanin and iron in substantia nigra and other areas of human brain. Neuroscience. 1996;73(2):407-15.

98. Zucca FA, Bellei C, Giannelli S, Terreni MR, Gallorini M, Rizzio E, et al. Neuromelanin and iron in human locus coeruleus and substantia nigra during aging: consequences for neuronal vulnerability. J Neural Transm (Vienna). 2006;113(6):757-67.

99. Zecca L, Stroppolo A, Gatti A, Tampellini D, Toscani M, Gallorini M, et al. The role of iron and copper molecules in the neuronal vulnerability of locus coeruleus and substantia nigra during aging. Proc Natl Acad Sci U S A. 2004;101(26):9843-8.

100. Michel PP, Alvarez-Fischer D, Guerreiro S, Hild A, Hartmann A, Hirsch EC. Role of activity-dependent mechanisms in the control of dopaminergic neuron survival. J Neurochem. 2007;101(2):289-97.

101. Guzman JN, Sanchez-Padilla J, Wokosin D, Kondapalli J, Ilijic E, Schumacker PT, et al. Oxidant stress evoked by pacemaking in dopaminergic neurons is attenuated by DJ-1. Nature. 2010;468(7324):696-700.

102. Goldberg JA, Guzman JN, Estep CM, Ilijic E, Kondapalli J, Sanchez-Padilla J, et al. Calcium entry induces mitochondrial oxidant stress in vagal neurons at risk in Parkinson's disease. Nat Neurosci. 2012;15(10):1414-21.

103. Sanchez-Padilla J, Guzman JN, Ilijic E, Kondapalli J, Galtieri DJ, Yang B, et al. Mitochondrial oxidant stress in locus coeruleus is regulated by activity and nitric oxide synthase. Nat Neurosci. 2014;17(6):832-40.

104. Reeve A, Simcox E, Turnbull D. Ageing and Parkinson's disease: Why is advancing age the biggest risk factor? Ageing Res Rev. 142014. p. 19-30.

105. Hell JW, Westenbroek RE, Warner C, Ahlijanian MK, Prystay W, Gilbert MM, et al. Identification and differential subcellular localization of the neuronal class C and class D L-type calcium channel alpha 1 subunits. J Cell Biol. 1993;123(4):949-62.

106. Hurley MJ, Gentleman SM, Dexter DT. Calcium CaV1 channel subtype mRNA expression in Parkinson's disease examined by in situ hybridization. Journal of molecular neuroscience : MN. 2015;55(3):715-24.

107. Schiemann J, Schlaudraff F, Klose V, Bingmer M, Seino S, Magill PJ, et al. K-ATP channels in dopamine substantia nigra neurons control bursting and novelty-induced exploration. Nat Neurosci. 2012;15(9):1272-80.

108. Liss B, Haeckel O, Wildmann J, Miki T, Seino S, Roeper J. K-ATP channels promote the differential degeneration of dopaminergic midbrain neurons. Nat Neurosci. 2005;8(12):1742-51.

109. Matsuda W, Furuta T, Nakamura KC, Hioki H, Fujiyama F, Arai R, et al. Single nigrostriatal dopaminergic neurons form widely spread and highly dense axonal arborizations in the neostriatum. J Neurosci. 2009;29(2):444-53.

110. Pissadaki EK, Bolam JP. The energy cost of action potential propagation in dopamine neurons: clues to susceptibility in Parkinson's disease. Front Comput Neurosci. 2013;7:13.

111. Takakusaki K, Shiroyama T, Yamamoto T, Kitai ST. Cholinergic and noncholinergic tegmental pedunculopontine projection neurons in rats revealed by intracellular labeling. The Journal of comparative neurology. 1996;371(3):345-61.

112. Gao K, Mason P. Somatodendritic and axonal anatomy of intracellularly labeled serotonergic neurons in the rat medulla. The Journal of comparative neurology. 1997;389(2):309-28.

113. Gao H, Glatzer NR, Williams KW, Derbenev AV, Liu D, Smith BN. Morphological and electrophysiological features of motor neurons and putative interneurons in the dorsal vagal complex of rats and mice. Brain Res. 2009;1291:40-52.

114. Gagnon D, Parent M. Distribution of VGLUT3 in highly collateralized axons from the rat dorsal raphe nucleus as revealed by single-neuron reconstructions. PLoS One. 2014;9(2):e87709.

115. Chazal G, Ma W. An ultrastructural analysis of serotoninergic neurons in the nucleus raphe magnus of the rat. Neuroscience. 1989;33(2):301-10.

116. Jones BE, Yang TZ. The efferent projections from the reticular formation and the locus coeruleus studied by anterograde and retrograde axonal transport in the rat. The Journal of comparative neurology. 1985;242(1):56-92.

117. Contant C, Umbriaco D, Garcia S, Watkins KC, Descarries L. Ultrastructural characterization of the acetylcholine innervation in adult rat neostriatum. Neuroscience. 1996;71(4):937-47.

118. Zhou FM, Wilson CJ, Dani JA. Cholinergic interneuron characteristics and nicotinic properties in the striatum. Journal of neurobiology. 2002;53(4):590-605.

119. Meitzen J, Pflepsen KR, Stern CM, Meisel RL, Mermelstein PG. Measurements of neuron soma size and density in rat dorsal striatum, nucleus accumbens core and nucleus accumbens shell: differences between striatal region and brain hemisphere, but not sex. Neurosci Lett. 2011;487(2):177-81.

120. Sian J, Dexter DT, Lees AJ, Daniel S, Agid Y, Javoy-Agid F, et al. Alterations in glutathione levels in Parkinson's disease and other neurodegenerative disorders affecting basal ganglia. Ann Neurol. 1994;36(3):348-55.

121. Pearce RK, Owen A, Daniel S, Jenner P, Marsden CD. Alterations in the distribution of glutathione in the substantia nigra in Parkinson's disease. J Neural Transm (Vienna). 1997;104(6-7):661-77.

122. Sofic E, Lange KW, Jellinger K, Riederer P. Reduced and oxidized glutathione in the substantia nigra of patients with Parkinson's disease. Neurosci Lett. 1992;142(2):128-30.

123. Tagliaferro P, Burke RE. Retrograde Axonal Degeneration in Parkinson Disease. J Parkinsons Dis. 2016;6(1):1-15.

124. O'Malley KL. The role of axonopathy in Parkinson's disease. Exp Neurobiol. 2010;19(3):115-9.

125. Kinghorn KJ, Asghari AM, Castillo-Quan JI. The emerging role of autophagic-lysosomal dysfunction in Gaucher disease and Parkinson's disease. Neural regeneration research. 2017;12(3):380-4.

126. Wong YC, Krainc D. Lysosomal trafficking defects link Parkinson's disease with Gaucher's disease. Movement disorders. 2016;31(11):1610-8.

127. Migdalska-Richards A, Schapira AH. The relationship between glucocerebrosidase mutations and Parkinson disease. J Neurochem. 2016;139 Suppl 1:77-90.

128. Sidransky E, Nalls MA, Aasly JO, Aharon-Peretz J, Annesi G, Barbosa ER, et al. Multicenter analysis of glucocerebrosidase mutations in Parkinson's disease. The New England journal of medicine. 2009;361(17):1651-61.

129. Gegg ME, Burke D, Heales SJ, Cooper JM, Hardy J, Wood NW, et al. Glucocerebrosidase deficiency in substantia nigra of parkinson disease brains. Ann Neurol. 2012;72(3):455-63.

130. Murphy KE, Halliday GM. Glucocerebrosidase deficits in sporadic Parkinson disease. Autophagy. 2014;10(7):1350-1.

131. Dehay B, Martinez-Vicente M, Caldwell GA, Caldwell KA, Yue Z, Cookson MR, et al. Lysosomal impairment in Parkinson's disease. Movement disorders. 2013;28(6):725-32.

132. Ashrafi G, Schwarz TL. Pink1- and PARK2-mediated local mitophagy in distal neuronal axons. Autophagy. 2015;11(1):187-9.

133. Matheoud D, Sugiura A, Bellemare-Pelletier A, Laplante A, Rondeau C, Chemali M, et al. Parkinson's disease-related proteins Pink1 and Parkin repress mitochondrial antigen presentation. Cell. 2016;166(2):314-27.

134. Sheng C, Heng X, Zhang G, Xiong R, Li H, Zhang S, et al. DJ-1 deficiency perturbs microtubule dynamics and impairs striatal neurite outgrowth. Neurobiology of aging. 2013;34(2):489-98.

135. Di Nottia M, Masciullo M, Verrigni D, Petrillo S, Modoni A, Rizzo V, et al. DJ-1 modulates mitochondrial response to oxidative stress: clues from a novel diagnosis of PARK7. Clin Genet. 2017;92(1):18-25.

136. MacLeod D, Dowman J, Hammond R, Leete T, Inoue K, Abeliovich A. The familial Parkinsonism gene LRRK2 regulates neurite process morphology. Neuron. 2006;52(4):587-93.

137. Yue M, Hinkle KM, Davies P, Trushina E, Fiesel FC, Christenson TA, et al. Progressive dopaminergic alterations and mitochondrial abnormalities in LRRK2 G2019S knock-in mice. Neurobiol Dis. 2015;78:172-95.

138. Surmeier DJ, Halliday GM, Simuni T. Calcium, mitochondrial dysfunction and slowing the progression of Parkinson's disease. Exp Neurol. 2017;298(Pt B):202-9.

139. Wang Z, Hou L, Huang L, Guo J, Zhou X. Exenatide improves liver mitochondrial dysfunction and insulin resistance by reducing oxidative stress in high fat diet-induced obese mice. Biochem Biophys Res Commun. 2017;486(1):116-23.

140. Li Y, Perry T, Kindy MS, Harvey BK, Tweedie D, Holloway HW, et al. GLP-1 receptor stimulation preserves primary cortical and dopaminergic neurons in cellular and rodent models of stroke and Parkinsonism. Proc Natl Acad Sci U S A. 2009;106(4):1285-90.

141. Athauda D, Maclagan K, Skene SS, Bajwa-Joseph M, Letchford D, Chowdhury K, et al. Exenatide once weekly versus placebo in Parkinson's disease: a randomised, double-blind, placebo-controlled trial. Lancet. 2017;390(10103):1664-75.

142. Gleave JA, Arathoon LR, Trinh D, Lizal KE, Giguere N, Barber JHM, et al. Sirtuin 3 rescues neurons through the stabilisation of mitochondrial biogenetics in the virally-expressing mutant alpha-synuclein rat model of parkinsonism. Neurobiol Dis. 2017;106:133-46.

143. Shi H, Deng HX, Gius D, Schumacker PT, Surmeier DJ, Ma YC. Sirt3 protects dopaminergic neurons from mitochondrial oxidative stress. Hum Mol Genet. 2017;26(10):1915-26.

144. Greenfield JG, Bosanquet FD. The brain-stem lesions in Parkinsonism. J Neurol Neurosurg Psychiatry. 1953;16(4):213-26.

145. Pakkenberg H, Brody H. The number of nerve cells in the substantia nigra in paralysis agitans. Acta neuropathologica. 1965;5(2):320-4.

146. Bernheimer H, Birkmayer W, Hornykiewicz O, Jellinger K, Seitelberger F. Brain dopamine and the syndromes of Parkinson and Huntington. Clinical, morphological and neurochemical correlations. J Neurol Sci. 1973;20(4):415-55.

147. Rajput AH, Rozdilsky B. Dysautonomia in Parkinsonism: a clinicopathological study. J Neurol Neurosurg Psychiatry. 1976;39(11):1092-100.

148. Gaspar P, Gray F. Dementia in idiopathic Parkinson's disease. A neuropathological study of 32 cases. Acta neuropathologica. 1984;64(1):43-52.

149. Tagliavini F, Pilleri G, Bouras C, Constantinidis J. The basal nucleus of Meynert in idiopathic Parkinson's disease. Acta neurologica Scandinavica. 1984;70(1):20-8.

150. Chan-Palay V. Galanin hyperinnervates surviving neurons of the human basal nucleus of Meynert in dementias of Alzheimer's and Parkinson's disease: a hypothesis for the role of galanin in accentuating cholinergic dysfunction in dementia. The Journal of comparative neurology. 1988;273(4):543-57.

151. Gibb WR, Lees AJ. A comparison of clinical and pathological features of young- and old-onset Parkinson's disease. Neurology. 1988;38(9):1402-6.

152. Rinne JO, Rummukainen J, Paljarvi L, Rinne UK. Dementia in Parkinson's disease is related to neuronal loss in the medial substantia nigra. Ann Neurol. 1989;26(1):47-50.

153. Zweig RM, Jankel WR, Hedreen JC, Mayeux R, Price DL. The pedunculopontine nucleus in Parkinson's disease. Ann Neurol. 1989;26(1):41-6.

154. Pakkenberg B, Moller A, Gundersen HJ, Mouritzen Dam A, Pakkenberg H. The absolute number of nerve cells in substantia nigra in normal subjects and in patients with Parkinson's disease estimated with an unbiased stereological method. J Neurol Neurosurg Psychiatry. 1991;54(1):30-3.

155. Xuereb JH, Perry RH, Candy JM, Perry EK, Marshall E, Bonham JR. Nerve cell loss in the thalamus in Alzheimer's disease and Parkinson's disease. Brain. 1991;114 (Pt 3):1363-79.

156. Moller A. Mean volume of pigmented neurons in the substantia nigra in Parkinson's disease. Acta Neurol Scand Suppl. 1992;137:37-9.

157. Zweig RM, Cardillo JE, Cohen M, Giere S, Hedreen JC. The locus ceruleus and dementia in Parkinson's disease. Neurology. 1993;43(5):986-91.

158. Mouatt-Prigent A, Agid Y, Hirsch EC. Does the calcium binding protein calretinin protect dopaminergic neurons against degeneration in Parkinson's disease? Brain Res. 1994;668(1-2):62-70.

159. Ma SY, Collan Y, Roytta M, Rinne JO, Rinne UK. Cell counts in the substantia nigra: a comparison of single section counts and disector counts in patients with Parkinson's disease and in controls. Neuropathol Appl Neurobiol. 1995;21(1):10-7.

160. Halliday GM, McRitchie DA, Cartwright H, Pamphlett R, Hely MA, Morris JG. Midbrain neuropathology in idiopathic Parkinson's disease and diffuse Lewy body disease. J Clin Neurosci. 1996;3(1):52-60.

161. Ma SY, Rinne JO, Collan Y, Roytta M, Rinne UK. A quantitative morphometrical study of neuron degeneration in the substantia nigra in Parkinson's disease. J Neurol Sci. 1996;140(1-2):40-5.

162. Ma SY, Roytta M, Rinne JO, Collan Y, Rinne UK. Correlation between neuromorphometry in the substantia nigra and clinical features in Parkinson's disease using disector counts. J Neurol Sci. 1997;151(1):83-7.

163. Greffard S, Verny M, Bonnet AM, Beinis JY, Gallinari C, Meaume S, et al. Motor score of the Unified Parkinson Disease Rating Scale as a good predictor of Lewy body-associated neuronal loss in the substantia nigra. Arch Neurol. 2006;63(4):584-8.

164. Beach TG, Adler CH, Lue L, Sue LI, Bachalakuri J, Henry-Watson J, et al. Unified staging system for Lewy body disorders: correlation with nigrostriatal degeneration, cognitive impairment and motor dysfunction. Acta neuropathologica. 2009;117(6):613-34.

165. Kordower JH, Olanow CW, Dodiya HB, Chu Y, Beach TG, Adler CH, et al. Disease duration and the integrity of the nigrostriatal system in Parkinson's disease. Brain. 2013;136(Pt 8):2419-31.

166. Kraemmer J, Kovacs GG, Perju-Dumbrava L, Pirker S, Traub-Weidinger T, Pirker W. Correlation of striatal dopamine transporter imaging with post mortem substantia nigra cell counts. Movement disorders. 2014;29(14):1767-73.

167. Chan-Palay V, Asan E. Alterations in catecholamine neurons of the locus coeruleus in senile dementia of the Alzheimer type and in Parkinson's disease with and without dementia and depression. The Journal of comparative neurology. 1989;287(3):373-92.

168. German DC, Manaye KF, White CL, 3rd, Woodward DJ, McIntire DD, Smith WK, et al. Disease-specific patterns of locus coeruleus cell loss. Ann Neurol. 1992;32(5):667-76.

169. Patt S, Gerhard L. A Golgi study of human locus coeruleus in normal brains and in Parkinson's disease. Neuropathol Appl Neurobiol. 1993;19(6):519-23.

170. Hoogendijk WJ, Pool CW, Troost D, van Zwieten E, Swaab DF. Image analyser-assisted morphometry of the locus coeruleus in Alzheimer's disease, Parkinson's disease and amyotrophic lateral sclerosis. Brain. 1995;118 (Pt 1):131-43.

171. Brunnstrom H, Friberg N, Lindberg E, Englund E. Differential degeneration of the locus coeruleus in dementia subtypes. Clinical neuropathology. 2011;30(3):104-10.

172. McMillan PJ, White SS, Franklin A, Greenup JL, Leverenz JB, Raskind MA, et al. Differential response of the central noradrenergic nervous system to the loss of locus coeruleus neurons in Parkinson's disease and Alzheimer's disease. Brain Res. 2011;1373:240-52.

173. Dugger BN, Murray ME, Boeve BF, Parisi JE, Benarroch EE, Ferman TJ, et al. Neuropathological analysis of brainstem cholinergic and catecholaminergic nuclei in relation to rapid eye movement (REM) sleep behaviour disorder. Neuropathol Appl Neurobiol. 2012;38(2):142-52.

174. Del Tredici K, Braak H. Dysfunction of the locus coeruleus-norepinephrine system and related circuitry in Parkinson's disease-related dementia. J Neurol Neurosurg Psychiatry. 2013;84(7):774-83.

175. Arendt T, Bigl V, Arendt A, Tennstedt A. Loss of neurons in the nucleus basalis of Meynert in Alzheimer's disease, paralysis agitans and Korsakoff's Disease. Acta neuropathologica. 1983;61(2):101-8.

176. Candy JM, Perry RH, Perry EK, Irving D, Blessed G, Fairbairn AF, et al. Pathological changes in the nucleus of Meynert in Alzheimer's and Parkinson's diseases. J Neurol Sci. 1983;59(2):277-89.

177. Nakano I, Hirano A. Neuron loss in the nucleus basalis of Meynert in parkinsonism-dementia complex of Guam. Ann Neurol. 1983;13(1):87-91.

178. Whitehouse PJ, Hedreen JC, White CL, 3rd, Price DL. Basal forebrain neurons in the dementia of Parkinson disease. Ann Neurol. 1983;13(3):243-8.

179. Nakano I, Hirano A. Parkinson's disease: Neuron loss in the nucleus basalis withouth concomitant Alzheimer's Disease. Ann Neurol. 1984;15(5):415-8.

180. Perry EK, Curtis M, Dick DJ, Candy JM, Atack JR, Bloxham CA, et al. Cholinergic correlates of cognitive impairment in Parkinson's disease: comparisons with Alzheimer's disease. J Neurol Neurosurg Psychiatry. 1985;48(5):413-21.

181. Rogers JD, Brogan D, Mirra SS. The nucleus basalis of Meynert in neurological disease: a quantitative morphological study. Ann Neurol. 1985;17(2):163-70.

182. Hirsch EC, Graybiel AM, Duyckaerts C, Javoy-Agid F. Neuronal loss in the pedunculopontine tegmental nucleus in Parkinson disease and in progressive supranuclear palsy. Proc Natl Acad Sci U S A. 1987;84(16):5976-80.

183. Jellinger K. The pedunculopontine nucleus in Parkinson's disease, progressive supranuclear palsy and Alzheimer's disease. J Neurol Neurosurg Psychiatry. 1988;51(4):540-3.

184. Schmeichel AM, Buchhalter LC, Low PA, Parisi JE, Boeve BW, Sandroni P, et al. Mesopontine cholinergic neuron involvement in Lewy body dementia and multiple system atrophy. Neurology. 2008;70(5):368-73.

185. Pienaar IS, Elson JL, Racca C, Nelson G, Turnbull DM, Morris CM. Mitochondrial abnormality associates with type-specific neuronal loss and cell morphology changes in the pedunculopontine nucleus in Parkinson disease. Am J Pathol. 2013;183(6):1826-40.

186. Kremer HP. The hypothalamic lateral tuberal nucleus: normal anatomy and changes in neurological diseases. Prog Brain Res. 1992;93:249-61.

187. Kremer HP, Bots GT. Lewy bodies in the lateral hypothalamus: do they imply neuronal loss? Movement disorders. 1993;8(3):315-20.

188. Purba JS, Hofman MA, Swaab DF. Decreased number of oxytocin-immunoreactive neurons in the paraventricular nucleus of the hypothalamus in Parkinson's disease. Neurology. 1994;44(1):84-9.

189. Nakamura S, Ohnishi K, Nishimura M, Suenaga T, Akiguchi I, Kimura J, et al. Large neurons in the tuberomammillary nucleus in patients with Parkinson's disease and multiple system atrophy. Neurology. 1996;46(6):1693-6.

190. Ansorge O, Daniel SE, Pearce RK. Neuronal loss and plasticity in the supraoptic nucleus in Parkinson's disease. Neurology. 1997;49(2):610-3.

191. Hoogendijk WJ, Purba JS, Hofman MA, de Vos RA, Jansen EN, Swaab DF. Depression in Parkinson's disease is not accompanied by more corticotropin-releasing hormone expressing neurons in the hypothalamic paraventricular nucleus. Biol Psychiatry. 1998;43(12):913-7.

192. Fronczek R, Overeem S, Lee SY, Hegeman IM, van Pelt J, van Duinen SG, et al. Hypocretin (orexin) loss in Parkinson's disease. Brain. 2007;130(Pt 6):1577-85.

193. Eadie MJ. The pathology of certain medullary nuclei in Parkinsonism. Brain. 1963;86:781-92.

194. Saper CB, Sorrentino DM, German DC, de Lacalle S. Medullary catecholaminergic neurons in the normal human brain and in Parkinson's disease. Ann Neurol. 1991;29(6):577-84.

195. Yamamoto T, Hirano A. Nucleus raphe dorsalis in parkinsonism-dementia complex of Guam. Acta neuropathologica. 1985;67(3-4):296-9.

196. Benarroch EE, Schmeichel AM, Sandroni P, Parisi JE, Low PA. Rostral raphe involvement in Lewy body dementia and multiple system atrophy. Acta neuropathologica. 2007;114(3):213-20.

197. Javoy-Agid F, Ruberg M, Taquet H, Bokobza B, Agid Y, Gaspar P, et al. Biochemical neuropathology of Parkinson's disease. Adv Neurol. 1984;40:189-98.

198. Dymecki J, Lechowicz W, Bertrand E, Szpak GM. Changes in dopaminergic neurons of the mesocorticolimbic system in Parkinson's disease. Folia neuropathologica. 1996;34(2):102-6.

199. Henderson JM, Carpenter K, Cartwright H, Halliday GM. Loss of thalamic intralaminar nuclei in progressive supranuclear palsy and Parkinson's disease: clinical and therapeutic implications. Brain. 2000;123 (Pt 7):1410-21.

200. Pedersen KM, Marner L, Pakkenberg H, Pakkenberg B. No global loss of neocortical neurons in Parkinson's disease: a quantitative stereological study. Mov Disord. 2005;20(2):164-71.

201. MacDonald V, Halliday GM. Selective loss of pyramidal neurons in the pre-supplementary motor cortex in Parkinson's disease. Movement disorders. 2002;17(6):1166-73.

202. Joelving FC, Billeskov R, Christensen JR, West M, Pakkenberg B. Hippocampal neuron and glial cell numbers in Parkinson's disease--a stereological study. Hippocampus. 2006;16(10):826-33.

2.10 Table I

REGIONS	PUBLICATIONS (reference #)	TECHNIQUE	N (ctrl)	LOSS OF NEURONS (%)	COMPARISON GROUP INFO (Healthy controls unless stated otherwise)	BLINDED / AGE MATCHED	STATED DIAGNOSIS, SCALE OF SEVERITY, DISEASE DURATION (expressed in range or mean, when available)	OTHER REGIONS COUNTED	CORRELATIONS (with disease severity, duration or age)
Substantia Nigra pars Compacta (SNc)	Greenfield, 1953 (144)	o	19 (22)	some	--	Not stated	iPA, <1-20 years	LC	--
	Pakkenberg, 1965 (145)	m	10 (10)	66	Healthy controls and two young controls	Not stated/Yes	iPA	--	--
	Bernheimer, 1973 (146)	o	69 (0)	some	No healthy controls, compared to type of PD and Huntington's disease	Not stated/Yes	PD, H&Y, 1-47 years	--	--
	Rajput, 1976 (147)	o	6 (1)	some	--	Not stated	iPA, H&Y, 3-18 years	LC, DMV, Cortex, Hypothalamus, Intermediolateral spinal cord, sympathetic ganglia	--
	Gaspar, 1984 (148)	o	32 (6)	some	--	Yes/Yes	iPD, 2-23 years	LC, NBM	--
	Tagliavini, 1984 (149)	o	6 (5)	some	--	Not stated/Yes	iPD, 5-13 years	NBM	--
	Chan-Palay, 1988 (150)	o	9 (22)	some	--	Yes/Not stated	PD	NBM	--
	Gibb, 1988 (151)	m	34 (-)	-	No healthy controls, compared young and old onset	Not stated	PD, 1-34 years	--	--
	Hirsch, 1988 (70)	c	4 (3)	77	--	Not stated	PD	A10, A8, CGS	--
	German, 1989 (71)	c	5 (3)	61	--	Not stated/Yes	PD, 5-27 years	VTA	--
	Rinne, 1989 (152)	s	12 (18)	60	--	Not stated/Yes	iPD, H&Y II-V	--	Yes
	Zweig, 1989 (153)	o	6 (8)	Mild to severe	Not compared - estimation	Not stated/Yes	PD, 5-14 years	PPN, DR, NBM	--
	Gibb, 1990 (46)	m	6 (6)	75	--	Not stated	PD	--	--
	Halliday, 1990 (72)	c	4 (4)	68	--	Not stated/Yes	PD	SNc + LC, RN, PPN, DMV	Yes (dementia score)
	Fearnley, 1991 (30)	m	20 (36)	20-90	--	Not stated/Yes	PD, 1.5-38 years	--	Yes (also in controls)
	Pakkenberg, 1991 (154)	s	7 (7)	66	--	Not stated/Yes	PD, 4-16 years	--	--
	Paulus, 1991 (73)	m	39 (14)	59	--	Not stated/Yes	PD, H&Y III-V, 1-31 years	LC, DRN, NBM	--
	Xuereb, 1991 (155)	o	5 (5)	some	--	Not stated/Yes	PD	Thalamus (multiple nuclei)	--
	Moller, 1992 (156)	c	3 (3)	80	--	Not stated/Yes	PD	--	--
	Zweig, 1993 (157)	m	13 (14)	some	--	Yes	PD, H&Y 4.5, 11 years	LC, VTA, NBM	--
	Mouatt-Prigent, 1994 (158)	c	4 (3)	76	--	Not stated/Yes	iPD	VTA	--
	Ma, 1995 (159)	s	4 (7)	70	--	Not stated	PD	--	--
	Halliday, 1996 (160)	s	11 (15)	37-75	--	Not stated/Yes	PD, 1-18 years	--	Yes
	Ma, 1996 (161)	c	20 (8)	76	--	Not stated/Yes	PD	--	--
	Ma, 1997 (162)	s	12 (12)	55	--	Not stated/Yes	PD, H&Y III-V, 3-17 years	--	Yes
	Damier, 1999 (56)	c	5 (5)	86	--	Not stated	iPD	VTA	Yes
	Henderson, 2000 (57)	c	9 (8)	69	--	Not stated/Yes	PD, H&Y II-V, 3-17 years	Centromedian–Parafascicular Complex, mediodorsal or anterior principal nucleus	--
	Zarrow, 2003 (74)	m	19 (13)	78	Healthy controls, AD	Not stated/Yes	iPD, 12.4 years	LC, NBM	
	Greffard, 2006 (163)	o	14 (5)	50	--	Not stated/Yes	iPD, UPDRS3 = 53, 8.5 years	--	Yes
	Rudow, 2008 (34)	s	8 (23)	~80 vs young, ~75 vs old controls	Young, middle aged and old healthy controls	Not stated/Yes	PD, 7-20 years	--.	Yes, in controls

	Beach, 2009 (164)	o	66 (87)	some	Healthy controls, ILDB, DLB, ADLB, ADNLB	Yes/Not stated	PD + DLB, UPDRS = 41, 10.6 years	--	--
	Karachi, 2010 (48)	s	12 (8)	69-88	--	Yes	PD, UPDRS	PPN	--
	Milber, 2012 (45)	s	13 (17)	70	Healthy controls, iLBD	Yes/Not stated	PD, Braak stage I-VI, 8.3 years.	--	Yes in iLBD
	Kordower, 2013 (165)	s	28 (9)	50-90	--	Yes	PD, 1-27 years	--	Yes
	Dijkstra, 2014 (43)	s	24 (12)	56	Healthy controls, iLBD	Yes	PD and iLBD, Braak stage 0-VI, H&Y, 13.6 years	--	Yes
	Kraemmer, 2014 (166)	m	4 (0)	-	No healthy controls, compared to AD, CJD, CBS, NPH	Yes/Not stated	PD and DLB, 2-4 years	--	--
	Cheshire, 2015 (54)	s	44 (17)	75	--	Yes	PD, LID severity, 14.8 years	RN	--
	Iacono, 2015 (44)	s	6 (6)	82	--	Yes	iPD and iLDB, Braak stage I-IV, H&Y 2-5,	--	--
Total:	**38**	**o10, m8, c8, s12**	**612(452)**						
Locus Coeruleus (LC)	Rajput, 1976 (147)	o	6(1)	some	--	Not stated	iPA H&Y, 3-18 years	SN, DMV, Cortex, Hypothalamus, Intermediolateral spinal cord, sympathetic ganglia	--
	Gaspar, 1984 (148)	o	32 (6)	some	--	Yes	iPD, 2-23 years	SNc, NBM	--
	Hirsch, 1988 (70)	c	4 (3)	55	--	Not stated	PD	SNc, A10, A8	--
	Chan-Palay, 1989 (167)	c	6 (3)	31-94*	--	Not stated/Yes	PD	--	--
	Zweig, 1989 (153)	o	6 (8)	Mild to severe	Not compared - estimation	Not stated/Yes	PD, 5-14 years	PPN, SNc, DR, NBM	--
	Halliday, 1990 (72)	c	4 (4)	68	--	Not stated/Yes	PD	SNc + LC, RN, PPN, DMV	--
	Gai, 1991 (51)	c	6 (5)	74	--	Not stated/Yes	iPD, 5-30 years	PPN, LTN, OPN, RN	Yes
	Paulus, 1991 (73)	m	37 (12)	63	--	Not stated/Yes	PD, H&Y III-V, 1-31 years	SNc, DRN, NBM	--
	German, 1992 (168)	c	6 (7)	21-93	Healthy controls, AD, down-syndrome	Not stated/Yes	PD, 5-16 years	--	--
	Patt, 1993 (169)	o	8 (8)	some	--	Not stated	PD	--	--
	Zweig, 1993 (157)	m	13 (14)	46-69	--	Yes/Yes	PD, H&Y 4.5, 11 years	SNc, VTA, NBM	--
	Hoogendijk, 1995 (170)	c	5 (5)	39 NS	Healthy controls, AD, ALS	Not stated/Yes	PD, 7 years	--	--
	Bertrand, 1997 (52)	c	11 (6)	58-78	--	Not stated	PD	--	Yes
	Zarrow, 2003 (74)	m	19 (13)	83	Healthy controls, AD	Not stated/Yes	iPD, 12.4 years	SNc, NBM	--
	Brunnstom, 2011 (171)	m	25(0)	mild-severe	Healthy controls, AD	Yes/Not stated	DLB and PD dementia	--	--
	Mc Millan, 2011 (172)	m	7 (8)	71-88	Healthy controls, AD, DLB	Yes	PD, 7-25 years	--	--
	Dugger, 2012 (173)	c	21 (11)	some	--	Not stated/Yes	LBD, 8.4 years	PPN	--
	Del Tredici, 2013 (174)	o	5 (1)	some	--	Not stated	PD, H&Y 3-5, 7-15 years	--	--
Total:	**18**	**o5, m4, c9, s0**	**221(115)**						--
	*31 w/o dementia, 48 w/ dementia, 94 if Non-responsive to L-DOPA								
Nucleus Basalis of Meynert (NBM)	Arendt, 1983 (175)	m	5 (14)	70	--	Not stated/Yes	Postencephalitic PD	--	--
	Candy, 1983 (176)	m	5 (5)	some	Healthy controls, AD	Not stated	PD	--	--
	NakaNo, 1983 (177)	m	2 (5)	90	--	Not stated/Yes	PD-dementia complex of Guam, 4-5 years	--	--
	Whitehouse, 1983 (178)	m	12 (10)	45-71	--	Yes	iPD, 4-26 years	--	--
	Gaspar, 1984 (148)	m	32 (6)	36	--	Yes	iPD, 2-23 years	SNc, LC	--
	NakaNo, 1984 (179)	m	11 (13)	60	--	Not stated/Yes	PD, 1-17 years	--	--
	Tagliavini, 1984 (149)	m	6 (5)	46-69	--	Not stated/Yes	iPD, 5-13 years	SNc	--
	Perry, 1985 (180)	m	4 (8)	17-72	Healthy controls, AD	Not stated/Yes	PD	--	--
	Rogers, 1985 (181)	m	4(5)	some	Healthy controls, PSP, Creutzfeldt-Jakob disease, ALS, MS and AD (+ individual cases of other diseases)	Not stated/Yes	PD	--	--

	Chan-Palay, 1988 (150)	m	9 (22)	~50	Healthy controls, AD	Yes/Not stated	PD	SNc	--
	Paulus, 1991 (73)	m	40 (17)	some	--	Not stated/Yes	PD, H&Y III-V, 1-31 years	SNc, LC, DRN	--
	Zweig, 1993 (157)	o	13 (14)	some	--	Yes	PD, H&Y 4.5, 11 years	LC, SNc, VTA	--
	Zarrow, 2003 (74)	m	19 (13)	37	Healthy controls, AD	Not stated/Yes	iPD, 12.4 years	SNc, LC	--
Total:	**13**	**o1, m12, c0, s0**	**162(137)**						
Pedunculopontine Nucleus (PPN)	Hirsch, 1987 (182)	c	6 (4)	57	Healthy controls, supranuclear palsy	Not stated	PD	--	--
	Jellinger, 1988 (183)	m	14 (15)	53	--	Not stated/Yes	PD, 10 years	--	--
	Zweig, 1989 (153)	m	4 (8)	46-69	--	Not stated/Yes	PD, 10-14 years	--	--
	Halliday, 1990 (72)	c	4 (4)	57	--	Not stated/Yes	PD	SNc + LC, RN, DMV	--
	Gai, 1991 (51)	c	6 (5)	43	--	Not stated/Yes	iPD, 5-30 years	LTN, OPN, RN, LC	Yes
	Rinne, 2008 (47)	s	11 (9)	40	--	Not stated/Yes	PD, H&Y 2.5 and 5, 9.3 years	--	Yes
	Schmeichel, 2008 (184)	m	13 (11)	65	Healthy controls, MSA	Yes/Not stated	DLB, 3-16 years	Laterodorsal tegmental nucleus	--
	Karachi, 2010 (48)	s	12 (8)	31-38	--	Yes	PD, UPDRS 0-IV	SN	--
	Dugger, 2012 (173)	c	21 (11)	some	--	Not stated/Yes	LBD, 8.4 years	LC	--
	Hepp, 2013 (49)	s	9 (9)	41	Healthy controls, DLB	Yes	PD, Braak stage IV-VI, H&Y IV-V, 8-26 years	--	--
	Pienaar, 2013 (185)	s	8 (5)	50	--	Yes	PD, Braak stage II-IV, 6-13 years	--	--
Total:	**11**	**o0, m3, c4, s4**	**108 (89)**						
Hypothalamus	Rajput, 1976 (147)	o	6 (1)	None	--	Not stated	iPA, H&Y, 3-18 years	SN, LC, DMV, Cortex, intermediolateral spinal cord, sympathetic ganglia	--
	Kremer, 1992 (186)	m	8 (15)	None	--	Not stated	PD	--	--
	Kremer, 1993 (187)	m	8 (7)	None	--	Not stated/Yes	iPD, 4-17 years	--	--
	Purba, 1994 (188)	m	6 (6)	20	--	Not stated/Yes	PD	--	--
	Nakamura, 1996 (189)	m	8 (6)	None	--	Not stated/Yes	iPD	--	--
	Ansorge, 1997 (190)	m	7 (8)	12-29	--	Not stated/Yes	PD, 18 years	--	--
	Hoogendijk, 1998 (191)	m	12 (6)	None	--	Yes	iPD	--	--
	Fronczek, 2007 (192)	c	9 (9)	45	--	Yes	PD, late-stage	--	--
	Thannickal, 2007 (59)	s	10 (5)	50	--	Not stated/Yes	PD, H&Y I-V, 4-23 years	--	Yes
Total:	**9**	**o1, m6, c1, s1**	**74(63)**						
Dorsal Motor Nucleus of the Vagus Nerve (DMV)	Eadie, 1963 (193)	m	8(5)	30	--	Not stated/Yes	PD	Hypoglossal nuclei, nucleus ambiguus	--
	Rajput, 1976 (147)	o	6(1)	some	--	Not stated	iPA, H&Y, 3-18 years	SN, LC, Cortex, Hypothalamus, Intermediolateral spinal cord, sympathetic ganglia	--
	Halliday, 1990 (75)	c	4 (4)	77	--	Not stated	PD	RN	--
	Halliday, 1990 (72)	c	4 (4)	77	--	Not stated/Yes	PD	SNc + LC, RN, PPN	--
	Saper, 1991 (194)	m	5(5)	60	--	Not stated	PD, 2-16 years	--	--
	Gai, 1992 (53)	s	8(6)	55	--	Not stated/Yes	PD, 5-24 years	Hypoglossal nucleus	Yes
	Benarroch, 2006 (67)	o	14(12)	50	--	Yes/Not stated	PD or LBD, 10 years	Nucleus ambiguus	--
Total:	**7**	**o2, m2, c2, s1**	**49(37)**						
Raphe Nuclei (RN)	Yamamoto, 1985 (195)	m	2 (1)	50-90	--	Not stated/Yes	iPD	--	--

	Halliday, 1990 (75)	c	4 (4)	0 dorsal-56 median	--	Not stated	PD	DMV	--
	Halliday, 1990 (72)	c	4 (4)	0 dorsal-44 obscurus-60 median	--	Not stated/Yes	PD	SNc + LC, PPN, DMV	--
	Gai, 1991 (51)	c	6 (5)	76	--	Not stated/Yes	iPD, 5-30 years	PPN, LTN, OPN, LC	--
	Paulus, 1991 (73)	m	23 (6)	37	--	Not stated/Yes	PD, H&Y III-V, 1-31 years	SNc, LC, RN, NBM	--
	Benarroch, 2007 (196)	m	14 (12)	60-67	--	Yes	DLB, 5-20 years	--	--
	Cheshire, 2015 (54)	s	44 (17)	None	--	Yes	PD, LID severity, 14.8 years	SNc	--
Total:	**7**	**o0, m3, c3, s1**	**97 (49)**						
Ventral Tegmental Area (VTA)	Javoy-Agid, 1984 (197)	m	2 (2)	77	--	Not stated	PD	--	--
	Hirsch, 1988 (70)	c	4 (3)	48	--	Not stated	PD	SNc, A10, A8, CGS	--
	German, 1989 (71)	c	5 (3)	42	--	Not stated/Yes	PD, 5-27 years	SNc	--
	Zweig, 1993 (157)	m	13 (14)	some	--	Yes	PD, H&Y 4.5, 11 years	LC, SNc, NBM	--
	Mouatt-Prigent, 1994 (158)	c	4 (3)	some	--	Not stated/Yes	iPD	SNc	--
	Dymecki, 1996 (198)	m	7 (6)	41-62	--	Not stated/Yes	PD, long-term	--	--
	McRitchie, 1997 (55)	s	3 (3)	31	--	Not stated/Yes	iPD, 1-27 years	A8, A10	--
	Damier, 1999 (56)	c	5 (5)	46	--	Not stated	iPD	SNc	Yes
Total:	**8**	**o0, m3, c4, s1**	**43 (39)**						
Olfactory Bulb (OB)	Pearce, 1995 (60)	m	7 (7)	57	--	Not stated/Yes	PD, 8-19 years	--	--
	Huisman, 2004 (61)	s	10 (10)	increase of 100	--	Not stated/Yes	PD, 4-23 years	--	--
	Huisman, 2008 (62)	s	20 (19)	increase of 100 in female	--	Yes	iPD, 3-30 years	--	--
	MundinaNo, 2011 (63)	s	6 (15)	increase of 100	--	Not stated/Yes	PD, Braak stage II-V	--	--
Total:	**4**	**o0, m1, c0, s3**	**43 (51)**						
Thalamus	Xuereb, 1991 (155)	m	5 (5)	None	--	Not stated/Yes	PD	Thalamus (multiple nuclei)	--
	Henderson, 2000 (199)	c	9 (10)	40-55	--	Not stated/Yes	PD, H&Y II-V, 7.2 years	Caudal intralaminar nuclei, limbic thalamic nuclei	--
	Henderson, 2000 (57)	s	9 (8)	50-70	--	Not stated/Yes	PD, H&Y II-V, 3-17 years	SNc, Centromedian–parafascicular complex, mediodorsal or anterior principal nucleus	--
	Halliday, 2005 (58)	s	9 (9)	None	--	Not stated/Yes	PD, H&Y II-V, 9 years	Motor thalamus, Cortex	--
Total:	**4**	**o0, m1, c1, s2**	**32(32)**						
Sympathic/parasympathic ganglia	Rajput, 1976 (147)	o	6 (1)	some	--	Not stated	iPA, H&Y, 3-18 years	SN, LC, DMV, Cortex, Hypothalamus	--
	Wakabayashi, 1997 (68)	m	25 (25)	31-43	--	Not stated/Yes	PD	--	--
	Benarroch, 2006 (67)	o	14 (12)	None	--	Yes/Not stated	PD or LBD, 10 years	DMV, nucleus ambiguus	--
Total:	**3**	**o2, m1, c0, s0**	**45 (38)**						
Cortex	Rajput, 1976 (147)	o	6 (1)	None	--	Not stated	iPA, H&Y, 3-18 years	SN, LC, DMV, Hypothalamus, Intermediolateral spinal cord, sympathetic ganglia	--

	Pedersen, 2005 (200)	s	10 (12)	None	--	Not stated/Yes	PD, 2-25 years	--	--
Total:	**2**	**o1, m0, c0, s1**	**16 (13)**						
Pre-supplementary and premotor cortex	MacDonald, 2002 (201)	m	5 (5)	32-45	--	Yes	PD, 10-17 years	--	--
	Halliday, 2005 (58)	s	9 (9)	None	--	Not stated/Yes	PD, H&Y II-V, 9 years	Motor thalamus	--
Total:	**2**	**o0, m1, c0, s1**	**14 (14)**						
Amygdala, corticomedial complex	Harding, 2002 (69)	s	**18 (16)**	30	--	Yes	PD, 13 years	--	--
Hippocampus	Joelving, 2006 (202)	s	**8 (8)**	None	--	Not stated/Yes	PD, 2-25 years	--	--
Laterodorsal tegmental Nucleus (LTN)	Gai, 1991 (51)	c	**6 (5)**	41	--	Not stated/Yes	iPD, 5-30 years	PPN, OPN, RN, LC	Yes
Oral pontine reticular Nucleus (OPN)	Gai, 1991 (51)	c	**6 (5)**	41	--	Not stated/Yes	iPD, 5-30 years	PPN, LTN, RN, LC	Yes

Table I. List of 90 studies quantifying the loss of neurons in the brain in PD.

Included in the table are the technique used for quantification (o, observation; m, manual c, computer assisted; s, stereological counting), the number of subjects and controls (ctrl) studied, the estimated % loss of neurons, any particularity in the comparison group, mention if studies were performed blind and with age-matched controls, the stated diagnosis, scale of severity and disease duration when mentioned and note on other regions counted. Where an average value of loss was not given by authors, this number was calculated from available data.

ABREVIATIONS: AD, Alzheimer Disease; ADLB, Alzheimer's Disease with Lewy bodies; ADNLB, Alzheimer's Disease with no Lewy bodies; ALS, Amyotrophic Lateral Sclerosis; CBS, corticobasal syndrome; CGS, central grey substance; CJD, Creutzfeldt-Jakob disease; ctrl, control; DLB, dementia with Lewy bodies; H&Y, Hoehn and Yahr scale; iPA, idiopathic paralysis agitans; LBD or iLBD, Lewy body disease or idiopathic Lewy body disease; LDB or iLDB, dementia with Lewy bodies or idiopathic dementia with Lewy bodies; LID, levodopa (L-DOPA)–induced dyskinesias; MS, multiple sclerosis; MSA, multiple system atrophy; NPH, normal pressure hydrocephalus; PD or iPD, Parkinson’s Disease or idiopathic Parkinson’s Disease; PSP, progressive supranuclear palsy; UPDRS, unified Parkinson Disease rating scale.

2.11 Figure 1

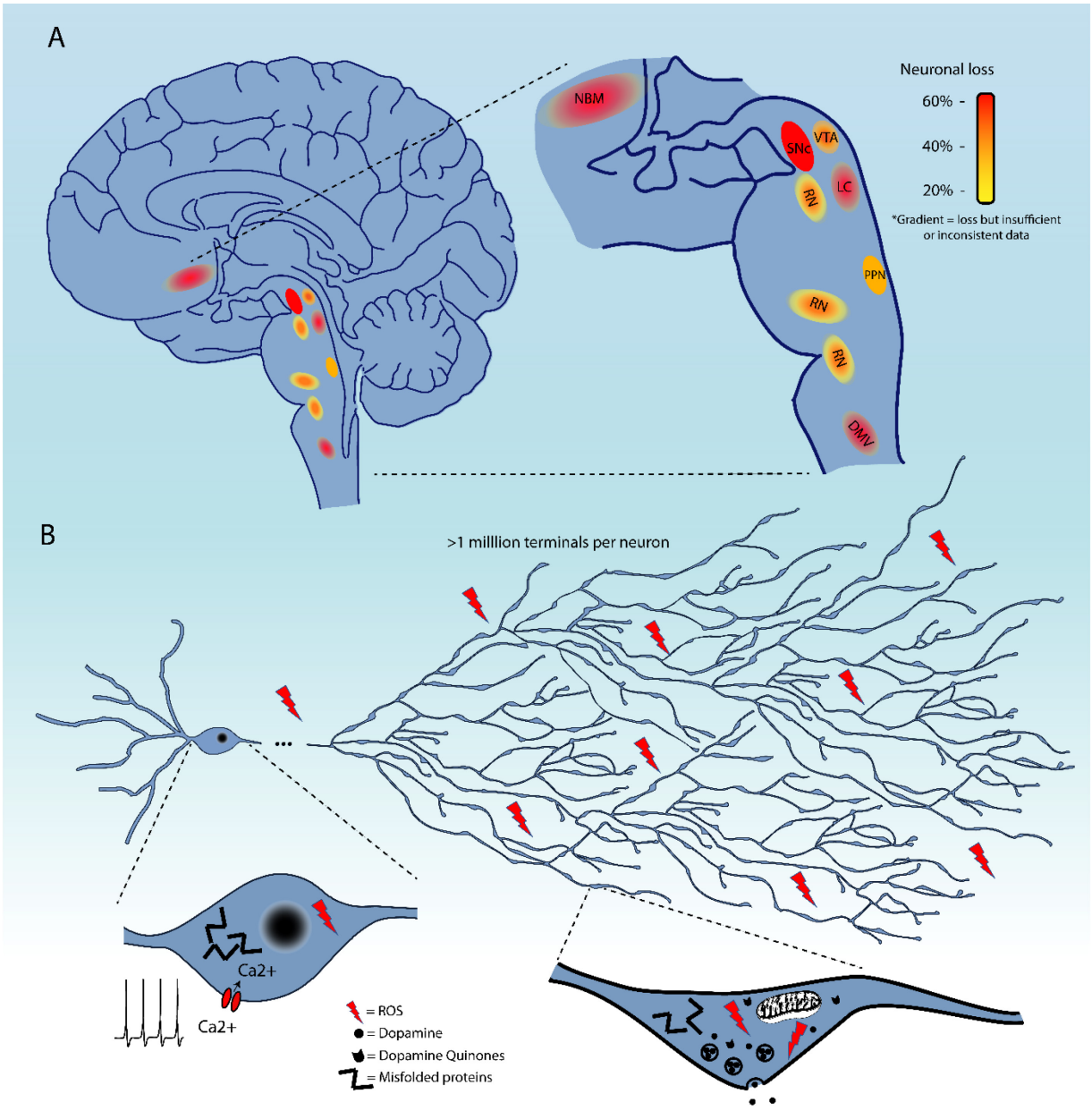
A
Neuronal loss
60% -
40% -
20% -
*Gradient = loss but insufficient or inconsistent data
NBM
SNc
VTA
LC
RN
PPN
RN
RN
DMV
B
>1 milllion terminals per neuron
Ca2+
Ca2+
= ROS
= Dopamine
= Dopamine Quinones
= Misfolded proteins

Figure 1. Selective vulnerability in Parkinson's Disease.

(A) Schematic representation of brain regions demonstrating cell loss in Parkinson's disease. These are colour-coded based on the evidence of cell loss. Red = 60%, orange = 40%, and yellow = 20%. Colour gradients indicate uncertainty in the extent of this cell loss.

(B) Summary of the converging hypotheses that may explain the origins of the selective vulnerability of neurons in Parkinson's disease. This includes the exceptionally large axonal arbor of PD-affected neurons, their electrophysiological properties, including calcium-dependent pacemaking, and high levels of oxidant stress in the somatodendritic and axonal domain, all thought to be contributing to cellular dysfunction and cell loss. Pathological protein aggregation and reactive dopamine quinones are considered as additional precipitating factors.

Chapitre 3 : Hypothèses et résultats

Tel que décrit dans la section précédente, il est fort possible que la vulnérabilité sélective des neurones dopaminergiques de la SNc dans la MP soit due à la demande métabolique massive induite par leur arborisation axonale de taille particulièrement importante, en comparaison aux neurones dopaminergiques voisins de la VTA qui semblent dégénérer de façon moins importante [61, 19]. Toutefois, une comparaison quantitative de la densité de l'arborisation axonale des neurones dopaminergiques de ces deux régions n'était pas disponible avant les travaux de cette thèse.

Notre première hypothèse, testée à l'aide d'une préparation de neurones dopaminergiques en culture, était que la susceptibilité plus importante des neurones dopaminergiques de la SNc par rapport à ceux de la VTA dans la MP pouvait s'expliquer par une différence dans la taille de leur arborisation axonale. En effet, le maintien d'une plus grande arborisation axonale chez les neurones de la SNc induirait une plus grande charge énergétique et rendrait ces neurones plus susceptibles à diverses toxines environnementales. La diminution subséquente de la taille de cette arborisation, à l'aide d'un facteur de guidage axonal, devrait réduire cette demande énergétique et du fait même la vulnérabilité (Article II). L'utilisation d'un modèle de culture primaire avait pour avantage de nous permettre de mesurer spécifiquement les besoins bioénergétiques des neurones dopaminergiques de la SNc et de la VTA à l'aide d'un analyseur de flux extracellulaire qui mesure en temps réel la variation de la concentration d'oxygène, ainsi que les changements de pH. Puisque la phosphorylation oxydative est le processus consommant la majorité de l'oxygène chez les neurones et puisqu'un des sous-produits de la glycolyse est l'acide lactique, il est possible d'extrapoler les changements de concentration d'oxygène et de pH pour déduire la production d'énergie par la phosphorylation oxydative et par la glycolyse respectivement. Le modèle de culture permet aussi de tester rapidement des molécules pouvant moduler la croissance axonale et la survie.

Notre seconde hypothèse était que les mutations présentes dans les formes familiales de la MP telles que Parkin, Pink1 et DJ-1 pourraient induire des changements détectables dans la

taille de l'arborisation axonale, dans la vulnérabilité et/ou dans les besoins énergétiques de façon différentielle chez les neurones dopaminergiques de la SNc et de la VTA (Article III). Nous avons choisi ces mutations parce qu'elles sont celles dont les liens avec la fonction mitochondriale sont les plus clairs. Nous avons choisi d'utiliser notre modèle de culture pour les mêmes raisons qui celles citées ci-haut.

Notre troisième hypothèse était que l'augmentation de la taille de l'arborisation axonale des neurones dopaminergiques de la SNc *in vivo*, à l'aide du knock-out sélectif du récepteur D2 chez ceux-ci, augmenterait la vulnérabilité de ces neurones à un modèle de lésion à la 6-OHDA ou à la surexpression de l'α-synucléine (Article IV). Nous avons choisi ce modèle parce qu'il nous permettait de moduler sélectivement la taille de l'arborisation axonale des neurones dopaminergiques, sans nous inquiéter des conséquences du knock-out sur les autres populations neuronales. Le modèle de lésion à la 6-OHDA a été sélectionné pour sa robustesse, pour sa spécificité pour les neurones dopaminergiques et parce qu'il réplique bien la pathologie initiée au niveau des terminaisons axonales. Nous avons aussi utilisé le modèle de surexpression de l'α-synucléine puisqu'il s'apparente mieux à la maladie, bien qu'il soit moins spécifique et qu'il induise généralement une neurodégénérescence moins importante.

Chapitre 4 : L'étendue axonale comme facteur de vulnérabilité *in vitro* (Article II)

L'article qui suit présente les travaux qui nous ont permis en culture d'affirmer que les neurones dopaminergiques de la SNc ont une arborisation axonale de taille particulièrement importante par rapport aux neurones de la VTA, ce qui augmente leurs besoins énergétiques et les rend plus vulnérables. Nous avons aussi montré que la diminution de la taille de cette arborisation réduit les besoins bioénergétiques et rend les neurones moins vulnérables à différentes toxines mitochondriales.

Contributions des auteurs

Nicolas Giguère : Conception et exécution des expériences reliées aux enregistrements électrophysiologiques et à l'imagerie et la survie neuronale. Analyse des données et écriture du manuscrit.

Consiglia Pacelli : Conception et exécution des expériences reliées à la fonction mitochondriale. Analyse des données et écriture du manuscrit.

Marie-Josée Bourque : Préparation des cultures cellulaires.

Martin Lévesque : Planification des expériences sur la sémaphorine 7A et révision du manuscrit.

Ruth S. Slack : Don de réactifs et révision du manuscrit.

Louis-Éric Trudeau : Conception, coordination et supervision du projet et écriture du manuscrit.

*Nicolas Giguère et Consiglia Pacelli sont co-premiers auteurs.

Publié dans la revue « Current Biology » le 20 juillet 2015.
https://doi.org/10.1016/j.cub.2015.07.050

Elevated mitochondrial bioenergetics and axonal arborization size are key contributors to vulnerability of dopamine neurons

Consiglia Pacelli[1,*], Nicolas Giguère[1,*], Marie-Josée Bourque[1], Martin Lévesque[2], Ruth S. Slack[3], Louis-Éric Trudeau[1]

[1]Departments of pharmacology and neurosciences
Central Nervous System Research Group (GRSNC)
Faculty of Medicine, Université de Montréal, Québec, H4T 1J4 Canada
[2]Department of psychiatry and neurosciences, Centre de Recherche de l'Institut Universitaire en Santé Mentale de Québec, Faculté de Médecine, Université Laval,
Québec, Québec, G1J 2G3 Canada
[3]Department of cellular and molecular medicine
Faculty of Medicine, University of Ottawa, Ottawa, Ontario, K1H 8M5 Canada

Author contribution: *These authors are co-first authors

4.1 Abstract

Although the mechanisms underlying the loss of neurons in Parkinson's disease are not well understood, impaired mitochondrial function and pathological protein aggregation are suspected as playing a major role. Why DA (dopamine) neurons and a select small subset of brain nuclei are particularly vulnerable to such ubiquitous cellular dysfunctions is presently one of the key unanswered questions in Parkinson's disease research. One intriguing hypothesis is that their heightened vulnerability is a consequence of their elevated bioenergetic requirements. Here we show for the first time that vulnerable nigral DA neurons differ from less vulnerable DA neurons such as those of the VTA (ventral tegmental area) by having a higher basal rate of mitochondrial OXPHOS (oxidative phosphorylation), a smaller reserve capacity, a higher density of axonal mitochondria, an elevated level of basal oxidative stress and a considerably more complex axonal arborization. Furthermore, we demonstrate that reducing axonal arborization by acting on axon guidance pathways with Semaphorin 7A reduces in parallel the basal rate of mitochondrial OXPHOS and the vulnerability of nigral DA neurons to the neurotoxic agents MPP+ (1-methyl-4-phenylpyridinium) and rotenone. Blocking L-type calcium channels with isradipine was protective against MPP+ but not rotenone. Our data provide the most direct demonstration to date in favor of the hypothesis that the heightened vulnerability of nigral DA neurons in Parkinson's disease is directly due to their particular bioenergetic and morphological characteristics.

4.2 Introduction

Parkinson's disease is a chronic progressive neurodegenerative disorder characterized by the selective loss of DA-containing neurons in the SNc (substantia nigra compacta). Although the mechanisms underlying the loss of neurons in idiopathic forms of Parkinson's disease are not well understood, impaired mitochondrial function and pathological protein aggregation are suspected as playing a major role. Why DA neurons and a select small subset of brain nuclei are particularly vulnerable to such ubiquitous cellular dysfunctions is presently one of the key unanswered questions in Parkinson's disease research.

A recent hypothesis proposes that SNc DA neurons are particularly vulnerable because they are autonomous pacemakers dependent on L-type voltage-dependent Ca^{2+} channels of the Cav1.3 type, leading to extensive Ca^{2+} influx and associated ATP-dependent extrusion mechanisms (1–3). The elevated rate of mitochondrial OXPHOS required to meet the cell's demands in ATP (4) has been hypothesized to lead to oxidative stress and contribute to the heightened vulnerability of these neurons (5).

Another emerging hypothesis proposes that the selectively vulnerability of DA neurons and other cell groups in Parkinson's disease can be explained in large part by the fact that they establish an unusually large axonal arborization and number of axon terminals (6–8). Such a morphological phenotype can be hypothesized to be associated with particularly high demands in ATP to sustain neurotransmission along profuse axons (9–11).

These two non-mutually excluding hypotheses both imply high energy demands with an expected elevated rate of OXPHOS and associated ROS (reactive oxygen species) production, potentially leading to cellular damage in the context of ageing. Crucial key information is presently missing to support this general model of DA neuron vulnerability in Parkinson's disease. So far, no published data has demonstrated that vulnerable DA neurons in the SNc indeed have elevated energetic requirements compared for example to DA neurons of the closely located VTA that are considerably less affected in Parkinson's disease. In addition, no

quantitative comparisons have been made comparing the axonal arborization of SNc and VTA DA neurons and it has never been demonstrated that a large axonal arborization increases basal energetic demands and OXPHOS.

Here we show that the more vulnerable SNc DA neurons differ from VTA DA neurons in that they show higher basal respiration, higher axonal mitochondrial density, elevated ROS production, a much more complex axonal arborization and increased vulnerability to neurotoxic agents MPP+ (1-methyl-4-phenylpyridinium), rotenone and H_2O_2. Furthermore, we provide evidence that manipulating basal energy demands has a predictable effect on neuronal vulnerability. Our data provide strong support in favor of the hypothesis that the particular bioenergetic and morphological characteristics of nigral DA neurons underlie their heightened vulnerability in Parkinson's disease.

4.3 Results

4.3.1 SNc DA neurons show elevated basal oxidative phosphorylation and elevated ROS production

Experiments were performed using a mouse DA neuron primary culture system in which DA neurons microdissected from the SNc and VTA (Figure S1) were grown on a supporting monolayer of astrocytes. The characteristics of SNc and VTA neurons were also compared to those of olfactory bulb (OB) DA neurons, expected to be quite different because they are local projection neurons and used here as a control, to demonstrate that our model is able to recapitulate some of the known morphological differences between different classes of DA neurons. As a first test of our global hypothesis, we estimated mitochondrial OXPHOS by measuring cellular respiration. We measured both basal and maximal (uncoupled with CCCP) OCR (oxygen consumption rate) in living neurons, examined at 10 days *in vitro* (DIV), a time point at which neurons are sufficiently mature and have a large number of functional axon

terminals. The OCR measured from purified astrocyte cultures, considerably lower compared to the signal measured from mixed neuron/astrocyte cultures, was subtracted in each experiment to estimate the signal arising from neurons (Figure S2).

An analysis of basal OCR in SNc, VTA and OB cultures revealed that OCR in SNc neurons was 64.6% higher compared to VTA neurons and more than 4-fold higher (423.2%) compared to OB (olfactory bulb) neurons (Figure 1A). In the presence of the mitochondrial uncoupler CCCP, maximal OCR in SNc and VTA cultures were not statistically different, although they were still elevated compared to OB neurons (Figure 1B). An evaluation of the RCR (respiratory control ratio), calculated as the ratio between basal and maximal OCR, revealed that this ratio was 19.3% lower in SNc compared to VTA neurons, with no statistically significant difference between VTA and OB neurons (Figure 1C). These results suggest that SNc DA neurons are near their maximal capacity at basal state and less capable than other DA neurons of increasing their production of energy when required. Basal glycolysis was not significantly different between SNc and VTA DA cultures (Figure S3A).

Because these primary cultures included other neuron types in addition to DA neurons, we validated our main conclusions using DA neurons FACS (fluorescence-activated cell sorting) purified from TH-EGFP transgenic mice (Figure 1D-F). We found that in these cultures, in which all neurons were dopaminergic, the difference in basal OCR between SNc and VTA or OB cultures was even larger than in standard mixed cultures, with SNc DA neurons showing a close to 3-fold increase (274 %) relative to VTA or OB (295%) DA neurons (Figure 1D). Importantly, GFP-negative non-DA neurons obtained from the same SNc tissue blocks did not show a similarly elevated basal OCR, thus revealing that the elevated basal OCR in SNc cultures arises specifically from DA neurons (Figure 1D). Additionally, the RCR in purified SNc DA neurons was even smaller than that estimated in mixed cultures, with a value close to 100% (122%), thus further highlighting the fact that SNc DA neurons operate at basal state close to their maximal rate of OXPHOS (Figure 1E). Basal glycolysis was also significantly elevated in purified SNc compared to VTA DA neurons (Figure S3B).

A consequence of OXPHOS is the generation of cellular ROS (13). Mitochondria are widely recognized as the main source of superoxide in cells (14). To evaluate if the elevated OCR in SNc DA neurons resulted in an increased mitochondrial ROS production, we took advantage of the cell-permeant superoxide indicator MitoSOX red, known to selectively target mitochondria where it is rapidly oxidized by superoxide (Figure 1G). Quantification of MitoSOX signal at the axon terminals of SNc and VTA DA neurons revealed highly elevated ROS production in SNc compared to VTA terminals (Figure 1H). Similar results were obtained with the broad-spectrum superoxide sensor DHE (Figure S4).

Elevated OXPHOS and glycolysis in SNc compared to VTA DA neurons could result from activity-dependent mechanisms such as neurotransmitter release (15). To test this hypothesis, we first examined basal firing rate in these neurons. Patch-clamp recording from GFP-positive DA neurons at 10 DIV (Figure 2A) revealed that the basal firing rate of SNc DA neurons was in fact lower than that of VTA DA neurons (Figure 2B), arguing that an elevated firing rate is not the main explanation for the increased oxidative metabolism in SNc neurons compared to VTA neurons. We next used the sodium channel blocker tetrodotoxin (TTX) (1µM) to block neuronal firing (complete block after 5 min; n= 10 for SNc and n= 11 for VTA; results not shown). We found that blocking firing caused a significant drop in basal OXPHOS selectively in SNc DA neurons (Figure 2C) without affecting basal ECAR (Figure S3C). In the presence of TTX, basal OCR was not significantly different between SNc and VTA DA neurons (Figure 2D), arguing that a larger proportion of basal OCR in SNc DA neurons derives from activity-dependent cellular processes such as firing and neurotransmitter release.

4.3.2 SNc DA neurons display a larger axonal arborization compared to VTA and OB DA neurons

Because this parameter is hypothesized to be one of the causes of the elevated metabolic activity of SNc DA neurons, we next compared the size of the axonal arborization of cultured SNc, VTA and OB DA neurons using semi-automated single neuron tracing (Figure 3A). At 3 and 7 DIV respectively, the axonal arborization of SNc DA neurons was 113% and 69% larger than that of VTA DA neurons and 545% and 326% larger than that of OB DA neurons (Figure

3B, C). Similar differences were observed when comparing the number of axonal processes at 3 and 7 DIV respectively (Figure 3D, E). Confirmatory results were obtained by analyzing axonal complexity using a Sholl analysis (Figure S5). A similar analysis of the dendritic arborization of DA neurons revealed modest differences between SNc and VTA DA neurons at 3 DIV and no significant differences at 7 DIV (Figure S6).

4.3.3 SNc DA neurons show enhanced density of mitochondria and elevated ATP production

An elevated rate of OXPHOS in SNc DA neurons could be due to more active mitochondria, a higher density of mitochondria or a combination of both. We took advantage of viral-mediated overexpression of DsRed2-mito to visualize the distribution and density of the mitochondrial network in cultured DA neurons (Figure 4A). Mitochondrial density, normalized over process length, was two-fold higher in the axonal compartment of SNc DA neurons compared to VTA DA neurons (Figure 4B). There was no such difference in the dendritic compartment (Figure 4C) or in the cell body (Figure 4D). This result suggests that the mitochondrial density or content of SNc DA neurons is increased in a spatially restricted manner. Taking into account the previously described increase in SNc axonal arborization size, the difference in total mitochondrial mass is thus expected to be even larger.

As an increase in mitochondrial density and basal rate of OXPHOS is predictive of increased ATP production, we next investigated the relative contribution of mitochondrial OXPHOS to ATP production. We measured intracellular basal ATP content in SNc, VTA and OB neurons both in the absence and in the presence of oligomycin, a specific inhibitor of the mitochondrial F1F0-ATP-synthase, used here to confirm the involvement of OXPHOS as the source of ATP production. Although it was not possible to distinguish between DA and non-DA neurons, SNc neurons showed a significantly increased oligomycin-sensitive ATP content compared to VTA neurons (Figure 4E), compatible with their elevated basal respiration. Oligomycin induced a decrease of approximately 80% of the levels of cellular ATP (Figure 4F), compatible with a primary role of OXPHOS rather than glycolysis in the production of ATP in our model.

Our observations showing increased mitochondrial density in SNc DA neurons suggest the possibility of an increased rate of mitochondrial biogenesis in these neurons. We used qPCR to examine the level of expression of PGC-1α (peroxisome proliferator-activated receptor γ coactivator), a well-known regulator of mitochondrial function and biogenesis (16). A significant increase in PGC-1α was detected in SNc DA neurons compared to VTA DA neurons (Figure 4G), compatible with an increased rate of mitochondrial biogenesis in these neurons.

4.3.4 SNc DA neurons show enhanced vulnerability to cytotoxic aggression

SNc DA neurons are well established to be more vulnerable to DA neuron-specific toxins such as 6-OHDA (6-dhydroxydopamine) and MPTP (1-methyl-4-phenyl-1,2,3,6-tetrahydropyridine) or its derivative MPP+ (17). However, whether this increased vulnerability is fully cell autonomous and maintained *in vitro* and whether it is also expressed in response to less selective agents such as mitochondrial toxins is less well established. Following our hypothesis, SNc DA neurons should be more affected by those toxins since they show less respiratory reserve capacity and increased ROS production due to their large bioenergetic requirements. We examined the DA neuron-specific neurotoxin MPP+, known to be up taken in DA neurons through the DA transporter (DAT) and the membrane-permeable mitochondrial complex-I blocker rotenone. We found that MPP+ at doses of 5 or 10 μM induced significantly more loss of SNc DA neurons compared to VTA DA neurons (Figure 5A). A similar increased vulnerability was observed for rotenone, tested at 25 and 50 nM, with again the SNc DA neurons being most vulnerable (Figure 5B). Finally, SNc DA neurons were also more vulnerable to direct oxidative stress induced by H_2O_2 (100 μM) (Figure 5C), illustrating that SNc DA neurons show elevated vulnerability to a broad range of cellular stressors, independently of the route of entry independently or of a direct toxic effect on mitochondria or microtubule function, two cellular targets of MPP+ and rotenone (18, 19), compatible with their higher basal level of OXPHOS and ROS production.

4.3.5 Sema7A Implication of L-type calcium channels in basal bioenergetics and vulnerability of SNc but not VTA neurons

Following initial experiments evaluating the impact of elevating basal OXPHOS using the AMPK (5'-AMP-activated protein kinase) activator AICAR, which proved unable to reduce vulnerability (Figure S7), we next examined the impact of reducing basal OXPHOS. Elevated intracellular Ca^{2+} resulting from Cav1.3 L-type Ca^{2+}channel activity, a class of channels known to contribute to the pacemaking of SNc DA neurons (3), has been proposed to place a high load on cellular energy stores and contribute to the vulnerability of these neurons (5). Reducing L-type channel activation is expected to decrease basal OCR in DA neurons, something that has not been previously demonstrated. Reducing activation of L-type Ca^{2+}channels with the negative allosteric regulator isradipine (1 µM) for 1h produced a small (22%) but significant reduction in basal OCR in SNc cultures compared to control (Figure 6A). No significant change was detected in VTA neurons. Interestingly, the small reduction in OCR observed in SNc neurons did not abolish the difference in basal OCR between SNc and VTA cultures (Figure 6B), arguing that other factors such as axonal arborization size are important determinants of basal bioenergetic expenditures in SNc DA neurons. As expected from previous studies (20, 21), isradipine had no effect on the average firing rate of SNc or VTA DA neurons (Figure 6C). However, it significantly reduced the vulnerability of SNc DA neurons to MPP+ (5 µM) (Figure 6D), with 28% more DA neurons surviving in the isradipine-treated group. However, isradipine had no pro-survival effect against rotenone (50 nM) toxicity (Figure 6E), even if applied chronically (Figure 6F).

4.3.6 Sema7A reduces axonal arborization, basal OXPHOS and ROS production in SNc but not VTA DA neurons

Recent work has demonstrated the expression of Sema7A in the ventral midbrain (22–24) and the importance of this guidance factor for the axonal arborization of DA neurons (25) (Chabrat & Lévesque, in preparation). Here we examined the possibility to directly manipulate the axonal arborization of DA neurons to allow a more direct test of the hypothesis that the selectively vulnerability of SNc DA neurons is due in part to their larger axonal arborization

and associated lower OCR and oxidative stress. Sema7A (0.5µg/mL at 0 and 5 DIV), significantly reduced the size of the axonal arborization of SNc DA neurons (46%) but not of VTA DA neurons (Figure 7A, B). This was not accompanied by any change in the dendritic arborization (Figure 7C) or basal survival (Figure 7D) of these neurons. In close parallel to this decrease in axonal arborization, basal OCR was significantly reduced (39%) in SNc neurons treated with Sema7A compared to control (Figure 7E), bringing basal OCR in SNc neurons to a level similar to that of VTA neurons (Figure 7F). A similar tendency was observed for uncoupled OCR (Figure 7G), although this did not reach statistical significance. A significant increase of 51% in the RCR was selectively detected in SNc DA neurons (Figure 7H). Strikingly, Sema7A treatment was neuroprotective, significantly decreasing the vulnerability of SNc DA neurons to both MPP+ (Figure 7I) and rotenone (Figure 7J). Neuronal survival was increased by 18% in response to MPP+ and 27% in response to rotenone in the Sema7A-treated groups. To evaluate if the effect of Sema7A on basal OXPHOS and axonal arborization decreased ROS production, we measured superoxide levels using MitoSOX red and DHE. Quantification of superoxide production using both of these indicators showed a significant reduction after Sema7A treatment only in SNc DA neurons (Figure 7K-L).

4.4 Discussion

Although a number of hypotheses have been raised, the particular vulnerability of SNc DA neurons remains unexplained and represents a central unresolved question in Parkinson's disease research. A recently proposed hypothesis suggests that the selective vulnerability of SNc DA neurons in Parkinson's disease can be explained in large part by the fact that these neurons have a particularly large axonal arborization and larger energetic requirements than less vulnerable neurons, leading to an increased rate of basal mitochondrial OXPHOS and associated production of ROS (1, 6, 8, 11). This hypothesis is not yet supported by direct published evidence.

We have here taken advantage of a novel *in vitro* system allowing direct comparisons of

DA neurons from different brain regions at the morphological and bioenergetic levels. In particular, we provide for the first time a comparison of energetic metabolism in vulnerable SNc DA neurons compared to the closely located and less vulnerable VTA DA neurons. We found that SNc DA neurons have significantly elevated basal and uncoupled mitochondrial respiration compared to VTA and OB DA neurons. Our results also highlight that SNc DA neurons have a smaller respiratory control ratio than VTA DA neurons, show an elevated ATP content and basal glycolytic flux (Figure S3). These findings suggest that at basal state, DA neurons already operate near the maximal capacity of their mitochondrial energy production capacity. This is not the case for glycolysis, which appears to be playing a more modest role in energy production at basal state (but see (15)). The combination of a chronically elevated level of ROS production together with a very small reserve capacity may make it difficult for these neurons to cope with activity-dependent fluctuations in bioenergetic demands as well as with various cellular stresses of genetic or environmental origin or associated with aging. Our second major observation is that SNc DA neurons have a much higher intrinsic capacity for axonal growth than the closely located VTA DA neurons. Together with our finding that reducing axonal arborization size with Sema7A causes a corresponding decrease in basal OXPHOS and vulnerability, our findings are compatible with the hypothesis that the development of a very large axonal arborization is one of the main reasons underlying the elevated bioenergetic demands of these neurons, thereby placing them at risk for degeneration.

SNc DA neurons are well known *in vivo* to be more vulnerable than VTA DA neurons to toxins such as 6-OHDA or MPTP (26, 27). Interestingly, OB DA neurons are also known to be more resistant to such toxins and to be preserved in Parkinson's disease (28, 29). Although mesencephalic DA neurons *in vitro* have also been shown to be sensitive to MPP+ (30, 31), the differential vulnerability of different subtypes of DA neurons *in vitro* had not been clearly demonstrated. Here we thus compared for the first time the vulnerability of SNc and VTA DA neurons, showing that as predicted, SNc DA neurons are more vulnerable to MPP+. Our finding of a similar increased vulnerability to rotenone, a membrane permeable mitochondrial complex I blocker and H_2O_2, a direct oxidative stressor, further argues that the differential vulnerability of SNc and VTA DA neurons is not simply due to differential expression of DA transporter (DAT), the main port of entry of MPP+, which is known to be expressed at higher levels in SNc

DA neurons relative to the VTA (32).

Oxidative damage due to mitochondrial dysfunction has been proposed to play an important role in Parkinson's disease pathogenesis (33). In the present work, we found that ROS content was higher in SNc compared to VTA DA neurons. Using MitoSOX red, we further demonstrate that elevated ROS is likely to be of mitochondrial origin and to occur throughout the neuron, including in axon terminals. Our results are compatible with the hypothesis that increased OXPHOS in SNc DA neurons is the main cause of the elevated ROS levels. Our finding of increased mitochondrial density in these neurons also supports this hypothesis. However, our results do not exclude that in addition, other sources of ROS such as those arising from the oxidative metabolism of DA itself (34) could also play a role.

A critical question is why DA neurons of the SNc have larger energetic requirements. A recent hypothesis proposes that a common characteristic of vulnerable neurons in Parkinson's disease is that they have a particularly large axonal arborization and a large number of axon terminals (6, 7, 9). Such a large axonal arborization and number of axon terminals would in turn place a large energetic burden on these neurons because of the need to maintain functional mitochondria and provide energy to all of these structures (8, 11). Although highly attractive, this hypothesis was not yet supported by any published evidence. In particular, no quantitative comparisons had been made comparing the axonal arborization of SNc DA neurons to that of less vulnerable DA neurons such as those of the VTA or OB. In addition, it had not been shown that a large axonal arborization indeed increases basal energetic demands, the rate of OXPHOS and the accumulation of ROS. In the present work, we found that the axonal arborization of SNc DA neurons *in vitro* is approximately two-fold larger than that of other DA neurons. This observation not only provides support for the cellular energetics/axonal arborization vulnerability hypothesis, but it also suggests that having a large axon arborization is an intrinsic property of these neurons that can be maintained *in vitro*, even in the absence of their normal target neurons. A large axonal arborization and a high number of axon terminals may underlie elevated energetic expenditures related to action potential conduction and activity-dependent axon terminal function. Compatible with this possibility, we found that blocking the firing of SNc DA neurons with TTX reduced OXPHOS to a level comparable to that of VTA neurons.

The higher energetic requirements of SNc DA neurons in relation to their large axonal arborization could in theory be met by a higher efficiency of mitochondrial ATP production and/or higher mitochondrial content. Our experiments revealed a substantially larger density of mitochondria in the axonal domain of SNc DA neurons compared to VTA DA neurons, with no significant change in the dendrites or cell body. This later finding stands in apparent contradiction with a previous brief report showing that in brain of three Swiss-Webster mice, the fractional area of the cell body of SNc DA neurons occupied by mitochondria was smaller than that of VTA DA neurons (35). However, it is unclear if the fractional area is a reliable indicator of the total mitochondrial mass. Our finding of increased expression of PGC-1α, a well-known master regulator of mitochondrial biogenesis, previously demonstrated to regulate mitochondrial density in neurons (36, 37) is also compatible with the hypothesis of increased mitochondrial biogenesis in SNc compared to VTA DA neurons. Much recent work has explored the involvement of PGC-1α in neurodegenerative diseases (38, 39), although the results of experiments evaluating the effects of overexpressing PGC-1α on the vulnerability of mouse DA have been controversial (36, 40–42). This may result from the difficulty to increase OXPHOS and ATP production without increasing oxidative stress. Compatible with this conclusion, we found that increasing OXPHOS with AICAR, a well-known activator of AMPK (43, 44), failed to decrease the vulnerability of SNc DA neurons (Figure S7). Although we found that AICAR caused a marked increase in OXPHOS that is likely to result from an increase in mitochondrial biogenesis (44), this increased mitochondrial function did not result in reduced vulnerability against MPP+ or rotenone (Figure S7), arguing that an increase in basal OXPHOS is not an ideal strategy to promote neuroprotection in SNc DA neurons, a conclusion that is compatible with previous results (36, 42).

A second characteristic that has been proposed to lead to increased energy expenditures and vulnerability in SNc DA neurons is autonomous pacemaking (2, 3, 20). It has been proposed that the pacemaker firing of SNc DA neurons is dependent on L-type voltage-dependent Ca^{2+} channels of the Cav1.3 type, leading to extensive Ca^{2+} influx (3), and that such elevated Ca^{2+} influx is associated with a considerable metabolic cost and oxidative stress (45). Although quite attractive heuristically and supported by recent work showing that L-type channel blockade can be neuroprotective (46–48), this hypothesis had not yet been supported by data demonstrating

that Ca^{2+} influx through L-type channels in SNc DA neurons indeed increases basal energetic expenditures. Our results showing that the L-type Ca^{2+} channel blocker isradipine reduces basal OCR and is protective against MPP+ fill this gap and provide support for this hypothesis. However, we found no such protective effect of isradipine on toxicity to rotenone, a finding that is at odds with a previous report (49). Further experiments will be required to test the possibility that this lack of neuroprotection is due to the broader nature of the action of this toxin.

Our observation that SNc and VTA DA neurons still differ in basal OCR in the presence of isradipine suggest that other factors such as the size of the axonal arborization are likely to be additional key players in determining the vulnerability of SNc DA neurons. Supporting this hypothesis, we found that decreasing axonal arborization size in SNc neurons by treating cells with Sema7A (25) (Chabrat & Lévesque, in preparation), dramatically decreased basal OCR, which was associated with increased neuronal survival, in essence switching SNc neurons to a VTA-like phenotype. Further experiments will be required to determine whether the neuroprotection induced by Sema7A is fully attributable to its ability to reduce axonal arborization size. It will also be interesting to determine the contribution of beta1-integrin or plexin C1 receptors in the effects of Sema7A, which is otherwise known to have positive effects of axonal growth in other systems (50, 51) (but see (52)). Finally, the developmental time course of the elevated bioenergetics and axonal characteristics of DA neurons would benefit from more detailed evaluation as the present studies were performed with neurons obtained from neonatal animals.

In summary, our work provides the most direct demonstration that the highly elaborate axonal arborization of SNc DA neurons places these neurons at risk in Parkinson's disease because it greatly increases their basal energy demands, leading to chronically elevated oxidative stress and rendering these neurons more vulnerable to perturbations of mitochondrial function, something that can occur in response to multiple factors including gene mutations, exposure to environmental toxicants and ageing.

4.5 Experimental procedures

Primary neuronal cultures and drug treatments

Cultures were prepared according to a previously described protocol, with minor variations (53). Neurons from transgenic mice expressing the GFP gene in catecholamine neurons under the control of TH promoter (TH-GFP mice) (54) were also used in electrophysiology experiments and purified by flow cytometry cell sorting for some of the metabolic flux experiments. In some experiments, MPP+ (Sigma) (5 or 10 µM) or H_2O_2 (Sigma) (100-200 µM) were added at 10 DIV (days *in vitro*) for 24 hours. In other experiments, the complex I blocker rotenone (Sigma) (25 or 50 nM) was added at 8 DIV for 72 hours. In some experiments, the L-type Ca^{2+} channel blocker isradipine (Tocris) (1 µM) was added 3h before MPP+ or rotenone for acute treatments. For chronic treatment, isradipine was additionally added after 24 and 48h in the presence of rotenone. Acute treatments with AICAR (5-aminoimidazole-4-carboxamide-1-*β*-D-ribofuranoside) (Sigma) (100 µM) were performed at 7DIV and chronic treatments with Sema7A (R&D System) (0.5µg/mL) were performed directly in the culture medium during at the time of culture preparation and again at 5 DIV. After 10 DIV, cells were used either for electrophysiology, metabolic flux experiments or immunocytochemistry. Cells treated with rotenone or MPP+ were fixed at 11 DIV and cells for single neuron morphological measurements were fixed after 3 or 7 DIV.

Metabolic flux experiments

The rate of oxygen consumption deriving from mitochondrial OXPHOS was assessed using an extracellular flux analyzer (Seahorse Biosciences).

Superoxide level determination in live primary neurons

To estimate cellular ROS production, superoxide levels were determined using the fluorescent indicator DHE (dihydroethidium) and MitoSOX.

Electrophysiology

Spontaneous firing rate was recorded in a gap-free protocol and the L-type voltage-dependent Ca^{2+} channel blocker isradipine (1 μM) was added after 5min.

Immunofluorescence

Primary antibodies used were TH-rabbit (Millipore, 1:2000), DAT-rat (Chemicon, 1:2000), MAP-2-mouse (Chemicon, 1:1000) and RFP (Rockland, 1:1000).

Mitochondrial network quantification

Mitochondria were labeled by infecting neurons with a lentivirus encoding DsRed2-mito (mitochondrially-targeted red fluorescent reporter protein) at 30 MOI at the time of plating and fixed at 10 DIV. Images were obtained by capturing confocal 1 micron z-stacks (10-15 images) at 20x.

Single neuron morphology, global neuronal morphology and survival assessment

At 3 and 7 DIV, isolated TH-positive DA neurons were randomly selected and imaged by acquiring confocal z-stacks at 20x and analyzed using NeuronJ plugin for ImageJ to reconstruct the axonal and dendritic arbor of each neuron using semi-automated tracing. When single neuron assessment was not necessary, the global size of the neurons' axonal arborization was estimated by capturing random images throughout the coverslip. These values were then normalized to the number of TH neurons with clear round nuclei on the coverslip, estimated by scanning the coverslip vertically and horizontally (cross counting) at 20x. The same counting method was used for MPP+ and rotenone survival experiments.

Real-time quantitative PCR

Cells were collected as described previously (55). Real-time quantitative PCR was performed using an Eco Real-Time PCR System (Illumina) in a volume of 15 µl. The reaction mixture included PerfeCTa® SYBR® Green FastMix (Quanta Biosciences), 5 µl of cDNA and 0.3 µM of each primer. CT values for gene products were normalized to GAPDH CT values, and comparisons were made between experimental groups, using the DCT method (CT gene of interest minus CT GAPDH) (56).

Measurement of total cellular ATP

Cellular ATP content was determined using the PerkinElmer "ATPlite" kit (PerkinElmer) according to the manufacturer's instructions.

Statistics

Parametric statistical tests were used because samples contained data with normal distributions. Data were always obtained from a minimum of 3 separate sets of experiments and presented as mean ± SEM. The level of statistical significance was established at $p < 0.05$ in one or two-way ANOVAs and two-tailed t-tests performed with the Prism 6 software (GraphPad Software, $p < 0.05$ = *, $p < 0.01$ = **, $p < 0.001$ = ***, $p < 0.0001$ = ****). The Tukey post-hoc test was used when all the means were compared to each other and the Sidak post-hoc test was used when only subsets of means were compared.

*Detailed materials and methods are available in Supplementary Materials and Methods

4.6 Acknowledgments

The authors wish to thank Dr. Kazuto Kobayashi from Fukushima University who provided the TH-GFP transgenic mice and Dr. David Park from the University of Ottawa for his comments and suggestions throughout this project. We also thank Séverine Maire and Caroline Saumure for their participation is some of the experiments. This work was funded by a grant from the Krembil Foundation and the Brain Canada Foundation as well as by a pilot project grant from Parkinson Society Canada. The GRSNC is supported by an infrastructure grant from the Fonds du Québec en Recherche, Santé (FRQS). C. Pacelli and N. Giguère both received salary support from Parkinson Society Canada.

4.7 References

1. Chan, C. S., Gertler, T. S., and Surmeier, D. J. (2010). A molecular basis for the increased vulnerability of substantia nigra dopamine neurons in aging and Parkinson's disease. Mov. Disord. *25 Suppl 1*, S63–70.

2. Guzman, J. N., Sánchez-Padilla, J., Chan, C. S., and Surmeier, D. J. (2009). Robust pacemaking in substantia nigra dopaminergic neurons. J. Neurosci. *29*, 11011–11019.

3. Surmeier, D. J., Guzman, J. N., Sanchez-Padilla, J., and Goldberg, J. A. (2011). The origins of oxidant stress in Parkinson's disease and therapeutic strategies. Antioxid. Redox Signal. *14*, 1289–1301.

4. Viola, H. M., and Hool, L. C. (2010). Cross-talk between L-type Ca2+ channels and mitochondria. Clin. Exp. Pharmacol. Physiol. *37*, 229–235.

5. Surmeier, D. J. (2007). Calcium, ageing, and neuronal vulnerability in Parkinson's disease. Lancet Neurol. *6*, 933–938.

6. Parent, M., and Parent, A. (2006). Relationship between axonal collateralization and neuronal degeneration in basal ganglia. J. Neural Transm. Suppl., 85–88.

7. Matsuda, W., Furuta, T., Nakamura, K. C., Hioki, H., Fujiyama, F., Arai, R., and Kaneko, T. (2009). Single nigrostriatal dopaminergic neurons form widely spread and highly dense axonal arborizations in the neostriatum. J. Neurosci. *29*, 444–453.

8. Bolam, J. P., and Pissadaki, E. K. (2012). Living on the edge with too many mouths to feed: why dopamine neurons die. Mov. Disord. *27*, 1478–1483.

9. Gauthier, J., Parent, M., Lévesque, M., and Parent, A. (1999). The axonal arborization of single nigrostriatal neurons in rats. Brain Res. *834*, 228–232.

10. Perier, C., and Vila, M. (2012). Mitochondrial biology and Parkinson's disease. Cold Spring Harb. Perspect. Med. *2*, a009332.

11. Pissadaki, E. K., and Bolam, J. P. (2013). The energy cost of action potential propagation in dopamine neurons: clues to susceptibility in Parkinson's disease. Front. Comput. Neurosci. *7*, 13.

12. Perier, C., and Vila, M. (2012). Mitochondrial biology and Parkinson's disease. Cold Spring Harb. Perspect. Med. *2*, a009332.

13. Balaban, R. S., Nemoto, S., and Finkel, T. (2005). Mitochondria, oxidants, and aging. Cell *120*, 483–495.

14. Lenaz, G. (2001). The mitochondrial production of reactive oxygen species: mechanisms and implications in human pathology. IUBMB Life *52*, 159–164.

15. Harris, J. J., Jolivet, R., and Attwell, D. (2012). Synaptic energy use and supply. Neuron *75*, 762–777.

16. Lin, J., Handschin, C., and Spiegelman, B. M. (2005). Metabolic control through the PGC-1 family of transcription coactivators. Cell Metab. *1*, 361–370.

17. Bove, J., Prou, D., Perier, C., and Przedborski, S. (2005). Toxin-induced models of Parkinson's disease. NeuroRx *2*, 484–494.

18. Ren, Y., Liu, W., Jiang, H., Jiang, Q., and Feng, J. (2005). Selective vulnerability of dopaminergic neurons to microtubule depolymerization. J. Biol. Chem. *280*, 34105–34112.

19. Choi, W.-S., Kruse, S. E., Palmiter, R. D., and Xia, Z. (2008). Mitochondrial complex I inhibition is not required for dopaminergic neuron death induced by rotenone, MPP+, or paraquat. Proc. Natl. Acad. Sci. U. S. A. *105*, 15136–15141.

20. Chan, C. S., Guzman, J. N., Ilijic, E., Mercer, J. N., Rick, C., Tkatch, T., Meredith, G. E., and Surmeier, D. J. (2007). "Rejuvenation" protects neurons in mouse models of Parkinson's disease. Nature *447*, 1081–1086.

21. Meredith, G. E., Totterdell, S., Potashkin, J. A., and Surmeier, D. J. (2008). Modeling PD pathogenesis in mice: advantages of a chronic MPTP protocol. Parkinsonism Relat. Disord. *14 Suppl 2*, S112–115.

22. Van den Heuvel, D. M. A., and Pasterkamp, R. J. (2008). Getting connected in the dopamine system. Prog. Neurobiol. *85*, 75–93.

23. Hernández-Montiel, H. L., Tamariz, E., Sandoval-Minero, M. T., and Varela-Echavarría, A. (2008). Semaphorins 3A, 3C, and 3F in mesencephalic dopaminergic axon pathfinding. J. Comp. Neurol. *506*, 387–397.

24. Pasterkamp, R. J., Kolk, S. M., Hellemons, A. J., and Kolodkin, A. L. (2007). Expression patterns of semaphorin7A and plexinC1 during rat neural development suggest roles in axon guidance and neuronal migration. BMC Dev. Biol. *7*, 98.

25. A. Chabrat, E. Metzakopian, P. De Koninck, S.-L. Ang, and M. Lévesque Transcription factors Lmx1a and Lmx1b regulate PlexinC1 expression and axon targeting of midbrain dopamine neurons. In Program No 126.20/B8. 2013 Neuroscience Meeting Planner.

26. Hung, H. C., and Lee, E. H. (1996). The mesolimbic dopaminergic pathway is more resistant than the nigrostriatal dopaminergic pathway to MPTP and MPP+ toxicity: role of BDNF gene expression. Brain Res. Mol. Brain Res. *41*, 14–26.

27. Luk, K. C., Rymar, V. V., van den Munckhof, P., Nicolau, S., Steriade, C., Bifsha, P., Drouin, J., and Sadikot, A. F. (2013). The transcription factor Pitx3 is expressed selectively in midbrain dopaminergic neurons susceptible to neurodegenerative stress. J. Neurochem. *125*, 932–943.

28. Yu, W. H., Matsuoka, Y., Sziráki, I., Hashim, A., Lafrancois, J., Sershen, H., and Duff, K. E. (2008). Increased dopaminergic neuron sensitivity to 1-methyl-4-phenyl-1,2,3,6-tetrahydropyridine (MPTP) in transgenic mice expressing mutant A53T alpha-synuclein. Neurochem. Res. *33*, 902–911.

29. Huisman, E., Uylings, H. B. M., and Hoogland, P. V. (2004). A 100% increase of dopaminergic cells in the olfactory bulb may explain hyposmia in Parkinson's disease. Mov. Disord. *19*, 687–692.

30. Fukuhara, Y., Takeshima, T., Kashiwaya, Y., Shimoda, K., Ishitani, R., and Nakashima, K. (2001). GAPDH knockdown rescues mesencephalic dopaminergic neurons from MPP+ -induced apoptosis. Neuroreport *12*, 2049–2052.

31. Hashimoto, T., Nishi, K., Nagasao, J., Tsuji, S., and Oyanagi, K. (2008). Magnesium exerts both preventive and ameliorating effects in an in vitro rat Parkinson disease model involving 1-methyl-4-phenylpyridinium (MPP+) toxicity in dopaminergic neurons. Brain Res. *1197*, 143–151.

32. Storch, A., Ludolph, A. C., and Schwarz, J. (2004). Dopamine transporter: involvement in selective dopaminergic neurotoxicity and degeneration. J. Neural Transm. Vienna Austria 1996 *111*, 1267–1286.

33. Chinta, S. J., and Andersen, J. K. (2008). Redox imbalance in Parkinson's disease. Biochim. Biophys. Acta BBA - Gen. Subj. *1780*, 1362–1367.

34. Graham, D. G. (1978). Oxidative pathways for catecholamines in the genesis of neuromelanin and cytotoxic quinones. Mol. Pharmacol. *14*, 633–643.

35. Liang, C.-L., Wang, T. T., Luby-Phelps, K., and German, D. C. (2007). Mitochondria mass is low in mouse substantia nigra dopamine neurons: Implications for Parkinson's disease. Exp. Neurol. *203*, 370–380.

36. Clark, J., Silvaggi, J. M., Kiselak, T., Zheng, K., Clore, E. L., Dai, Y., Bass, C. E., and Simon, D. K. (2012). Pgc-1α overexpression downregulates Pitx3 and increases susceptibility to MPTP toxicity associated with decreased Bdnf. PloS One *7*, e48925.

37. Wareski, P., Vaarmann, A., Choubey, V., Safiulina, D., Liiv, J., Kuum, M., and Kaasik, A. (2009). PGC-1{alpha} and PGC-1{beta} regulate mitochondrial density in neurons. J. Biol. Chem. *284*, 21379–21385.

38. Zheng, B., Liao, Z., Locascio, J. J., Lesniak, K. A., Roderick, S. S., Watt, M. L., Eklund, A. C., Zhang-James, Y., Kim, P. D., Hauser, M. A., et al. (2010). PGC-1α, a potential

therapeutic target for early intervention in Parkinson's disease. Sci. Transl. Med. *2*, 52ra73.

39. Pacelli, C., De Rasmo, D., Signorile, A., Grattagliano, I., di Tullio, G., D'Orazio, A., Nico, B., Comi, G. P., Ronchi, D., Ferranini, E., et al. (2011). Mitochondrial defect and PGC-1α dysfunction in parkin-associated familial Parkinson's disease. Biochim. Biophys. Acta *1812*, 1041–1053.

40. St-Pierre, J., Drori, S., Uldry, M., Silvaggi, J. M., Rhee, J., Jäger, S., Handschin, C., Zheng, K., Lin, J., Yang, W., et al. (2006). Suppression of reactive oxygen species and neurodegeneration by the PGC-1 transcriptional coactivators. Cell *127*, 397–408.

41. Mudò, G., Mäkelä, J., Di Liberto, V., Tselykh, T. V., Olivieri, M., Piepponen, P., Eriksson, O., Mälkiä, A., Bonomo, A., Kairisalo, M., et al. (2012). Transgenic expression and activation of PGC-1α protect dopaminergic neurons in the MPTP mouse model of Parkinson's disease. Cell. Mol. Life Sci. CMLS *69*, 1153–1165.

42. Ciron, C., Lengacher, S., Dusonchet, J., Aebischer, P., and Schneider, B. L. (2012). Sustained expression of PGC-1α in the rat nigrostriatal system selectively impairs dopaminergic function. Hum. Mol. Genet. *21*, 1861–1876.

43. Zong, H., Ren, J. M., Young, L. H., Pypaert, M., Mu, J., Birnbaum, M. J., and Shulman, G. I. (2002). AMP kinase is required for mitochondrial biogenesis in skeletal muscle in response to chronic energy deprivation. Proc. Natl. Acad. Sci. U. S. A. *99*, 15983–15987.

44. Jäger, S., Handschin, C., St-Pierre, J., and Spiegelman, B. M. (2007). AMP-activated protein kinase (AMPK) action in skeletal muscle via direct phosphorylation of PGC-1alpha. Proc. Natl. Acad. Sci. U. S. A. *104*, 12017–12022.

45. Dryanovski, D. I., Guzman, J. N., Xie, Z., Galteri, D. J., Volpicelli-Daley, L. A., Lee, V. M.-Y., Miller, R. J., Schumacker, P. T., and Surmeier, D. J. (2013). Calcium entry and α-synuclein inclusions elevate dendritic mitochondrial oxidant stress in dopaminergic neurons. J. Neurosci. *33*, 10154–10164.

46. Kupsch, A., Sautter, J., Schwarz, J., Riederer, P., Gerlach, M., and Oertel, W. H. (1996). 1-Methyl-4-phenyl-1,2,3,6-tetrahydropyridine-induced neurotoxicity in non-human primates is antagonized by pretreatment with nimodipine at the nigral, but not at the striatal level. Brain Res. *741*, 185–196.

47. Guzman, J. N., Sanchez-Padilla, J., Wokosin, D., Kondapalli, J., Ilijic, E., Schumacker, P. T., and Surmeier, D. J. (2010). Oxidant stress evoked by pacemaking in dopaminergic neurons is attenuated by DJ-1. Nature *468*, 696–700.

48. Ilijic, E., Guzman, J. N., and Surmeier, D. J. (2011). The L-type channel antagonist isradipine is neuroprotective in a mouse model of Parkinson's disease. Neurobiol. Dis. *43*, 364–371.

49. Yu, X., Li, X., Jiang, G., Wang, X., Chang, H. C., Hsu, W. H., and Li, Q. (2013). Isradipine prevents rotenone-induced intracellular calcium rise that accelerates senescence in human neuroblastoma SH-SY5Y cells. Neuroscience *246*, 243–253.

50. Pasterkamp, R. J., Peschon, J. J., Spriggs, M. K., and Kolodkin, A. L. (2003). Semaphorin 7A promotes axon outgrowth through integrins and MAPKs. Nature *424*, 398–405.

51. Jongbloets, B. C., Ramakers, G. M. J., and Pasterkamp, R. J. (2013). Semaphorin7A and its receptors: pleiotropic regulators of immune cell function, bone homeostasis, and neural development. Semin. Cell Dev. Biol. *24*, 129–138.

52. Uesaka, N., Uchigashima, M., Mikuni, T., Nakazawa, T., Nakao, H., Hirai, H., Aiba, A., Watanabe, M., and Kano, M. (2014). Retrograde semaphorin signaling regulates synapse elimination in the developing mouse brain. Science *344*, 1020–1023.

53. Fasano, C., Thibault, D., and Trudeau, L.-E. (2008). Culture of postnatal mesencephalic dopamine neurons on an astrocyte monolayer. Curr. Protoc. Neurosci. Editor. Board Jacqueline N Crawley Al *Chapter 3*, Unit 3.21.

54. Matsushita, N., Okada, H., Yasoshima, Y., Takahashi, K., Kiuchi, K., and Kobayashi, K. (2002). Dynamics of tyrosine hydroxylase promoter activity during midbrain dopaminergic neuron development. J. Neurochem. *82*, 295–304.

55. Mendez, J. A., Bourque, M.-J., Dal Bo, G., Bourdeau, M. L., Danik, M., Williams, S., Lacaille, J.-C., and Trudeau, L.-E. (2008). Developmental and target-dependent regulation of vesicular glutamate transporter expression by dopamine neurons. J. Neurosci. *28*, 6309–6318.

56. Livak, K. J., and Schmittgen, T. D. (2001). Analysis of relative gene expression data using real-time quantitative PCR and the $2^{-\Delta\Delta CT}$ method. Methods *25*, 402–408.

4.8 Figures

Figure 1. Increased basal respiration and ROS production in SNc compared to VTA and OB DA neurons.

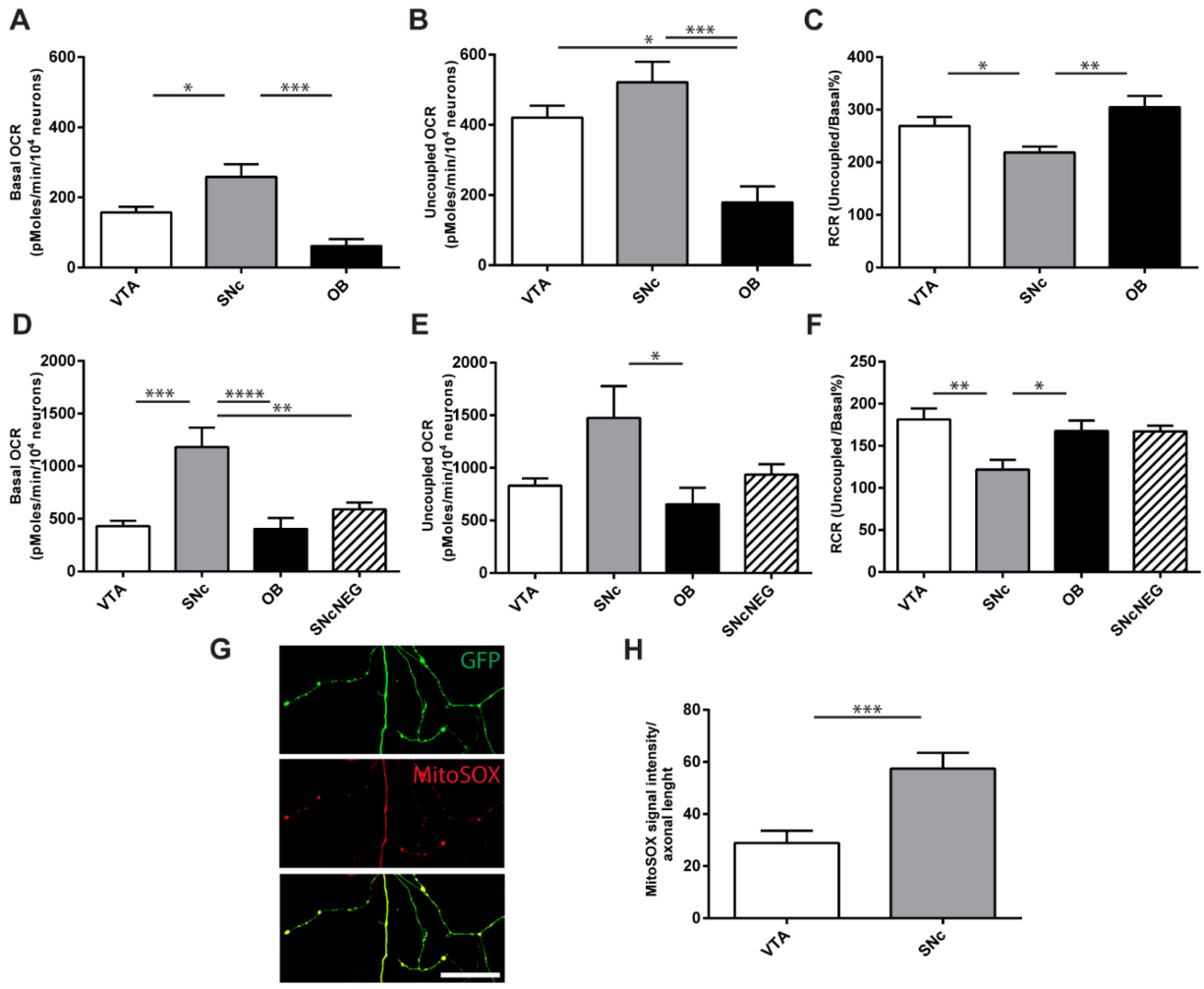

Oxygen consumption rates (OCR) were measured using a XF24 Analyzer from mixed co-cultures (A-C) and FACS-purified DA neurons (D-F) from the VTA, SNc or OB. Non-DA neurons from the SNc (SNc NEG) were analyzed as a negative control. Basal OCR was measured in mixed co-cultures (A) and FACS-purified DA neurons (D). Maximal or uncoupled OCR was measured in the presence of 0.5 μM CCCP in mixed co-cultures (B) and FACS-purified DA neurons (E). The respiratory control ratio (RCR) was calculated by dividing uncoupled by basal OCR, in mixed co-cultures (C) and FACS-purified DA neurons (The values represent the mean ± SEM, n=10-30 wells from at least 3 different cultures. * $p<0.05$; ** $p<0.01$; *** $p<0.001$; **** $p<0.0001$). G-H Intracellular ROS levels were determined using the superoxide-sensitive fluorescent dye MitoSOX. SNc and VTA DA neurons FACS-purified from TH-GFP mice were incubated 1 μM MitoSOX for 30 min. G. Representative confocal images of TH-GFP neurons and MitoSOX fluorescence. Scale bar=50μm. H. Average MitoSOX signal intensity in SNc and VTA DA neurons. Scale bars =25μm. The values represent the mean ± SEM, n=10-15 coverslips from 5 different cultures *$p<0.05$; *** $p<0.001$.

Figure 2. Decreased basal firing in SNc compared to VTA DA neurons and effect of TTX on respiration.

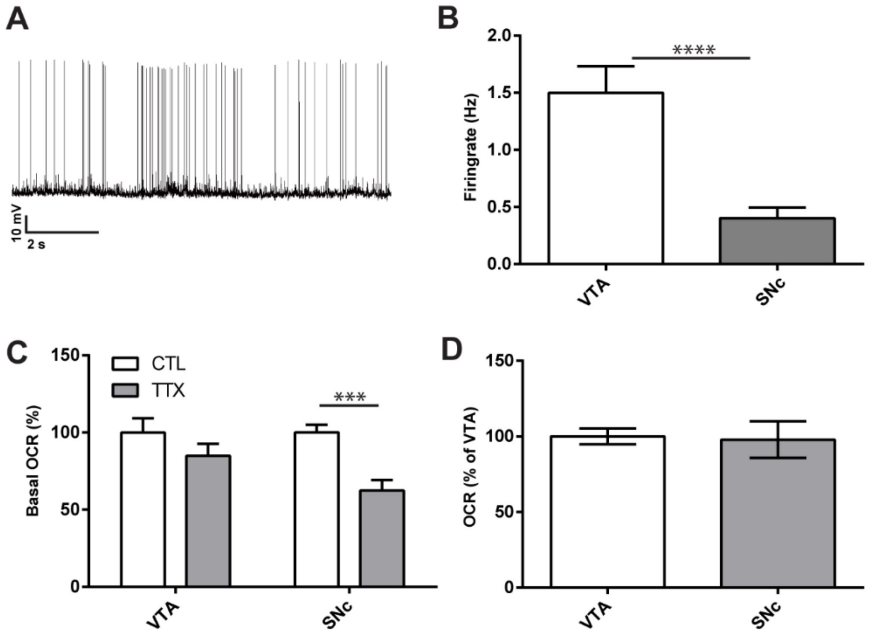

A-B. Firing rates were determined by whole cell patch-clamping. (A) Representative trace illustrating the basal firing of a cultured DA neuron. B. Average firing rate of SNc and VTA DA neurons from TH-GFP mice during 10 min recordings. The values represent the mean ± SEM, n=25 neurons, from at least 4 different cultures.**** $p<0.0001$. C-D. Effect of TTX on basal OCR. After quantifying basal respiration, 1 μM TTX was added to VTA or SNc cultures and the OCR was monitored for 1h. The effect of the Na channel blocker on basal respiration was calculated from the ratio of basal OCR to OCR in the presence of TTX. The values represent the mean ± SEM, n=10-15 wells from 4 different cultures. *** $p<0.001$. D. In the presence of TTX, basal OCR was no longer higher in SNc compared to VTA DA neurons. The values, expressed as a percentage of VTA, represent the mean ± SEM (n=10-15 wells from 4 different cultures).

Figure 3. The axonal arborization of SNc neurons is larger and more complex than that of VTA and OB DA neurons.

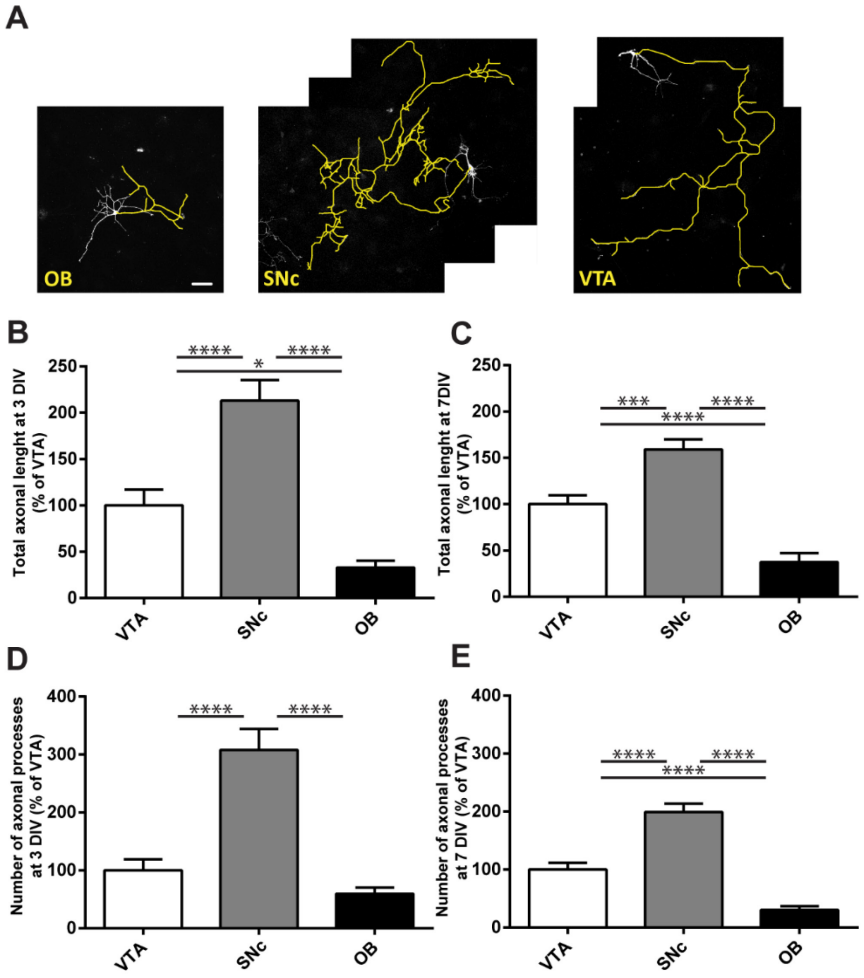

The axonal arborization of individual TH-positive DA neurons was measured by semi-automated tracing from confocal image stacks. Isolated DA neurons were randomly selected and imaged by acquiring confocal z-stacks at 20x. The longest process, which was 3 to 20 times longer than the others, was considered as the axon. The axonal arborization of cultured SNc, VTA and OB DA neurons was measured at 3 DIV and 7 DIV. The images show examples of isolated TH immunopositive neurons from each region (A) Scale bars =100µm. The total length (B, C) and number of axonal processes (D, E) were measured at 3 and 7 DIV, respectively. The data represent the mean ± SEM, n=20-35 neurons from 4 different cultures. * $p<0.05$; ** $p<0.01$; *** $p<0.001$; **** $p<0.0001$.

Figure 4. Increased density of mitochondria and ATP content in SNc compared to VTA DA neurons.

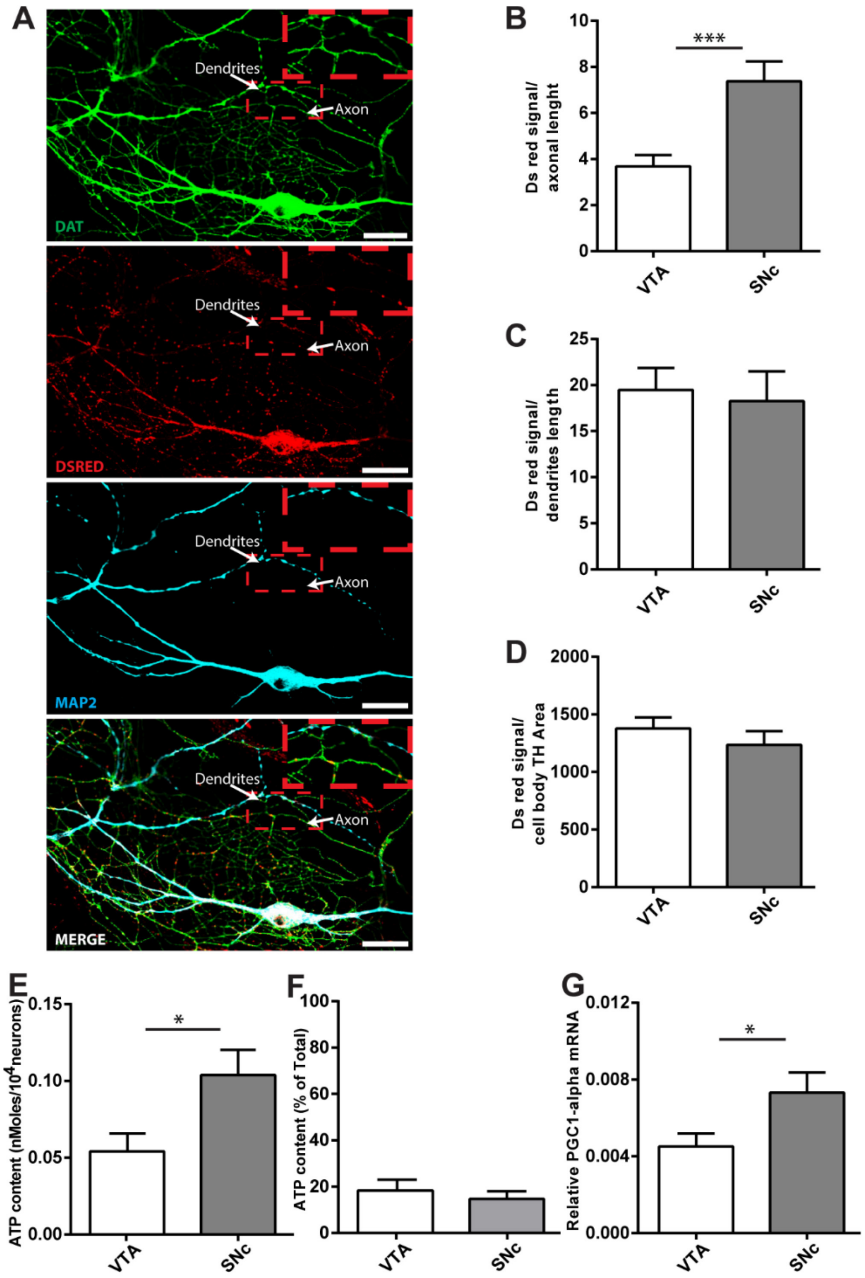

A-D. Mitochondria were localized in DA neurons after viral infection with mitoDsRed. A. Representative confocal images from DA neurons immunolabelled with DAT (green), RFP (red) and MAP-2 (cyan) antibodies. Scale bar=25µm, 1.6x zoomed area. The bar graph shows DsRed signal quantified from axons (B), dendrites (C) (normalized on axonal or dendritic length) and the cell body (D) (normalized on TH area). Values represent the mean ± SEM, n=20-40 neurons from 4 different cultures. ***$p<0.001$. E. Oligomycin-sensitive cellular ATP content under basal conditions was quantified in co-cultures prepared from the VTA, SNc and OB. Values represent the mean ± SEM, n=6 coverslips from 6 different cultures. *$p<0.05$. F. Oligomycin-insensitive cellular ATP content under basal conditions was quantified after incubation with 1 µg/ml oligomycin for 30 min. Values, expressed as a percentage of the total ATP content, represent the mean ± SEM, n=6 coverslips from 6 different cultures. G. PGC-1α mRNA levels were determined by RTqPCR from total RNA extracted from pools of ten TH-GFP DA neurons. Values were normalized to GAPDH. Values represent the mean ± SEM, n=15 samples from 5 different cultures. *$p<0.05$.

Figure 5. SNc DA neurons are more vulnerable to MPP+, rotenone and H_2O_2 than VTA DA neurons.

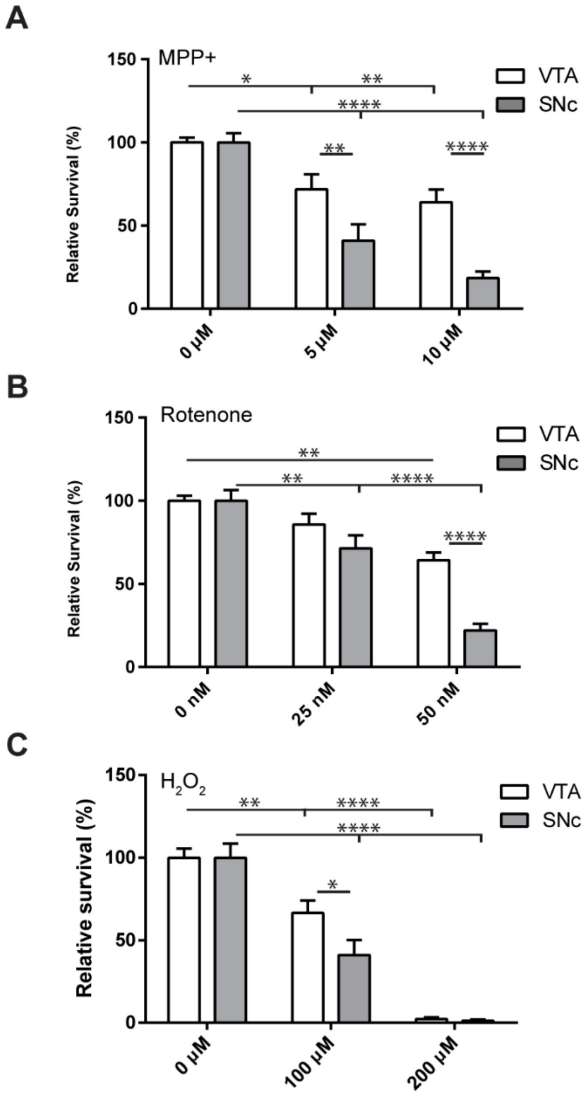

A. SNc and VTA DA neurons were treated with MPP+ (5 and 10µM, 24h) and the proportion of surviving neurons was determined by counting the number of TH-positive neurons with clear round nuclei. B. SNc and VTA DA neurons were treated with rotenone (25 and 50nM, 72h) and the proportion of surviving neurons was determined. C. SNc and VTA DA neurons were treated with H_2O_2 (100 and 200µM, 24h) and the proportion of surviving neurons was determined. Values represent the mean ± SEM, n=10-15 coverslips from at least 3 different cultures. * $p<0.05$; ** $p<0.01$; **** $p<0.0001$.

Figure 6. The L-type calcium channel blocker isradipine reduces basal respiration and vulnerability to MPP+.

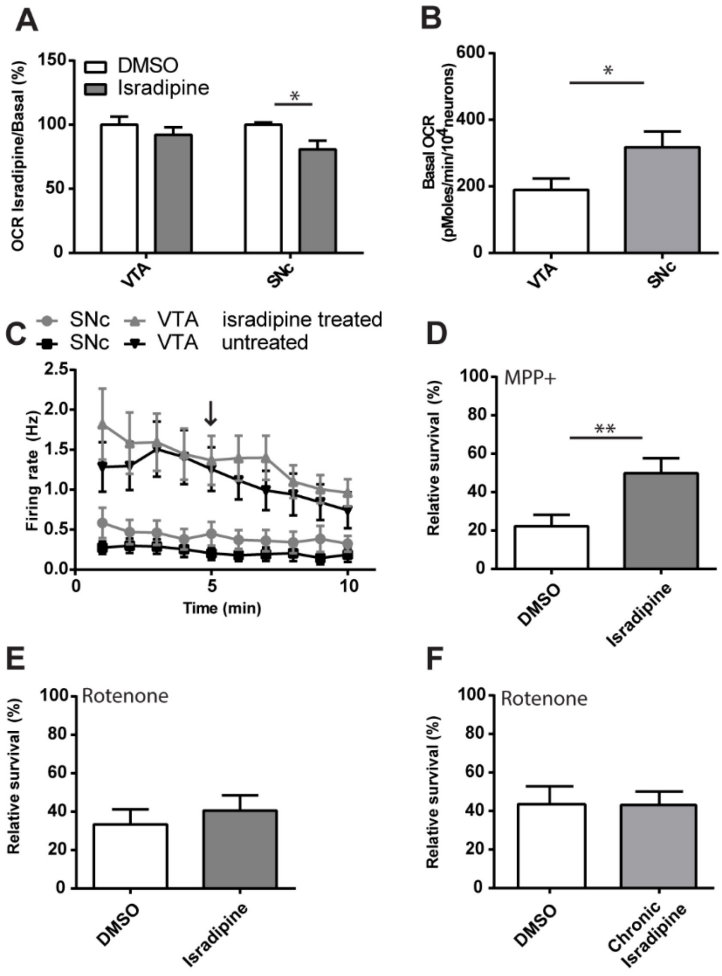

A. After quantifying basal respiration, 1 μM isradipine was added to VTA or SNc cultures and the OCR was monitored for 1h. The effect of the channel blocker on basal respiration was calculated from the ratio of basal OCR to OCR in the presence of isradipine. The values represent the mean ± SEM, n=10-15 wells from 4 different cultures. *p<0.05. B. In the presence of isradipine, basal OCR was still significantly higher in SNc compared to VTA DA neurons. The values represent the mean ± SEM, n=10-15 wells from 4 different cultures and statistically analyzed using a t-test. *p<0.05. C. The effect of isradipine on firing rate was measured using whole-cell patch-clamp recording from SNc or VTA neurons cultured from TH-GFP mice. After 5 min of baseline recording, isradipine was added for another 5 min (arrow). The values (average firing rate per one min bins) represent the mean ± SEM, n=15-20 neurons from at least 4 different cultures. The vulnerability of SNc DA neurons to MPP+ (5 μM, 24h) (D) or rotenone (50 nM, 72h) (E) was determined after a 3h pre-treatment with isradipine (1 uM) or DMSO or (F) in the case of rotenone, after a 3h pre-treatment with isradipine (1 uM) or DMSO followed by 2 additional treatments after 24 and 48h. Cells were fixed and TH-positive neurons with clear round nuclei were counted. The values represent the mean ± SEM, n=15-25 coverslips from 3 different cultures. ** p<0.01.

Figure 7. Sema7A reduces axonal arborization size, basal OCR, ROS production and vulnerability of SNc DA neurons.

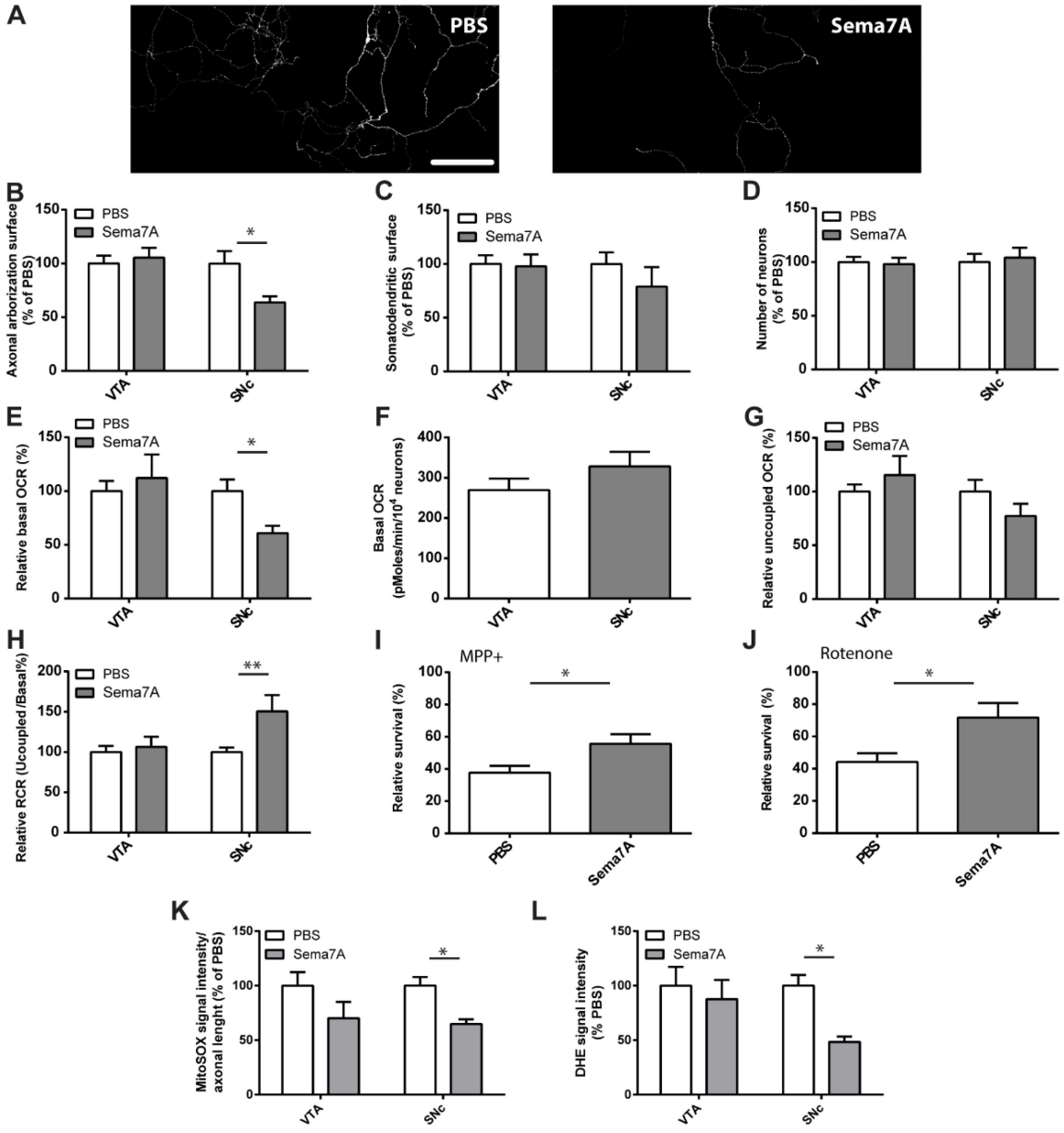

Sema7A (0.5 µg/mL) was added to the cultures at the time of cell plating and at 5 DIV. Neurons were subsequently evaluated at 10 DIV to quantify changes in basal survival and axonal arborization. A. Example of axonal TH-immunolabelling of SNc DA neurons after chronic treatment with vehicle (right) or Sema7A (left). Scale bar=100µm. B. Quantification of axonal arborization surface. C. Quantification of dendritic surface. D. Quantification of the number of TH-positive neurons in VTA and SNc cultures. The values obtained were then normalized to the number of TH neurons counted previously. The values represent the mean ± SEM, n=15 coverslips from 4 different cultures. *p<0.05. At 10 DIV, the effect of Sema7A treatment on basal OCR (E, F), uncoupled OCR (G) and RCR (H) was also measured. The values represent the mean ± SEM, n=15-20 wells from 4 different cultures. * p<0.05; ** p<0.01. The effect of Sema7A pre-treatment on the vulnerability of SNc DA neurons to MPP+ (5 µM, 24h) (I) or rotenone (50 nM, 72h) (J) was quantified. The values represent the mean ± SEM, n=15-25 coverslips. *p<0.05. K-L. Intracellular ROS levels were determined using the superoxide-sensitive fluorescent dyes Mitosox and DHE. K. Average MitoSOX signal intensity in SNc and VTA DA neurons. The values represent the mean ± SEM, n=8 coverslips from 4 different cultures. L. Average DHE signal intensity in SNc and VTA DA neurons. The values represent the mean ± SEM, n=30 neurons from 6 different cultures. *p<0.05.

4.9 Supplementary Figures

Figure S1. Dissection of SNc and VTA.

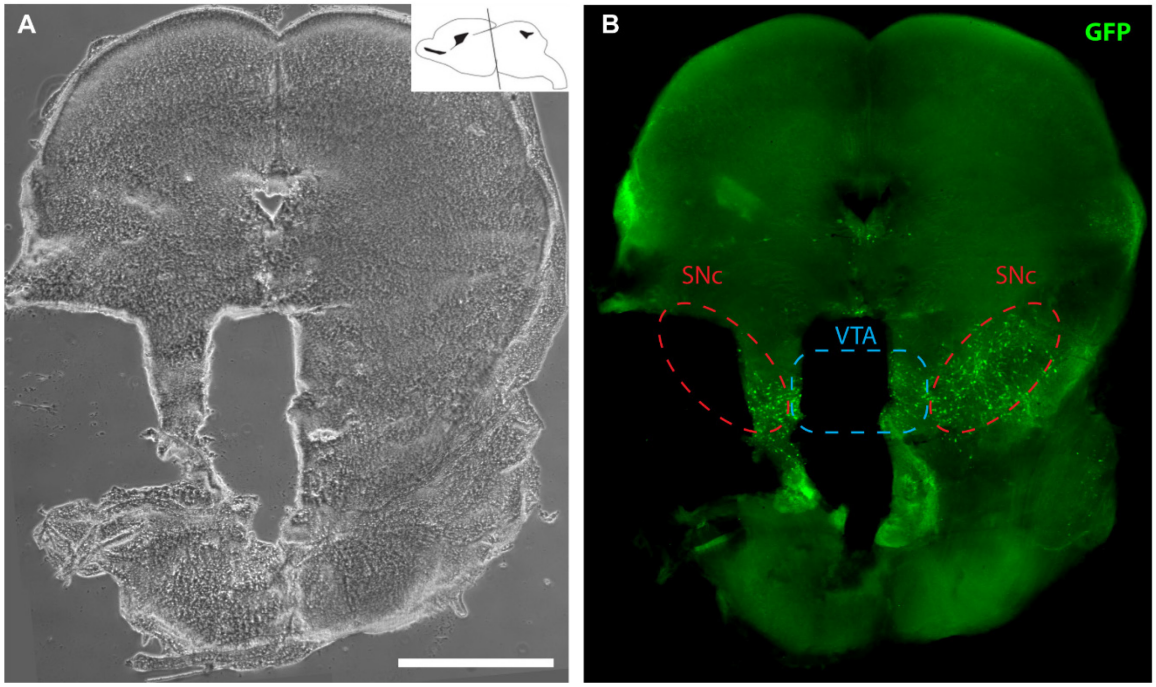

A coronal mesencephalic brain section was prepared as described previously(Fasano, Thibault, and Trudeau 2008). The VTA was micro-dissected from the ventro-medial region of the brain section (blue dotted lines). The SNc was micro-dissected from the ventro-lateral regions of the brain section (red dotted lines). The intermediate area between the SNc and VTA was discarded to increase the likelihood of selectively isolating VTA and SNc neurons. (A) Phase contrast image of a hemi-dissected mesencephalic brain section from a P0 TH-GFP mouse. The inset shows a representative profile of the brain to illustrate the region selected to prepare the section (modified from the Atlas of the Developing Mouse Brain at E17.5, P0 and P6, 1st Edition, Paxinos, Halliday, Watson, Koutcherov and Wang, 2006. (B) Immunofluorescence image of the same brain section after immunostaining for GFP. Red dashed line, SNc. Blue dashed line, VTA. Scale bar: 1 mm.

Figure S2. Oxygen consumption rate (OCR) and extracellular acidification rate (ECAR) were assessed using an XF24-flux analyzer.

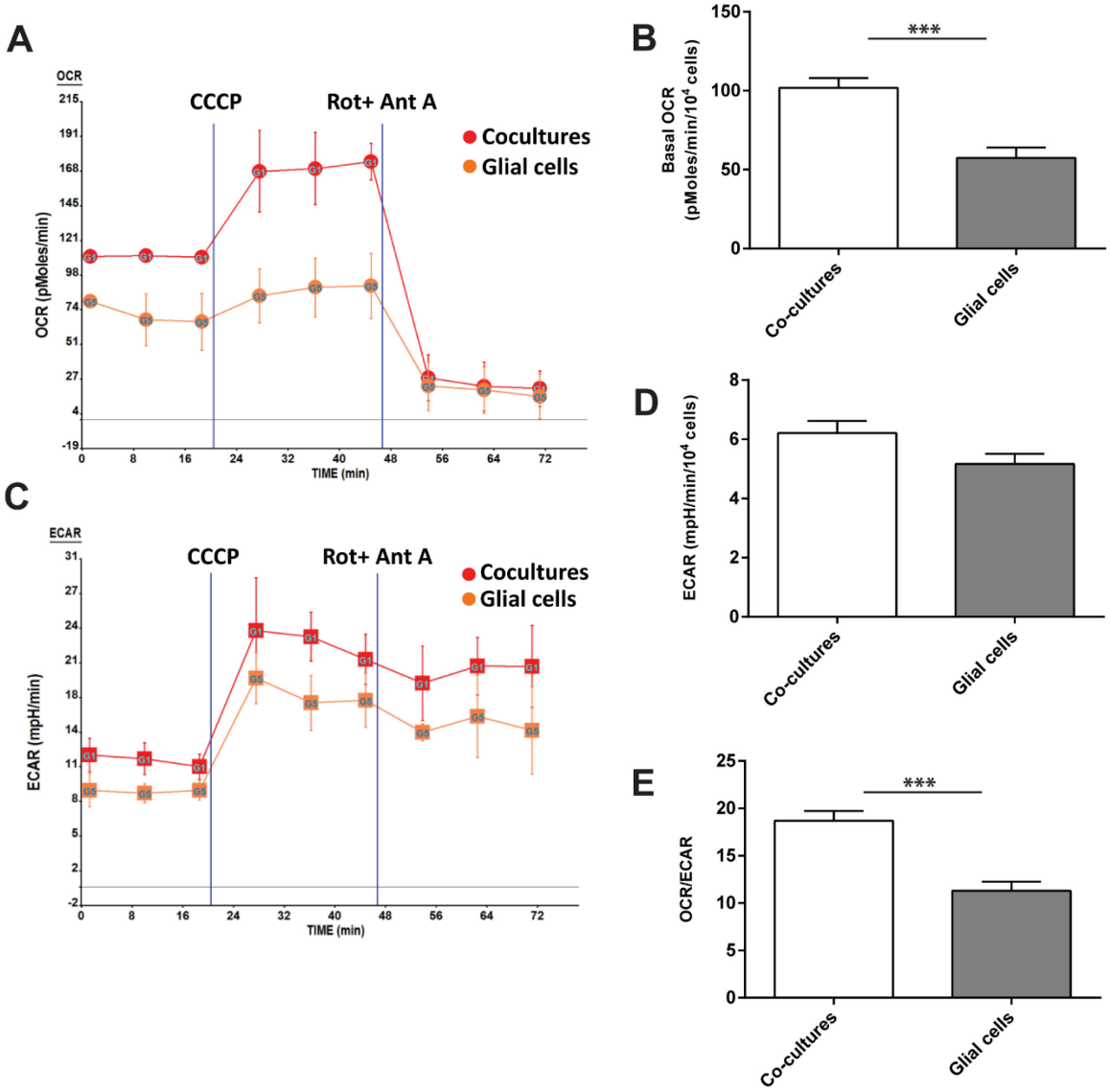

(A) Representative time course of OCR in co-cultures and in glial cells alone. Cultures were exposed sequentially to the mitochondrial uncoupler CCCP (0.5μM) to measure maximal OCR and to a respiratory inhibitor cocktail (rotenone/antimycin-A) to quantify non-mitochondrial OCR. (B) The bar graph shows average basal OCR in co-cultures and glial cells alone, normalized to the total cell number. (C) Representative time course of ECAR in co-cultures and glial cells alone. (D) The bar graph shows basal ECAR normalized to the total cell number. (E) Bar graph showing the ratio between basal OCR and ECAR, demonstrating the higher mitochondrial metabolism in neurons compared to glia cells. The values represent the mean ± SEM, n=15-30 wells from 4 different cultures and statistically analyzed by t test. *** $p<0.001$.

Figure S3. SNc DA neurons show elevated glycolysis.

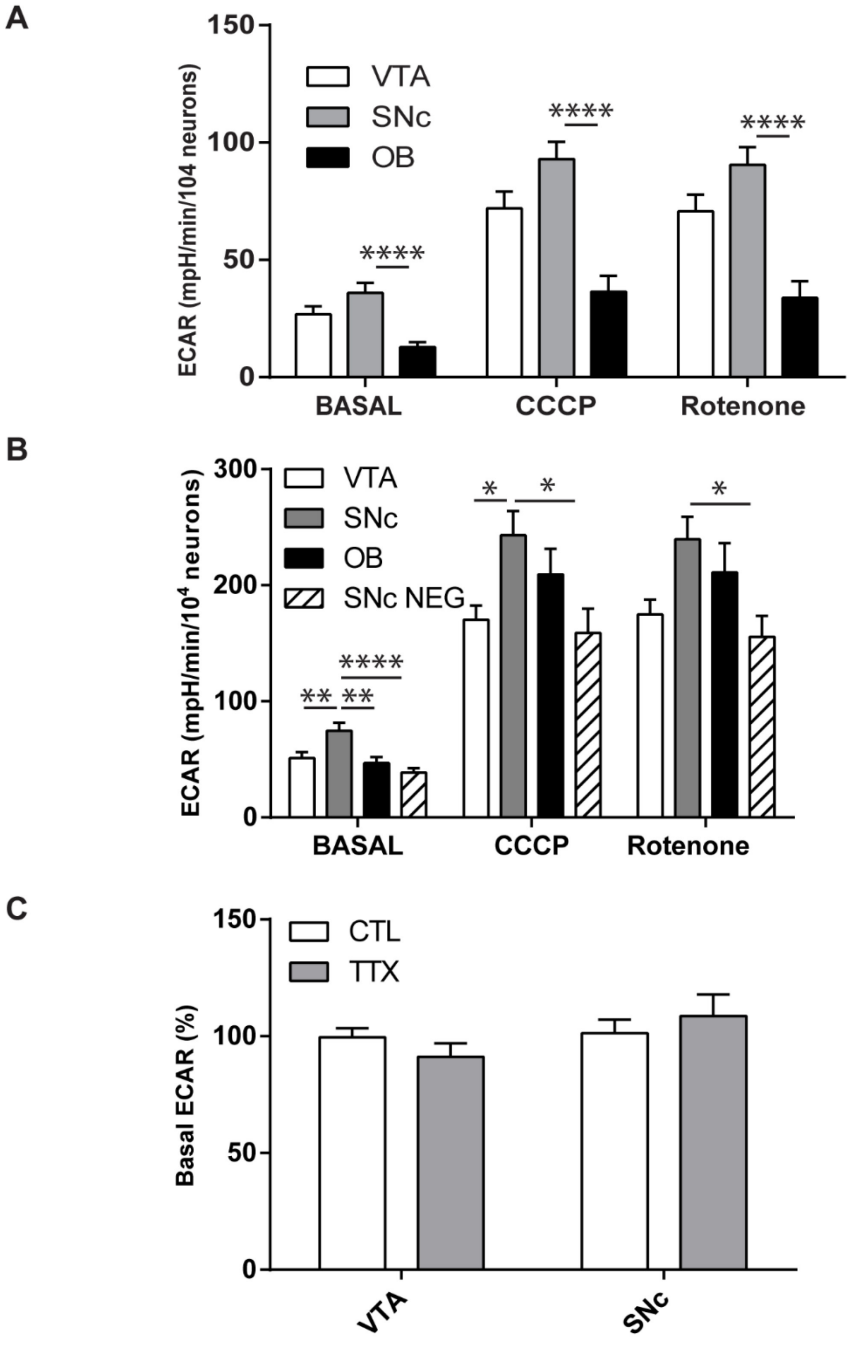

Neurons can produce ATP through glycolysis, a process that can be measured in living neurons by monitoring the extracellular acidification rate (ECAR), resulting from the production of lactic acid. (A) SNc neurons did not show a significantly different basal ECAR compared to VTA neurons, although it was significantly higher compared to OB. As expected, glycolysis was up-regulated following blockade of mitochondrial ATP production by the mitochondrial uncoupler CCCP or by the complex I-inhibitor rotenone; however, such maximal glycolytic flux was not significantly different between SNc and VTA neurons, although SNc neurons displayed significantly higher ECAR compared to OB. (B) We confirmed this results in FACS-purified SNc DA neurons that displayed significantly higher basal ECAR compared to VTA, OB and GFP-negative SN neurons. Maximal glycolytic flux, measured in the presence of CCCP was also significantly higher in SNc compared to VTA DA neurons, although this was not significant in the presence of rotenone. The large difference between basal and maximal glycolysis reveals that at basal level, only 28 % and 29 % of the maximal glycolytic capacity is used by SNc and VTA DA neurons, respectively, thus arguing that under our experimental conditions, the majority of ATP synthesis derives from OXPHOS rather than from glycolysis. The values represent the mean ± SEM, n=10-30 wells from at least 3 different cultures. * $p<0.05$; ** $p<0.01$; *** $p<0.001$; ****. (C) Effect of TTX on basal ECAR. After quantifying basal ECAR, 1 µM TTX was added to VTA or SNc cultures and the ECAR was monitored for 1h. TTX caused no significant change in ECAR. The values represent the mean ± SEM, n=10-15 wells from 4 different cultures.

Figure S4. SNc DA neurons show elevated ROS production.

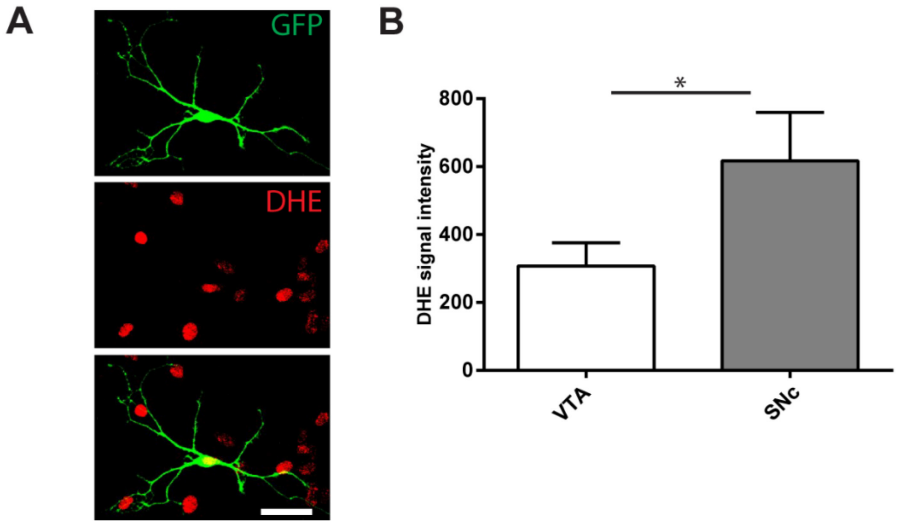

We measured superoxide levels in living TH-GFP DA neurons using the fluorescent indicator DHE, incubated for a 20 min period. DHE oxidation by superoxide leads to its accumulation in the cell nucleus, thus providing an estimation of steady-state superoxide production. (A) Representative confocal images of DHE fluorescence from TH-GFP neurons. Scale bar=50μm. (B) Average DHE signal intensity in SNc and VTA DA neurons. The values represent the mean ± SEM, n=20 neurons from 4 different cultures. *$p<0.05$.

Figure S5. SNc DA neurons display a more complex axonal arborization compared to VTA and OB DA neurons.

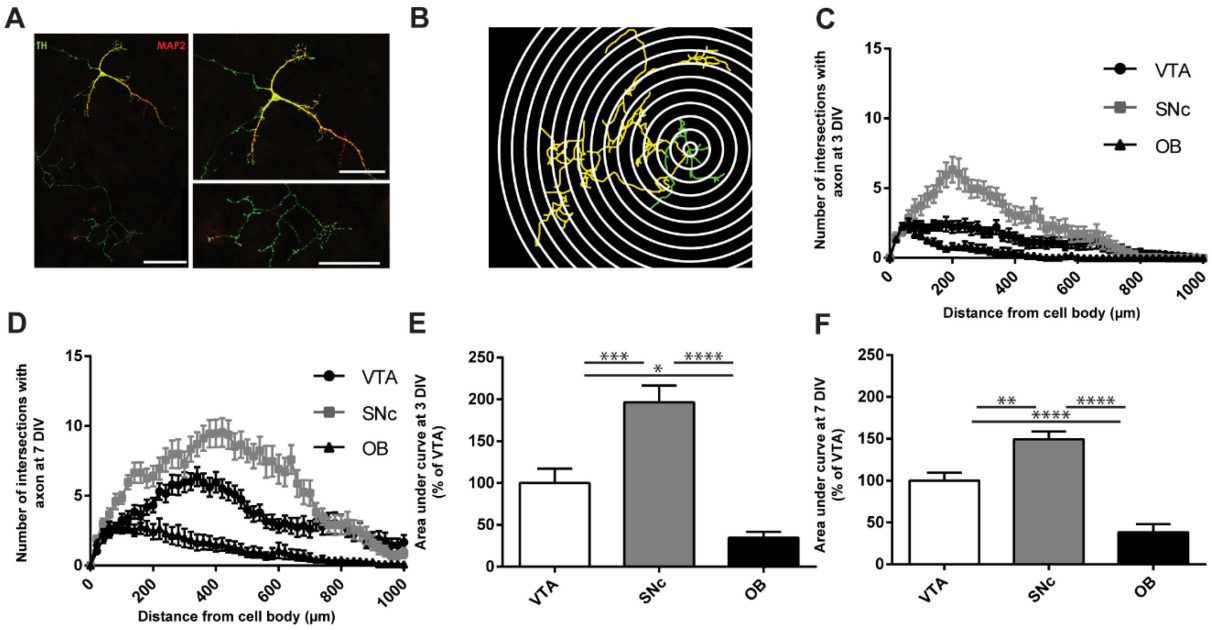

The results of the quantification of the axonal arborization size of cultured SNc, VTA and OB DA neurons, carried out using semi-automated single neuron tracing, were confirmed using a Sholl analysis. (A) The images show examples of isolated TH immunopositive neurons and MAP2/TH colabelling to identify the somatodendritic compartment of DA neurons. Scale bars =100µm. A Sholl analysis (B) was performed to quantify axonal complexity (C-D) at 3 and 7 DIV, respectively. Quantification of the area under the Sholl curves (E, F) was used for quantitative comparisons. The data represent the mean ± SEM, n=20-35 neurons from 4 different cultures. * $p<0.05$; ** $p<0.01$; *** $p<0.001$; **** $p<0.0001$.

Figure S6. The dendritic arborization of SNc and VTA neurons is comparable after 7 days in vitro.

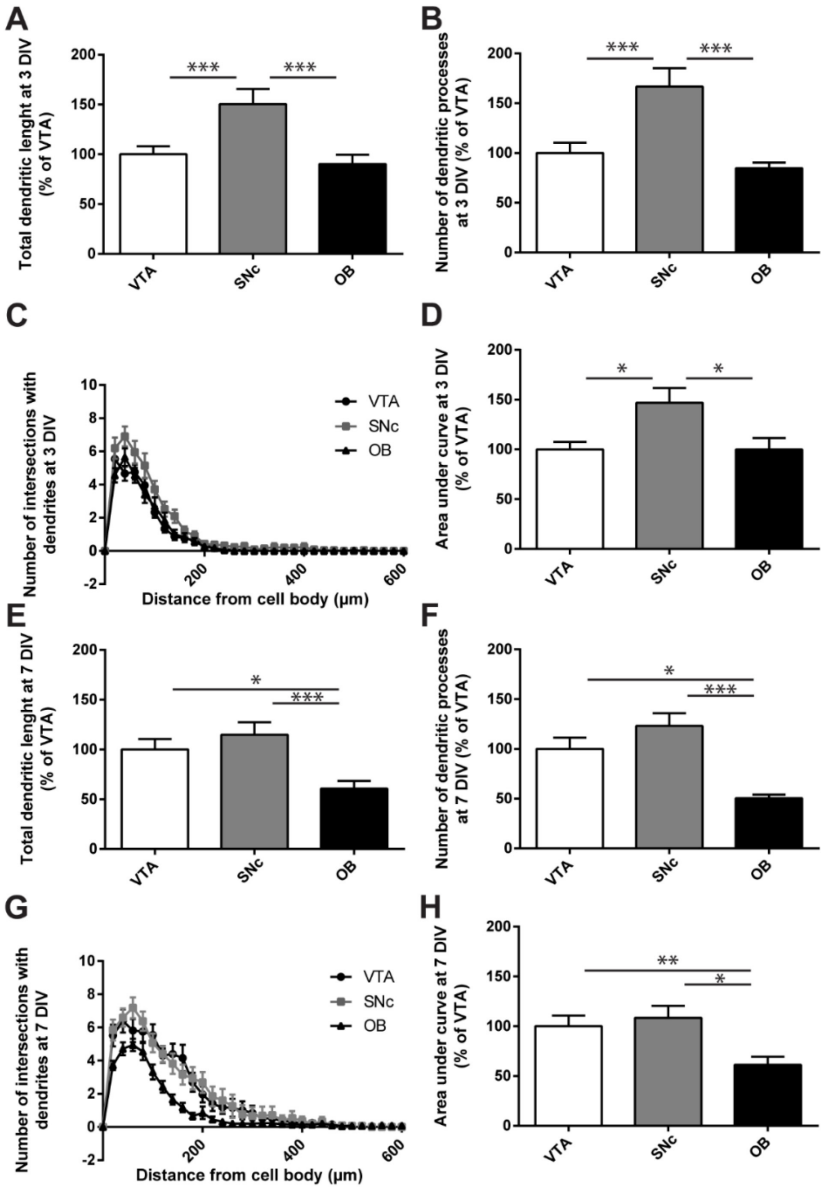

Dendritic arborization was measured using single neuron tracings from confocal images. Isolated TH-positive DA neurons were randomly selected and imaged by acquiring confocal z-stacks at 20x. Dendritic arborization was measured from cultured SNc, VTA and OB DA neurons at 3 DIV (A-D) and 7 DIV (E-H). The total length (A, E) and number of dendritic processes (B, F) were measured and a Sholl analysis was performed (C, G) to assed dendritic complexity. The area under the Sholl curves (D, H) was used for quantitative comparisons. Data are presented as a percentage of VTA values. Data represent the mean ± SEM, n=20-35 neurons from 4 different cultures. * $p<0.05$; ** $p<0.01$; *** $p<0.001$; **** $p<0.0001$.

Figure S7. The AMPK activator AICAR increases respiration but fails to protect SNc DA neurons.

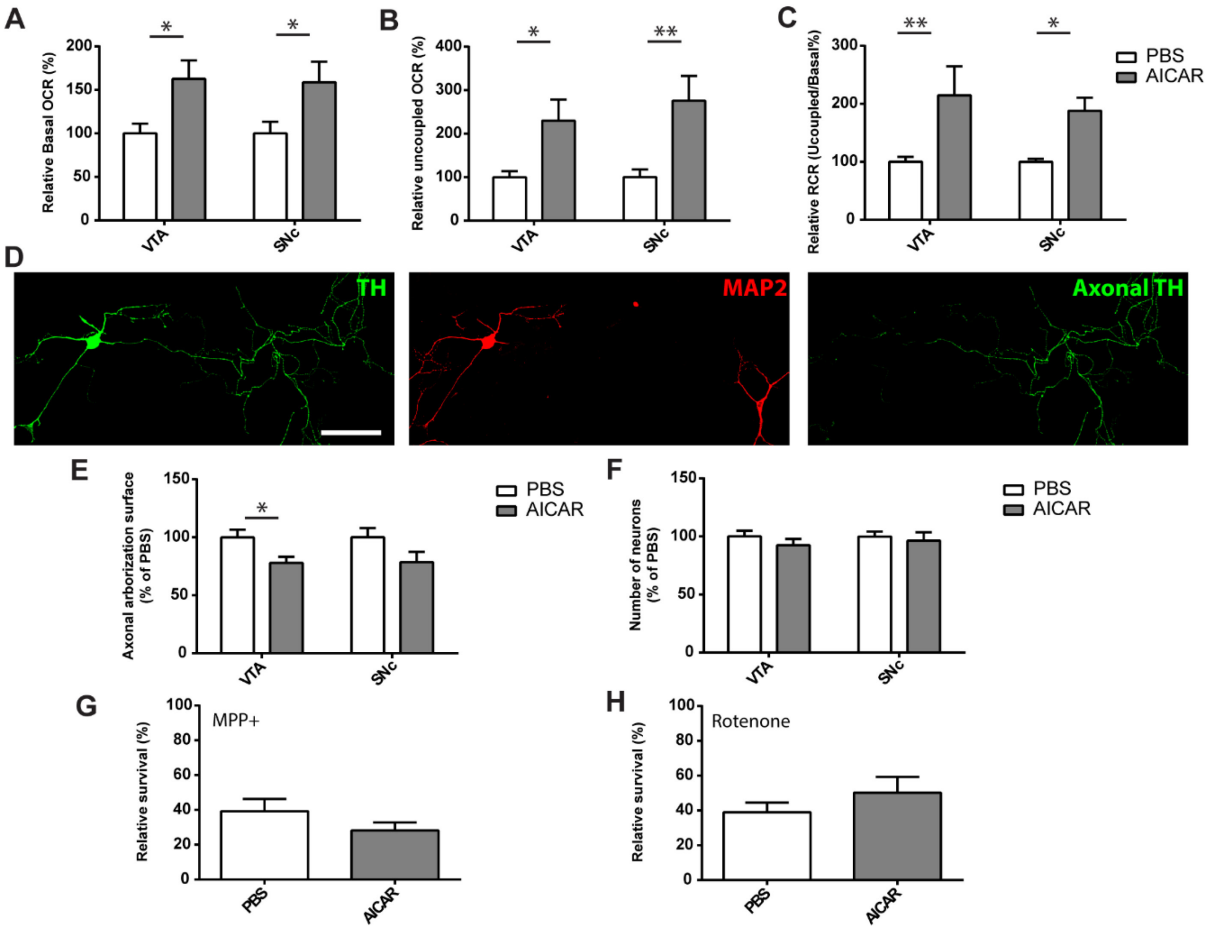

Complex SNc DA neurons could be more vulnerable to toxic stress than more simple VTA DA neurons because they lack sufficient energy to maintain key cellular functions under conditions that challenge cellular bioenergetics. If this were the case, increasing OXPHOS could be neuroprotective. Alternately, the high basal OXPHOS could put DA neurons at risk because of its association with oxidative stress, in which case it would be predicted that elevating OXPHOS would fail to protect SNc DA neurons. To distinguish between these two hypotheses, we exposed SNc and VTA DA neurons to AICAR (100 μM), an agent well known to increase basal OCR in many cell types due to activation of AMPK (5'-AMP-activated protein kinase), an energy sensor that regulates cellular energetic metabolism. A-C. AICAR (100 μM) was added to VTA and SNc cultures at 7 DIV and its effects on basal OCR (A), uncoupled OCR (B) and RCR (C) were quantified at 10 DIV. The values represent the mean ± SEM, n=15-25 wells from 5 different cultures and statistically analyzed using an ANOVA followed by Sidak's Post Hoc test. * $p<0.05$; ** $p<0.01$. As a control, we examined the effect of AICAR on axonal growth and basal survival (D-H). (D-E) Example of SNc DA neurons after treatment with AICAR. TH-immunolabelling is shown on the left (green) and MAP-2 immunolabelling in the middle (red). The image on the right represents TH-positive axons obtained by subtracting MAP2-labelled dopaminergic somatodendritic signal from total TH signal. Scale bar=100μm. AICAR caused a small reduction in axonal arborization size in VTA but not in SNc DA neurons and failed to change basal neuronal survival (F). AICAR treatment failed to change the vulnerability of DA neurons to MPP+ (5 μM, 24h) (G) or rotenone (50 nM, 72h) (H). The values represent the mean ± SEM, n=10-20 coverslips from 4 different cultures.

4.10 Supplemental experimental procedures

Animals

All procedures involving animals were conducted in strict accordance with the Guide to care and use of experimental animals (2nd Ed.) of the Canadian Council on Animal Care. The experimental protocols were approved by the animal ethics committee (CDEA) of the Université de Montréal. Housing was at a constant temperature (21°C) and humidity (60%), under a fixed 12 hours light/dark cycle and free access to food and water.

Primary neuronal cultures and drug treatments

Dissociated neurons micro-dissected from the SNc, VTA or olfactory bulb (OB) of P0-P2 C57BL6 mice were seeded on a monolayer of cortical astrocytes grown on collagen/poly-L-lysine-coated glass coverslips. The total seeded neuron density was 100 000 cells/ml for all the experiments, except for the metabolic flux experiments in mixed co-cultures for which the density was 250 000 cells/ml and for the single neuron morphological tracings for which the density was 20 000 cells/ml. All cultures were incubated at 37 °C in 5 % CO_2 and maintained in 2/3 of Neurobasal™-A enriched with 1 % penicillin/streptomycin, 1 % Glutamax™-1, 2 % B-27 supplement and 5 % fetal bovine serum (Invitrogen) plus 1/3 of minimum essential medium (MEM) enriched with 1 % penicillin/streptomycin, 1 % GlutamaxTM-1, 20 mM Glucose, 1mM sodium pyruvate, 100 µl MITO+ serum-extender. The proportion of DA neurons was 26 % for SNc, 36% for VTA and 11% for OB cultures.

Metabolic flux experiments

Cells were plated on XF24 tissue culture plates and maintained in culture for 10 days. Before experiments, cells were incubated for 1 h at 37°C in a CO2-free incubator in bicarbonate-free DMEM (Sigma) supplemented with 200 mM GlutaMax™-1 (Invitrogen), 100mM sodium pyruvate (Sigma), 25 mM D-glucose (Sigma), 63.3 mM NaCl (Sigma) and phenol red (Sigma). The pH was adjusted to 7.4 with NaOH. Oxygen consumption was sequentially measured under

basal conditions in the presence of the mitochondrial uncoupler CCCP (0.5 μM) and mitochondrial inhibitors rotenone (1 μM) and antimycin A (1 μM), to assess respectively the maximal oxidative capacity and non-mitochondrial oxygen consumption. After the assays, the cells were immediately fixed for immunofluorescence. Oxygen consumption rates were normalized to cell number identified with DAPI staining. Since neurons were cultured together with astrocytes, we also performed parallel measurements from pure astrocyte cultures. After subtraction of the OCR measured from astrocytes, the resulting OCR values measured from mixed cultures were normalized in a second step on the total neuron of neurons identified with MAP-2 immunostaining. The OCR measured from mixed DA neurons/astrocytes cultures was considerably higher than that measured in pure astrocyte cultures (Figure S2A, B), thus confirming our ability to measure signal originating from DA neurons. Our results show a marked increase in OCR (43%) in mixed cultures compared to astrocytes alone. The rate of glycolysis, estimated by measuring the extracellular acidification rate (ECAR), was not different in co-cultures compared to purified astrocyte cultures (Figure S2C, D). The OCR/ECAR ratio was significantly larger in neuron co-cultures than in purified astrocyte cultures, thus demonstrating the higher rate of mitochondrial oxidative phosphorylation in neurons compared to astrocytes (Figure S2E). Since ECAR values in co-cultures were close to those of astrocytes, we did not subtract the contribution of glial cells. We normalized ECAR values on the total cell number and then on the total number of neurons.

Superoxide level determination in live primary neurons

TH-GFP DA neurons were incubated with 10μM DHE for 20 min or with 1 μM MitoSOX for 30 min in physiological saline solution before images were acquired using a laser scanning confocal microscope (FV1000 MPE, Olympus) equipped with multi-argon and helium/neon lasers and a 20x water-immersion objective for DHE images and 60 X oil-immersion objective for MitoSOX images. For DHE, a 100 μm^2 region of interest was selected in GFP-positive cell body and the total intensity was then measured (mean pixel intensity x signal area). Excitation was achieved using the 488 nm laser line and emitted light was acquired between 520 and 610 nm.

For MitoSOX quantifications, regions of interest were limited to isolated GFP-positive axon segments. 10 pictures per coverslips were captured. The total intensity of MitoSOX signal (mean pixel intensity x signal area) was normalized on the length of analyzed processes. Images were analyzed using Image-J software. Background fluorescence was subtracted from every image.

Electrophysiology

Glass coverslips plated with neurons were inserted in a recording chamber affixed to the stage of an inverted Nikon Eclipse TE-200 fluorescent microscope and gravitationally perfused with a physiological saline solution composed of (in mM): 140 NaCl, 5 KCl, 2 $MgCl_2$, 2 $CaCl_2$, 10 HEPES, 6 sucrose, 10 glucose. Whole-cell patch-clamp recordings were performed on GFP expressing neurons using borosilicate pipettes (4.5-6.5 MΩ) filled with an intra-pipette solution composed of (in mM): 145 KMeSO4, 10 NaCl, 0.1 EGTA, 2 ATP (Mg salt), 0.6 GTP (Tris salt), 10 HEPES, 10 phosphocreatine (Tris salt), and pH 7.35 and osmolarity 300-305 mOsm. The signal was amplified and controlled using a PC-505 patch-clamp amplifier (Warner), filtered at 2 kHz, digitized at 10 kHz and analyzed with pClamp10 software (Molecular Devices).

Immunofluorescence

Cultures were fixed 30 min with 4% paraformaldehyde (PFA) in PBS, permeabilized, and nonspecific binding sites blocked. Cells were incubated overnight with a primary antibody solution containing 1% bovine serum albumin (BSA), 0.1% Triton-X-100 in PBS, 5% goat serum and 0.02% NaN_3. Cells were washed several times in PBS before incubation for 1h with the appropriate Alexa-labeled secondary antibodies (Invitrogen).

Mitochondrial network quantification

Image analysis was performed using ImageJ software. Only DAT-positive infected DA neurons were selected for analysis. Regions of interest were determined to separately measure DsRed2-mito signal in the cell body, isolated dendrite segments (identified as DAT and MAP2-

positive regions) and isolated axon segments (identified as DAT positive and MAP2 negative). The intensity of DsRed2 signal (mean pixel intensity x signal area) was normalized on TH area for cell body and on the length of analyzed processes for dendrite and axon segments (as described before for MitoSOX).

Single neuron morphology, global neuronal morphology

Neurons were examined at 3 or 7 DIV to compare data from isolated developing (3 DIV) and morphologically more mature (7 DIV) DA neurons. The axon was identified as the longest neurite, a criterion confirmed by identifying dendrites with MAP2 immunostaining (Figure S5A). A Sholl analysis estimating the complexity and branching of the neurons' arborization was also performed using the plugin included in the Fiji distribution of ImageJ (Figure S5B).

To analyze the isolated TH neurons, one to fifteen image stacks per neuron were captured depending on the extent of the neuron's arborization and then stitched together using Photoshop CS6 to display the neurons' complete arborization. The longest process, which was 3 to 20 times longer than the others, was considered as the axon. This distinction was also confirmed with MAP2 dendritic staining and neurons where this distinction was not possible were rejected from further analysis. Total process length and total number of processes were measured for axon and dendrites. In non-isolated neuron cultures, axonal arborization was estimated by capturing 5 image stacks per coverslip randomly throughout the coverslip. Using a home-made macro in ImageJ, MAP2 and TH signal were thresholded to remove background and then binarised. MAP2 signal area was then removed from TH signal area and the remaining axonal signal surface was measured.

Real-time quantitative PCR

GFP-positive DA neurons cultured on glass coverslips were mounted into a recording chamber and continuously perfused. Pools of ten GFP-expressing DA neurons were collected under RNase-free conditions by using autoclaved borosilicate patch pipettes. After sample

collection, the content of the pipette was transferred immediately into a prechilled 200 µl tube containing 6 µl of a freshly prepared solution of 20Uof RNaseOUT and 8.3 mM DTT (Invitrogen) and then frozen on dry ice until use. Frozen samples were thawed on ice and subjected to the RT reaction as previously described [48]. The primers used for Real-time quantitative PCR were: PGC-1α Fw: 5'- TGCCATTGTTAAGACCGAGA-3', PGC-1α Rv: 5'-CTGTGGGTTTGGTGTGAGG-3'. GAPDH was used as housekeeping gene (Fw 5'-GGAGAAACCTGCCAAGTATGA-3', Rv: 5'-TGAAGTCGCAGGAGACAACC-3').

Measurement of total cellular ATP

The cells were collected by trypsinization and centrifugation at 500 ×g and then re-suspended in phosphate-buffered saline, pH 7.4. Cellular ATP content was determined using the PerkinElmer "ATPlite" kit (PerkinElmer) according to the manufacturer's instructions. Measurements were performed on a Wallac Victor plate reader (PerkinElmer). One coverslip from each sample was labelled with DAPI to quantify total cell number. ATP values were then normalized on total cell number. Oligomycin-insensitive ATP production (from glycolysis) was subtracted. Values obtained from measurements from glial cells alone were subtracted. The remaining values, representing the ATP derived from OXPHOS in neurons only, were then normalized on the total number of neurons identified with MAP-2 immunostaining.

4.11 Supplementary references

(S1) Fasano, C., Thibault, D., and Trudeau, L.-E. (2008). Culture of postnatal mesencephalic dopamine neurons on an astrocyte monolayer. Curr. Protoc. Neurosci. Editor. Board Jacqueline N Crawley Al Chapter 3, Unit 3.21.

(S2) Paxinos, G., Halliday, G.M., Watson, C., Koutcherov, Y., and Wang, H. (2006). Atlas of the Developing Mouse Brain at E17.5, P0 and P6, 1st Edition (San Diego: Elsevier Academic Press).

Chapitre 5 : Vulnérabilité dans les formes familiales de la maladie de Parkinson (Article III)

Pour rappel, notre hypothèse initiale était que la vulnérabilité plus importante des neurones de la SNc dans le contexte de la MP était due à l'importante demande énergétique induite par leur arborisation axonale particulièrement complexe. L'article précédent nous a permis de valider cette notion, en plus de développer plusieurs outils nous permettant d'évaluer la croissance axonale, la survie et la fonction mitochondriale de ces neurones en culture.

Dans l'article qui suit, nous avons tiré avantage de ces techniques pour évaluer les mêmes paramètres dans les modèles murins de trois formes familiales de la maladie qui sont étroitement liés à la fonction mitochondriale; soit les knock-out pour Parkin, Pink1 et DJ-1.

Contributions des auteurs

Nicolas Giguère : Conception et exécution des expériences reliées à l'imagerie et la survie neuronale, à une partie des mesures de la fonction et densité mitochondriale et aux expériences de « *rescue* ». Analyse des données et écriture du manuscrit.

Consiglia Pacelli : Conception et exécution d'une partie des mesures de la fonction mitochondriale et des mesures d'ATP. Analyse des données et révision du manuscrit.

Marie-Josée Bourque : Préparation des cultures cellulaires.

Diana Matheoud : Aide dans les expériences de Western Blot.

Caroline Saumure : Exécution des mesures de la prolifération gliale mésencéphalique.

Daniel Lévesque : Conception et exécution de l'expérience de radioligand. Analyse des données et révision du manuscrit.

David Park : Don de réactifs et révision du manuscrit.

Ruth S. Slack : Don de réactifs et révision du manuscrit.

Louis-Éric Trudeau : Conception, coordination et supervision du projet et écriture du manuscrit.

*Nicolas Giguère et Consiglia Pacelli sont co-premiers auteurs.

Publié dans la revue « Journal of Biological Chemistry » le 26 avril 2018.
https://doi.org/10.1074/jbc.RA117.000499

Comparative analysis of Parkinson's disease–associated genes reveals altered survival and bioenergetics of parkin-deficient dopamine neurons in mice

Nicolas Giguère[1,2,*], Consiglia Pacelli[4,*], Caroline Saumure[1,2], Marie-Josée Bourque[1,2], Diana Matheoud[2,5], Daniel Levesque[6,7], Ruth S. Slack[8], David Park[8], Louis-Éric Trudeau[1-2-7]

From [1]Departments of pharmacology and physiology, [2]Department of neurosciences, [3]Central Nervous System Research Group (GRSNC), Faculty of Medicine, Université de Montréal, Québec, H4T 1J4 Canada, [4]Department of Clinical and Experimental Medicine, University of Foggia, Foggia, 71122 Italy, [5]Centre de recherche du Centre hospitalier de l'Université de Montréal (CRCHUM), H2X 0A9 Canada, [6]Faculty of Pharmacy, Université de Montréal, Québec, H4T 1J4 Canada, [7]Groupe de Recherche Universitaire sur le Médicament (GRUM), [8]Department of cellular and molecular medicine, University of Ottawa, Ottawa, K1M 8M5 Ontario.

Author contribution: *These authors are co-first authors

Keywords: Parkinson's disease, Parkin, PTEN‐induced putative kinase 1, Pink1, DJ-1, substantia nigra, dopamine neuron, bioenergetics, axonal arborization, glial cell

5.1 Abstract

Many mutations in genes encoding proteins such as parkin, PTEN-induced putative kinase 1 (Pink1), protein deglycase DJ-1 (DJ-1 or PARK7), leucine-rich repeat kinase 2 (LRRK2), and α-synuclein have been linked to familial forms of Parkinson's disease (PD). The consequences of these mutations, such as altered mitochondrial function and pathological protein aggregation, are starting to be better understood. However, little is known about the mechanisms explaining why alterations in such diverse cellular mechanisms lead to the selective loss of dopamine (DA) neurons in the substantia nigra (SNc) in the brain of individuals with PD. Recent work has shown that one of the reasons for the high vulnerability of SNc DA neurons is their high basal rate of mitochondrial oxidative phosphorylation (OXPHOS), resulting from their highly complex axonal arborization. Here, we examined whether axonal growth and basal mitochondrial function are altered in SNc DA neurons from Parkin-, Pink1-, or DJ-1KO mice. We provide evidence for increased basal OXPHOS in Parkin-KO DA neurons and for reduced survival of DA neurons that have a complex axonal arbor. The surviving smaller neurons exhibited reduced vulnerability to the DA neurotoxin and mitochondrial complex I inhibitor MPP+, and this reduction was associated with reduced expression of the DA transporter. Finally, we found that glial cells play a role in the reduced resilience of DA neurons in these mice and that WT Parkin overexpression rescues this phenotype. Our results provide critical insights into the complex relationship among mitochondrial function, axonal growth, and genetic risk factors for PD.

5.2 Introduction

In PD, chronic progressive loss of SNc DA neurons leads to some of the characteristic motor symptoms of the disease. Over the past years, many mutations in genes coding for proteins such as the E3 ubiquitin ligase Parkin, PTEN-induced putative kinase 1 (Pink1), protein deglycase DJ-1, leucine-rich repeat kinase 2 (LRRK2) and α-synuclein have been linked to familial forms of the disease.

Although the mechanisms underlying the effects of these mutations, such as alteration in mitochondrial function, mitophagy, lysosomal and proteasome function and protein aggregation, are slowly starting to be better understood (1), little is known about the reason why alterations in such ubiquitous cellular mechanisms lead to selective loss of sub-populations of neurons, including SNc DA neurons. An emerging hypothesis suggests that the selective vulnerability of DA neurons and other cell groups in PD can be explained in large part by the fact that they establish an unusually complex axonal arborization (2–4). This characteristic has been associated with particularly high demands in ATP needed to sustain neurotransmission along profuse axons (5–8).

Arguing in favor of this hypothesis, recent work showed that SNc DA neurons have a higher basal rate of mitochondrial OXPHOS and ATP production and a smaller reserve capacity compared to less vulnerable DA neurons of the ventral tegmental area (VTA) (9), characteristics that appear to be the result of the highly complex axonal arborization of these neurons and that are also associated with a high level of oxidative stress. Based on these results, a question that arises is whether bioenergetic parameters or axon growth are perturbed in genetic mouse models of PD. Here we examined primary SNc and VTA DA neurons obtained from Parkin, Pink1 or DJ-1 KO mice. We found *in vitro* that basal survival, axonal growth and mitochondrial function are altered in SNc DA neurons from Parkin KO mice but not from Pink1 or DJ-1 KO mice, resulting in an increased oxygen consumption rate (OCR) but lower ATP content. We also found that astrocytes from Parkin KO mice had a slower growth rate and lower OCR and that their replacement with WT astrocytes abolished the reduction in basal survival observed in Parkin

KO SNc DA neurons. Finally, we show that overexpression of WT Parkin rescues the survival, axonal morphology and bioenergetics of SNc Parkin KO cultures. Our data provide new insights in the complex relationship between cellular bioenergetics, axonal development and survival of DA neurons in Parkin, Pink1 and DJ-1 KO mouse models of PD, highlighting a critical role for Parkin.

5.3 Results

5.3.1 SNc DA neurons in Parkin but not Pink1 or DJ-1 KO PD mouse models show altered basal survival and growth.

Experiments were performed using a mouse primary culture system including DA neurons microdissected from the SNc and VTA of newborn Parkin-, Pink1- or DJ-1-KO mice. The neurons were grown on a supporting monolayer of astrocytes of corresponding genotype. As previously reported (9), in such cultures, WT SNc DA neurons show increased basal respiration, increased ATP production and a larger axonal arborization compared to WT VTA DA neurons (Supplemental Figure S1).

We first evaluated the rate of spontaneous loss of DA neurons *in vitro* over a period of 11 days as an index of the neurons' basal resilience. At 11 DIV, a time point at which DA neurons are mature at the morphological and metabolic levels, we found that Parkin KO SNc DA neurons showed a pronounced rate of spontaneous degeneration, with 56% more cell loss compared to WT SNc DA neurons (Figure 1A). We did not observe any similar enhancement of SNc DA neuron loss in Pink1 KO or DJ-1 KO neurons (Figure 1B and C) or in VTA cultures from any of the 3 genotypes (Figure 1D-F). Interestingly, there was also no change in survival at an earlier time point in SNc Parkin KO culture (5DIV, Supplemental Figure S2A), arguing for the need of sustained stress for this increased vulnerability to be revealed. We next examined axonal arborization size in the remaining Parkin KO SNc DA neurons at 11 DIV and found that

it was 40% smaller compared to WT (Figure 1G, 1H), with no change in Parkin KO VTA neurons. Again, we did not observe any differences between Pink1 WT and KO DA neurons, between DJ-1 WT and KO DA neurons (Figure 1I and J) or at an earlier time point in Parkin WT vs KO DA neurons (Supplemental Figure S2B). These results suggest that Parkin KO SNc DA neurons have a higher intrinsic vulnerability and that the most arborized DA neurons are degenerating preferentially or, alternately, that axonal development is slowed in these neurons after prolonged development *in vitro*.

5.3.2 Parkin but not Pink1 or DJ-1 KO DA neurons show altered mitochondrial function.

Because recent work has provided evidence for a close relationship between survival, axonal arborization size and mitochondrial bioenergetics in DA neurons (9), we next evaluated mitochondrial OXPHOS by measuring cellular respiration. At 10 DIV, basal and maximal (uncoupled with CCCP) oxygen consumption rates (OCR) were measured in living neurons. The respiratory control ratio (RCR), corresponding to the ratio between basal and maximal OCR was also determined to estimate the respiratory reserve capacity. We found that basal OCR was significantly increased by 50% in Parkin KO SNc DA neurons compared to WT (Figure 2A). However, maximal OCR or the RCR were unchanged in these neurons (Figure 2A). OCR was unchanged in SNc DA neurons from Pink1 KO or DJ-1 KO mice (Figure 2B and C) or at 5 DIV in SNc Parkin KO culture (Supplemental Figure S2C). Interestingly, basal OCR was significantly increased by 181% in Parkin KO VTA DA neurons, accompanied by an increase of maximal OCR of 120%, with no changes in RCR (Figure 2D). OCR was unchanged in VTA DA neurons form Pink1 or DJ-1 KO mice.

Considering previous work suggesting a critical role or Parkin in the turnover of mitochondria (10–12), a possible interpretation of the increase in basal OCR in Parkin KO DA neurons is that loss of Parkin leads to the presence of dysfunctional mitochondria that are partially uncoupled. If this were the case, a prediction is that the increase in OCR should not be accompanied by an increase in ATP production and could even be accompanied by a decrease in ATP. To test this hypothesis, we measured ATP content in each culture and discovered a

significant reduction of 44% in ATP levels in Parkin KO SNc cultures, with no change in Pink1 KO or DJ-1 KO cultures (Figure 2G-I). Such a possible uncoupling between OCR and ATP production appears to be particularly exacerbated in Parkin KO VTA DA neurons cultures, perhaps because more of these neurons survived to this impairment, compatible with their higher resilience in response to oxidative stress (9). Interestingly, contrarily to SNc DA neurons (Figure 3A), VTA DA neurons from Parkin KO mice showed an increase in basal glycolysis (Figure 3B), perhaps representing a compensatory mechanism for impaired mitochondrial function. This was not observed in SNc or VTA neurons from either Pink1 or DJ-1 KO mice. (Figure 3C-F).

Considering our data arguing for defective mitochondrial function in SNc DA neurons from Parkin KO mice, the distribution and density of mitochondria in DA neurons from this genetic background were also directly examined by infecting cells with a mitochondrially-tagged DsRed protein (DsRed2-mito lentivirus) (Figure 4A). No significant difference was detected in the density of mitochondria in the soma, axon or dendrites of SNc DA neurons from Parkin KO mice compared to WT (Figure 4B).

5.3.3 Parkin KO glia show altered growth, extracellular acidification rate (ECAR) and OCR and influence basal survival of SNc DA neurons.

The reduced resilience of SNc DA neurons in Parkin KO mice could be due to a cell-intrinsic perturbation, to perturbation of non-neuronal cells such as astrocytes or microglia or a combination of the two. Previous work has indeed demonstrated reduced proliferation of astrocytes, increased density of microglia and reduced neuroprotective effects of glial-conditioned medium in Parkin KO mice (13). We therefore evaluated the implication of glial cells in the altered survival of the Parkin KO SNc DA neurons by growing Parkin KO DA neurons with WT glia. We found that this completely reverted this reduced survival phenotype (Figure 5A). Compatible with previous results (13), there were 33% fewer cells in Parkin KO cortical glial cultures after 7DIV, 36% less at 10 DIV and 39% fewer cells at 10 DIV with a mitotic inhibitor was added when glial cells reached confluence, conditions that mimicked those used to prepare neuronal cultures (Figure 5B-C). The proliferation of mesencephalic glial cells was similarly reduced (Supplemental Figure S3). Glial cells in Parkin KO cultures were also

perturbed at the metabolic level, as revealed by the fact that basal OCR was reduced by 24% and maximal OCR by 25%, with no change in RCR (Figure 5D). In addition, basal glycolysis was increased by 52% (Figure 5E) and no change was observed in ATP levels (Figure 5F), suggesting the possibility of a compensation by glycolysis of the reduced OXPHOS. Similar measurements performed in Pink1 KO and DJ-1 KO cultures revealed a decreased basal and maximal OCR in glial cells from Pink1 KO but not DJ-1 KO mice, with no changes in any other measurements (Supplemental Figure S4).

5.3.4 Vulnerability to the neurotoxin MPP+ is altered in Parkin, DJ-1 but not Pink1 KO SNc DA neurons.

The reduced basal survival of SNc DA neurons from Parkin KO mice (Figure 1A), together with the observation of reduced axonal arborization size (Figure 1H) in these surviving neurons suggests the possibility that the surviving smaller neurons might be more resilient, as per a recent model (4, 9). To test this possibility, we next examined the vulnerability of DA neurons at 10 DIV to cellular stress induced by the DA neuron specific neurotoxin and mitochondrial complex I inhibitor MPP+. Interestingly, the surviving SNc DA neurons from the Parkin KO cultures were significantly less vulnerable to MPP+ (Figure 6A). No change in vulnerability was observed in SNc DA neurons from Pink1 KO mice (Figure 6B). Finally, SNc DA neurons from DJ-1 KO mice were to the contrary more vulnerable to MPP+ (Figure 6C). Compatible with previous work showing higher resilience of VTA DA neurons, MPP+ caused much smaller cell loss in VTA DA neurons and no difference was found between genotype (Figure 6D-F).

5.3.5 Reduced DA transporter expression in surviving SNc DA neurons in Parkin KO mice.

Although reduced vulnerability of surviving SNc DA neurons from Parkin KO mice could be due to a number of factors, an obvious possibility is that reduced toxicity could be due to lower levels of the DA transporter (DAT), which is the route of entry of MPP+ in DA neurons

(14). We measured DAT density using a radio ligand assay and found that surviving DA neurons indeed showed 60% less DAT compared to WT SNc DA neurons (Figure 7A). Also arguing in favor of this hypothesis, vulnerability to DAT-independent toxic treatments such as hydrogen peroxide (Figure 7B) or the complex I blocker rotenone (Figure 7C) was similar in Parkin KO and WT SNc DA neuron cultures. Finally, vulnerability to MPP+ of Parkin KO SNc DA neurons growth together with WT glia, conditions that prevent the loss of SNc DA neurons, was similar to that of WT SNc DA neurons (Figure 7D).

5.3.6 Partial rescue of Parkin KO SNc DA neurons by WT Parkin overexpression

Finally, to further strengthen the idea that the reduced basal survival, axonal length and increased basal OCR in SNc DA neurons from Parkin KO mice is a direct consequence of the loss of Parkin expression, we overexpressed WT Parkin using an AAV vector (Figure 8A). We found that the basal survival of SNc DA Parkin KO neurons was partially rescued by Parkin overexpression (Figure 8B) and that their axonal length and basal OCR were also back to WT levels (Figure 8C,D), without changing maximal OCR or RCR (Figure 8E,F).

5.4 Discussion

Since the discovery of the first human mutations causing familial forms of Parkinson's disease, extensive work has been performed to identify the mechanisms by which loss or gain of function of gene products including Parkin, Pink1, DJ-1, LRRK2 and alpha-synuclein trigger the disease process. One of the approaches used has been to create knockout animals in species such as flies and mice in the hope of obtaining valid models of the disease. Unfortunately, in mice, constitutive KO of these genes typically does not lead to age-dependent loss of DA neurons *in vivo* (but see (15–17)). A possible explanation could be that it is difficult to model age-dependent neurodegeneration in species with a short life span or that mice need to be

exposed to a second hit to trigger the disease. Another possibility is that the cumulative burden of oxidative stress in mouse DA neurons is not sufficiently high to lead to cell loss. Whatever the case may be, using these models is still of interest to examine some of the early stages of the disease, prior to cell loss. Indeed, various cellular and subcellular dysfunctions have been reported in such models during the past decade (18–22). In this present work, we aimed to determine whether basal resilience *in vitro* and parameters linked to cellular bioenergetics such as mitochondrial OXPHOS and axonal arborization size are altered in Parkin, Pink1 or DJ-1 KO mice.

5.4.1 Morphological and bioenergetic alterations in Parkin KO SNc cultures

We discovered that basal survival *in vitro*, axonal growth and mitochondrial function are altered in SNc DA neurons from Parkin KO mice, with little if any changes in Pink1 KO or DJ-1 KO mice. Our finding of reduced basal survival of SNc DA neurons in Parkin KO mice argues that SNc DA neurons in these mice have a higher basal vulnerability to cellular stress, a conclusion that is in keeping with previous results (9, 23, 24). Interestingly, we found that the subset of SNc DA neurons that survived up to 11 DIV in Parkin KO cultures possessed a smaller axonal arborization and produced less ATP, findings that are compatible with previous work proposing that cellular bioenergetics are directly related to axon length and to vulnerability (9). Further experiments directly evaluating the links between ATP levels and axon growth in DA neurons would help establish more direct links between these parameters. Our observation of reduced axonal arborization size is also in line with recent work showing reduced complexity of neuronal processes in iPSC-derived human neurons carrying Parkin mutations (25). However, somewhat surprisingly, surviving Parkin KO SNc DA neurons at 10 days *in vitro* showed higher basal OCR, suggesting an uncoupling between oxygen consumption and ATP production. This observation could be the result of the accumulation of damaged mitochondria and as such would be compatible with previous work showing mitochondrial dysfunction in Parkin KO mutant drosophila (26). However, no increase in OCR was reported in mouse cortical or striatal primary cultures or in mesencephalic post-nuclear supernatants prepared from adult Parkin KO mice (27). Since such cultures do not contain any DA neurons and since OCR measurements from mesencephalic post-nuclear supernatants are necessarily contaminated by non-DA neurons and

other cells, it is possible that a change in OCR occurring principally in DA neurons may have been missed in these previous studies.

5.4.2 Impaired mitochondrial function in SNc Parkin-KO cultures

Considering that Parkin is normally recruited by Pink1 to damaged mitochondria to initiate mitophagy, it is possible that the increase in OCR with a reduction in ATP levels that we observed in residual SNc DA neurons after 10 days *in vitro* is the results of the accumulation of malfunctioning, uncoupled mitochondria. Although we cannot exclude this possibility, our observation of a lack of change in mitochondrial density, evaluated with Mito-DsRed, does not provide support for such an interpretation. One possibility is that other mechanisms compensate for the lack of Parkin-mediated mitophagy. Such mechanisms could either get rid of some of the damaged mitochondria in a Parkin-independent manner and/or slow down the production of new mitochondria, explaining the lack of change of total mitochondrial density. Although recent work suggests that the rate of mitophagy in axons may be very limited (28), additional experiments directly quantifying mitochondrial turnover could help clarify this issue. Nonetheless, the increase in OCR combined with decreased ATP production argues for malfunctioning mitochondria (9, 22, 29, 30). In this context, the resulting metabolic stress could favor the survival of neurons with smaller bioenergetic needs such as those that have a smaller axonal arborization. Arguing in favor of this interpretation, VTA DA neurons, which are less vulnerable in PD and normally have a smaller axonal arborization than SNc DA neurons (9), did not show altered survival in the absence of Parkin under our experimental conditions. We found that even if they showed a much higher basal OCR, their ATP production and axonal arborization was unchanged. This highlights the higher basal resilience of these neurons. Further experiments quantifying basal ROS production and antioxidant defense mechanisms in VTA DA neurons would be helpful to further characterize and explain such resilience.

Our finding of a lack of change in bioenergetics and axonal growth in DA neurons from Pink1 and DJ-1 KO mice is puzzling, especially concerning the implication of Pink1 in mitochondrial quality control, in a common pathway with Parkin. A partial explanation could come from recent work showing that mitochondrial quality control in tissues with elevated

metabolic demands such as the brain can be Pink1-independent (31). If this is also the case in our model, this could explain why we only see alterations in Parkin KO cultures. Except for a recent study reporting age-dependent unilateral loss of SNc DA neurons in a new sub-strain of DJ-1 KO mice (15), there has been no previous reports of altered basal growth and survival of DA neurons in Pink1 or DJ-1 KO mouse lines. However, previous work has reported impaired respiration and increased glycolytic activity in mixed neuronal culture from the midbrain of Pink1 KO mice (32). The relative abundance of DA neurons in such cultures was not reported, making it unclear if results reflected the bioenergetic properties of SNc DA neurons. In addition, mitochondrial membrane potential was used to indirectly evaluate OXPHOS, making a comparison with our present results difficult. Concerning DJ-1, previous work using a neuronal-like cell line showed reduced OCR and ATP production (33). It is very difficult to compare our findings to such results because of the major morphological and bioenergetic differences between such cell lines and primary DA neurons, in addition to the major difference in cell maturity between the two studies (18h in the Heo et al. study compared to 10 days for the present study). In the present study, while increased cell loss was apparent after 11 days in Parkin KO cultures, we found no change after 5 days. Similarly, loss of Pink1 or DJ-1 might thus need more time to reveal an increased vulnerability, as suggested by work on aged Pink1 KO mice (34). Further studies evaluating neuronal survival in DA neurons from Pink1 or DJ-1 KO mice after longer time points in culture might thus be useful to determine whether changes in vulnerability do exist, but simply need a higher level of cellular stress or time to be revealed.

5.4.3 WT Parkin overexpression rescues morphological and bioenergetic defects in Parkin KO SNc cultures

Since the KO used in this work was constitutive, the increased vulnerability of SNc DA neurons we detected in Parkin KO cultures could result from changes occurring during embryonic development of the neurons and not be a direct consequence of the lack of Parkin expression in cells. To explore this possibility, we performed a rescue experiment and reintroduced WT Parkin using an AAV vector. We found that such overexpression was sufficient to rescue the changes in basal survival, axonal growth and mitochondrial OXPHOS in Parkin KO SNc DA neurons, observations that are compatible with previous work showing

that overexpression of WT Parkin is neuroprotective (35, 36). An important limitation of the present rescue experiment is that Parkin expression was driven through a strong CBA promoter, likely leading to expression levels much higher than WT levels (Supplemental Figure S5).

5.4.4 Parkin-KO glial cell alterations and implications for neuronal defects

The increased vulnerability of SNc DA neurons we detected in Parkin KO cultures could result from cell-autonomous alterations, from non-cell autonomous mechanisms, such as a change in glial cell function, as reported previously (13), or a combination of the two. To explore the implication of astrocytes, cells that play a key role in the trophic support of DA neurons (37, 38), we prepared mixed cultures containing WT glia and Parkin KO DA neurons. In such cultures, we observed no significant differential loss of SNc DA neurons over 10 days *in vitro*, arguing for a major implication of glia cell dysfunction in the reduced survival of SNc DA neurons in cultures prepared from Parkin KO mice. Compatible with glial cell dysfunction in such mice, we found slower proliferation of Parkin KO glial cells, an observation that is in line with previous work (13, 39). Such slower proliferation of glial cells (mostly astrocytes) led to a reduced density of such cells at 10 DIV, accompanied by a reduction in OCR, but an increase in glycolysis, with no changes in ATP levels. It is possible that the reduction in glial cell number itself influenced neuronal survival in Parkin KO cultures. However, we feel that this is unlikely because we found that very large reductions in glial cell density are required to negatively impact DA neuron survival (data not shown). Here, the reduction in glial cell density was modest (~33%) and was not accompanied by a decrease in ATP production. Future work will be required to determine if the secretion of glial-cell derived neurotrophic factors or the regulation of lactate or pyruvate shuttling is altered in Parkin KO astrocytes, providing a potential explanation for the reduced survival of SNc DA neurons.

5.4.5 Lower DAT level in surviving Parkin-KO SNc neurons

SNc DA neurons are well-known to be particularly vulnerable to mitochondrial toxins such as MPP+, which enter DA neurons through the DAT (14). DA neurons in Pink1 and DJ-1 KO mice have been reported to be more vulnerable to different toxin models, suggesting

increased cell vulnerability (21, 40–45). Surprisingly, this is not the case for Parkin KO mice (30, 46–49). We therefore also investigated this issue in the present study using MPP+, the active metabolite of MPTP. Interestingly, we found increased vulnerability to MPP+ only in SNc DA neurons cultured from DJ-1 KO mice, but not in cultures prepared from Pink1 or Parkin KO mice, arguing that some of the properties of DJ-1, such as its antioxidant role is important to prevent toxicity to MPP+, even if it is not necessary for survival up to 11 DIV under our basal culture conditions. Since the MPTP experiments cited previously were performed in adult mice, it is possible that the developing state of our neurons prevented us from seeing such increased vulnerability in Pink1 KO cultures. Surprisingly, in Parkin KO SNc cultures, the neurons surviving after 10 DIV were actually less vulnerable to MPP+. A number of models can be considered to explain this result. First, this could be caused by a lower expression of DAT in surviving DA neurons; a down-regulation reported previously when this mouse was first characterized (48) and more recently in Parkin mutant human midbrain DA neurons derived from induced pluripotent stem cells (50). Compatible with this, we did observe a lower expression of DAT in Parkin KO cultures. In addition, we found no change in survival in response to DAT-independent oxidative stress such as that induced by rotenone or H_2O_2. This last finding is in apparent contradiction with previously published data showing that embryonic midbrain DA neurons from Parkin KO mice show an increased vulnerability to rotenone (51). The different type of cultures used (embryonic vs. postnatal), density of DA neurons (low vs. high), age of cultures (7 vs 10 DIV) and the different duration of rotenone application are all factors that should be considered to explain such different results. Interestingly, in the present study, we found no differential effect of MPP+ on the survival of Parkin KO DA neurons when Parkin KO SNc DA neurons were cultured together with WT glia; this finding could be taken to suggest that the differential expression of DAT alone is not sufficient to explain the differential survival of SNc DA neurons to MPP+ in Parkin KO cultures. However, a more comprehensive explanation is that in Parkin KO SNc cultures, the impaired functioning of astrocytes lead to the preferential death of highly arborized DA neurons, a population of neurons that are otherwise more vulnerable to cellular stressors in general (9). Because of this differential survival, the remaining SNc DA neurons in Parkin KO cultures would have lower axonal arborization and reduced DAT expression with consequent reduced vulnerability to MPP+. DAT levels were not quantified in cultures prepared from Pink1 KO or DJ-1 KO mice.

Our data provide new insights into the complex relationship between mitochondrial function, axonal growth and genetic risk factors linked to PD. Previous work has shown that overexpression of Parkin, Pink1 or DJ-1 in DA neurons is neuroprotective against mitochondrial toxins (35, 36, 52). Such results argue for a direct role of these gene products in regulating the vulnerability of DA neurons. The present results also uncover a role of Parkin in regulating mitochondrial function and OXPHOS in DA neurons. However, our findings also argue for the existence of more indirect roles through an impact on glial cells. Further work will be required to examine if such changes might be key to explain the heightened vulnerability of SNc DA neurons over multiple decades, as occurs in PD.

5.5 Experimental procedures

Animals

All procedures involving animals were conducted in strict accordance with the Guide to care and use of experimental animals (2nd Ed.) of the Canadian Council on Animal Care. The experimental protocols were approved by the animal ethics committee (CDEA) of the Université de Montréal. Housing was at a constant temperature (21°C) and humidity (60%), under a fixed 12 hours light/dark cycle and free access to food and water.

Genotyping

All animals used were genotyped using a KAPA2G Fast HotStart DNA Polymerase kit from Kapa Biosystem. Primer used were:

Pink1 WT upper primer (0.2µM)	TCCCTCTATGGCGTCCTCTT
Pink1 WT lower primer (0.2µM)	CAGCAACTGCAAGGTCATCA
Pink1 KO upper primer (0.2µM)	GCACCCTGACCTTGGTTCCTA
Pink1 KO lower primer (0.2µM)	GGGGGAACTTCCTGACTAGG
Parkin WT upper primer (1µM)	TGCTCTGGGGTTCGTC
Parkin WT lower primer (1µM)	TCCACTGGCAGAGTAAATGT
DJ-1 WT upper primer (0.5µM)	TGGTGAAGTGAGCAGACAGG
DJ-1 WT lower primer (0.5µM)	AGGAGCCAAAGAAACAAGCA
Parkin (0.25µM) or DJ-1 (0.5µM) Neo upper primer	CCTGCTTGCCGAATATCAT
Parkin (0.25µM) or DJ-1 (0.5µM) Neo lower primer	AAGGCGATAGAAGGCGATG

Primary neuronal cultures and drug treatments

Cultures were prepared according to a previously described protocol (53), with minor variations (9). Dissociated neurons micro-dissected from the SNc or VTA of postnatal days 0-2 (P0-P2) Parkin KO (48), Pink1 KO (54) or DJ-1 KO (40) mice were seeded on a monolayer of corresponding cortical astrocytes grown on collagen/poly-L-lysine-coated glass coverslips. The total seeded neuron density was 100 000 cells/ml for all experiments, except for the metabolic flux experiments for which the density was 250 000 cells/ml. All cultures were incubated at 37 °C in 5 % CO_2 and maintained in 2/3 of Neurobasal^{TM}-A medium enriched with 1 % penicillin/streptomycin, 1 % Glutamax^{TM}-1, 2 % B-27 supplement and 5 % fetal bovine serum (Invitrogen) plus 1/3 of minimum essential medium (MEM) enriched with 1 % penicillin/streptomycin, 1 % GlutamaxTM-1, 20 mM Glucose, 1mM sodium pyruvate and 100 µl MITO+ serum-extender. In some experiments, MPP+ (Sigma) (5 or 10 µM) or H_2O_2 (Sigma) (100-150 µM) were added at 10 DIV (days *in vitro*) for 24h. In other experiments, the complex I blocker rotenone (Sigma) (50 nM) was added at 8 DIV for 72h. For the rescue experiments, AAV encoding GFP (AAV-CBA-emGFP) or WT Parkin fused with GFP (AAV-CBA-emGFP-flag-Parkin WT) were applied to the cells the day of the culture, leading to infection of more than 95% of the cells.

Metabolic flux experiments

The rate of oxygen consumption deriving from mitochondrial OXPHOS and the extracellular acidification rate (ECAR) deriving from glycolysis were assessed using an extracellular flux analyzer (Seahorse Biosciences), as previously described (9). Cells were plated on XF24 tissue culture plates and maintained in culture for 5 or 10 days. Before experiments, cells were incubated for 1 h at 37°C in a CO2-free incubator in bicarbonate-free DMEM (Sigma) supplemented with 2 mM GlutaMax^{TM}-1 (Invitrogen), 1 mM sodium pyruvate (Sigma), 25 mM D-glucose (Sigma), 63.3 mM NaCl (Sigma) and phenol red (Sigma). The pH was adjusted to 7.4 with NaOH. These concentrations of substrates represent saturating concentrations to ensure that they did not limit the rate of respiration and glycolysis. Oxygen consumption was sequentially measured under basal conditions, in the presence of the

mitochondrial uncoupler CCCP (0.5 μM) to assess the maximal oxidative capacity and in the presence of the mitochondrial inhibitors rotenone (1 μM) and antimycin A (1 μM), to assess non-mitochondrial oxygen consumption. After the assays, the cells were immediately fixed for immunofluorescence. For 10 DIV cultures, the oxygen consumption rate (OCR) was normalized to cell number, as assessed by DAPI staining. Since neurons were cultured together with astrocytes, parallel measurements were also performed from pure astrocyte cultures. After subtraction of the OCR measured from astrocytes, the resulting OCR values measured from mixed cultures were normalized in a second step on the total number of neurons identified with MAP-2 immunostaining. For 5 DIV cultures, OCR and all ECAR measurements, the contribution of glial cells was not subtracted since values in co-cultures were close to those of astrocytes. Values were normalized on total cell number and then on the total number of neurons.

Immunofluorescence

Cultures were fixed 30 min with 4% paraformaldehyde (PFA) in PBS, permeabilized, and nonspecific binding sites blocked. Cells were incubated overnight with a primary antibody solution containing 1% bovine serum albumin (BSA), 0.1% Triton-X-100 in PBS, 5% goat serum and 0.02% NaN3. Cells were washed several times in PBS before incubation for 1h with the appropriate Alexa-labelled secondary antibodies (Invitrogen). Primary antibodies used were TH-rabbit (Millipore, 1:2000), MAP-2-mouse (Chemicon, 1:1000) and RFP-rabbit (Rockland, 1:1000).

Mitochondrial network quantification

Mitochondria were labelled by infecting neurons with a lentivirus encoding DsRed2-mito (mitochondrially-targeted red fluorescent reporter protein) at 30 MOI at the time of plating and fixed at 10 DIV. Images were obtained by capturing confocal 0.5 micron z-stacks (10-15 images) using a 60x oil-immersion objective (NA 1.42) on a Olympus Fluoview FV100 confocal using Fluoview version 3.1b software. Image analysis was performed using ImageJ software. Only TH-positive infected DA neurons were selected for analysis. Regions of interest

were determined to separately measure DsRed2-mito signal in the cell body, isolated dendrite segments and isolated axon segments. The percentage of TH-positive area covered by DsRed signal was measured in each cellular compartment.

Global neuronal morphology and survival assessment

At 10 DIV, TH-positive axonal arborization surface was estimated by capturing 5 confocal image stacks per coverslip randomly throughout the coverslip with a 20X water immersion objective (NA 0.5). Using a home-made macro in ImageJ, MAP2 and TH signal were thresholded to remove background and then binarised. MAP2 signal area was then removed from TH signal area and the remaining axonal signal surface was measured. For survival assessment, the number of TH neurons with clear round nuclei on the coverslip were estimated by scanning the coverslip vertically and horizontally (cross-counting) with a 20X dry objective (NA 0.40) on a Nikon Eclipse TE200 inverted microscope.

Parkin KO glial cells proliferation measurements

Glial cells were grown on coverslips for 1, 3, 7 and 10 DIV. On a separate series of coverslips, FUDR was added once glial cell reached confluence as is typically performed for neuronal cultures. The number of glial cells was measured by counting cells in 5 random pictures per coverslip after DAPI staining.

Measurement of total cellular ATP

Cellular ATP content was determined using the PerkinElmer “ATPlite” kit (PerkinElmer) according to the manufacturer's instructions. The cells were collected by trypsinization and centrifugation at 500 ×g and then re-suspended in phosphate-buffered saline, pH 7.4. Measurements were performed on a Wallac Victor plate reader (PerkinElmer). One coverslip from each sample was labelled with DAPI to quantify total cell number. ATP values were then normalized on total cell number. Oligomycin-insensitive ATP production (from glycolysis) was subtracted. Values obtained from measurements from glial cells alone were

subtracted. The remaining values, representing the ATP derived from OXPHOS in neurons only, were then normalized on the total number of neurons identified with MAP-2 immunostaining.

Radioligand assay

10 DIV cultures were incubated with trypsin a 37^{O}C during 10 min and collected in 20% FBS in PBS after subsequent centrifugation at 900 and 1500g for 5 min. One mL of PBS was added between the two centrifugations. The cell pellets were resuspended in cold 200 µL of a binding buffer solution (Na2HPO4 10.1 mM, KH2PO4 1.8 mM, KCl 2 mM, NaCl 137 mM) and then stored at -80 ^{O}C until use. Tissue homogenates were washed by centrifugation at 13,000 g (4°C) for 15 min. Supernatants were discarded and pellets resuspended in the same buffer. DAT labelling was performed by adding 20 pM of (125I)RTI-55 ligand (specific activity, 2200 Ci/mmol, PerkinElmer, Woodbride, ON, Canada) to the tissue homogenates in a final volume of 200 uL. Each sample was evaluated in triplicate. Nonspecific binding was estimated in the presence of 1 µM of the selective reuptake inhibitor GBR12909 (Sigma-Aldrich, St-Louis, MO, USA). Incubation at room temperature for 1 h was terminated by rapid filtration through Whatman GF/C glass filters under vacuum, followed by 3 rinses (4 ml each) with the same ice-cold buffer. Radioactivity was counted by γ scintigraphy.

Statistics

Parametric statistical tests were used because samples contained data with normal distributions. Data were always obtained from a minimum of 3 separate sets of experiments and presented as mean ± SEM. The level of statistical significance was established at $p < 0.05$ in one or two-way ANOVAs or two-tailed t-tests. A ROUT outlier analysis was performed when needed (Q=1%). Statistical analyses were performed with the Prism 7 software (GraphPad Software, $p < 0.05$ = *, $p < 0.01$ = **, $p < 0.001$ = ***, $p < 0.0001$ = ****). The Tukey post-hoc test was used when all the means were compared to each other and the Sidak post-hoc test was used when only subsets of means were compared.

5.6 Acknowledgements

The GRSNC is supported by an infrastructure grant from the Fonds du Québec en Recherche, Santé (FRQS). N. Giguère and C. Pacelli both received salary support from Parkinson Society Canada and N. Giguère received salary support from Fonds du Québec en Recherche, Santé (FRQS).

5.7 References

1. De Rosa, P., Marini, E. S., Gelmetti, V., and Valente, E. M. (2015) Candidate genes for Parkinson disease: Lessons from pathogenesis. Clin. Chim. Acta Int. J. Clin. Chem. 449, 68–76

2. Parent, M., and Parent, A. (2006) Relationship between axonal collateralization and neuronal degeneration in basal ganglia. J. Neural Transm. Suppl.

3. Matsuda, W., Furuta, T., Nakamura, K. C., Hioki, H., Fujiyama, F., Arai, R., and Kaneko, T. (2009) Single nigrostriatal dopaminergic neurons form widely spread and highly dense axonal arborizations in the neostriatum. J. Neurosci. 29, 444–453

4. Bolam, J. P., and Pissadaki, E. K. (2012) Living on the edge with too many mouths to feed: why dopamine neurons die. Mov. Disord. 27, 1478–1483

5. Gauthier, J., Parent, M., Lévesque, M., and Parent, A. (1999) The axonal arborization of single nigrostriatal neurons in rats. Brain Res. 834, 228–232

6. Perier, C., and Vila, M. (2012) Mitochondrial biology and Parkinson's disease. Cold Spring Harb. Perspect. Med. 2, a009332

7. Franco-Iborra, S., and Perier, C. (2015) Neurodegeneration: the size takes it all. Curr. Biol. 25, R797–R800.

8. Pissadaki, E. K., and Bolam, J. P. (2013) The energy cost of action potential propagation in dopamine neurons: clues to susceptibility in Parkinson's disease. Front. Comput. Neurosci. 7, 13

9. Pacelli, C., Giguère, N., Bourque, M.-J., Lévesque, M., Slack, R. S., and Trudeau, L.-É. (2015) Elevated mitochondrial bioenergetics and axonal arborization size are key contributors to the vulnerability of dopamine neurons. Curr. Biol. CB. 25, 2349–2360

10. Yamano, K., Matsuda, N., and Tanaka, K. (2016) The ubiquitin signal and autophagy: an orchestrated dance leading to mitochondrial degradation. EMBO Rep. 17, 300–316

11. Pickrell, A. M., Huang, C.-H., Kennedy, S. R., Ordureau, A., Sideris, D. P., Hoekstra, J. G., Harper, J. W., and Youle, R. J. (2015) Endogenous Parkin preserves dopaminergic substantia nigral neurons following mitochondrial DNA mutagenic stress. Neuron. 87, 371–381

12. McLelland, G.-L., Soubannier, V., Chen, C. X., McBride, H. M., and Fon, E. A. (2014) Parkin and Pink1 function in a vesicular trafficking pathway regulating mitochondrial quality control. EMBO J. 33, 282–295

13. Solano, R. M., Casarejos, M. J., Menéndez-Cuervo, J., Rodriguez-Navarro, J. A., García de Yébenes, J., and Mena, M. A. (2008) Glial dysfunction in parkin null mice: effects of aging. J. Neurosci. 28, 598–611

14. Javitch, J. A., D'Amato, R. J., Strittmatter, S. M., and Snyder, S. H. (1985) Parkinsonism-inducing neurotoxin, N-methyl-4-phenyl-1,2,3,6-tetrahydropyridine: uptake of the metabolite N-methyl-4-phenylpyridine by dopamine neurons explains selective toxicity. Proc Natl Acad Sci U A. 82, 2173–7

15. Rousseaux, M. W. C., Marcogliese, P. C., Qu, D., Hewitt, S. J., Seang, S., Kim, R. H., Slack, R. S., Schlossmacher, M. G., Lagace, D. C., Mak, T. W., and Park, D. S. (2012) Progressive dopaminergic cell loss with unilateral-to-bilateral progression in a genetic model of Parkinson disease. Proc. Natl. Acad. Sci. U. S. A. 109, 15918–15923

16. Stevens, D. A., Lee, Y., Kang, H. C., Lee, B. D., Lee, Y.-I., Bower, A., Jiang, H., Kang, S.-U., Andrabi, S. A., Dawson, V. L., Shin, J.-H., and Dawson, T. M. (2015) Parkin loss leads to PARIS-dependent declines in mitochondrial mass and respiration. Proc. Natl. Acad. Sci. U. S. A. 112, 11696–11701

17. Lee, Y., Stevens, D. A., Kang, S.-U., Jiang, H., Lee, Y.-I., Ko, H. S., Scarffe, L. A., Umanah, G. E., Kang, H., Ham, S., Kam, T.-I., Allen, K., Brahmachari, S., Kim, J. W., Neifert, S., Yun, S. P., Fiesel, F. C., Springer, W., Dawson, V. L., Shin, J.-H., and Dawson, T. M. (2017) Pink1 Primes Parkin-Mediated Ubiquitination of PARIS in Dopaminergic Neuronal Survival. Cell Rep. 18, 918–932

18. Hauser, D. N., and Hastings, T. G. (2013) Mitochondrial dysfunction and oxidative stress in Parkinson's disease and monogenic parkinsonism. Neurobiol. Dis. 51, 35–42

19. Dias, V., Junn, E., and Mouradian, M. M. (2013) The role of oxidative stress in Parkinson's disease. J. Park. Dis. 3, 461–491

20. Zhang, W., Wang, T., Pei, Z., Miller, D. S., Wu, X., Block, M. L., Wilson, B., Zhang, W., Zhou, Y., Hong, J.-S., and Zhang, J. (2005) Aggregated alpha-synuclein activates microglia: a process leading to disease progression in Parkinson's disease. FASEB J. 19, 533–542

21. Canet-Avilés, R. M., Wilson, M. A., Miller, D. W., Ahmad, R., McLendon, C., Bandyopadhyay, S., Baptista, M. J., Ringe, D., Petsko, G. A., and Cookson, M. R. (2004) The Parkinson's disease protein DJ-1 is neuroprotective due to cysteine-sulfinic acid-driven mitochondrial localization. Proc. Natl. Acad. Sci. U. S. A. 101, 9103–9108

22. Greene, J. C., Whitworth, A. J., Kuo, I., Andrews, L. A., Feany, M. B., and Pallanck, L. J. (2003) Mitochondrial pathology and apoptotic muscle degeneration in Drosophila parkin mutants. Proc. Natl. Acad. Sci. U. S. A. 100, 4078–4083

23. Luk, K. C., Rymar, V. V., van den Munckhof, P., Nicolau, S., Steriade, C., Bifsha, P., Drouin, J., and Sadikot, A. F. (2013) The transcription factor Pitx3 is expressed

selectively in midbrain dopaminergic neurons susceptible to neurodegenerative stress. J. Neurochem. 125, 932–943

24. Hung, H. C., and Lee, E. H. (1996) The mesolimbic dopaminergic pathway is more resistant than the nigrostriatal dopaminergic pathway to MPTP and MPP+ toxicity: role of BDNF gene expression. Brain Res. Mol. Brain Res. 41, 14–26

25. Ren, Y., Jiang, H., Hu, Z., Fan, K., Wang, J., Janoschka, S., Wang, X., Ge, S., and Feng, J. (2015) Parkin mutations reduce the complexity of neuronal processes in iPSC-derived human neurons. Stem Cells Dayt. Ohio. 33, 68–78

26. Burman, J. L., Yu, S., Poole, A. C., Decal, R. B., and Pallanck, L. (2012) Analysis of neural subtypes reveals selective mitochondrial dysfunction in dopaminergic neurons from parkin mutants. Proc. Natl. Acad. Sci. U. S. A. 109, 10438–10443

27. Damiano, M., Gautier, C. A., Bulteau, A.-L., Ferrando-Miguel, R., Gouarne, C., Paoli, M. G., Pruss, R., Auchère, F., L'Hermitte-Stead, C., Bouillaud, F., Brice, A., Corti, O., and Lombès, A. (2014) Tissue- and cell-specific mitochondrial defect in Parkin-deficient mice. PloS One. 9, e99898

28. Cao, X., Wang, H., Wang, Z., Wang, Q., Zhang, S., Deng, Y., and Fang, Y. (2017) In vivo imaging reveals mitophagy independence in the maintenance of axonal mitochondria during normal aging. Aging Cell. 16, 1180–1190

29. Pacelli, C., De Rasmo, D., Signorile, A., Grattagliano, I., di Tullio, G., D'Orazio, A., Nico, B., Comi, G. P., Ronchi, D., Ferranini, E., Pirolo, D., Seibel, P., Schubert, S., Gaballo, A., Villani, G., and Cocco, T. (2011) Mitochondrial defect and PGC-1α dysfunction in parkin-associated familial Parkinson's disease. Biochim. Biophys. Acta. 1812, 1041–1053

30. Palacino, J. J., Sagi, D., Goldberg, M. S., Krauss, S., Motz, C., Wacker, M., Klose, J., and Shen, J. (2004) Mitochondrial dysfunction and oxidative damage in parkin-deficient mice. J. Biol. Chem. 279, 18614–18622

31. McWilliams, T. G., Prescott, A. R., Montava-Garriga, L., Ball, G., Singh, F., Barini, E., Muqit, M. M. K., Brooks, S. P., and Ganley, I. G. (2018) Basal mitophagy occurs independently of Pink1 in mouse tissues of high metabolic demand. Cell Metab. 27, 439-449.e5

32. Yao, Z., Gandhi, S., Burchell, V. S., Plun-Favreau, H., Wood, N. W., and Abramov, A. Y. (2011) Cell metabolism affects selective vulnerability in Pink1-associated Parkinson's disease. J. Cell Sci. 124, 4194–4202

33. Heo, J. Y., Park, J. H., Kim, S. J., Seo, K. S., Han, J. S., Lee, S. H., Kim, J. M., Park, J. I., Park, S. K., Lim, K., Hwang, B. D., Shong, M., and Kweon, G. R. (2012) DJ-1 null dopaminergic neuronal cells exhibit defects in mitochondrial function and structure: involvement of mitochondrial complex I assembly. PloS One. 7, e32629

34. Gispert, S., Ricciardi, F., Kurz, A., Azizov, M., Hoepken, H.-H., Becker, D., Voos, W., Leuner, K., Müller, W. E., Kudin, A. P., Kunz, W. S., Zimmermann, A., Roeper, J., Wenzel, D., Jendrach, M., García-Arencíbia, M., Fernández-Ruiz, J., Huber, L., Rohrer, H., Barrera, M., Reichert, A. S., Rüb, U., Chen, A., Nussbaum, R. L., and Auburger, G. (2009) Parkinson phenotype in aged Pink1-deficient mice is accompanied by progressive mitochondrial dysfunction in absence of neurodegeneration. PLOS ONE. 4, e5777

35. Paterna, J.-C., Leng, A., Weber, E., Feldon, J., and Büeler, H. (2007) DJ-1 and Parkin modulate dopamine-dependent behavior and inhibit MPTP-induced nigral dopamine neuron loss in mice. Mol. Ther. J. Am. Soc. Gene Ther. 15, 698–704

36. Benskey, M. J., Manfredsson, F. P., Lookingland, K. J., and Goudreau, J. L. (2015) The role of parkin in the differential susceptibility of tuberoinfundibular and nigrostriatal dopamine neurons to acute toxicant exposure. Neurotoxicology. 46, 1–11

37. Rappold, P. M., and Tieu, K. (2010) Astrocytes and therapeutics for Parkinson's disease. Neurother. J. Am. Soc. Exp. Neurother. 7, 413–423

38. Nakajima, K., Hida, H., Shimano, Y., Fujimoto, I., Hashitani, T., Kumazaki, M., Sakurai, T., and Nishino, H. (2001) GDNF is a major component of trophic activity in DA-depleted striatum for survival and neurite extension of DAergic neurons. Brain Res. 916, 76–84

39. Shaltouki, A., Sivapatham, R., Pei, Y., Gerencser, A. A., Momčilović, O., Rao, M. S., and Zeng, X. (2015) Mitochondrial alterations by Parkin in dopaminergic neurons using PARK2 patient-specific and PARK2 knockout isogenic iPSC lines. Stem Cell Rep. 4, 847–859

40. Kim, R. H., Smith, P. D., Aleyasin, H., Hayley, S., Mount, M. P., Pownall, S., Wakeham, A., You-Ten, A. J., Kalia, S. K., Horne, P., Westaway, D., Lozano, A. M., Anisman, H., Park, D. S., and Mak, T. W. (2005) Hypersensitivity of DJ-1-deficient mice to 1-methyl-4-phenyl-1,2,3,6-tetrahydropyrindine (MPTP) and oxidative stress. Proc. Natl. Acad. Sci. U. S. A. 102, 5215–5220

41. Haque, M. E., Mount, M. P., Safarpour, F., Abdel-Messih, E., Callaghan, S., Mazerolle, C., Kitada, T., Slack, R. S., Wallace, V., Shen, J., Anisman, H., and Park, D. S. (2012) Inactivation of Pink1 gene in vivo sensitizes dopamine-producing neurons to 1-methyl-4-phenyl-1,2,3,6-tetrahydropyridine (MPTP) and can be rescued by autosomal recessive Parkinson disease genes, Parkin or DJ-1. J. Biol. Chem. 287, 23162–23170

42. Martinat, C., Shendelman, S., Jonason, A., Leete, T., Beal, M. F., Yang, L., Floss, T., and Abeliovich, A. (2004) Sensitivity to oxidative stress in DJ-1-deficient dopamine neurons: An ES-derived cell model of primary Parkinsonism. PLOS Biol. 2, e327

43. Inden, M., Taira, T., Kitamura, Y., Yanagida, T., Tsuchiya, D., Takata, K., Yanagisawa, D., Nishimura, K., Taniguchi, T., Kiso, Y., Yoshimoto, K., Agatsuma, T., Koide-Yoshida, S., Iguchi-Ariga, S. M. M., Shimohama, S., and Ariga, H. (2006) PARK7 DJ-1

protects against degeneration of nigral dopaminergic neurons in Parkinson's disease rat model. Neurobiol. Dis. 24, 144–158

44. Mullett, S. J., and Hinkle, D. A. (2009) DJ-1 knock-down in astrocytes impairs astrocyte-mediated neuroprotection against rotenone. Neurobiol. Dis. 33, 28–36

45. Lev, N., Barhum, Y., Ben-Zur, T., Melamed, E., Steiner, I., and Offen, D. (2013) Knocking out DJ-1 attenuates astrocytes neuroprotection against 6-hydroxydopamine toxicity. J. Mol. Neurosci. 50, 542–550

46. Aguiar, A. S., Tristão, F. S. M., Amar, M., Chevarin, C., Lanfumey, L., Mongeau, R., Corti, O., Prediger, R. D., and Raisman-Vozari, R. (2013) Parkin-knockout mice did not display increased vulnerability to intranasal administration of 1-methyl-4-phenyl-1,2,3,6-tetrahydropyridine (MPTP). Neurotox. Res. 24, 280–287

47. Thomas, B., von Coelln, R., Mandir, A. S., Trinkaus, D. B., Farah, M. H., Leong Lim, K., Calingasan, N. Y., Flint Beal, M., Dawson, V. L., and Dawson, T. M. (2007) MPTP and DSP-4 susceptibility of substantia nigra and locus coeruleus catecholaminergic neurons in mice is independent of parkin activity. Neurobiol. Dis. 26, 312–322

48. Itier, J.-M., Ibanez, P., Mena, M. A., Abbas, N., Cohen-Salmon, C., Bohme, G. A., Laville, M., Pratt, J., Corti, O., Pradier, L., Ret, G., Joubert, C., Periquet, M., Araujo, F., Negroni, J., Casarejos, M. J., Canals, S., Solano, R., Serrano, A., Gallego, E., Sanchez, M., Denefle, P., Benavides, J., Tremp, G., Rooney, T. A., Brice, A., and Garcia de Yebenes, J. (2003) Parkin gene inactivation alters behaviour and dopamine neurotransmission in the mouse. Hum. Mol. Genet. 12, 2277–2291

49. Perez, F. A., Curtis, W. R., and Palmiter, R. D. (2005) Parkin-deficient mice are not more sensitive to 6-hydroxydopamine or methamphetamine neurotoxicity. BMC Neurosci. 6, 71

50. Jiang, H., Ren, Y., Yuen, E. Y., Zhong, P., Ghaedi, M., Hu, Z., Azabdaftari, G., Nakaso, K., Yan, Z., and Feng, J. (2012) Parkin controls dopamine utilization in human midbrain dopaminergic neurons derived from induced pluripotent stem cells. Nat. Commun. 3, 668

51. Casarejos, M. J., Menéndez, J., Solano, R. M., Rodríguez-Navarro, J. A., García de Yébenes, J., and Mena, M. A. (2006) Susceptibility to rotenone is increased in neurons from parkin null mice and is reduced by minocycline. J. Neurochem. 97, 934–946

52. Haque, M. E., Thomas, K. J., D'Souza, C., Callaghan, S., Kitada, T., Slack, R. S., Fraser, P., Cookson, M. R., Tandon, A., and Park, D. S. (2008) Cytoplasmic Pink1 activity protects neurons from dopaminergic neurotoxin MPTP. Proc. Natl. Acad. Sci. U. S. A. 105, 1716–1721

53. Fasano, C., Thibault, D., and Trudeau, L. E. (2008) Culture of postnatal mesencephalic dopamine neurons on an astrocyte monolayer. Curr. Protoc. Neurosci. Chapter 3, Unit 3 21

54. Akundi, R. S., Huang, Z., Eason, J., Pandya, J. D., Zhi, L., Cass, W. A., Sullivan, P. G., and Büeler, H. (2011) Increased mitochondrial calcium sensitivity and abnormal expression of innate immunity genes precede dopaminergic defects in Pink1-deficient mice. PloS One. 6, e16038

5.8 Footnotes

This work was funded by a grant from the Krembil Foundation and the Brain Canada Foundation to R.S., D.P. and L-E.T., as well as by the CIHR and by a pilot project grant from Parkinson Society Canada.

The abbreviations used are: DA, dopamine; DAT, dopamine transporter; DIV, days in vitro; ECAR, extracellular acidification rate; LRRK2, leucine-rich repeat kinase 2; OCR, oxygen consumption rate; OXPHOS, oxidative phosphorylation; PD, Parkinson's disease; Pink1, PTEN-induced putative kinase 1; SNc, substantia nigra *par compacta*; VTA, ventral tegmental area.

5.9 Figures

Figure 1. Altered basal survival and axonal arbor size of Parkin but not Pink1 or DJ-1 ko SNc DA neurons.

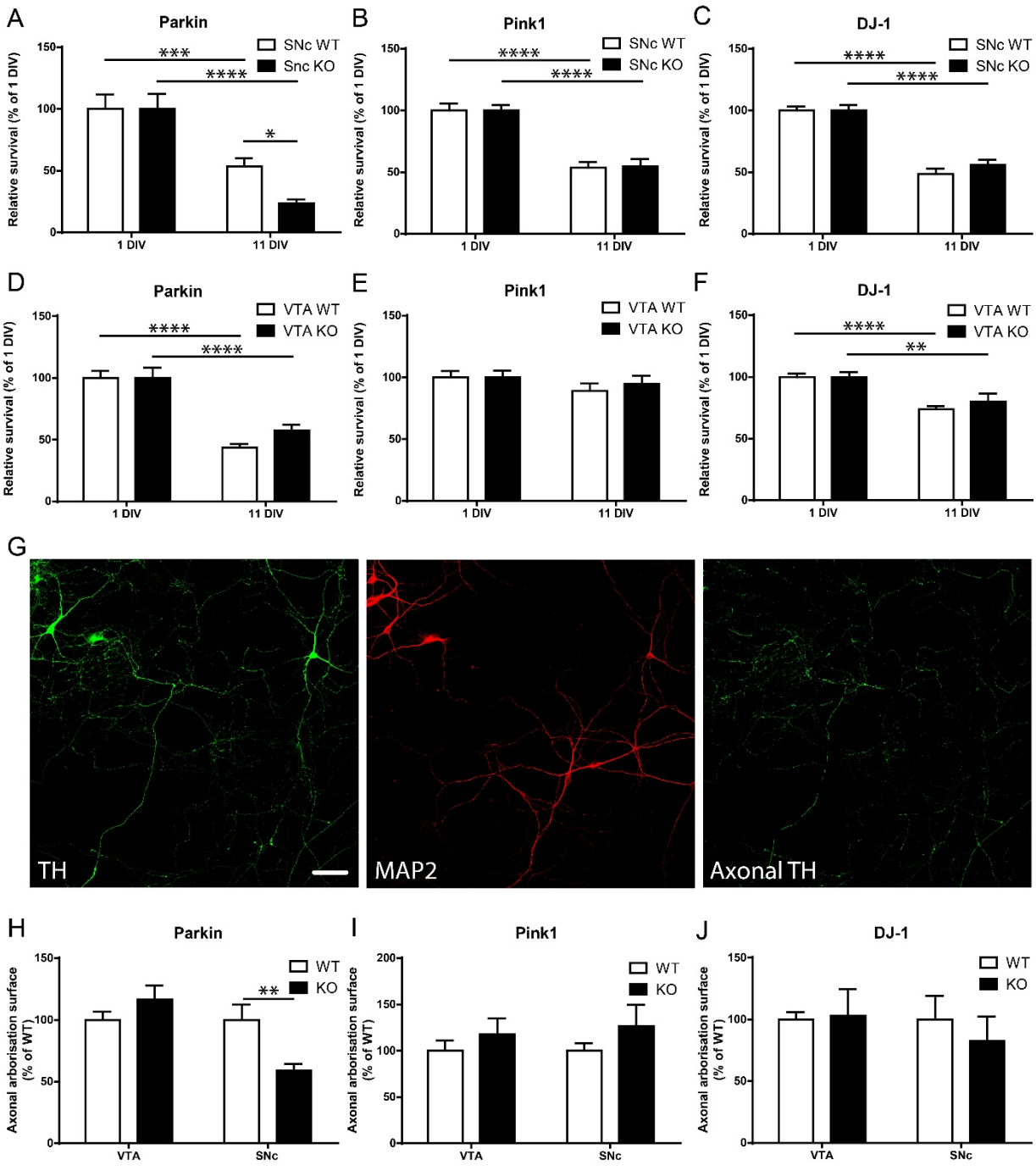

(A-F) Basal survival rate was measured by counting the proportion of DA neurons with a clear round nucleus at 1 DIV that survived until 11 DIV in Parkin KO (A, D), Pink1 KO (B, E) or DJ-1 KO (C, F) SNc or VTA cultures. The values represent the mean ± SEM, n = 8-24 coverslips from at least 3 different cultures. *$p < 0.05$; **$p < 0.01$; ***$p < 0.001$; ****$p < 0.0001$. (G-J) Axonal arborization size was measured by removing somatodendritic (MAP2 signal) surface from TH surface in random fields (G), scale bar = 100 µm. The values obtained were normalized to the number of TH-positive SNc or VTA DA neurons in Parkin (H), Pink1 (I) and DJ-1 (J) cultures. The values represent the mean ± SEM, n = 13-17 coverslips from at least 3 different cultures. **$p < 0.01$.

Figure 2. Altered mitochondrial function in Parkin but not Pink1 or DJ-1 KO DA neurons.

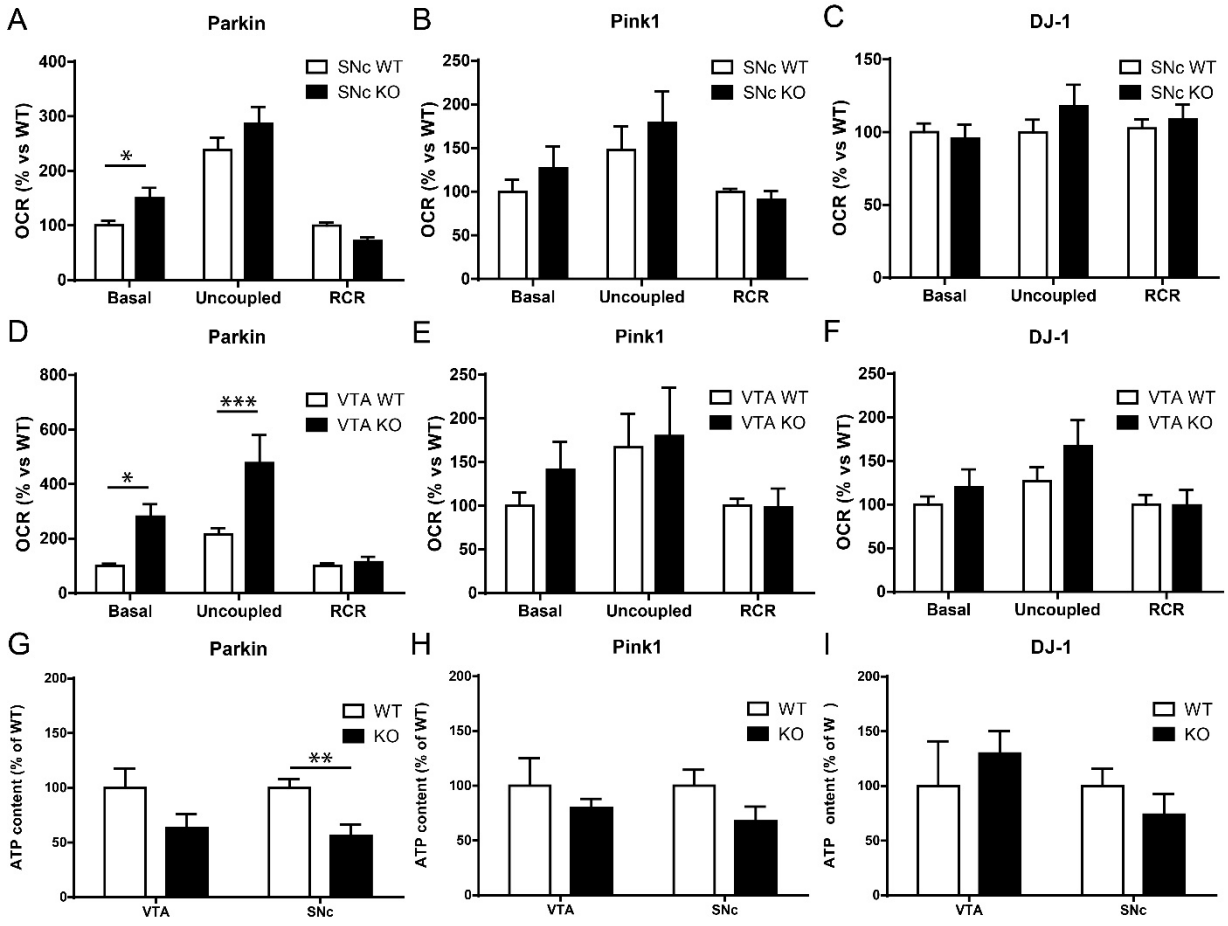

(A–F) Oxygen consumption rates (OCR) were measured using a XF24 Analyzer from Parkin (A), Pink1 (B) and DJ-1 (C) SNc cultures and from Parkin (D), Pink1 (E) and DJ-1 (F) VTA cultures. Basal OCR, uncoupled OCR in the presence of 0.5 mM CCCP and the respiratory control ratio (RCR), calculated by dividing uncoupled by basal OCR, were measured. The values represent the mean ± SEM, n = 7–27 wells from at least 3 different cultures. *$p < 0.05$; ***$p < 0.001$. (G) ATP content under basal conditions was quantified in SNc and VTA DA neurons from Parkin (G), Pink1 (H) and DJ-1 (I) cultures. Values represent the mean ± SEM, n = 5-7 coverslips from at least 3 different cultures. **$p < 0.005$.

Figure 3. No change of glycolysis in Parkin, Pink1 or DJ-1 KO DA neurons from SNc or VTA cultures.

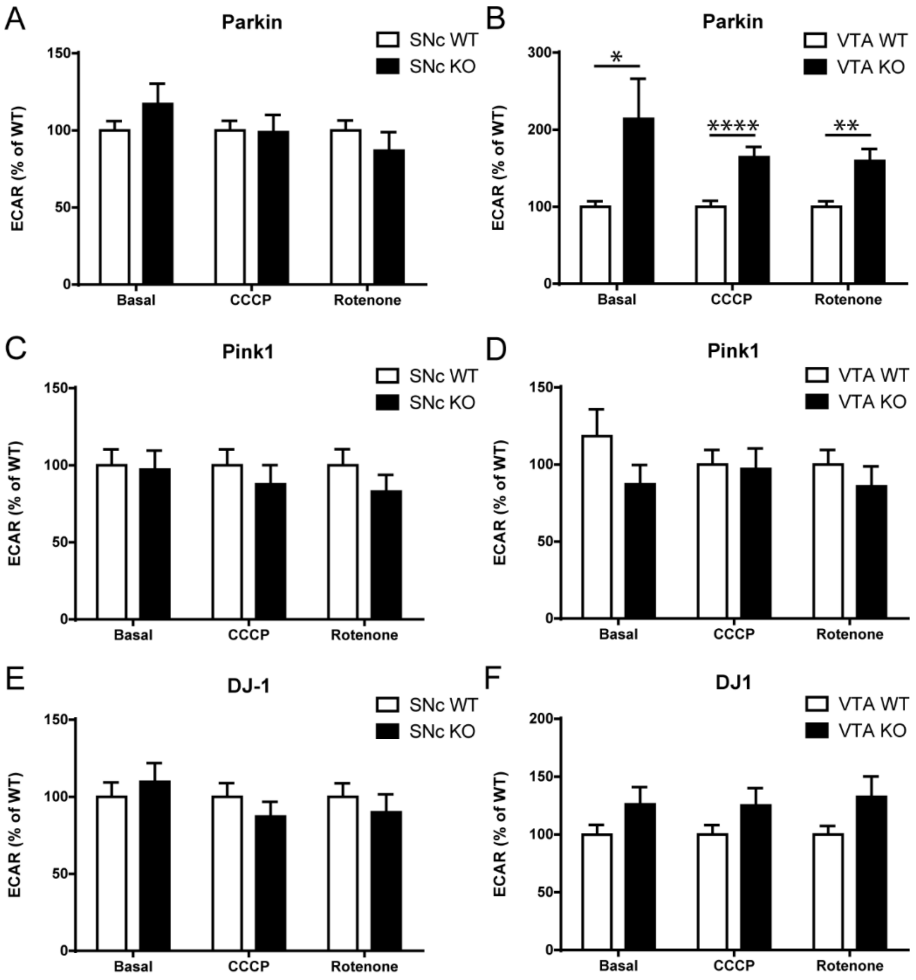

(A–F) Extracellular acidification rates (ECAR) were measured using a XF24 Analyzer from Parkin (A), Pink1 (C) and DJ-1 (E) KO SNc cultures and from Parkin (B), Pink1 (D) and DJ-1 (F) VTA KO cultures. ECAR under basal condition (Basal), in the presence of 0.5 mM CCCP (CCCP) and in the presence of 1 μM rotenone (Rotenone) were measured. The values represent the mean ± SEM, n = 17–27 wells from at least 3 different cultures. *$p < 0.05$; **$p < 0.01$; ****$p < 0.0001$.

Figure 4. No change in neuronal mitochondrial density in Parkin KO SNc DA neurons.

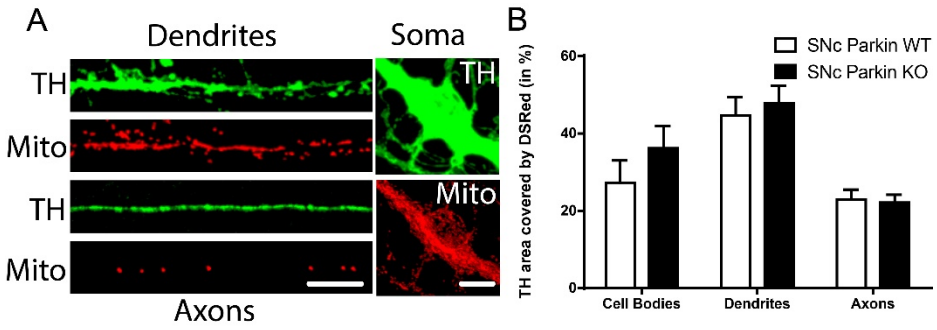

(A-B) SNc DA neurons were infected with DsRed2-mito at the time of plating. The density of mitochondria (A) was measured in TH-positive neurons using confocal microscopy. Scale Bar = 10 μm. (B) Proportion of TH signal covered by DSRed in cell bodies, dendrites and axons. The values represent the mean ± SEM, n = 20-26 neurons from at least 3 different cultures.

Figure 5. Parkin KO glial cell dysfunction is implicated in basal survival of Parkin KO SNc DA neurons.

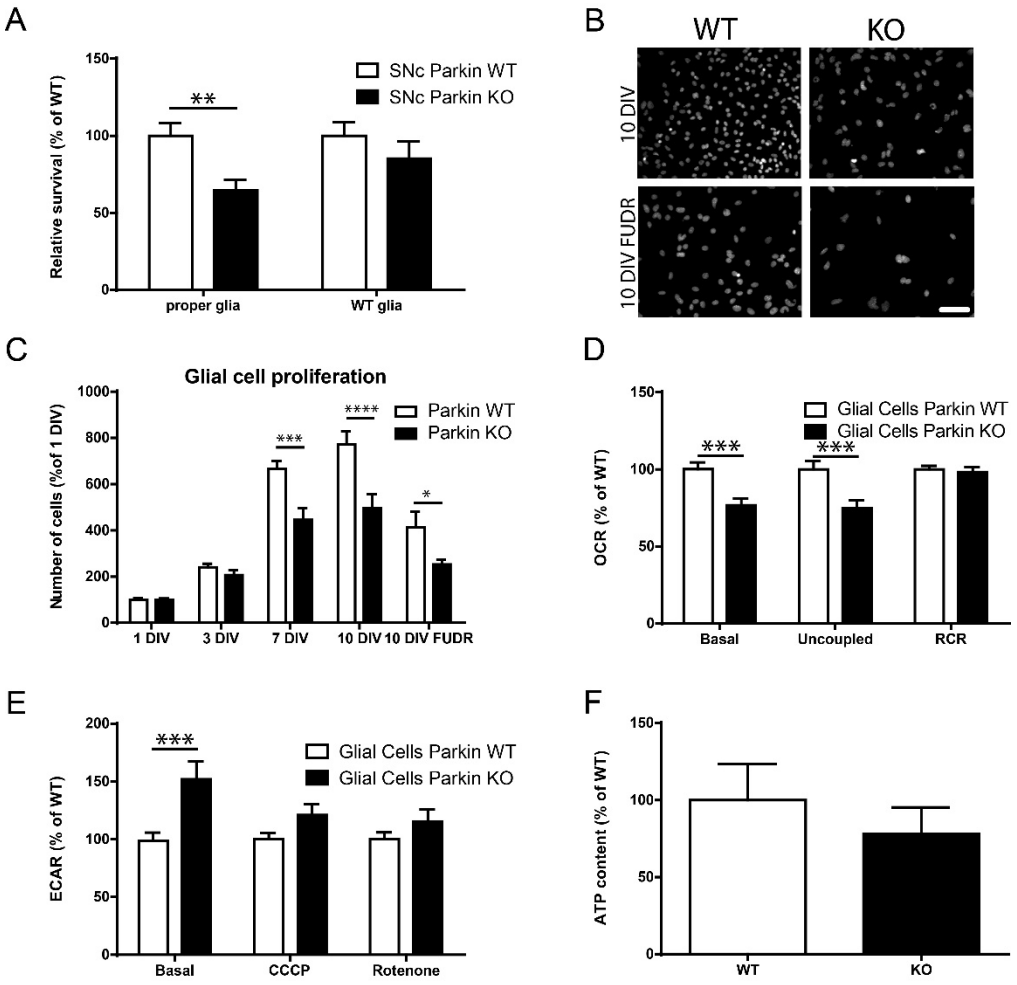

(A) SNc Parkin KO and WT DA neurons were grown on corresponding or WT glial cells and survival was measured by counting the proportion of DA neurons with a clear round nucleus. The values represent the mean ± SEM, n = 18–31 coverslips from at least 3 different cultures. **p < 0.01. (B-C) Parkin KO glial cells were grown on coverslips for 1, 3, 7 and 10 DIV. In another group of coverslips, the mitotic inhibitor FUDR was added once glial cells reached confluence as per the procedure typically used to prepare neuronal cultures. The number of glial cells was measured by DAPI staining. Scale bar = 100 μm. The values represent the mean ± SEM, n = 8–12 coverslips from at least 3 different cultures. *p < 0.05; ***p < 0.001, ****p < 0.0001. (D-E) OCR (D) and ECAR (E) were measured using a XF24 Analyzer from Parkin glial cell cultures. The values represent the mean ± SEM, n = 16–36 wells from at least 4 different cultures. **p < 0.01; ***p < 0.001. (F) ATP content under basal conditions was quantified in Parkin KO glial cell cultures. The values represent the mean ± SEM, n = 6–7 coverslips from at least 3 different cultures.

Figure 6. Altered survival to MPP+ of SNc DA neurons in Parkin, DJ-1 but not Pink1-KO cultures.

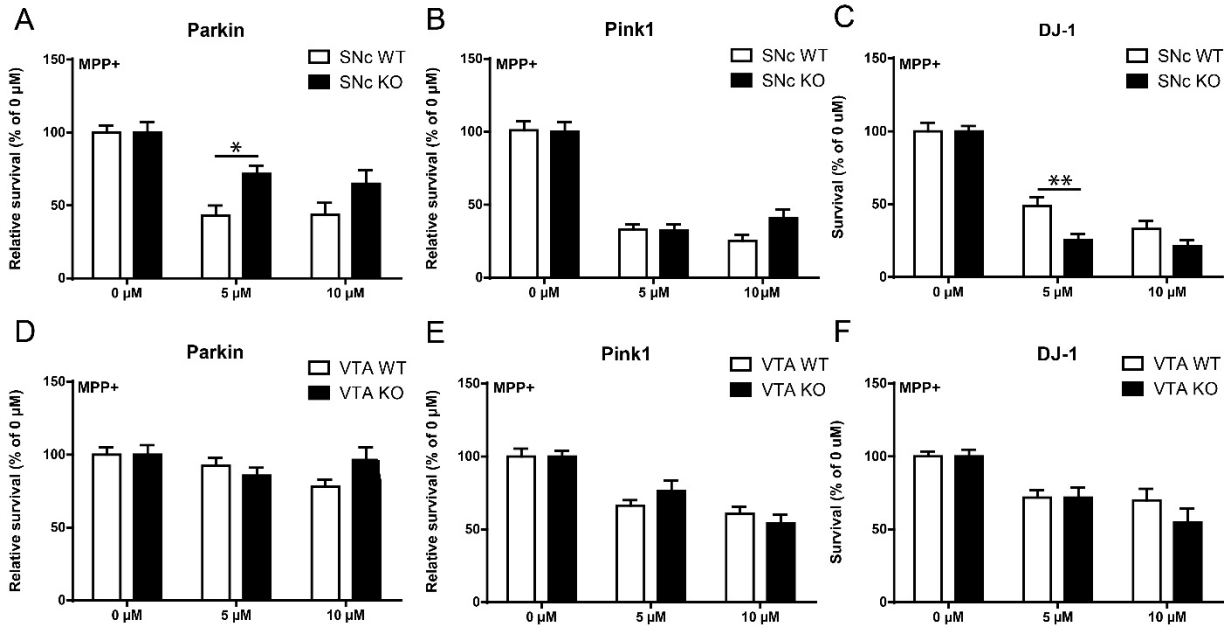

(A-F) DA neurons were treated with MPP+ (5 and 10 μM, 24 hr) and the proportion of surviving neurons was determined by counting the number of TH-positive neurons with a clear round nucleus in SNc cultures prepared from Parkin (A), Pink1 (B) or DJ-1 (C) KO mice or in VTA cultures (D, E, F). The values represent the mean ± SEM, n = 12-25 coverslips from at least 3 different cultures. *$p < 0.05$; **$p < 0.01$.

Figure 7. Differential vulnerability to MPP+ of Parkin KO SNc DA neurons associated with lower DAT expression in surviving neurons.

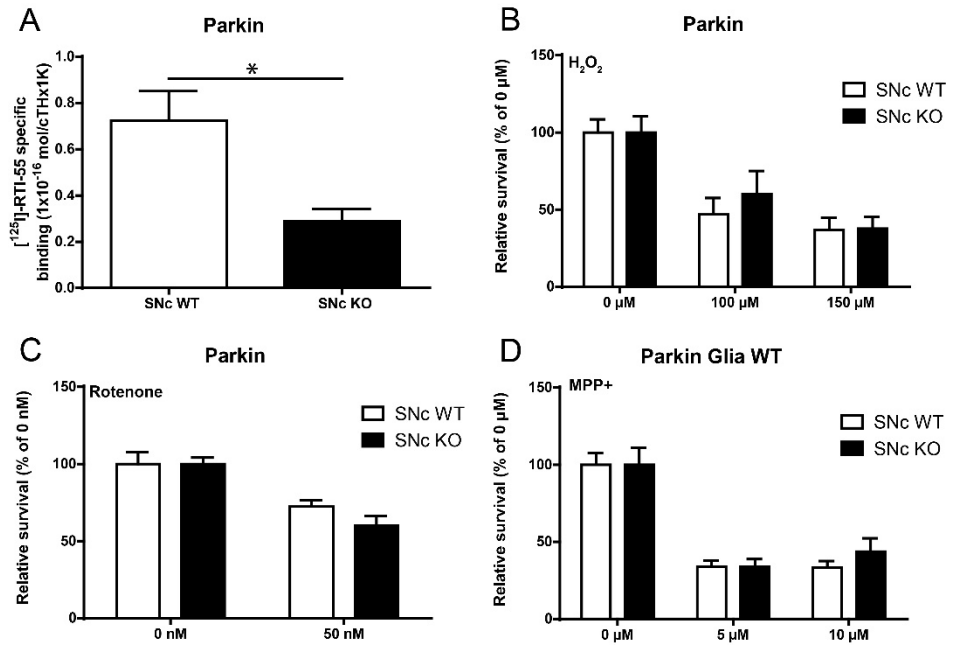

(A) The density of DAT was measured by radioligand assay in Parkin KO SNc cultures. The values represent the mean ± SEM, n = 3 samples from 3 different cultures. *$p < 0.05$. (B-C) Parkin KO SNc neurons were treated with H_2O_2 (100 and 150 μM, 24 hr) (B) or rotenone (50nM, 72h) (C) and the proportion of surviving neurons was determined by counting the number of TH-positive neurons with a clear round nucleus. The values represent the mean ± SEM, n = 8-20 coverslips from at least 3 different cultures. (D) Parkin KO SNc cultures under WT glia were treated with MPP+ (5 and 10 μM, 24 hr), and the proportion of surviving neurons was determined by counting the number of TH-positive neurons with a clear round nucleus. The values represent the mean ± SEM, n = 10-20 coverslips from at least 3 different cultures.

Figure 8. Partial rescue of basal survival, axonal length and bioenergetics in Parkin KO SNc cultures by AAV overexpression of WT parkin.

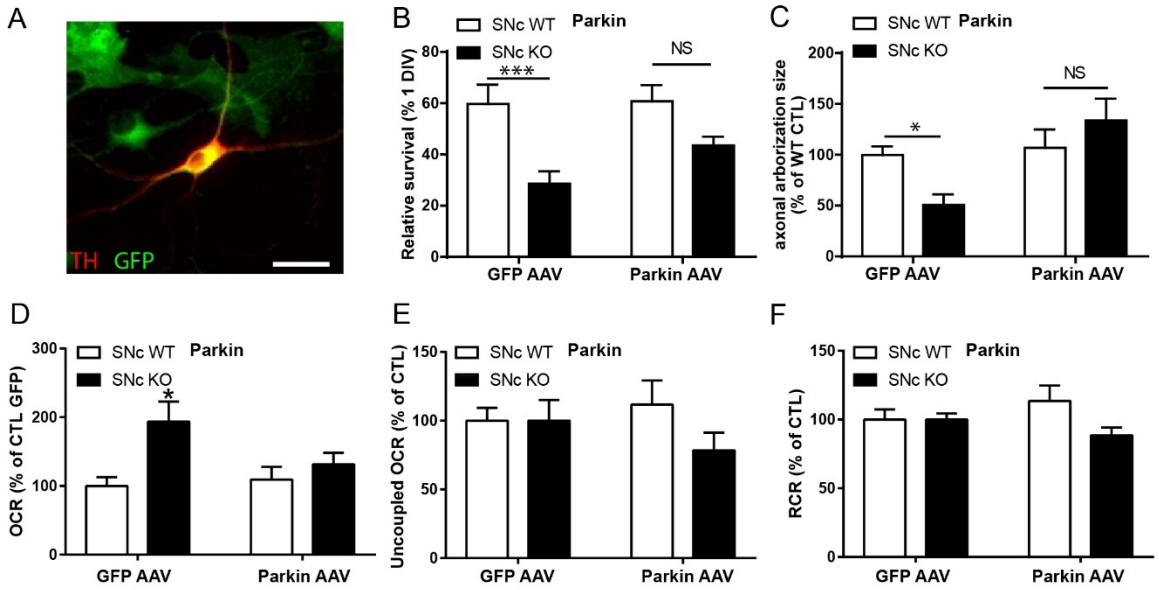

(A) Parkin WT and KO SNc cultures were infected with Parkin WT-GFP AAV or GFP only AAV and cultured for 10 DIV. Scale bar = 25 μm. (B) Basal survival rate was measured by counting the proportion of DA neurons with a clear round nucleus at 1 DIV that survived until 10 DIV. (C) Axonal arborization size was measured by removing somatodendritic (MAP2 signal) surface from TH surface in random fields. Data were normalized by the control condition. The values represent the mean ± SEM, n =8-12 coverslips from at least 3 different cultures. *$p < 0.05$, ***$p < 0.001$. Oxygen consumption rates (OCR) were measured using a XF24 Analyzer. Basal OCR (D), uncoupled OCR (E) in the presence of 0.5 mM CCCP and the respiratory control ratio (RCR) (F), calculated by dividing uncoupled by basal OCR, were measured. Data were normalized to the control condition. The values represent the mean ± SEM, n =15-25 wells from at least 6 different cultures. *$p < 0.05$.

5.10 Supplementary Figures

Figure S1. Increased respiration, ATP content and axonal arborization size of SNc DA neurons compared to VTA.

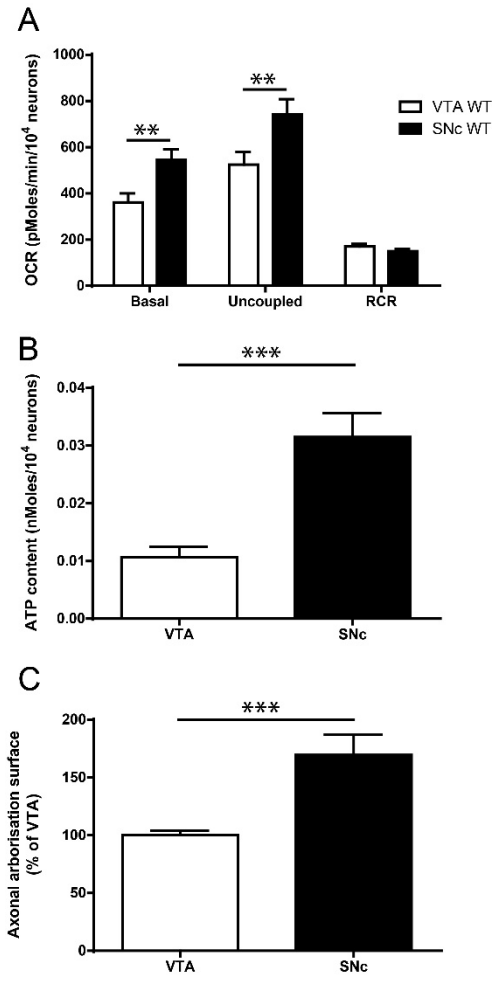

OCR (A), ATP content (B) and axonal arborization surface (C) of SNc and VTA DA neurons pooled from the WT non-normalized data from Parkin, Pink1 and DJ-1 cultures. OCR (A) was measured using a XF24 Analyzer from all WT SNc and VTA cultures. The values represent the mean ± SEM, n = 39-78 wells from at least 12 different cultures. **$p < 0.01$. ATP content under basal conditions was quantified in all WT SNc and VTA cultures. The values represent the mean ± SEM, n = 19-20 coverslips from at least 9 different cultures ***$p < 0.001$. (C) Axonal arborization size was measured removing MAP2 signal surface from TH signal surface in random fields. The values obtained were normalized to the number of TH-positive SNc or VTA DA neurons in all WT cultures. The values represent the mean ± SEM, n = 46-47 coverslips from at least 9 different cultures. ***$p < 0.001$.

Figure S2. No change in survival, axonal arborization size and oxygen consumption at 5 DIV in SNc DA neurons from Parkin-KO culture.

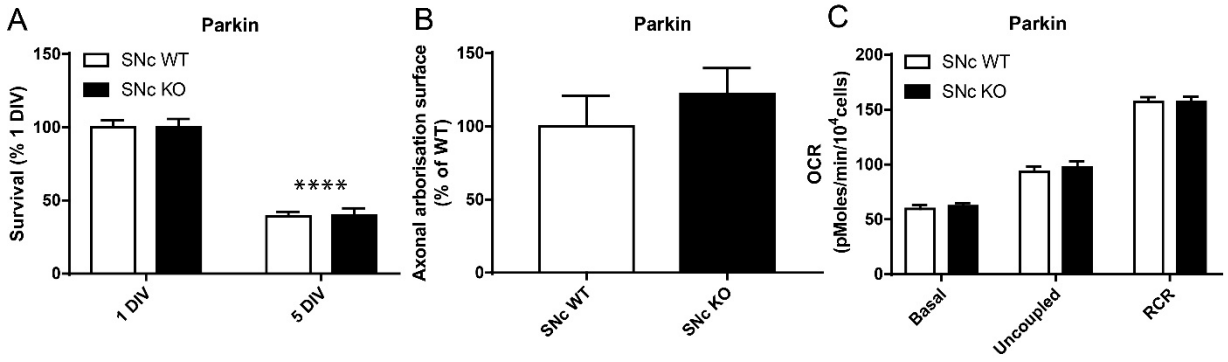

Parkin WT and KO SNc cultures at 5 DIV (A) Basal survival rate was measured by counting the proportion of DA neurons with a clear round nucleus at 1 DIV that survived until 5 DIV. (B) Axonal arborization size was measured by removing somatodendritic (MAP2 signal) surface from TH surface in random fields. Data were normalized by the control condition. The values represent the mean ± SEM, n =20-24 coverslips from at least 3 different cultures. *$p < 0.05$, ***$p < 0.001$. (C) Oxygen consumption rates (OCR) were measured using a XF24 Analyzer. Basal OCR, uncoupled OCR in the presence of 0.5 mM CCCP and the respiratory control ratio (RCR), calculated by dividing uncoupled by basal OCR, were measured. Data were normalized to the control condition. The values represent the mean ± SEM, n =18-21 wells from at least 3 different cultures. ****$p < 0.0001$.

Figure S3. Parkin KO glial cell dysfunction is also present in mesencephalic glial cultures.

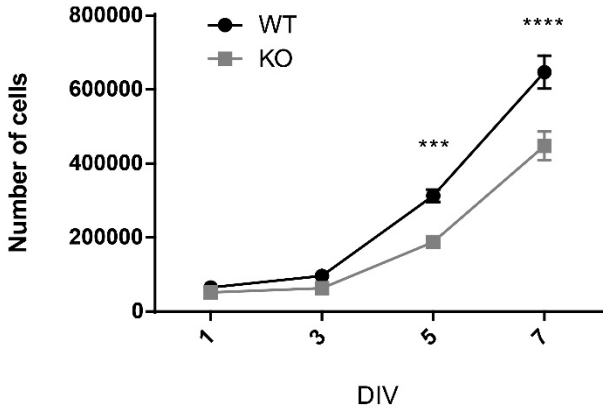

Mesencephalic Parkin KO glial cells were grown for 1, 3, 5 and 7 DIV. The number of glial cells was measured by DAPI staining. The values represent the mean ± SEM, n = 12 coverslips from at least 3 different cultures. ***$p < 0.001$, ****$p < 0.0001$.

Figure S4. Decrease OCR in Pink1 but not DJ-1-KO glial cell culture, with no change in ECAR or ATP content.

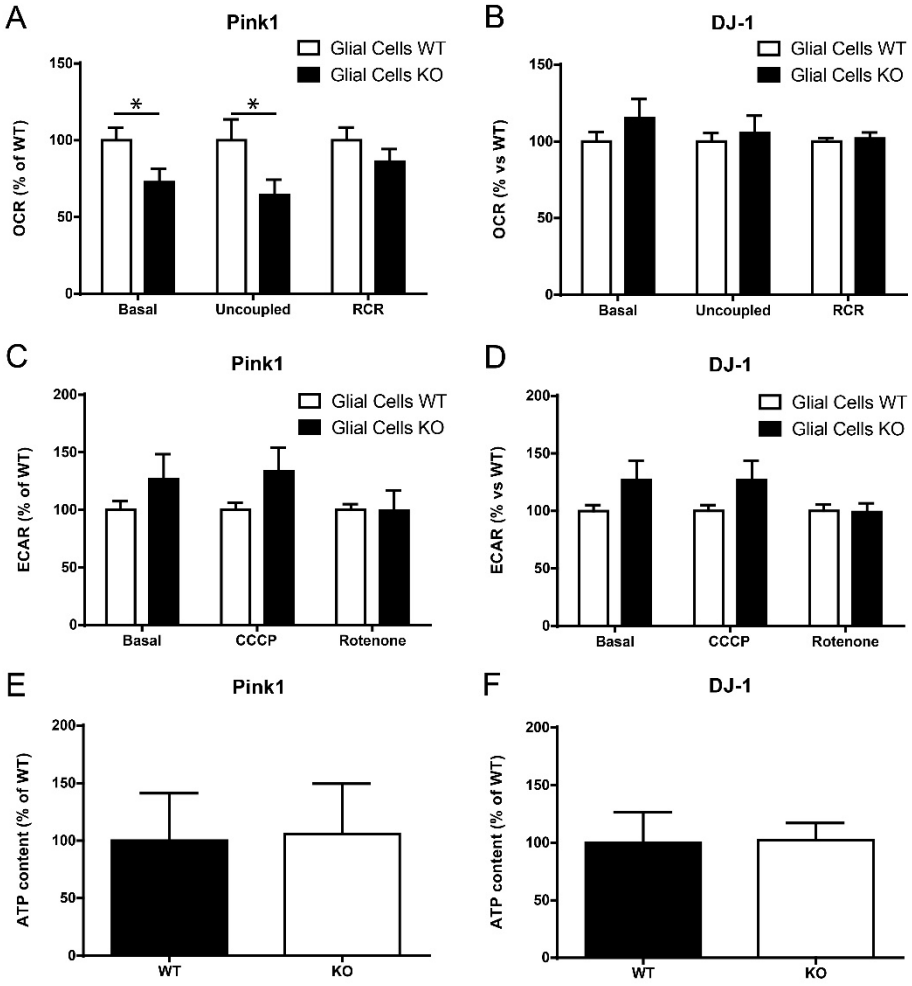

OCR (A-B) and ECAR (C-D) were measured using a XF24 Analyzer from Pink1 (A, C) and DJ-1 (B, D) glial cell cultures. The values represent the mean ± SEM, n = 16–21 wells from at least 4 different cultures. *$p < 0.05$. ATP content under basal conditions was quantified in Pink1 (E) and DJ-1 (F) glial cell cultures. The values represent the mean ± SEM, n = 7 coverslips from at least 3 different cultures.

Figure S5. Parkin protein expression from Parkin WT and KO tissue and from Parkin WT culture and Parkin KO culture rescued with Parkin WT-GFP overexpression.

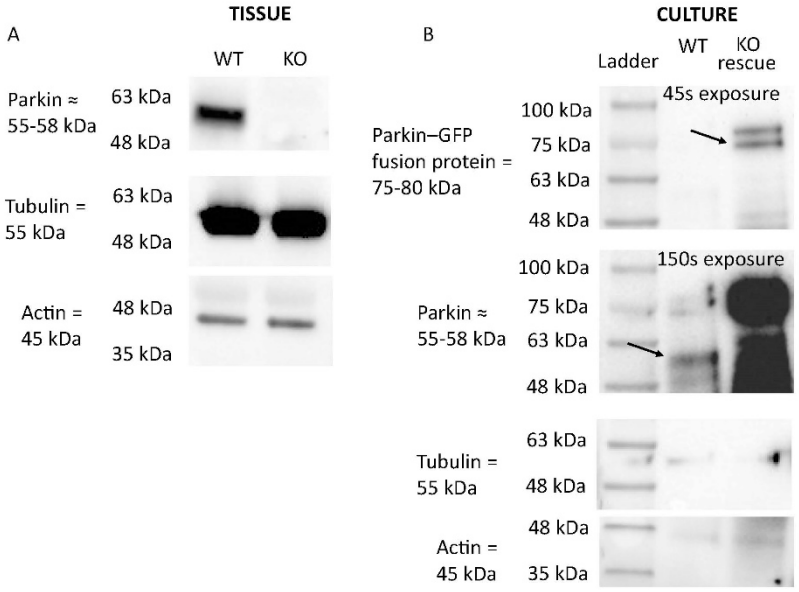

Parkin expression was measured by western blot in Parkin WT and KO P0 mouse brain tissue (A) and in Parkin WT and KO (with Parkin-GFP AAV rescue) SNc cultures. (B). Parkin overexpression in cultures was strong (B top, arrow), and the presence of the second band is likely due to parkin's ability to self-ubiquitinate. It was necessary to increase blot exposure to reveal the WT band in the WT culture condition (B middle, arrow). The bands for reference genes are weak for cultures because the amount of material obtained from culture coverslips is limited (B bottom). Antibodies used were anti-Parkin mouse 1:200 (sc-32282, Santa Cruz Biotechnology), anti-α/β-Tubulin rabbit 1: 1000 (2148S, Cell Signaling Technology) and anti-β-Actin mouse 1:2500 (ab6276, Abcam).

Chapitre 6 : Modulation de la taille de l'arborisation axonale et de la vulnérabilité *in vivo* (Article IV)

Nous savions maintenant *in vitro* que la vulnérabilité plus importante des neurones de la SNc était due à l'importante demande énergétique induite par leur arborisation axonale particulièrement complexe, et que cette vulnérabilité était exacerbée par le modèle Parkin KO.

L'article qui suit nous a permis de valider cette notion *in vivo*, en comparant la taille de l'arborisation axonale des neurones dopaminergiques de la SNc à ceux de la VTA, puis en utilisant un modèle de KO conditionnel du récepteur D2 chez ceux-ci pour exacerber cette différence et augmenter la vulnérabilité des neurones de la SNc.

Contributions des auteurs

Nicolas Giguère : Conception et exécution de toutes les expériences, hormis la voltamétrie et le compte stéréologique de cellules YFP. Analyse des données et écriture du manuscrit.

Benoît Delignat-Lavaud : Conception, exécution et analyse des expériences de voltamétrie.

Aurore Voisin : Compte stéréologique des cellules YFP de la Figure 1.

Vincent Jacquemet : Analyse de la cinétique des tracés de voltamétrie cyclique.

Bruno Giros : Don des souris $D2^{lox}$.

Louis-Éric Trudeau : Conception, coordination et supervision du projet et écriture du manuscrit.

Soumis

Increased vulnerability of nigral dopamine neuron after expansion of their axonal arborization size trough D2 dopamine receptor conditional knockout

Nicolas Giguère[1], Benoît Delignat-Lavaud [1], Aurore Voisin[1], Vincent Jacquemet[2], Bruno Giros[3], Louis-Éric Trudeau[1]

From [1]Departments of pharmacology and physiology, Department of neurosciences, Central Nervous System Research Group (GRSNC), Faculty of Medicine, Université de Montréal, Québec, H4T 1J4 Canada, [2]Department of pharmacology and physiology, Research Center of the Hôpital de Sacré-Coeur de Montréal, [3]Department of Psychiatry, McGill University Faculty of Medicine, Douglas Mental Health University Institute

Keywords: Parkinson's disease, axonal arborization, dopamine D2 receptor, vulnerability.

6.1 Abstract

Parkinson's disease (PD) is a neurodegenerative disorder characterized by the loss of dopamine (DA) neurons in the substantia nigra pars compacta (SNc). Rare genetic mutations in genes such as Parkin, Pink1, DJ-1, α-synuclein, LRRK2 and GBA are found to be responsible for the disease in about 15% of the cases. A key unanswered question in PD pathophysiology is why would these mutations, impacting basic cellular processes such as mitochondrial function and neurotransmission, lead to selective degeneration of SNc DA neurons? We previously showed *in vitro* that SNc DA neurons have an extremely high rate of mitochondrial oxidative phosphorylation and ATP production, characteristics that appear to be the result of their highly complex axonal arborization. To test the hypothesis *in vivo* that axon arborization size is a key determinant of vulnerability, we selectively labeled SNc or VTA DA neurons using floxed YFP viral injections in DAT-cre mice and showed that SNc DA neurons have a much more arborized axon than those of the VTA. To further enhance this difference, which may represent a limiting factor in the basal vulnerability of these neurons, we selectively deleted the DA D2 receptor (D2-cKO), a key negative regulator of the axonal arbour of DA neurons. In these mice, SNc DA neurons have a 2-fold larger axonal arborization, release less DA and are more vulnerable to a 6-OHDA lesion, but not to α-synuclein overexpression when compared to control SNc DA neurons. This work adds to the accumulating evidence that the axonal arborization size of SNc DA neurons plays a key role in their vulnerability in the context of PD.

6.2 Introduction

PD is a neurodegenerative disorder primarily characterized by a massive loss of DA neurons in the SNc that is also thought to be accompanied by the loss of other types of neurons in a select subset of brain regions including the locus coeruleus and the pedunculopontine nucleus (1). Canonical symptoms include a range of motor deficits, but PD patients also often suffer from non-motor symptoms including olfactory deficits and constipation. Inherited mutations in gene products such as Parkin, Pink1, DJ-1, α-synuclein, LRRK2 or GBA are found in approximately 15% of cases. These gene products are involved in basic cellular processes including mitophagy, oxidative stress handling, mitochondrial antigen presentation, vesicular trafficking and lysosomal function. One of the key unanswered questions in PD research is why alterations in such ubiquitous processes lead to selective degeneration of a select subset of neuronal populations in the brain including SNc DA neurons. One striking example of this selectivity is the much higher resilience of the neighboring DA neurons of the ventral tegmental area (VTA), which are far less affected than SNc DA neurons in PD (1). In the last few decades, many hypotheses have been raised about the core characteristics of SNc neurons that are responsible for their large bioenergetic requirements and that could explain their selective vulnerability. These include, but are not limited to, pacemaking activity (2), high DA- and iron-related toxicity (3,4) and possessing a highly elaborate, long-range axonal arborization (5–8). All these characteristics are thought to exert an important pressure on the capacity of these cells to efficiently produce energy and cope with the associated oxidative stress. In this context, any other subsequent cellular stresses associated with some of the genetic alterations mentioned above, as well as aging and exposure to environmental toxins could trigger the disease. We have previously showed *in vitro* that SNc DA neurons have a higher basal rate of mitochondrial oxidative phosphorylation and ATP production and a smaller reserve capacity compared with the less vulnerable DA neurons of the VTA, characteristics that appear to be the result of the highly complex axonal arborization of these neurons (8). We therefore postulated that the size of this axonal arborization might be a significant contributor to the differential vulnerability of SNc and VTA DA neurons in PD.

Based on our previous work and on modelling of the impact of the axonal arborization size on energy requirements (9,8), it is possible that the relatively small size of the axonal arborization of mouse DA neurons compared to humans (10 fold smaller) could explain the apparently high resilience of mouse DA neurons and the associated difficulty to produce optimal animal models in this species. Indeed, mouse models with genetic deletions of the key genes found in familial forms of the disease generally do not present age-dependent neuronal loss (10–14). If the smaller axonal arborization size of mouse DA neurons is a key limiting factor for their vulnerability, it might be possible to increase this vulnerability by increasing their axonal arborization size *in vivo*. In order to reach this objective and test our hypothesis, we generated mice with a conditional deletion of the DA D2 receptor in DA neurons (D2-cKO). Increased DA terminal density has been suggested to occur under chronic D2 antagonist administration (15,16) and in the constitutive knockout model of this receptor (17) and D2 agonists have been shown to reduce the density of axon terminals established by DA neurons (15,18). Here we surmised that a cell-specific knockout of this receptor in DA neurons could lead to an increased size and complexity of the axonal arborization of these neurons and increase their intrinsic vulnerability.

We find that in the intact mouse brain, the axonal arborization size of SNc DA neurons is 3-fold larger than that of less vulnerable VTA DA neurons. We further demonstrate that in D2-cKO mice, the axonal arborization size of SNc DA neurons is 2-fold larger relative to control mice, while evoked DA release is reduced and that they show increased vulnerability to 6-OHDA, but not to α-synuclein overexpression. This work provides strong evidence in favor of the hypothesis that the axonal arborization size of SNc DA neurons plays a key role in regulating their basal vulnerability in the context of PD.

6.3 Results

6.3.1 SNc DA neurons have a much more elaborated striatal axonal arborization than VTA DA neurons in the mouse brain

If axonal arborization size is to be a critical determinant of the selective vulnerability of SNc DA neurons, a prediction is that the axonal domain of these neurons should be more arborized than that of the more resilient VTA DA neurons *in vivo*. Since there is no specific axonal marker to distinguish between SNc and VTA DA neurons, we injected a small amount of floxed AAV2-eYFP in the SNc or the VTA of adult $DAT^{Cre/+}$ mice to label a few hundred (~300-1000) DA neurons from one or the other population (Fig. 1A). We then quantified the extent of their axonal arborization within the striatum (Fig. 1B), normalized by the number of labelled neurons, and plotted it as a function of bregma coordinates for SNc (Fig. 1C) and VTA (Fig. 1D) targeted infections. As expected, the majority of SNc DA neurons projections were found in the dorsal striatum and the majority of VTA DA neurons projections were found in the ventral striatum. Comparing the extent of the total arborization revealed a 3-fold larger axonal arbour for SNc compared to VTA DA neurons (Fig. 1E,F).

6.3.2 Increase in DAT but not TH striatal expression in D2-cKO without change in the number of neurons

Because an increase in axonal arbour size could increase the vulnerability of DA neurons, we aimed at increasing the axonal arborization of DA neurons by selective genetic deletion of the DA D2 receptor. To do so, we crossed $DAT^{IRES\text{-}Cre}$ mice with $Drd2^{loxP}$ mice and generated $DAT^{IRES\text{-}Cre/+}$; $Drd2^{loxP/loxP}$ mice as previously described (19). Control mice were heterozygotes for Cre expression ($DAT^{IRES\text{-}Cre/+}$; $Drd2^{+/+}$). In these D2-cKO adult mice, we examined the axonal varicosities of DA neurons by measuring TH and DAT immunolabeled structures using confocal imaging in the ventral and dorsal striatum (Fig. 2A,B). We observed no change in the area covered by TH signal (Fig. 2C), the TH mean signal intensity (Fig. 2D) or total TH signal (Fig. 2E) in any part of the striatum. However, we observed an increased area

covered by the DAT signal in the dorsal striatum (Fig. 2F) with an increased DAT signal intensity (Fig. 2G), which resulted in a more than 2-fold increase in total DAT signal (Fig. 2H). No changes were observed in the ventral striatum. This increased DAT signal in the dorsal striatum was not the result of changes in the number (Fig. 2I) or size (Fig. 2J) of striosomes and was not a result of an increased number of DA neurons in the SNc, VTA or retrorubral field (RRF), as determined by unbiased stereological counting (Fig. 2K).

6.3.3 Increased axonal arborization size of SNc but not VTA DA neurons in D2-cKO mice

To confirm that this increased dorsal striatal DAT signal was the result of an increase in the axonal arborization size of SNc DA neurons, we again used conditional viral labelling to visualize the axonal domain of SNc and VTA DA neurons in D2-cKO mice. We observed a 2-fold increase in the axonal arborization size of SNc DA neurons in D2-cKO mice (Fig. 3A), with no change for VTA DA neurons (Fig. 3B). Comparing axonal arborization size of SNc and VTA DA neurons from control mice again showed a 3-fold difference between the two populations (fig. 3A vs B). To better characterise this expanded axonal arbour originating from SNc D2-cKO DA neurons, we next measured the level of colocalization of virally-expressed YFP with DAT or TH (Fig. 3C). There was increased colocalization of TH or DAT with the YFP-labelled axonal varicosities of D2-cKO mice and a general increased colocalization of TH and DAT inside these processes (Fig. 3D). This increase of TH and DAT colocalization was also observed in the non-YFP fibers (data not shown). To evaluate if these new processes were likely to be functional and able to release DA, we measured the colocalization of VMAT2 with YFP (Fig. 3E) and found it to be unchanged (Fig. 3F). We also found an increased colocalization of VMAT2 and DAT inside these processes. This increase of VMAT2 and DAT colocalization was also visible in the non-YFP fibers (data not shown).

6.3.4 Reduced striatal DA release in D2-cKO mice without changes in DA reuptake kinetics

An increased density of dopaminergic axonal fibers in the striatum, as well as the genetic removal of the pre-synaptic D2R known to control DA synthesis and release, could lead to increased DA release. Alternately, the enhanced bioenergetic requirements associated with a broader axonal arbour could lead to impaired DA neurotransmission. To distinguish between these possibilities, we quantified DA release evoked by single electrical pulses in acutely prepared striatal brain sections from D2-cKO and control mice using fast-scan cyclic voltammetry (Fig. 4A). We found that DA release was greatly reduced in dorsal and ventral striatum (Fig. 4B). However, this difference was greatly reduced following incubation with the DAT antagonist nomifensine (Fig. 4C). This observation of a partial rescue with nomifensine, coupled with our observation of increased striatal DAT immunoreactivity (Fig. 2C-E) could imply that increased DAT function in D2-cKO mice was the cause of the reduced activity-dependent DA overflow. Alternately, as DAT blockers including nomifensine and cocaine have been reported to also promote DA release through other mechanisms (20–22), the apparent rescue could result from an enhancement of DA release and not reuptake. To distinguish between these two possibilities, we examined the kinetics of DA release. Comparing D2-cKO and control mice, we found no change in kinetics of DA reuptake (tau) or in the maximal rate of reuptake (Vmax) in the dorsal (Fig. 4D), or ventral (Fig. 4E) striatum, suggesting no robust change in DAT function in D2-cKO mice.

6.3.5 SNc DA neurons from D2-cKO are more vulnerable to 6-OHDA but not to α-synuclein overexpression

As an increase in axonal arbour size in D2-cKO SNc DA neurons is predicted to induce a larger bioenergetic burden on these neurons, we next examined their vulnerability in two different mouse models of PD: the α-synuclein viral overexpression model and the intra-striatal 6-OHDA model. AAV-mediated wild-type α-synuclein overexpression was achieved by stereotaxic injection into the mesencephalon (Fig. 5A). Three months after virus injection, stereological counting revealed a loss of 25-35% of DA neurons in the SNc and RRF (Fig.

5B,C), with no change in the number of non-DA neurons (Fig. 5D) and no significant change in the VTA (Fig. 5E). This cell loss in the SNc and RRF was not significantly different in D2-cKO mice compared to control mice. We also observed the presence of phosphorylated α-synuclein positive cell bodies (Fig. 5A), a good indicator of the toxicity induced by the overexpression. In the dorsal striatum only (Fig. 5F), we observed a small 20% decrease in TH signal area (Fig. 5G) and total signal (Fig. 5H) with no change in signal intensity (Fig. 5I).

In keeping with the very small level of cell loss and striatal denervation in this model, as well as the lack of genotype difference, only a modest increased preference for ipsilateral paw use was detected in mice overexpressing α-synuclein (Supplementary Fig. S1A), with no change in the total number of steps (Fig. S1B). In the rotation test, neither basal nor amphetamine-induced rotational preferences were altered (Fig. S1C,D), with amphetamine inducing the expected increase in total number of rotations (Fig. S1E).

We next examined the vulnerability of DA neurons using a second, different model of PD using the DA neuron-specific toxin 6-OHDA. Unilateral injection in the dorsal striatum at a low dose (1.5µg in 0.5 µL) (Fig. 6A) was performed in order to produce a partial loss of dopaminergic cell bodies (Fig. 6B). In control mice, one month after the 6-OHDA lesion, we measured an approximate 40% loss of DA neurons in the SNc (Fig. 6C) and the RRF (Fig. 6D), with no significant loss in the VTA (Fig. 6E) or for SNc non-DA neurons (Fig. 6F). Interestingly, in the D2-cKO mice, approximately 60% of SNc DA neurons were lost, representing almost 50% more neurodegeneration than for control mice (60% loss vs 42% loss for CTL) (Fig. 6C). As for axon terminals, TH signal area (Fig. 6G) and total TH signal (Fig. 6H) were both reduced by approximately 50% in the dorsal striatum, with no change detected in the ventral striatum, confirming the specificity of the lesion. In addition, DAT signal area (Fig. 6J) and total signal (Fig. 6K) were reduced by approximately 75% in the dorsal striatum. There were no significant changes in TH and DAT signal intensity (Fig. 6I,L), suggesting loss of axonal terminals rather than simply reduced TH and DAT levels. Even if more neurons were lost in the SNc in D2-cKO mice compared to control mice, no significant difference was observed between the two genotypes (Fig. 6G-L) at the terminal level, compatible with compensatory axonal sprouting.

In line with the modest decrease in TH signal within the striatum of these mice and the absence of genotype effect in striatal denervation, we failed to detect a difference between D2-cKO mice and controls in motor behaviors (Fig. 7). However, the 6-OHDA lesion caused an increased preference for the ipsilateral paw in the stepping test (Fig. 7A) with no change in total number of steps (Fig. 7B). In the rotation test, we observed no changes in rotational preference at basal level (Fig. 7C), but an increased preference for ipsilateral rotations under amphetamine was detected (Fig. 7D). Finally, the total number of rotations was significantly increased following amphetamine administration (Fig. 7E).

6.4 Discussion

One of the key unanswered questions in PD research is why DA neurons of the SNc are particularly vulnerable to the disease. In the last few decades, a number of hypotheses have been raised regarding the core characteristic responsible for this vulnerability, including DA and iron toxicity, pacemaking activity and the establishment of a large and complex axonal arborization (7,3,4,23). One commonality between these features is that they all lead to increased oxidative stress and bioenergetic demands, that are easily destabilized in pathology. Compatible with this model, we previously showed *in vitro* that SNc DA neurons have a higher rate of mitochondrial oxidative phosphorylation and basal oxidative stress compared with less vulnerable DA neurons of the VTA, characteristics that appear to be the result of their highly complex axonal arborization (8). These results suggest that the size of this axonal arborization might be a critical determinant differentiating between surviving and degenerating neurons in PD.

6.4.1 Relative axonal arborization size of VTA and SNc DA neurons

The size of the axonal arbour of SNc DA neurons was measured previously in the intact rat brain (24,25) but no direct comparison of this parameter with less vulnerable VTA DA neurons was available prior to the present work. However, by dividing the estimated number of terminals in the rat ventral and dorsal striatum with the corresponding number of DA neurons

in the VTA and SNc, it had been previously estimated that SNc DA neurons have an 8-fold broader axonal arborization compared to VTA DA neurons (7). In the present work, we directly measured axonal arborization size of both neuronal populations in the entire striatum and similarly found a much larger axonal (3-fold) arborization for SNc compared to VTA DA neurons in mice. The smaller difference between our finding (3-fold) and the previous estimate (8-fold) could be due to the use of different species (rats vs mice), but we additionally took into account that VTA DA neurons also project to the dorsal striatum; projections which were not considered in the previous estimation (7). The projections of VTA neurons to the dorsal striatum were much more diffuse, but because of the much larger size of the dorsal striatum compared to the ventral striatum, they accounted for a significant amount of the total projections from the VTA. These projections were also previously examined in single neuron tracing study in mice (26), but in this work, the authors did not compare VTA to SNc neurons. They nonetheless confirmed that part of VTA DA neurons projections were outside of the ventral striatum, compatible with previous classical work describing mesocortical and mesolimbic pathways (27). In the present study, we did not quantify axonal processes outside of the striatum, which could have led to an overestimated difference between SNc DA neurons and VTA DA neurons. However, as we found only a very low relative density of dopaminergic processes outside of the striatum, for example in the prefrontal cortex, amygdala and septum (data not shown), we do not expect that our estimates were significantly affected by this focus on striatal projections.

6.4.2 Using D2-cKO to increase SNc DA neurons axonal arbour size

In the present study, we used D2-cKO mice to examine the vulnerability of DA neurons under conditions where these neurons develop an even larger axonal arborization. Increased DA terminal density in the dorsal striatum had been previously described in a constitutive (17) knockout model of this receptor. In order to focus on cell-autonomous mechanisms of vulnerability, we deleted the D2R gene selectively in DA neurons by crossing $Drd2^{loxP}$ mice with $DAT^{IREScre}$ mice. Using these $DAT^{IREScre}/Drd2^{loxP}$mice, we observed a significant increase in DAT immunoreactive processes in the dorsal striatum with no increase in the number of DA neurons, similar to what has been observed previously in the hippocampus of this model (19). We did not find any changes in TH signal in the striatum, an observation that could reflect the

highly plastic and homeostatic nature of TH expression in response to perturbations such as neurotoxins, which might make it less reliable to assess the extent of loss of axonal processes (28–34).

To confirm that this increase in DAT immunoreactive processes reflected an increase in axonal arborization size and was originating from SNc DA neurons and not from DA neurons from other regions such as the VTA, we took advantage of a viral labelling strategy to conditionally express a fluorescent reporter protein in SNc or VTA DA neurons. Doing so, we confirmed that SNc but not VTA DA neurons have an increased number of axonal processes in the striatum of the D2-cKO mice. To validate whether expanded axonal domain contained terminals that were likely to release DA, we also quantified the presence of TH, DAT and VMAT2 in these virally-labelled axonal processes. We found that there was an increase in colocalization with TH and DAT and no change in VMAT2 density in axonal processes, arguing that the increase in axonal size did not come at the expense of a loss in neurochemical identity.

We next used fast scan cyclic voltammetry to measure DA release in the striatum and to gain further insight into the functionality of dopaminergic axons in this model. We found a general decrease in DA release that was partially rescued in the presence of a DAT antagonist. Our finding of a decrease in evoked DA overflow, although somewhat counter-intuitive when considering the autoreceptor function of the D2 receptor, is in line with previous observations of constitutive or conditional D2R KO mice (35–37) (but see (38)). However, the use of a DAT antagonist was not sufficient to return DA levels to normal in previous work using a engrailed1-based D2-cKO (35). It should be noted however that in this later work, while the control condition had both alleles of englailed1, the D2-cKO mice had only one allele of this transcription factor, which is otherwise critical for the development of DA neurons. Since knockout of even only one allele of engrailed1 has been shown to affect the number of DA neurons and the density of their terminals (39,40), it is possible that DA release in this model was affected by both the KO of the D2 receptor and the reduced engrailed1 expression as well as by the possible removal of the D2 receptor in non-DA neurons in the VTA and SNc.

It is also important to note that there have been reports that activation of D2 receptors in dopaminergic terminals regulates positively the localization of the DAT to the plasma membrane (41–44). In our D2-cKO mice, although we detected an increase in DAT levels by immunofluorescence, we did not observe any significant change in reuptake kinetics as assessed from cyclic voltammetry recordings. However, a reduction in Vmax has been observed in a previous study in which the D2 receptor was knocked down acutely using siRNA (37), although reuptake kinetics (tau) were not reported. The difference with our data could be explained by the acute nature of the deletion in this previous study. In the context of the absence of a change in reuptake kinetics, our finding of an apparent rescue of DA release in the presence of the DAT blocker nomifensine is puzzling. One possibility is that nomifensine was able to rescue a deficit in axon terminal function at a step which is independent from DAT activity. Previous work has indeed shown that DAT blockers including cocaine and nomifensine are able to enhance the exocytotic release of DA through a mechanism that is not yet clearly defined but that has been suggested to involve synapsin (20–22).

6.4.3 Axonal arborization size as vulnerability factor

The goal of this work was to provide a first *in vivo* test of the importance of axonal arborization size on the vulnerability of SNc DA neurons. We confirm here that D2-cKO mice represent a model in which an expansion of the axonal arborization of SNc DA neurons can be detected. Based on our previous work performed with primary DA neurons (8), we predicted that this should lead to increased vulnerability of SNc DA neurons. In keeping with this hypothesis, we found that D2-cKO SNc DA neurons were more vulnerable to a 6-OHDA lesion initiated at the axon terminal level. However, this increased neuronal loss did not lead to exacerbation in the behavioral changes induced by the partial dopaminergic denervation observed in this model. This finding is in line with the similar loss in striatal TH and DAT fiber density in D2-cKO mice compared to control mice, suggesting increased axonal sprouting from surviving neurons in the D2-cKO mice. An alternate interpretation of this increased neuronal loss in D2-cKO mice could be that the basal increase in DAT-positive varicosities observed in these mice led to an increased uptake of 6-OHDA. Although this possibility cannot be formally

excluded, its likelihood is limited because our cyclic voltammetry reuptake kinetic measurements argue for an absence of change in DAT functionality at the plasma membrane.

Future work will be required to determine the origins of the enhanced neuronal loss of SNc DA neurons in D2-cKO mice exposed to 6-OHDA, but an increased level of basal oxidative stress in SNc DA neurons could be implicated and synergistically lead to sufficient oxidant stress to initiate apoptotic death of DA neurons (45–47). ROS production induced by 6-OHDA has also been reported to impair axonal transport in dopaminergic neurons (48) and to deplete ATP content and antioxidant reserve (49), which could affect to a greater extent D2-cKO SNc DA neurons since they have a larger axonal compartment to maintain. Additionally, increased phosphorylation of α-synuclein to its pSyn-129 toxic form has been reported in the 6-OHDA model (50), which could play a role in the observed toxicity. However, it is unlikely that this effect on α-synuclein is the main mechanism leading to cell death in the present study because we failed to detect any change in vulnerability when we overexpressed α-synuclein, even if we observed presence of pSyn-129 in surviving cells bodies.

This lack of an increased vulnerability to α-synuclein overexpression in the present model is presently unresolved, but it might be explained by the fact that pathology is initially induced in the cell bodies, as opposed to in the terminals in the 6-OHDA model and that the time course of neurodegeneration is much longer in the overexpression model (months vs days for 6-OHDA). Additionally, the α-synuclein model is thought to trigger degeneration by causing pathological protein aggregation and impaired proteasome/lysosome function (51–53), unlike the 6-OHDA model, which directly impairs mitochondrial function by inhibiting mitochondrial complex I and IV and by inducing oxidative stress (54,55).

However, it has been suggested that α-synuclein overexpression can also influence mitochondrial function, but through different mechanisms. It has been proposed that once oligomerized, α-synuclein influences mitochondrial fusion/fission, transport, clearance and protein import mechanisms (56,57), as well as complex I and ATP-synthase function (58) and therefore increases oxidative stress (59). Since α-synuclein oligomerization seems to be a necessary step for all these alterations, overexpression of WT α-synuclein should take much

more time than 6-OHDA injections to elevate oxidative stress to critical levels. It should therefore also leave much more time for neurons to attempt to compensate for these changes compared to the 6-OHDA model where ATP and antioxidant depletion and oxidative stress are rapidly induced. In combination with the much more modest loss of striatal TH immunoreactive processes in the α-synuclein overexpression model, this could in part explain why behavioral alterations were almost absent in this model.

Interestingly, even in the absence of exogenous triggers such as 6-OHDA or α-synuclein overexpression, features of PD pathophysiology such as loss of processes and presence of α-synuclein aggregates in the dorsal striatum have been reported in aged constitutive D2-KO mice (60). In the present work, we did not produce nor examine aged D2-cKO mice, but it is possible that similar pathology would be observed.

In conclusion, this work demonstrates for the first time that SNc DA neurons in the intact brain possess a larger axonal arbour size compared to VTA DA neurons. This work also provides strong additional supportive evidence for the hypothesis that a very large axonal arbour places DA neurons at increased risk in PD.

6.5 Experimental Procedures

Animals

All procedures involving animals were conducted in strict accordance with the Guide to care and use of experimental animals (2nd Ed.) of the Canadian Council on Animal Care. The experimental protocols were approved by the animal ethics committee (CDEA) of the Université de Montréal. Housing was at a constant temperature (21°C) and humidity (60%), under a fixed 12h light/dark cycle and free access to food and water. Initial comparison of the axonal arborization size of SNc and VTA DA neurons was performed using DAT-Cre knock-in mice (61). The rest of the experiments were performed using DAT^{IRES}cre mice obtained from Jackson Labs (62) and crossed with $Drd2^{loxP}$ mice (38). Mouse background was mixed 129SV/C57BL6 and both males and females were used.

Genotyping

All animals were genotyped using a KAPA2G Fast HotStart DNA Polymerase kit from Kapa Biosystem. Primer used were:

DAT-Cre

DAT-CRE up	ACCAGCCAGCTATCAACTCG
DAT-CRE lw	TTACATTGGTCCAGCCACC

DAT^{IRES}cre

oIMR6625 Common	TGG CTG TTG GTG TAA AGT GG
oIMR6626 WTReverse	GGA CAG GGA CAT GGT TGA CT
oIMR8292 Mutant Reverse	CCA AAA GAC GGC AAT ATG GT

$Drd2^{loxP}$

D2LOX-A#2	GCT TCA CAG TGT GCT GCC TA
D2LOX-B	CCA TTG CTG CCT CTA CCA AG

Axonal arborization labelling, α-synuclein and 6-OHDA lesions

Two-month-old DAT-Cre or DAT^{IRES}cre positive mice were anesthetized with isoflurane (Aerrane; Baxter, Deerfield, IL, USA) and fixed on a stereotaxic frame

(Stoelting,Wood Dale, IL, USA). Fur on top of the head was trimmed, and the surgical area was disinfected with iodine alcohol. Throughout the entire procedure, eye gel (Lubrital, CDMV, Canada) was applied to the eyes, and a heat pad was placed under the animal and kept at 37°C. Next, bupivacaine (5 mg/ml and 2 mg/kg, Marcaine; Hospira, Lake Forest, IL, USA) was subcutaneously injected at the surgical site, an incision of about 1 cm made with a scalpel blade, and the cranium was exposed. Using a dental burr, one hole of 1 mm diameter was drilled above the site of injection (AP (anterior–posterior; ML (medial–lateral); DV (dorsal-ventral), from bregma). The following injection coordinates were used:

- SNc for axonal arborization labelling [AP -3.0 mm; ML 1.5 mm; DV -4.0 mm]
- VTA for axonal arborization labelling [AP -2.7 mm; ML 0.0 mm; DV -4.5 mm]
- Mesencephalon for α-synuclein virus injection [AP -3.0 mm; ML 1.0 mm; DV -4.3 mm]
- Dorsal striatum for 6-OHDA injection [AP 0.5 mm; ML 2.0 mm; DV -3.0 mm]

Note that the coordinates for SNc and VTA injections were 0.3 mm more anterior then for direct targeting of the region. These coordinates were adjusted to prevent infection of RRF, rostral linear nucleus (RLI) or caudal linear nucleus (CLI) DA neurons. Next, borosilicate pipettes were pulled using a pipet (prepared using a Sutter Instrument, P-2000 puller), coupled to a 10 µL Hamilton syringe (Hamilton, 701RN) using a RN adaptor (Hamilton, 55750-01) and the whole setup was filled with mineral oil. Using a Quintessential Stereotaxic Injector (Stoelting), solutions to be injected were pulled up in the glass pipet. For the axonal arborization size quantification, 0.1 µL (SNc) or 0.05 µL (VTA) of sterile NaCl containing $1.15x10^{12}$ viral genome particles/mL of AAV2-EF1a-DIO-eYFP (UNC Vector Core, Chapel Hill, NC, USA) was injected. For α-synuclein over-expression, 0.8 µL of AAV2-CBA-alpha-Syn ($3.8x10^{12}$ viral genome particles/mL, MJF Foundation, USA) or AAV2-CBA-eGFP ($2.0x10^{12}$ viral genome particles/mL MJF Foundation, USA) was injected. For 6-OHDA lesions, 0.5 µL 6-OHDA (3 mg/mL) in 0.2% ascorbic acid solution was injected. Forty minutes prior to 6-OHDA injections, the norepinephrine transporter blocker desipramine (25mg/Kg) was injected intraperitoneally to the animals to prevent lesions of the noradrenergic fibers. After the unilateral injection, the pipette was left in place for 10 min to allow diffusion and then slowly withdrawn. Finally, the scalp skin was sutured and a subcutaneous injection of the anti-inflammatory drug carprofen

(Rimadyl, 50 mg/mL) was given. Animals recovered in their home cage and were closely monitored for 24h. A second dose of carprofen (5 mg/kg) was given if deemed necessary. The brains were collected 1 month after the 6-OHDA injection (P90), 2 months after viral injection for axonal arborization labeling (P120) or 3 months after viral injection for α-synuclein overexpression studies (P150).

Tissue Preparation

Mice were anesthetized using pentobarbital NaCl saline solution (7 mg/mL) injected intraperitoneally and then were perfused with 50mL of PBS followed by 100 mL of paraformaldehyde (PFA) 4% using an intracardiac needle at a rate of 25 mL/min. The brains were extracted, placed 48h in PFA followed by 48h in a 30% sucrose solution and frozen in isopentane at -30ºC for 1 minute. 40 microns thick coronal sections were then produced using a cryostat (Leica CM1800) and placed in antifreeze solution at -20 ºC until used.

Immunohistochemistry

One out of every 6th slice was used for immunofluorescence. After a PBS wash, the tissue was permeabilized, nonspecific binding sites blocked and incubated overnight with a rabbit anti-TH antibody (1:1000, AB152, Millipore Sigma, USA), a rat anti-DAT antibody (1:1000, MAB369; MilliporeSigma, USA), a chicken anti-GFP (1:2000, GFP-1020; Aves Labs, USA), a mouse anti-p-S129-α-synuclein (1:2000, 328100, Invitrogen, USA), a chicken anti-α-synuclein (1:2000, AB190376, Cedarlane, USA) or rabbit anti-VMAT2 (1:2000, kindly provided by Dr. G.W. Miller (63)) Primary antibodies were subsequently detected with a rabbit or chicken Alexa Fluor-488–conjugated secondary antibody, a rabbit Alexa Fluor-546–conjugated secondary antibody, and/or a rat Alexa Fluor-647–conjugated secondary antibody (1:400; Thermo Fisher Scientific).

One out of every 6th slice was used for DAB immunostaining. After a PBS wash, the tissue was incubated for 10 min with 0.9% H_2O_2 solution, then washed with PBS again and incubated for 48h with a rabbit anti-TH antibody (1:1000, AB152, Millipore Sigma, USA) at 4ºC, 12h with goat anti-rabbit biotin-SP-AffiniPure secondary antibody (111-065-003, Jackson ImmunoResearch Laboratories, USA) at 4ºC and 3h with horseradish peroxidase streptavidine

(016-030-084, Cedarlane, USA). The DAB reaction was carried out for 45s, then stopped by incubation with 0.1M acetate buffer and slices were mounted on Superfrost/Plus microscope slides. They were left to dry for 96h after which they were stained with cresyl violet and went through subsequent incubations with increasing concentrations of alcohol. After short isopropanol and xylene baths, slides were sealed with Permount mounting medium (SP15-100, Fisher, USA) using glass coverslips.

Confocal Imaging

All of the imaging quantification analyses were performed on images captured using confocal microscopy. Images were acquired using an Olympus Fluoview FV1000 microscope (Olympus). Images acquired using 488 and 546 laser excitation were scanned sequentially to reduce nonspecific bleed-through signal. For each slice, up to 4 images were acquired in the dorsal striatum and up to 2 in the ventral striatum. All image quantifications were performed using ImageJ (National Institutes of Health) software. We first applied a background correction and then measured the surface and intensity of the signal.

For quantification of TH, DAT and VMAT2 positive terminals in the ventral or dorsal striatum, images were acquired using a 60x oil-immersion objective and averaged from slices at bregma 1.18, 0.14 and -0.94 mm. For axonal arborization size quantification with eYFP viral expression, images were acquired on one every 6th slices from bregma -2.2 to 1.94 mm using a 20x water immersion objective since the fibers were easily distinguishable at lower magnification. The proportion of the area percentage covered by eYFP fibers was extrapolated to the size of the striatum for each slice based on The Mouse Brain in Stereotaxic Coordinates 3rd Edition by George Paxinos (64) and normalized by the number of infected neurons counted manually (300-1000 neurons) and plotted in relation to the bregma coordinates. Stereological counting was not used for this quantification since the number of neurons was too low to get a reliable count using random sampling. The volume of eYFP positive axonal arborization was then approximated using the area under the curve.

The number of striosomes and their size was also quantified using the integrated particles analyzer in Image J. Colocalization measurements were performed using the Jacop plugin for

ImageJ on 60x confocal images (65). Mander's M1 and M2 coefficients were obtained after manual thresholding of the images to remove background. A mask of the YFP signal was applied to the other signals for measurement of their colocalization inside YFP fibers.

Stereological counting

TH-immunoreactive neurons were counted in every sixth section using a 100x oil-immersion objective on a Leica microscope equipped with a motorized stage. A 60 x 60 μm^2 counting frame was used in the Stereo Investigator (MBF Bioscience) sampling software with a 12 µm optical dissector (2 µm guard zones) and counting site intervals of 150 µm after a random start (100 µm intervals for unilateral lesion). Mesencephalic DA nuclei, including the VTA, SNc and RRF were examined. Stereological estimates of the total number of TH-immunoreactive neurons within each nucleus were obtained.

Fast scan cyclic voltammetry

Acute brain slices from 3-month-old mice were obtained using a protective slicing method (66). Matched pairs of CTL and D2-cKO mice were used on each experimental day. After intracardiac perfusion, brains were quickly dissected, submersed in ice-cold NMDG cutting solution and coronal striatal brain slices of 300 µm (from bregma 1.34 to 0.98 mm) were prepared with a Leica VT1000S vibrating microtome in ice-cold (0 to 4°C) NMDG protective cutting solution. Slices recovered for 12 min in 32° NMDG solution and were then transferred to oxygenated HEPES-buffered resting solution at RT for at least 1h. For recordings, slices were put in a custom-made recording chamber superfused with artificial cerebral spinal fluid (aCSF) at 1 ml/min and maintained at 32°C. All solutions were adjusted at pH 7.35-7.4, 300 mOsm/kg and saturated with 95% O2-5% CO2 at least 30 min prior to each experiment.

Electrically induced DA release was measured by fast-scan cyclic voltammetry (FSCV) using a 7 µm diameter carbon-fiber electrode placed into the dorsal or ventral striatum ~100 µm below the surface and a bipolar electrode (Plastics One, Roanoke, VA, USA) placed ~200 µm away. Carbon-fiber electrodes were fabricated as previously described (67). Electrodes were polished and filled with 4M potassium acetate and 150 mM potassium chloride. Carbon fibers were then cut using a scalpel blade to obtain maximal basal currents of 100 to 180 nA. Electrodes

were finally selected for their sensitivity to DA using *in vitro* calibration with 1 µM DA in aCSF before each experiment. Before and after use, electrodes were cleaned with isopropyl alcohol. The potential of the carbon fiber electrode was scanned at a rate of 300 V/s according to a 10 ms triangular voltage wave (−400 to 1000 mV vs Ag/AgCl) with a 100 ms sampling interval, using a CV203BU headstage preamplifier (Axon instrument, Union City, CA)) and an Axopatch 200B amplifier (Axon Instruments). Data were acquired using a Digidata 1440A analog to digital converter board (Axon Instruments) connected to a computer using Clampex (Axon Instruments). Slices were left to stabilize for 20 min before any electrochemical recordings.

After positioning of the bipolar stimulation and carbon fiber electrodes in the striatum, single pulses (400 µA, 1ms) were applied to the nucleus accumbens core (referred to as ventral striatum) and then to the dorso-lateral part of the dorsal striatum to trigger DA release. Stimulations were applied every 2 min. After recording in the dorsal striatum, the media was changed to ACSF containing 5 µM of nomifensine (Sigma) and single stimuli were applied to the dorsal striatum. Electrode calibration was performed before and after the recording of each slices and the average value for the current at the peak oxidation potential was used to normalize the recorded *in vivo* current signals to DA concentrations.

DA release was analyzed as the peak height of DA concentrations and DA reuptake was determined from the clearance rate of DA which was assumed to follow Michaelis-Menten kinetics. A nonlinear least square optimization was applied to fit a three-parameter exponential function with baseline shift to the reuptake phase of the DA response. Uptake parameters (tau and Vmax) were calculated based on the exponential fitting. To determine whether DAT-mediated DA uptake was compromised in D2-cKO mice, the initial portion of the falling phase of single pulse evoked [DA]o curves was used to calculate the Vmax (maximal rate of DA uptake) after setting the Km parameter to 0.2 µM, based on the affinity of DA for the DAT, measured in mouse synaptosome preparations (68) and with the assumption that the Km is not altered in the KO mouse line.

Behavior testing

All mice were habituated to the user by handling them once a day during 3 consecutive days before experiments. Mice were moved to the experimental room 1h before the test.

Mice first went through a stepping test recorded with a digital camera (DMK 22BUC03, ImagingSource) and IC Capture 2.4 software. Mice were gently lifted by the base of the tail at one end of a 1-meter corridor leaving only forepaws touching the surface and were pulled backward for 4s over a distance of 1-meter. Recordings were then watched in slow motion and the number of steps of each forepaw were counted. After 1h of rest, animals were placed in a 4L beaker with the digital camera recording their movements from underneath to assess rotation. After 20 min, amphetamine 5 mg/kg was intraperitoneally injected and mice were placed back in the beaker for 40 min. Recordings were then watched to count the ispilateral and contralateral rotations made by the mice during the first (basal) and the last (amphetamine) 20 min.

Statistics

All experiments were performed blind to the experimental groups, from surgery to image analysis. Parametric statistical tests were used because samples contained data with normal distributions. Data were presented as mean ± SEM. The level of statistical significance was established at $p < 0.05$ in one or two-way ANOVAs or two-tailed t-tests with Welch's correction if needed. A ROUT outlier analysis was performed when required (Q=1%). Statistical analyses were performed with the Prism 7 software (GraphPad Software, $p < 0.05$ = *, $p < 0.01$ = **, $p < 0.001$ = ***, $p < 0.0001$ = ****). The Tukey post-hoc test was used when all the means were compared to each other and the Sidak post-hoc test was used when only subsets of means were compared.

6.6 Acknowledgements

This work was supported by the Brain Canada and Krembil foundations, as well as by the Canadian Institutes of Health Research (MOP106556) and by a pilot project grant from Parkinson Canada. The GRSNC was supported by an infrastructure grant from the Fonds du Québec en Recherche, Santé (FRQS). N. Giguère received salary support from Parkinson Society Canada and from the FRQS. We thank Dr. Lionel Carmant for access to the StereoInvestigator stereological analysis workstation.

6.7 References

1 Giguère N, Burke Nanni S, Trudeau L-E. On cell loss and selective vulnerability of neuronal populations in Parkinson's disease. Front Neurol 2018;9:455.

2 Surmeier DJ. Calcium, ageing, and neuronal vulnerability in Parkinson's disease. Lancet Neurol 2007;6:933–8.

3 Segura-Aguilar J, Paris I, Muñoz P, Ferrari E, Zecca L, Zucca FA. Protective and toxic roles of dopamine in Parkinson's disease. J Neurochem 2014;129:898–915.

4 Hare DJ, Double KL. Iron and dopamine: a toxic couple. Brain J Neurol 2016;139:1026–35.

5 Parent M, Parent A. Relationship between axonal collateralization and neuronal degeneration in basal ganglia. J Neural Transm Suppl 2006:85–8.

6 Matsuda W, Furuta T, Nakamura KC, Hioki H, Fujiyama F, Arai R, et al. Single nigrostriatal dopaminergic neurons form widely spread and highly dense axonal arborizations in the neostriatum. J Neurosci 2009;29:444–53.

7 Bolam JP, Pissadaki EK. Living on the edge with too many mouths to feed: why dopamine neurons die. Mov Disord 2012;27:1478–83.

8 Pacelli C, Giguère N, Bourque M-J, Lévesque M, Slack RS, Trudeau L-É. Elevated mitochondrial mioenergetics and axonal arborization size are key contributors to the vulnerability of dopamine neurons. Curr Biol CB 2015;25:2349–60.

9 Pissadaki EK, Bolam JP. The energy cost of action potential propagation in dopamine neurons: clues to susceptibility in Parkinson's disease. Front Comput Neurosci 2013;7:13.

10 Goldberg MS, Fleming SM, Palacino JJ, Cepeda C, Lam HA, Bhatnagar A, et al. Parkin-deficient mice exhibit nigrostriatal deficits but not loss of dopaminergic neurons. J Biol Chem 2003;278:43628–35.

11 Chandran JS, Lin X, Zapata A, Höke A, Shimoji M, Moore SO, et al. Progressive behavioral deficits in DJ-1 deficient mice are associated with normal nigrostriatal function. Neurobiol Dis 2008;29:505–14.

12 Ramsey CP, Tsika E, Ischiropoulos H, Giasson BI. DJ-1 deficient mice demonstrate similar vulnerability to pathogenic Ala53Thr human α-syn toxicity. Hum Mol Genet 2010;19:1425–37.

13 Aguiar AS, Tristão FSM, Amar M, Chevarin C, Lanfumey L, Mongeau R, et al. Parkin-knockout mice did not display increased vulnerability to intranasal administration of 1-methyl-4-phenyl-1,2,3,6-tetrahydropyridine (MPTP). Neurotox Res 2013;24:280–7.

14 Moisoi N, Fedele V, Edwards J, Martins LM. Loss of Pink1 enhances neurodegeneration in a mouse model of Parkinson's disease triggered by mitochondrial stress. Neuropharmacology 2014;77:350–7.

15 Parish CL, Stanic D, Drago J, Borrelli E, Finkelstein DI, Horne MK. Effects of long-term treatment with dopamine receptor agonists and antagonists on terminal arbor size. Eur J Neurosci 2002;16:787–94.

16 Tripanichkul W, Stanic D, Drago J, Finkelstein DI, Horne MK. D2 Dopamine receptor blockade results in sprouting of DA axons in the intact animal but prevents sprouting following nigral lesions. Eur J Neurosci 2003;17:1033–45.

17 Tinsley RB, Bye CR, Parish CL, Tziotis-Vais A, George S, Culvenor JG, et al. Dopamine D2 receptor knockout mice develop features of Parkinson disease. Ann Neurol 2009;66:472–84.

18 Fasano C, Poirier A, DesGroseillers L, Trudeau LE. Chronic activation of the D2 dopamine autoreceptor inhibits synaptogenesis in mesencephalic dopaminergic neurons in vitro. Eur J Neurosci 2008;28:1480–90.

19 Rocchetti J, Isingrini E, Dal Bo G, Sagheby S, Menegaux A, Tronche F, et al. Presynaptic D2 dopamine receptors control long-term depression expression and memory processes in the temporal hippocampus. Biol Psychiatry 2015;77:513–25.

20 Carboni E, Imperato A, Perezzani L, Di Chiara G. Amphetamine, cocaine, phencyclidine and nomifensine increase extracellular dopamine concentrations preferentially in the nucleus accumbens of freely moving rats. Neuroscience 1989;28:653–61.

21 Venton BJ, Seipel AT, Phillips PEM, Wetsel WC, Gitler D, Greengard P, et al. Cocaine increases dopamine release by mobilization of a synapsin-dependent reserve pool. J Neurosci 2006;26:3206–9.

22 Aragona BJ, Cleaveland NA, Stuber GD, Day JJ, Carelli RM, Wightman RM. Preferential enhancement of dopamine transmission within the nucleus accumbens shell by cocaine is attributable to a direct increase in phasic dopamine release events. J Neurosci 2008;28:8821–31.

23 Surmeier DJ, Schumacker PT, Guzman JD, Ilijic E, Yang B, Zampese E. Calcium and Parkinson's disease. Biochem Biophys Res Commun 2017;483:1013–9.

24 Prensa L, Parent A. The nigrostriatal pathway in the rat: A single-axon study of the relationship between dorsal and ventral tier nigral neurons and the striosome/matrix striatal compartments. J Neurosci 2001;21:7247–60.

25 Matsuda W, Furuta T, Nakamura KC, Hioki H, Fujiyama F, Arai R, et al. Single nigrostriatal dopaminergic neurons form widely spread and highly dense axonal arborizations in the neostriatum. J Neurosci 2009;29:444–53.

26 Aransay A, Rodríguez-López C, García-Amado M, Clascá F, Prensa L. Long-range projection neurons of the mouse ventral tegmental area: a single-cell axon tracing analysis. Front Neuroanat 2015;9.

27 Bjorklund A, Dunnett SB. Dopamine neuron systems in the brain: an update. Trends Neurosci 2007;30:194–202.

28 Berod A, Biguet NF, Dumas S, Bloch B, Mallet J. Modulation of tyrosine hydroxylase gene expression in the central nervous system visualized by in situ hybridization. Proc Natl Acad Sci 1987;84:1699–703.

29 Rose S, Nomoto M, Jenner P, Marsden CD. Transient depletion of nucleus accumbens dopamine content may contribute to initial akinesia induced by MPTP in common marmosets. Biochem Pharmacol 1989;38:3677–81.

30 Otto D, Unsicker K. Basic FGF reverses chemical and morphological deficits in the nigrostriatal system of MPTP-treated mice. J Neurosci 1990;10:1912–21.

31 Strong R, Moore MA, Hale C, Wessels-Reiker M, Armbrecht HJ, Richardson A. Modulation of tyrosine hydroxylase gene expression in the rat adrenal gland by age and reserpine. Brain Res 1990;525:126–32.

32 Tatton WG, Kwan MM, Verrier MC, Seniuk NA, Theriault E. MPTP produces reversible disappearance of tyrosine hydroxylase-containing retinal amacrine cells. Brain Res 1990;527:21–31.

33 McMillan CR, Sharma R, Ottenhof T, Niles LP. Modulation of tyrosine hydroxylase expression by melatonin in human SH-SY5Y neuroblastoma cells. Neurosci Lett 2007;419:202–6.

34 Lim H, Jang S, Lee Y, Moon S, Kim J, Oh S. Enhancement of anxiety and modulation of TH and pERK expressions in amygdala by repeated injections of corticosterone. Biomol Ther 2012;20:418–24.

35 Anzalone A, Lizardi-Ortiz JE, Ramos M, De Mei C, Hopf FW, Iaccarino C, et al. Dual control of dopamine synthesis and release by presynaptic and postsynaptic dopamine D2 receptors. J Neurosci 2012;32:9023–34.

36 Masoud S, Vecchio L, Bergeron Y, Hossain M, Nguyen L, Bermejo M, et al. Increased expression of the dopamine transporter leads to loss of dopamine neurons, oxidative stress and L-DOPA reversible motor deficits. Neurobiol Dis 2015;74:66–75.

37 Budygin EA, Oleson EB, Lee YB, Blume LC, Bruno MJ, Howlett AC, et al. Acute depletion of D2 receptors from the rat substantia nigra alters dopamine kinetics in the dorsal striatum and drug responsivity. Front Behav Neurosci 2017;10.

38 Bello EP, Mateo Y, Gelman DM, Noaín D, Shin JH, Low MJ, et al. Cocaine supersensitivity and enhanced motivation for reward in mice lacking dopamine D2 autoreceptors. Nat Neurosci 2011;14:1033–8.

39 Sonnier L, Le Pen G, Hartmann A, Bizot J-C, Trovero F, Krebs M-O, et al. Progressive loss of dopaminergic neurons in the ventral midbrain of adult mice heterozygote for Engrailed1. J Neurosci 2007;27:1063–71.

40 Veenvliet JV, Santos MTMA dos, Kouwenhoven WM, Oerthel L von, Lim JL, Linden AJA van der, et al. Specification of dopaminergic subsets involves interplay of En1 and Pitx3. Development 2013;140:3373–84.

41 Lee FJS, Pei L, Moszczynska A, Vukusic B, Fletcher PJ, Liu F. Dopamine transporter cell surface localization facilitated by a direct interaction with the dopamine D2 receptor. EMBO J 2007;26:2127–36.

42 Bolan EA, Kivell B, Jaligam V, Oz M, Jayanthi LD, Han Y, et al. D2 receptors regulate dopamine transporter function via an extracellular signal-regulated kinases 1 and 2-dependent and phosphoinositide 3 kinase-independent mechanism. Mol Pharmacol 2007;71:1222–32.

43 Garcia-Olivares J, Torres-Salazar D, Owens WA, Baust T, Siderovski DP, Amara SG, et al. Inhibition of dopamine transporter activity by G protein βγ subunits. PloS One 2013;8:e59788.

44 Chen R, Daining CP, Sun H, Fraser R, Stokes SL, Leitges M, et al. Protein kinase Cβ is a modulator of the dopamine D2 autoreceptor-activated trafficking of the dopamine transporter. J Neurochem 2013;125:663–72.

45 Elkon H, Melamed E, Offen D. Oxidative stress, induced by 6-hydroxydopamine, reduces proteasome activities in PC12 cells: implications for the pathogenesis of Parkinson's disease. J Mol Neurosci MN 2004;24:387–400.

46 Hanrott K, Gudmunsen L, O'Neill MJ, Wonnacott S. 6-Hydroxydopamine-induced apoptosis is mediated via extracellular auto-oxidation and caspase 3-dependent activation of protein kinase Cδ. J Biol Chem 2006;281:5373–82.

47 Latchoumycandane C, Anantharam V, Jin H, Kanthasamy A, Kanthasamy A. Dopaminergic neurotoxicant 6-OHDA induces oxidative damage through proteolytic activation of PKCδ in cell culture and animal models of Parkinson's disease. Toxicol Appl Pharmacol 2011;256:314–23.

48 Lu X, Kim-Han JS, Harmon S, Sakiyama-Elbert SE, O'Malley KL. The Parkinsonian mimetic, 6-OHDA, impairs axonal transport in dopaminergic axons. Mol Neurodegener 2014;9:17.

49 Tirmenstein MA, Hu CX, Scicchitano MS, Narayanan PK, McFarland DC, Thomas HC, et al. Effects of 6-hydroxydopamine on mitochondrial function and glutathione status in SH-SY5Y human neuroblastoma cells. Toxicol Vitro 2005;19:471–9.

50 Ganapathy K, Datta I, Sowmithra S, Joshi P, Bhonde R. Influence of 6-hydroxydopamine toxicity on α-synuclein phosphorylation, resting vesicle expression, and vesicular dopamine release. J Cell Biochem 2016;117:2719–36.

51 Ebrahimi-Fakhari D, Cantuti-Castelvetri I, Fan Z, Rockenstein E, Masliah E, Hyman BT, et al. Distinct roles in vivo for the ubiquitin-proteasome system and the autophagy-lysosomal pathway in the degradation of α-synuclein. J Neurosci 2011;31:14508–20.

52 Bourdenx M, Bezard E, Dehay B. Lysosomes and α-synuclein form a dangerous duet leading to neuronal cell death. Front Neuroanat 2014;8:83.

53 Mazzulli JR, Zunke F, Isacson O, Studer L, Krainc D. α-synuclein–induced lysosomal dysfunction occurs through disruptions in protein trafficking in human midbrain synucleinopathy models. Proc Natl Acad Sci 2016;113:1931–6.

54 Glinka YY, Youdim MBH. Inhibition of mitochondrial complexes I and IV by 6-hydroxydopamine. Eur J Pharmacol Environ Toxicol Pharmacol 1995;292:329–32.

55 Smith MP, Cass WA. Oxidative stress and dopamine depletion in an intrastriatal 6-hydroxydopamine model of Parkinson's disease. Neuroscience 2007;144:1057–66.

56 Di Maio R, Barrett PJ, Hoffman EK, Barrett CW, Zharikov A, Borah A, et al. α-synuclein binds TOM20 and inhibits mitochondrial protein import in Parkinson's disease. Sci Transl Med 2016;8:342ra78.

57 Pozo Devoto VM, Falzone TL. Mitochondrial dynamics in Parkinson's disease: a role for α-synuclein? Dis Model Mech 2017;10:1075–87.

58 Ludtmann MHR, Angelova PR, Horrocks MH, Choi ML, Rodrigues M, Baev AY, et al. α-synuclein oligomers interact with ATP synthase and open the permeability transition pore in Parkinson's disease. Nat Commun 2018;9:2293.

59 Parihar MS, Parihar A, Fujita M, Hashimoto M, Ghafourifar P. Mitochondrial association of alpha-synuclein causes oxidative stress. Cell Mol Life Sci CMLS 2008;65:1272–84.

60 Tinsley RB, Bye CR, Parish CL, Tziotis-Vais A, George S, Culvenor JG, et al. Dopamine D2 receptor knockout mice develop features of Parkinson disease. Ann Neurol 2009;66:472–84.

61 Zhuang X, Masson J, Gingrich JA, Rayport S, Hen R. Targeted gene expression in dopamine and serotonin neurons of the mouse brain. J Neurosci Methods 2005;143:27–32.

62 Bäckman CM, Malik N, Zhang Y, Shan L, Grinberg A, Hoffer BJ, et al. Characterization of a mouse strain expressing Cre recombinase from the 3' untranslated region of the dopamine transporter locus. Genes N Y N 2000 2006;44:383–90.

63 Cliburn RA, Dunn AR, Stout KA, Hoffman CA, Lohr KM, Bernstein AI, et al. Immunochemical localization of vesicular monoamine transporter 2 (VMAT2) in mouse brain. J Chem Neuroanat 2017;83–84:82–90.

64 Franklin KBJ, Paxinos G. The mouse brain in stereotaxic coordinates. 3. ed. Amsterdam: Elsevier, AP; 2008.

65 Bolte S, Cordelières FP. A guided tour into subcellular colocalization analysis in light microscopy. J Microsc 2006;224:213–32.

66 Ting JT, Daigle TL, Chen Q, Feng G. Acute brain slice methods for adult and aging animals: application of targeted patch clampanalysis and optogenetics. Methods Mol Biol Clifton NJ 2014;1183:221–42.

67 Martel P, Leo D, Fulton S, Bérard M, Trudeau L-E. Role of Kv1 potassium channels in regulating dopamine release and presynaptic D2 receptor function. PLOS ONE 2011;6:e20402.

68 Ross SB. Synaptic concentration of dopamine in the mouse striatum in relationship to the kinetic properties of the dopamine receptors and uptake mechanism. J Neurochem 1991;56:22–9.

6.8 Figures

Figure 1. SNc DA neurons have a longer axonal arborization than VTA DA neurons *in vivo*.

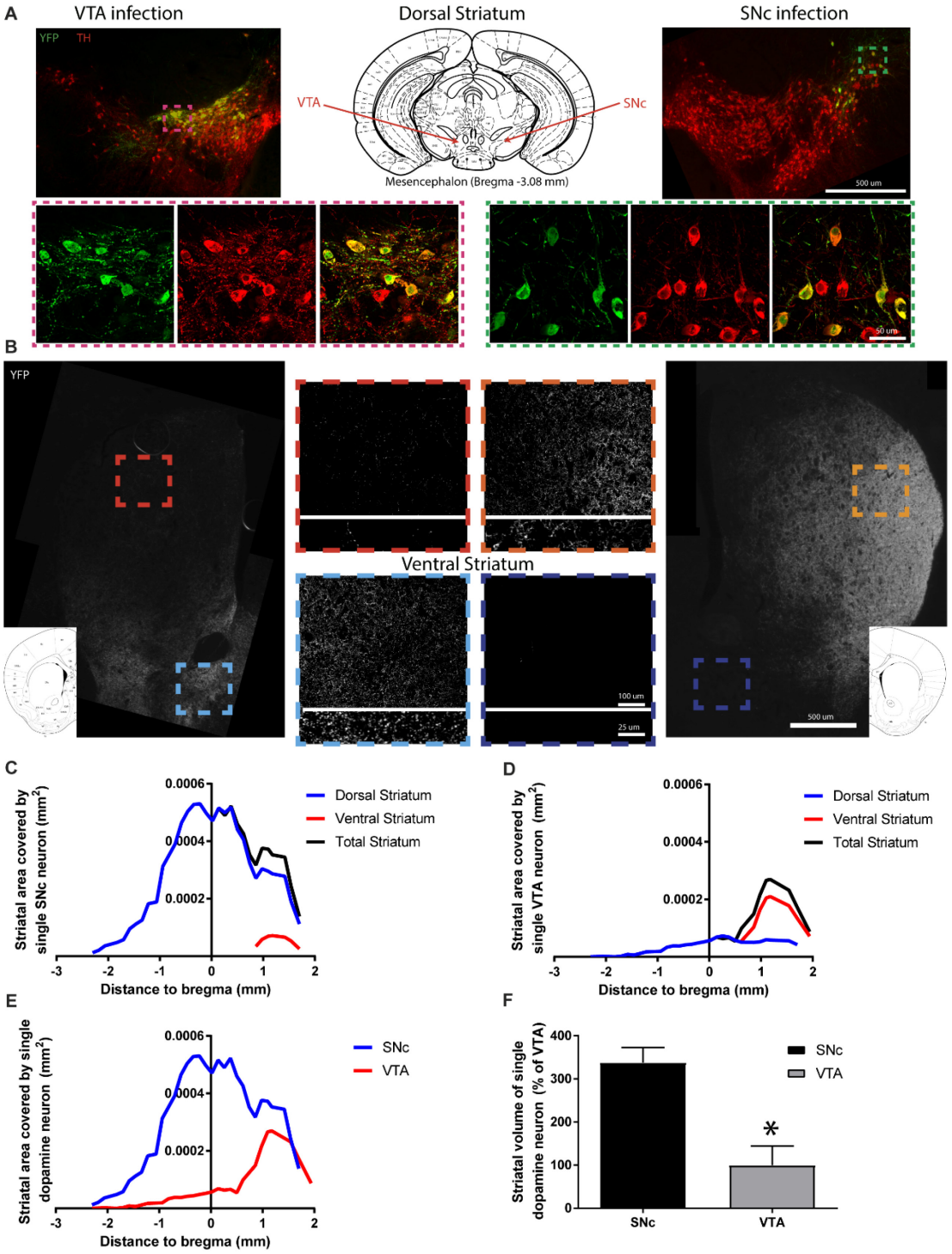

Axonal arborization was estimated by performing AAV injections in adult DAT-Cre mice to conditionally express eYFP in either SNc or VTA SNc DA neurons (A). The extent of the axonal arborization was then observed in the striatum (B) and measured thought-out the ventral and dorsal striatum for SNc (C) and VTA (D) targeted injections. Direct (E) and relative (F) comparisons of the total striatal axonal arborization size was performed. N=3 brains/group, mean ± SEM, *p>0.05. Brain schematics modified from The Mouse Brain in Stereotaxic Coordinates 3rd Edition by George Paxinos and Keith B.J. Franklin (64).

Figure 2. Increase in DAT but not TH striatal expression in D2-cKO mice, without a change in the number of DA neurons.

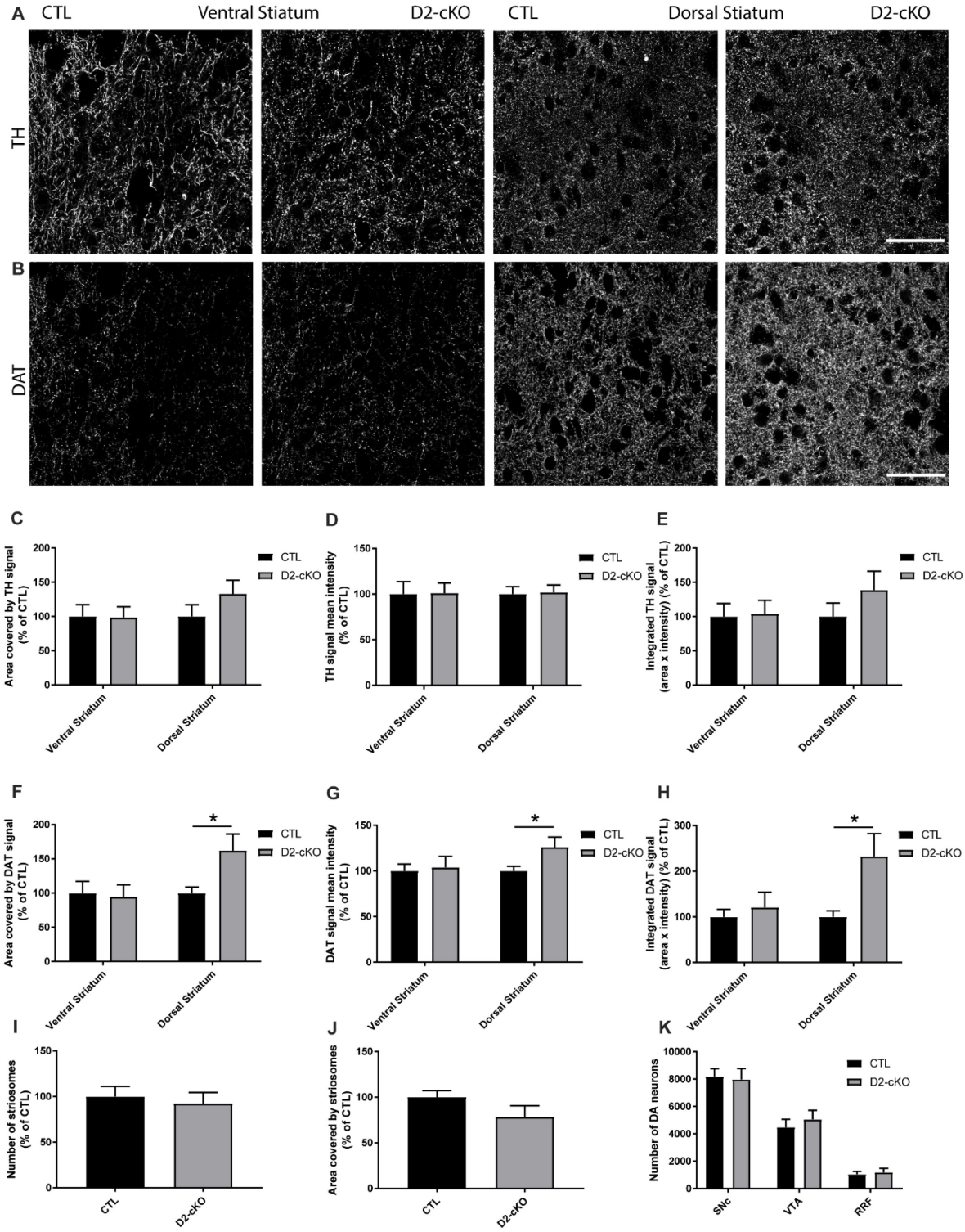

TH (A) and DAT (B) immunofluorescence levels were measured in the ventral and dorsal striatum in controls and D2-cKO mice. Scale bar = 50 μm. % area covered (C,F), mean signal intensity (D,G) and integrated signal (E,H) were quantified for TH and DAT signals as well as the number of striosomes (I) and their size (J) using DAT signal. N=15-22 brains/group, mean ± SEM, *p>0.05. The number of DA neurons in the SNc, VTA and RRF was measured using stereological counting. N=4-5 brains/group, mean ± SEM.

Figure 3. Increased axonal arborization size of SNc but not VTA DA neurons in D2-cKO mice.

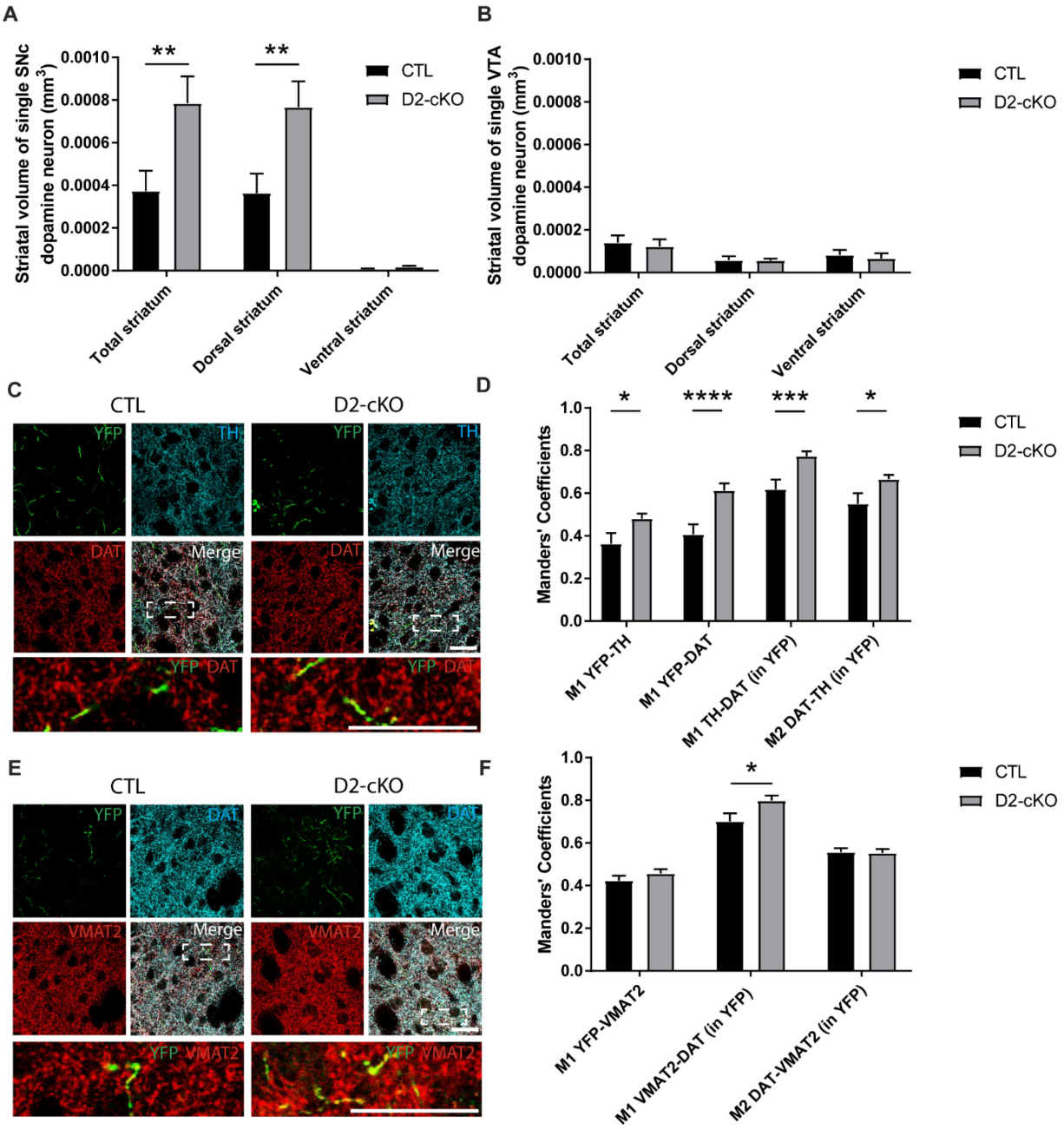

The axonal arborization of SNc or VTA DA neurons was selectively visualized using AAV injections in adult $DAT^{IRES\text{-}Cre/+}$;$DRD2^{LOX/LOX}$ mice to express eYFP in either SNc or VTA DA neurons. The extent of the axonal arborization was observed in the striatum and measured throughout the ventral and dorsal striatum for SNc (A) and VTA (B) targeted injections. N=6-10 brains/group, mean ± SEM, **p>0.01. Colocalization of YFP-positive SNc dopaminergic axonal processes (C) with TH and DAT, and the colocalization of TH and DAT were measured with Mander's coefficients (M1 and M2) (D). Colocalization of YFP-positive SNc dopaminergic axonal processes (E) with VMAT2 and colocalization of VMAT2 and DAT were measured with Mander's coefficients (F). M1= proportion of signal 1 that colocalize with signal 2, M2 = proportion of signal 2 that colocalize with signal 1. Scale bar = 80 μm. N=24-35 images/group, mean ± SEM, *p>0.05, ***p>0.001, ****p>0.0001.

Figure 4. Decrease in striatal DA release in D2-cKO mice without changes in DA reuptake kinetics.

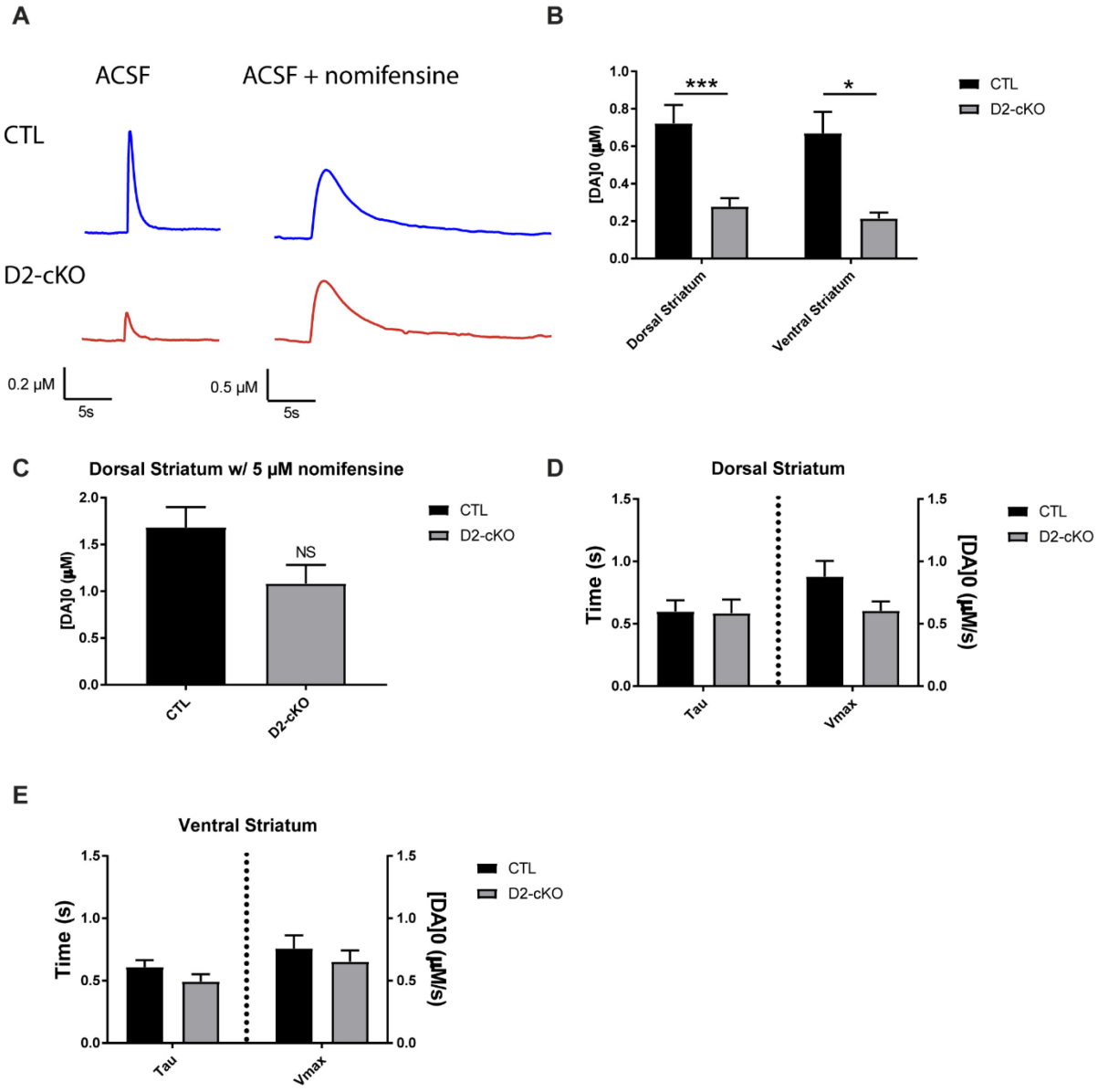

Cyclic voltammetry was used to measure the amount of DA released during single electrical stimuli on acute brain slices (A) in the ventral and dorsal striatum (B). Single stimulations were also used in the presence of the DAT antagonist nomifensine (C). DA reuptake kinetics were extracted from recordings obtained in response to single pulse stimulation by fitting an exponential curve based on the Michaelis-Menten equation for the dorsal (D) and ventral (E) striatum. N=8-9 brain/group, mean ± SEM, *p>0.05, ***p>0.001.

Figure 5. SNc DA neurons from D2-cKO are not more vulnerable to α-synuclein overexpression.

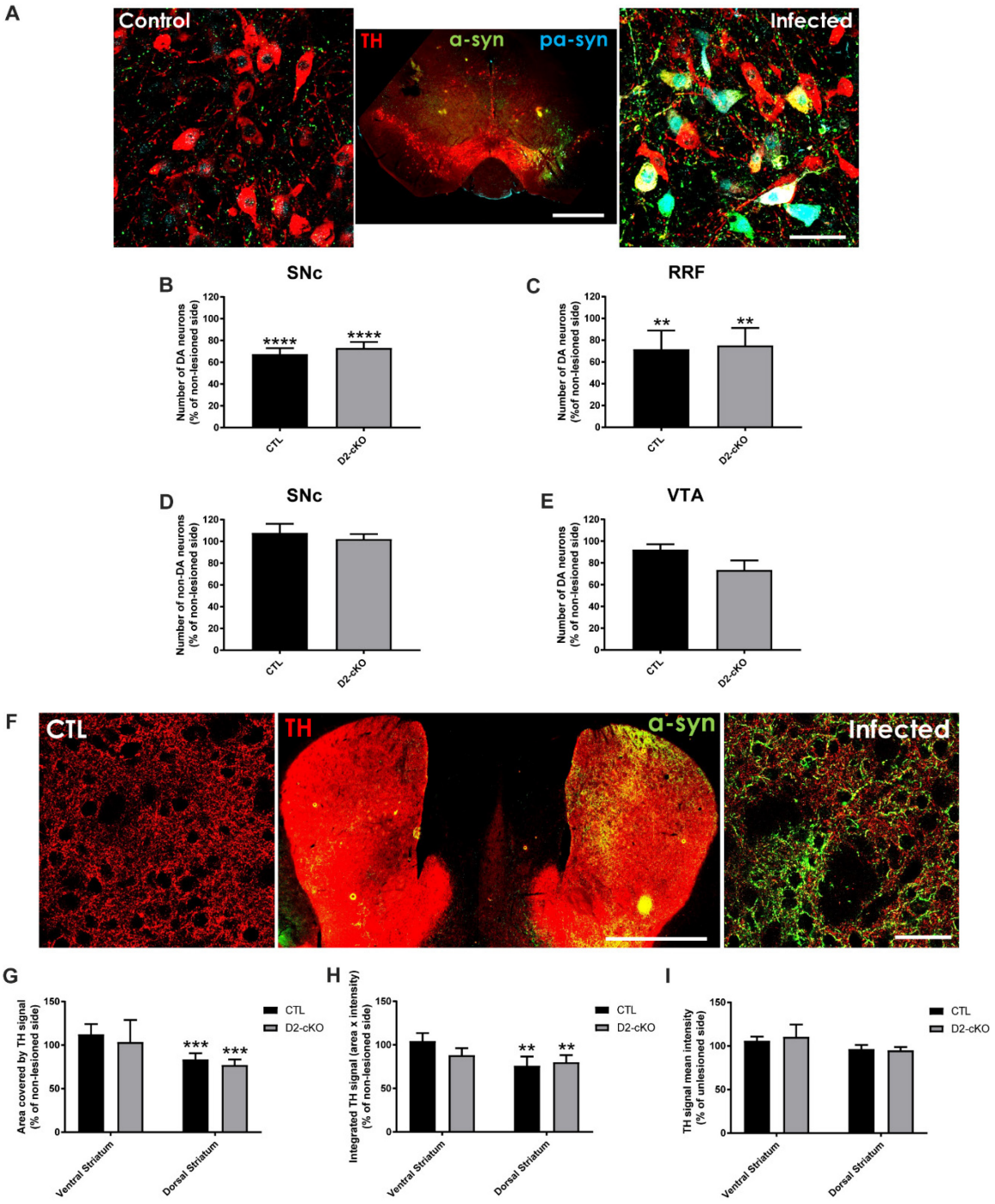

α-synuclein viral overexpression in the mesencephalon was used to evaluate the impact the increased axonal arborization size of D2-cKO SNc DA neurons on their vulnerability. In the mesencephalon (A), SNc TH+ (B), RRF TH+ (C), SNc TH- (D) and VTA DA neurons (E) were counted using stereological methods. N=9 brain/group, mean ± SEM, ** p>0.01, **** p>0.0001. Scale bars = 1mm and 50 µm. In the dorsal and ventral striatum (F), TH signal area (G), mean signal intensity (H) and integrated signal (I) were measured. N=9-12 brain/group, mean ± SEM, ** p>0.01, *** p>0.001. Scale bars = 1mm and 50 µm.

Figure 6. SNc DA neurons from D2-cKO mice are more vulnerable to 6-OHDA.

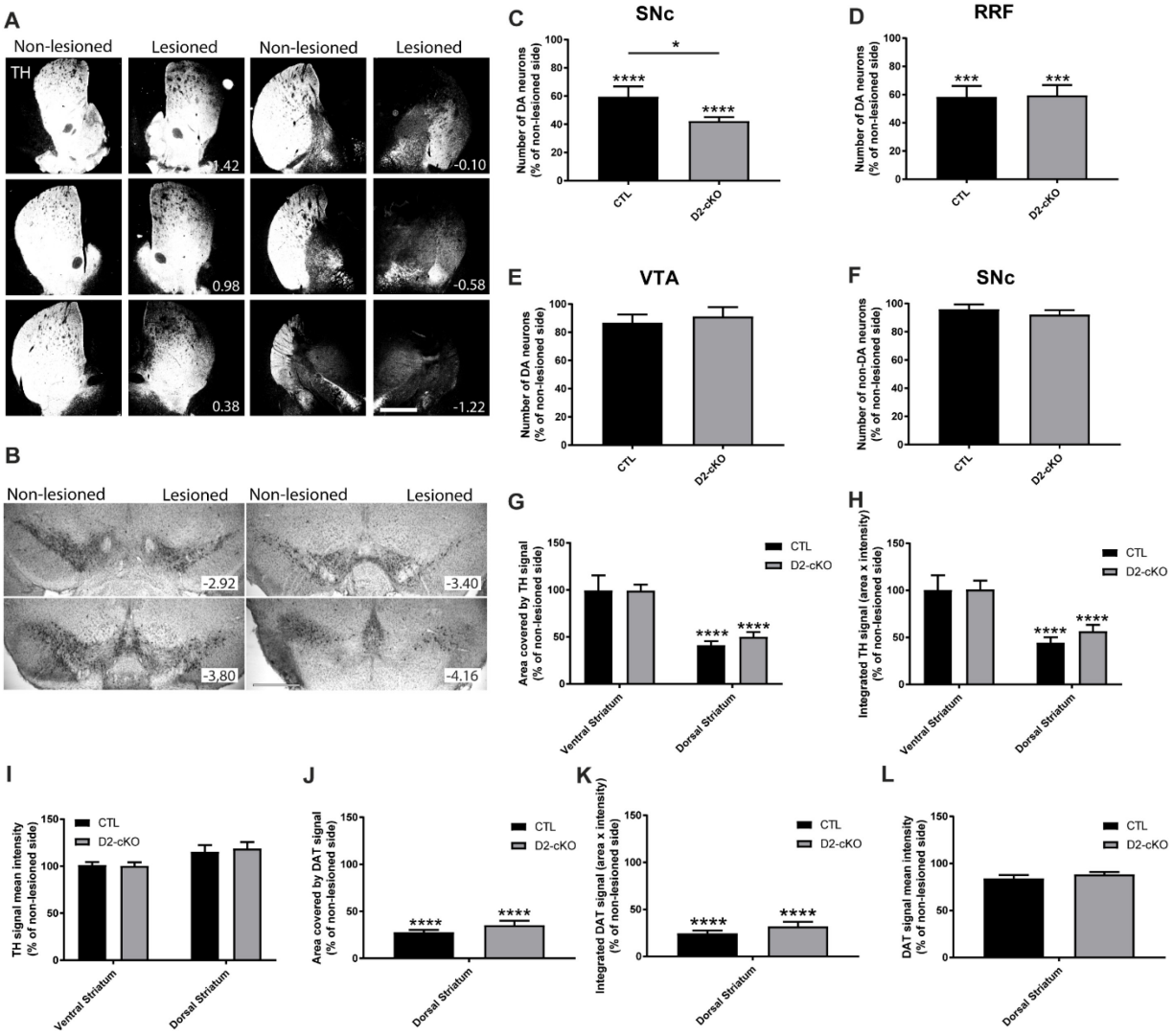

6-OHDA partial lesion in the dorsal striatum (A) was used to evaluate the impact of the increased axonal arborization size of D2-cKO SNc DA neurons on their vulnerability (B). Scale bar = 1 mm. Survival of TH+ SNc (C), RRF (D), VTA (E) and TH- SNc neurons (F) was measured using stereological counting. N=10-11 brain/group, mean ± SEM, *p>0.05, *** p>0.001, **** p>0.0001. TH (G) and DAT (J) signal area, total signal (H,K) and signal intensity (I,L) were measured in the dorsal striatum for both markers and in the ventral striatum only for TH. N=6-8 brain/group, mean ± SEM, **** p>0.0001.

Figure 7. Behavioral changes following 6-OHDA injection.

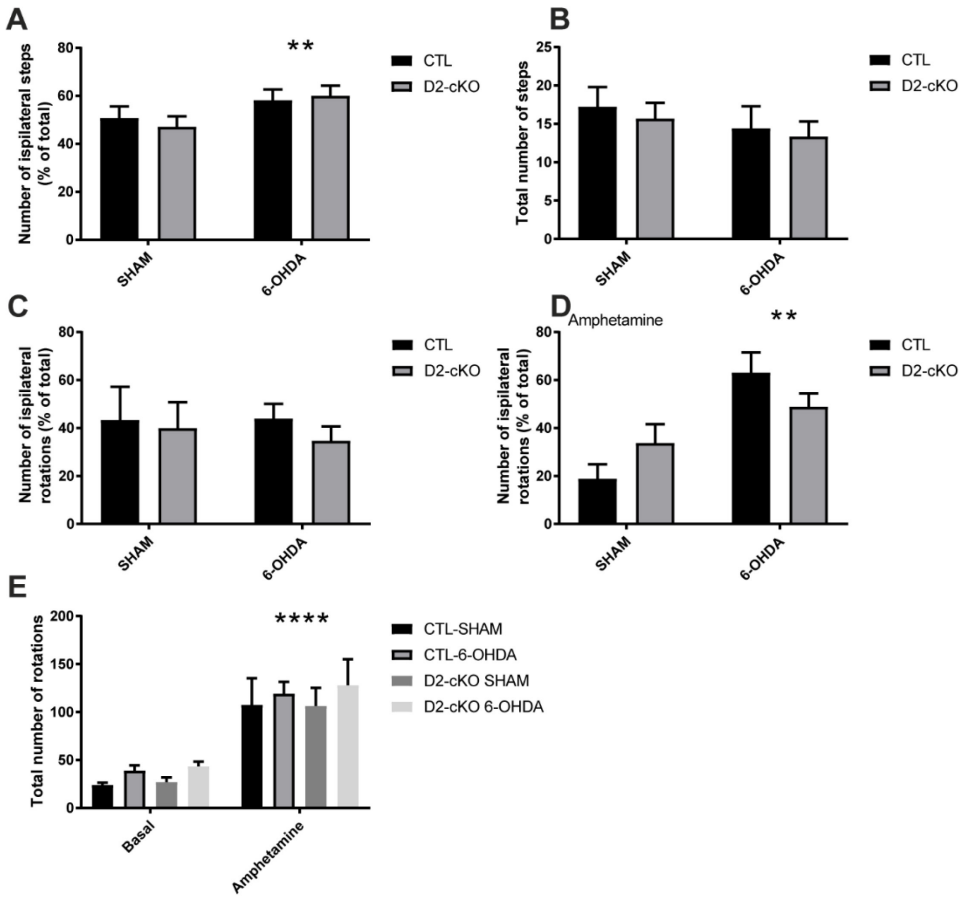

Paw preference (A) and total number of steps (B) were measured during a stepping test. Rotational behaviour was assessed at basal state (C) and after amphetamine administration (D). Total number of rotations were also measured (E). N=4-11 brain/group, mean ± SEM, ** p>0.01, **** p>0.0001.

6.9 Supplementary Figure

Figure S1. Behavioral changes following α-synuclein overexpression.

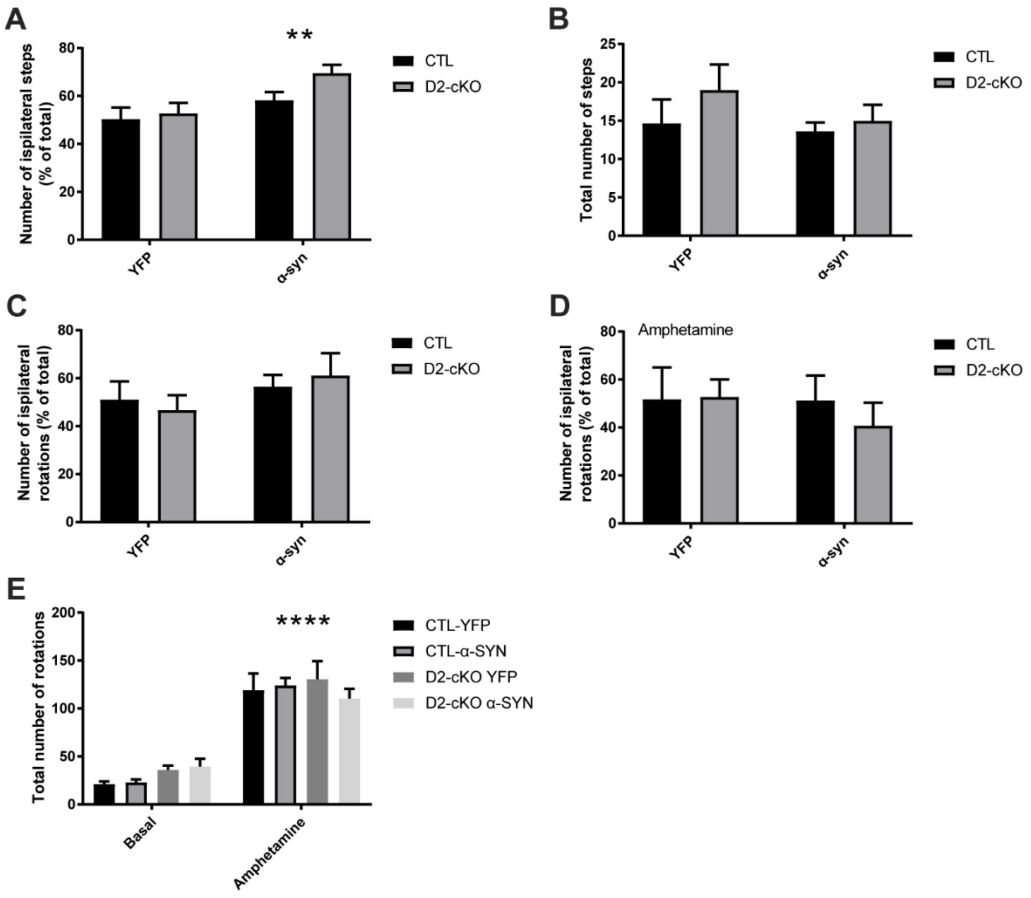

Paw preference (A) and total number of steps (B) were measured during a stepping test in 6-OHDA and α-synuclein overexpression models respectively. Rotational behaviour was assessed at basal state (C) and after amphetamine administration (D) in 6-OHDA and α-synuclein overexpression models respectively. Total number of rotations were also measured (E). N=4-11 brain/group, mean ± SEM, ** $p>0.01$, **** $p>0.0001$.

Chapitre 7 : Discussion

Les travaux inclus dans cette thèse avaient pour but de mieux comprendre les causes de la vulnérabilité sélective des neurones dopaminergiques de la SNc dans le contexte de la MP. Dans un premier temps, nous avons démontré en culture primaire chez la souris que ces neurones ont une arborisation axonale plus développée que d'autres populations dopaminergiques moins vulnérables telles que les neurones de la VTA et que cette arborisation s'accompagne de besoins énergétiques et d'un stress oxydatif plus important. De plus, en réduisant la taille de cette arborisation à l'aide de la sémaphorine 7A (Sema7A), un facteur de guidage axonal, nous avons réduit les besoins énergétiques et la vulnérabilité de ces neurones.

Dans un deuxième temps, nous avons évalué ces mêmes paramètres dans trois modèles génétiques des formes familiales de la MP, soit le KO pour Parkin, Pink1 et DJ-1 chez la souris. Nous avons découvert que les neurones dopaminergiques de la SNc KO pour Parkin ont une vulnérabilité augmentée à notre modèle de culture et qu'ils possèdent une efficacité mitochondriale grandement réduite. De plus, ces effets ont pu être renversés par leur croissance sur un tapis de glie WT ou par la surexpression de Parkin par vecteur viral.

Dans un troisième temps, nous avons démontré *in vivo* que les neurones dopaminergiques de la SNc ont un axone dont l'étendue est environ 3 fois plus importante que les neurones moins vulnérables de la VTA et que l'augmentation de la taille de cette arborisation axonale à l'aide du KO conditionnel du récepteur D2 les rend plus vulnérables au modèle de lésion à la 6-OHDA. Ensemble, ces travaux amènent pour la première fois des preuves directes que la taille de l'arborisation axonale est un facteur majeur dans la vulnérabilité des neurones dopaminergiques de la SNc dans le contexte de la MP.

7.1 Hypothèses de vulnérabilité sélective : emphase sur la taille de l'arborisation axonale

Au cours des dernières décennies, plusieurs caractéristiques propres aux neurones dopaminergiques ont été proposées comme potentiellement responsables de la vulnérabilité sélective des neurones dopaminergiques (voir premier article pour plus de détails [143]).

La présence de dopamine elle-même a été initialement suggérée comme un facteur de vulnérabilité à cause de son oxydation en quinones toxiques dans certaines conditions pathologiques [144]. Toutefois, plusieurs éléments semblent aller à l'encontre de cette hypothèse. Par exemple, les neurones de la VTA, voisins des neurones de la SNc, sont bien moins vulnérables dans la MP, bien qu'ils soient eux aussi dopaminergiques. À l'inverse, plusieurs populations neuronales non-dopaminergiques sont aussi affectées dans la MP [143]. De plus, l'augmentation dans le cerveau des niveaux de dopamine découlant de l'administration de L-DOPA lors du traitement de la MP n'accélère pas la mort neuronale [145, 146]. Bien que la toxicité reliée à la dopamine puisse contribuer à la vulnérabilité basale des neurones dopaminergiques, il est fort probable que son apport délétère soit relativement modeste.

Une seconde caractéristique proposée comme potentiellement responsable de la vulnérabilité sélective des neurones dopaminergiques est qu'ils possèdent un patron de décharge constant et autonome. Chez les neurones dopaminergiques de la SNc plus particulièrement, ces décharges s'accompagnent de lentes oscillations des concentrations intracellulaires de calcium, induites par l'ouverture de canaux calciques voltage dépendants (Cav1.1 et 1.3) [147]. Ces niveaux calciques, bien qu'importants pour maintenir le taux de décharge et la production d'énergie des neurones, nécessitent l'action de pompes calciques énergivores et induisent aussi une augmentation chronique du stress oxydatif par des mécanismes encore mal compris [148–150]. Cependant, en plus d'être présents chez les neurones dopaminergiques de la SNc, ces canaux sont aussi retrouvés chez plusieurs autres populations neuronales dont certaines sont épargnées dans la MP, telles que les neurones striataux et hippocampiques [151, 152]. Leur

expression est même maintenue chez les neurones dopaminergiques de la SNc qui survivent à la maladie [152]. D'autres mécanismes sont donc certainement en cause.

Une troisième hypothèse, privilégiée dans les travaux de cette thèse, est que les neurones dopaminergiques de la SNc sont particulièrement vulnérables à cause de la taille importante de leur arborisation axonale, induisant d'immenses besoins énergétiques et de hauts niveaux chroniques de stress oxydatif [153]. L'étendue de cet axone a précédemment été mesurée chez le rat (Figure 6) [154, 155, 62], mais seule une estimation indirecte était disponible avant les travaux de cette thèse en ce qui concerne la comparaison avec les neurones moins vulnérables de la VTA [19]. Pour faire cette estimation, la densité des terminaisons dopaminergiques striatales a été mise en relation avec le nombre de neurones dopaminergiques de chacune des deux régions. Ce calcul a permis d'estimer que les neurones de la SNc formeraient jusqu'à 245 103 terminaisons dans le striatum dorsal du rat, en comparaison à un maximum de 29 644 terminaisons dans le striatum ventral pour les neurones de la VTA [19]. Les neurones dopaminergiques de la SNc seraient donc jusqu'à 8 fois plus arborisés que ceux de la VTA, appuyant d'autant plus la relation entre la taille de l'arborisation axonale et la vulnérabilité neuronale dans la MP.

Dans le quatrième article de cette thèse, nous avons obtenu pour la première fois une comparaison directe de la taille de l'arborisation axonale striatale de ces deux populations neuronales chez la souris. Nous avons démontré que les neurones dopaminergiques de la SNc ont une arborisation environ 3 fois plus importante que ceux de la VTA. Cette différence est toutefois moins grande qu'estimée précédemment chez le rat [19], potentiellement à cause de différences entre les deux espèces de rongeurs. Cependant, nos données montrent aussi qu'une grande proportion des projections de la VTA s'étendent dans le striatum dorsal, projections ignorées dans la précédente estimation. Puisque le striatum dorsal est une structure au volume bien plus important que le striatum ventral, ces projections sont bien plus diffuses et donc donnent visuellement l'impression que les neurones de la VTA projettent presque exclusivement dans le striatum ventral. Par contre, lorsqu'on normalise la densité des projections par la taille de la structure, une portion non négligeable des projections striatales de la VTA sont en fait dans

le striatum dorsal, en accord avec de précédents travaux de traçages unitaires de ces neurones [156].

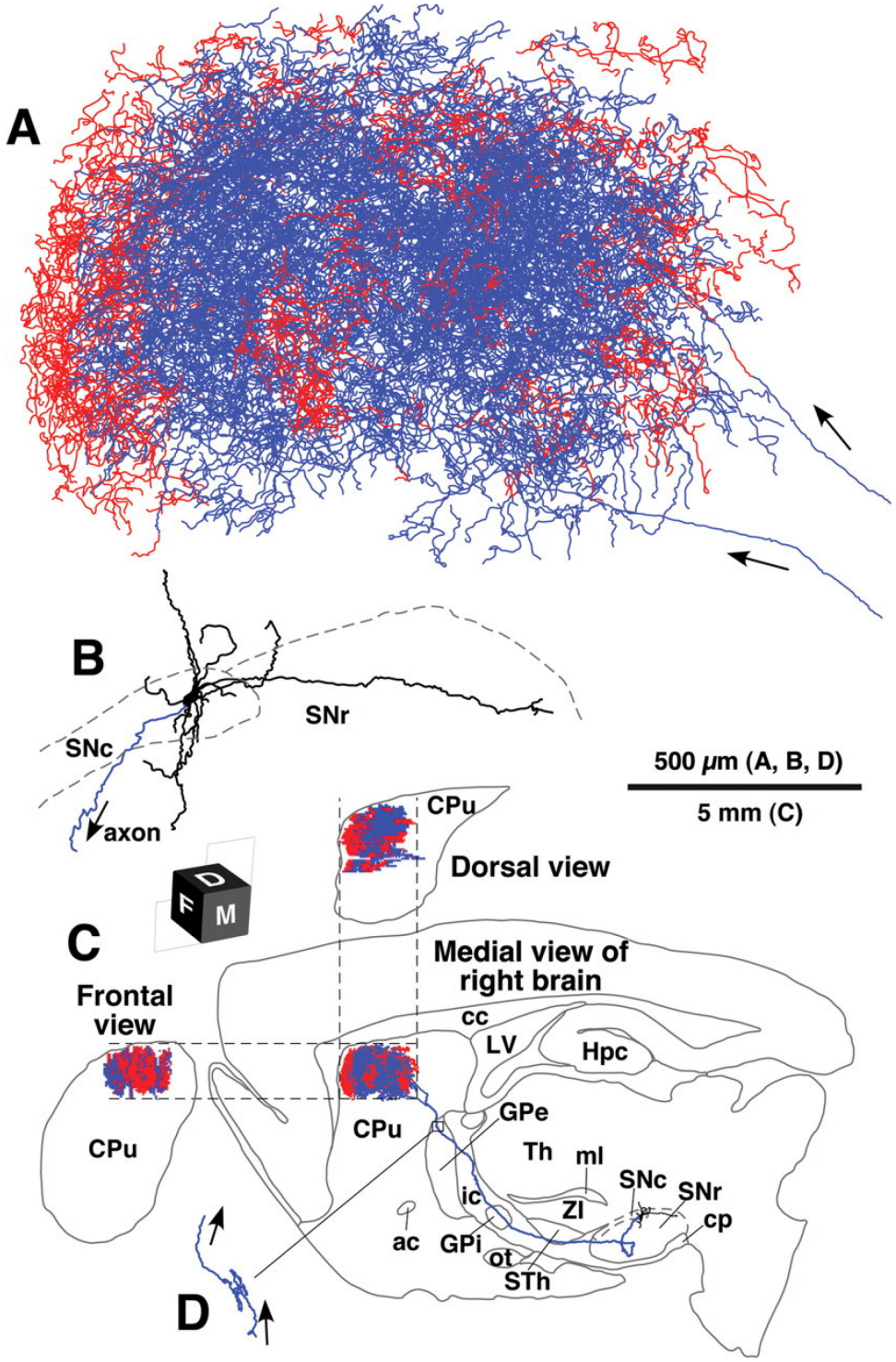

Figure 6. Arborisation axonale d'un neurone dopaminergique individuel de la SNc chez le rat [62]**.** Reproduction avec permission.

Un autre élément appuyant d'autant plus l'importance de la taille de l'arborisation axonale pour la vulnérabilité sélective des populations neuronales dans la MP est que la plupart des populations possiblement affectées dans la maladie sont de petits groupes de neurones qui projettent dans de vastes territoires cérébraux; tels que les neurones dopaminergiques de la SNc, les neurones cholinergiques du noyau basal de Meynert, du noyau pédonculopontin et du noyau dorsal du nerf vague et les neurones noradrénergiques du locus coeruleus. Toutefois, le lien direct entre la taille cette arborisation et les besoins énergétiques neuronaux était manquant avant les travaux de cette thèse, bien que cette relation ait été modélisée par le passé [157]. De plus, cette thèse démontre pour la première fois l'impact de la modulation de l'étendue de cet axone sur la vulnérabilité des neurones dopaminergiques de la SNc.

7.2 La taille de l'arborisation axonale *in vitro*

Dans le deuxième article de cette thèse [158], nous avons exploré l'hypothèse que la vulnérabilité neuronale serait dépendante de la taille de l'arborisation axonale. Pour ce faire, nous avons comparé, en culture primaire de neurones de souris, l'axone des neurones dopaminergiques de la SNc, de la VTA et du bulbe olfactif. Brièvement, nous avons démontré que les neurones de la SNc ont une arborisation axonale de taille plus importante, ont des besoins énergétiques plus grands et ont une capacité relative de production d'énergie supplémentaire moins importante que les neurones moins vulnérables de la VTA ou du bulbe olfactif. Du côté de la taille de l'arborisation axonale, il semble donc que ces neurones aient une capacité intrinsèque de croissance axonale plus importante, puisqu'ils conservent cette caractéristique lorsque mis en culture. De plus, l'axone des neurones de la SNc présente une densité mitochondriale et un stress oxydatif basal plus important. Ces neurones sont donc à la limite de leurs capacités bioénergétiques et doivent évoluer dans des conditions leur laissant peu de marge de manœuvre. Subséquemment, nos résultats démontrent qu'ils sont plus vulnérables à des toxines affectant la production d'énergie mitochondriale comme le MPP+, la roténone et le peroxyde d'hydrogène.

Par la suite, nous avons utilisé un facteur de guidage axonal, la Sema7A, pour réduire la taille de cette arborisation, ayant comme conséquence de réduire les besoins énergétiques, le stress oxydatif et la vulnérabilité qui en découlent. De manière intéressante, les effets de la Sema7A étaient spécifiques aux neurones dopaminergiques de la SNc et n'ont eu aucun impact observable sur ceux de la VTA. Plusieurs raisons pourraient potentiellement expliquer cette différence d'effets entre les neurones de la VTA et de la SNc, mais la plus logique est la possibilité que l'expression des récepteurs pour la Sema7A soit différente entre les deux populations neuronales. Nous avons donc effectué des expériences de RT-qPCR pour ceux-ci à l'aide de suspensions de cellules provenant de la SNc et de la VTA de souris néonatales (Annexe I H). Il faut savoir que la Sema7A est une molécule sécrétée, exprimée de façon plus importante dans le striatum dorsal [159] et qui peut se lier à deux récepteurs, soit le récepteur plexine C1 et le récepteur β1-intégrine [160]. Des travaux dans des lignées cellulaires ont précédemment montré que la modulation de la croissance cellulaire induite par la Sema7A passait par le récepteur β1-intégrine, mais que l'activation concomitante du récepteur plexine C1 avait pour effet de court-circuiter la signalisation de ce récepteur [161–163]. La balance des niveaux d'expression de ces deux récepteurs serait donc cruciale à la présence ou l'absence d'effet de la Sema7A. Chez les neurones utilisés pour produire nos cultures, bien que l'expression du récepteur β1-intégrine soit la même entre les neurones de la SNc et de la VTA, l'expression du récepteur plexine C1 est bien plus faible chez les neurones de la SNc (Annexe I H). Ces résultats pourraient donc expliquer la spécificité de l'effet de la Sema7A pour les neurones de la SNc. Nos résultats semblent toutefois en contradiction avec d'autres travaux qui montrent un effet inhibiteur de la croissance axonale par application aiguë de Sema7A, spécifique aux neurones dopaminergiques de la VTA en culture primaire embryonnaire, sans effets sur les neurones de la SNc [159]. Malheureusement, ces travaux n'ont pas évalué l'implication du récepteur β1-intégrine sur leurs effets. D'autres expériences seront nécessaires pour réconcilier ces résultats, mais des changements dans les niveaux d'expression des récepteurs de la Sema7A ou dans la régulation des voies de signalisation de ceux-ci entre E14.5 et P0 pourraient être en cause.

Dans ce même article [158], nous avons aussi brièvement exploré l'influence des canaux calciques de type L voltage-dépendant (CAV1.3), une autre caractéristique proposée comme responsable de la vulnérabilité sélective des neurones dopaminergiques de la SNc (voir la

section 2.5.3 pour plus de détails). Suite à l'inhibition de ces canaux dans nos cultures, nous avons mesuré une diminution des besoins énergétiques et de la vulnérabilité au MPP+, mais pas à la roténone. Ces effets étaient toutefois moins importants que lors de l'application de Sema7A, mais pourraient être expliqués par le fait que les courants calciques induits par les canaux CAV1.3 sont moins importants chez les jeunes neurones, en comparaison aux neurones adultes [164]. Des travaux supplémentaires seront nécessaires pour mieux comprendre comment cette neuroprotection est induite. Néanmoins, ces résultats confirment que plus d'une caractéristique puisse influencer la vulnérabilité des neurones dopaminergiques de la SNc dans la MP et donc que les hypothèses de vulnérabilité sélective ne sont pas mutuellement exclusives.

7.3 Knock-out de Parkin, Pink1 et DJ-1 *in vitro*

En parallèle à nos travaux sur la taille de l'arborisation axonale comme critère de vulnérabilité sélective, nous nous sommes intéressés à ces mêmes caractéristiques chez trois modèles génétiques de la MP; soit la délétion constitutive des gènes Parkin, Pink1 ou DJ-1 chez la souris. Des mutations causant la perte de fonction de ces gènes sont en effet retrouvées dans certaines formes familiales de la MP [165–168]. Bien qu'aucun de ces modèles ne réplique fidèlement la maladie chez la souris [122–126], nous pensions pouvoir détecter de plus subtils changements dans la croissance et la bioénergétique des neurones dopaminergiques de la SNc à l'aide de notre modèle de culture.

Nos travaux sur ces modèles, présentés dans le troisième article de cette thèse [169], démontrent que le KO de Parkin, mais pas de Pink1 ou de DJ-1, rend les neurones dopaminergiques de la SNc plus vulnérables aux conditions de culture et que cet effet peut être renversé par leur croissance en présence de cellules gliales provenant de souris Parkin WT ou par la surexpression de Parkin par vecteur viral chez les cellules gliales et les neurones. De plus en plus de travaux semblent démontrer une influence majeure des cellules gliales et microgliales dans la MP [170]. En accord avec nos données, il a été démontré que la perte de fonction de

Parkin dans les cellules gliales mène à une diminution de leur prolifération et à une réduction de leur sécrétion de l'antioxydant glutathion [171, 172], important pour la défense antioxydante neuronale, en plus de son implication dans la réponse inflammatoire [173]. De nombreuses données appuient par ailleur l'hypothèse d'un lien entre l'inflammation, l'activation de cellules microgliales, la sécrétion de cytokines et la progression de la maladie [174–176].

Du côté neuronal, les neurones survivant dans la culture Parkin KO présentent de claires altérations dans leurs productions d'énergie, ayant une consommation d'oxygène mitochondriale plus élevée, malgré une production d'ATP réduite et un compartiment axonal de taille plus modeste. Basé sur ces résultats, il serait tentant de conclure que seuls les neurones de la SNc établissant normalement de plus petits compartiments axonaux ont pu survivre en l'absence de Parkin. Il est toutefois aussi possible que le KO de Parkin réduise globalement la croissance axonale et qu'un sous-groupe de neurones de la SNc soit particulièrement vulnérable à cet effet. De leur côté, les neurones dopaminergiques de la VTA ne semblent pas être affectés de la même façon, montrant une consommation d'oxygène encore plus élevée, mais sans changement dans leur production d'ATP ou dans leur survie. Contrairement aux neurones de la SNc, ils semblent toutefois avoir la capacité d'augmenter leur activité glycolytique pour compenser la perte de production d'énergie mitochondriale induite par le KO de Parkin. Aucun de ces effets n'a été observé dans les cultures KO pour Pink1 ou DJ-1. Il pourrait sembler étrange que les cultures KO pour Pink1 et Parkin n'aient pas montré les mêmes résultats, sachant que la fonction de ces deux protéines est grandement interreliée dans les processus de mitophagie. Par contre, de récents travaux ont démontré que la mitophagie dépendante de Parkin s'effectuait sans problème en l'absence de Pink1 dans les tissus à forte demande énergétique comme le cerveau [177].

Nos résultats mettent aussi en doute la nécessité même de Parkin pour les processus mitophagiques. En théorie, Parkin est nécessaire au remplacement des mitochondries endommagées par mitophagie [87]. Toutefois, l'absence de ce processus ne semble pas induire d'accumulation de mitochondrie dans nos cultures, suggérant soit une diminution de la production de nouvelles mitochondries ou un remplacement des mitochondries endommagées par des mécanismes de mitophagie indépendants de Parkin. Récemment, plusieurs protéines ont

été suggérées comme capable d'induire la mitophagie en l'absence de Parkin, telles que ARIH1/HHARI [178], FKBP8 à l'aide de LC3a [179], Nix [180], MARCH5 [181] et Bcl2-L-13 [182], et donc leur action potentielle pourrait expliquer l'absence d'accumulation de mitochondries chez les neurones KO pour Parkin. Toutefois, l'expression et le rôle de ces protéines chez les neurones dopaminergiques restent à déterminer. Ultimement, l'étude des processus pouvant remplacer la fonction de Parkin chez la souris, mais aussi l'étude de leur rôle chez l'humain, pourrait nous permettre de mieux comprendre la différence d'effet de la perte de fonction de Parkin entre les modèles murins et les formes familiales de la MP.

L'absence de mort neuronale dans les modèles murins KO pour Parkin, Pink1 et DJ-1 est un réel mystère dans l'étude de la MP [122–126]. Chez l'humain au contraire, l'inactivation d'un de ces trois gènes est suffisante à induire l'apparition de formes précoces de la maladie [165–168]. Il existe bien sûr une multitude de possibilités pouvant expliquer cette différence d'effets, telles que la durée de vie et l'exposition à l'environnement qui diffèrent entre l'humain et la souris de laboratoire, sans exclure la possibilité que les fonctions exactes de ces gènes y soient régulées différemment. Toutefois, il est intéressant de se pencher sur la possibilité que l'étendue relative de l'axone des neurones dopaminergiques de la SNc chez ces deux mammifères puisse différer largement et influencer grandement l'importance de l'expression de ces gènes. En ce sens, des mesures indirectes du nombre de terminaisons striatales par neurones dopaminergiques de la SNc chez l'humain et les modèles murins ont précédemment permis d'estimer que ces neurones auraient jusqu'à 10 fois plus de terminaisons chez l'humain [19]. Serait-il possible que pour un neurone dopaminergique de souris ayant une arborisation axonale de taille relativement modeste, le rôle de Parkin, Pink1 ou DJ-1 soit plutôt accessoire? Il paraît logique de penser que chez les neurones aux axones moins arborisés, les besoins en mitophagie et en régulation du stress oxydatif pourraient être moins importants et donc possiblement plus facilement comblés par des mécanismes indépendants de l'expression ces gènes. Au contraire, lorsque la taille de l'arborisation axonale atteint un seuil critique comme chez l'humain, serait-il possible que la fonction de ces gènes devienne alors essentielle? De manière intéressante, l'inactivation de ces mêmes gènes, chez le rat cette fois, a montré l'induction de mort neuronale [183, 184]. Bien qu'aucune mesure directe de la taille de l'arborisation axonale des neurones dopaminergiques de la SNc de rat en comparaison à celle des neurones de souris n'existe, il est

possible d'estimer indirectement la taille de cette arborisation en nous basant sur la taille du striatum [185, 186], le nombre de neurones dopaminergiques [187, 188] et la densité des terminaisons dopaminergiques striatales [189, 190] de ces deux espèces. Basé sur ces données, l'axone dopaminergique de rat devrait alors avoir une arborisation de taille intermédiaire, soit au moins 2 fois plus importante que chez la souris, mais toujours 10 fois moins importante que chez l'humain. Il semble alors possible que l'étendue plus modeste de l'axone des neurones dopaminergiques de souris, en comparaison à celle du rat ou de l'humain, puisse expliquer l'absence d'effet de l'inactivation de Parkin, Pink1 ou DJ-1 sur la vulnérabilité de ces neurones chez la souris. D'autres travaux seront bien sûr nécessaires pour évaluer cette hypothèse, mais la possibilité que la taille de l'arborisation axonale soit un critère décisif dans la vulnérabilité de différentes espèces à la MP nous a encouragés à tenter de trouver une façon d'augmenter la taille de cette arborisation chez la souris, pour potentiellement y exacerber la vulnérabilité des neurones dopaminergiques et peut-être créer un meilleur modèle de la maladie.

7.4 Modulation de la taille de l'arborisation axonale *in vivo*

7.4.1 Knock-out de la Sema7A

Nous avons initialement tenté d'augmenter la taille de l'arborisation axonale des neurones dopaminergiques de la SNc par l'utilisation du KO de la Sema7A. Puisque l'application de Sema7A nous avait permis de réduire la taille de cette arborisation *in vitro* dans le deuxième article de cette thèse [158], il était logique de penser que son KO pourrait induire au contraire une croissance augmentée. Malheureusement, nous n'avons détecté aucun changement dans la surface du signal TH (Annexe I A,B), son intensité moyenne (Annexe I C,D) ou son signal total (Annexe I E,F) dans le striatum dorsal (Annexe I A,C,E) ou ventral (Annexe I B,D,F) chez les souris Sema7A-KO. Il était toutefois encore possible que le signal présent provienne d'un moins grand nombre de neurones dopaminergiques ou que la balance de

fibres dopaminergiques provenant de la SNc et de la VTA soit différente chez les souris KO pour la Sema7A. Puisque des travaux précédents avaient montré l'absence de mort neuronale dopaminergique dans ce modèle [159], nous avons exploré la deuxième option en croisant ces souris avec le modèle Dat^{Cre} pour pouvoir spécifiquement marquer les projections provenant de chacune de ces régions, en utilisant la même méthode d'injection virale décrite dans le quatrième article de cette thèse. Malheureusement, nous n'avons détecté aucun changement dans l'étendue des axones provenant des neurones dopaminergiques de la SNc ou de la VTA avec cette méthode (Annexe I G).

Plusieurs raisons pourraient potentiellement expliquer cette différence d'effet entre nos cellules en culture et le modèle KO *in vivo*, mais la plus logique est la possibilité que l'expression des récepteurs pour la Sema7A soit différente entre P0 et P60; âge auquel nous avons collecté les neurones pour la culture et âge auquel nous avons effectué nos mesures *in vivo*. Les neurones réagissent peut-être différemment à ce facteur de guidage axonal à différents âges. Nous avons donc effectué des expériences de RT-qPCR pour les récepteurs de la Sema7A sur des suspensions de cellules provenant de la SNc et de la VTA de souris adultes (P60), pour ensuite comparer leurs niveaux d'expression avec nos mesures précédemment effectuées sur des animaux néonataux (P0) (Annexe I H,I). De façon similaire, l'expression du récepteur plexine C1 s'est avérée plus faible chez les neurones de la SNc chez la souris adulte, mais l'expression de récepteur β1-intégrine y était au contraire augmentée (Annexe I I). Ceux-ci auraient donc dû être plus sensibles à la Sema7A à l'âge adulte. Bien que ces niveaux d'expression soient en accord avec des expériences d'hybridation *in situ* publiées précédemment et que la Sema7A soit toujours exprimée dans le striatum adulte [191], d'autres travaux seront nécessaires à la compréhension du rôle de la Sema7A chez les neurones dopaminergiques. Par exemple, il est possible que les voies de signalisation de ces deux récepteurs soient régulées différemment chez la souris néonatale comparativement à la souris adulte. Nous avons toutefois abandonné le modèle Sema7A-KO puisqu'il ne parvient pas à augmenter la taille de l'arborisation axonale des neurones dopaminergiques de la SNc chez la souris adulte.

7.4.2 Knock-out conditionnel du récepteur D2 et son impact sur la vulnérabilité

Nous avons donc continué notre quête d'un modèle augmentant la taille de l'arborisation axonale des neurones dopaminergiques de la SNc *in vivo* en nous tournant vers le KO du récepteur D2. Des travaux précédents avaient montré que l'application d'antagonistes du récepteur D2 [192, 193], ainsi que le KO constitutif de ce récepteur [194], augmentaient la densité des fibres dopaminergiques dans le striatum dorsal. Bien que cette augmentation ne fût pas montrée comme spécifique aux neurones dopaminergiques de la SNc, ces données nous ont encouragés à utiliser ce modèle pour tenter de moduler la taille de l'arborisation de ces neurones. Nous avons privilégié l'approche conditionnelle pour nous assurer d'un minimum d'effets chez les neurones non-dopaminergiques exprimant ce récepteur. Chez nos souris D2-cKO, nous avons confirmé que l'arborisation axonale des neurones dopaminergiques de la SNc avait doublé de taille, sans changement pour les neurones de la VTA. Nous avons aussi confirmé que la capacité de relâche de dopamine n'était pas augmentée chez les souris KO et donc qu'une augmentation de la toxicité potentielle liée à la dopamine [144, 195] était peu probable.

Pour évaluer l'impact de l'augmentation de la taille de l'arborisation axonale des neurones dopaminergiques de la SNc sur leur vulnérabilité dans le modèle D2-cKO, nous avons utilisé deux modèles de la MP; soit une lésion partielle à la 6-OHDA et la surexpression d'α-synucléine par vecteur viral. Appuyant l'importance de la taille de l'arborisation axonale comme facteur de vulnérabilité, nous avons observé une augmentation de la mort neuronale des neurones dopaminergiques de la SNc suite à la lésion à la 6-OHDA chez nos souris D2-cKO. Des travaux supplémentaires seront nécessaires pour expliquer les mécanismes impliqués dans cette augmentation de la vulnérabilité des neurones D2-cKO, mais il est possible que l'augmentation théorique de leurs besoins bioénergétiques, liées à l'augmentation de la taille de leur arborisation axonale, en synergie avec l'augmentation du stress oxydatif [196–198], l'altération du transport axonal [199] et la déplétion d'ATP et d'antioxydants [200] observées dans les modèles 6-OHDA, aient potentialisé leur neurodégénérescence. Dans une perspective future, la mesure de ces différents paramètres suite à l'application de 6-OHDA, mais avant

l'apparition de mort neuronale, pourrait nous permettre de mieux comprendre l'importance relative de ceux-ci dans la vulnérabilité augmentée des neurones D2-cKO.

Bien que le modèle de surexpression d'α-synucléine ait induit de la mort neuronale, aucune mort supplémentaire n'a été observée chez les souris D2-cKO. Bien qu'en contradiction avec notre hypothèse, cette absence d'effet supplémentaire pourrait s'expliquer par le fait que ce modèle induit une neurodégénérescence de moindre importance et plus lente, due au temps nécessaire à l'oligomérisation de la protéine sous sa forme pathologique, et qu'il ne touche pas de façon uniforme tous les neurones de la SNc [201]. En effet, les neurones les plus éloignés du site d'injection sont souvent épargnés. De plus, les mécanismes impliqués dans la mort neuronale dans ce modèle, soit l'agrégation de protéines et les dysfonctions du protéasome/lysosome [202–204], sont bien différents de ceux du modèle 6-OHDA ou un stress oxydatif est directement induit par le blocage des complexes I et IV mitochondriaux [205, 206]. Pour ces raisons, il est aussi probable que le modèle de surexpression d'α-synucléine laisse bien plus de temps aux neurones pour s'adapter à ses effets toxiques. Par conséquent, il est possible que l'augmentation théorique des besoins énergétiques et du stress oxydatif, induite par l'élaboration d'une arborisation axonale de taille plus importante chez les neurones D2-cKO, se synergise plus facilement avec les modèles qui provoquent un stress oxydatif direct et rapide, plutôt que des stress protéiques plus lents.

De manière intéressante, des symptômes parkinsoniens sans neurodégénérescence ont été rapportés chez le KO constitutif du récepteur D2, mais seulement chez des souris âgées de près de 2 ans [207]. Bien que l'impact initial de ce KO sur la taille de l'arborisation axonale des neurones dopaminergiques de la SNc n'ait pas été mesuré, l'augmentation de la densité de fibres striatale DAT positive dans ce modèle, observée chez des souris plus jeunes [194], suggère que ces symptômes soient dus à une augmentation de la vulnérabilité des neurones dopaminergiques à arborisation axonale augmentée. Des expériences futures de croisement du modèle D2-cKO ou KO constitutif avec les modèles génétiques de la MP utilisés dans le troisième article de cette thèse seraient grandement utiles à l'avancement de l'hypothèse de vulnérabilité sélective liée à la taille de l'arborisation axonale des neurones dopaminergiques. Il est possible que chez ces souris, l'augmentation de la taille de l'arborisation axonale par le KO du récepteur D2, couplée

aux délétions liées à certaines formes familiales de la MP, soit suffisante à induire l'apparition précoce de la maladie. Tel que suggéré précédemment dans la section 7.3, il est possible que l'absence de mort neuronale dans les modèles du KO de Parkin, Pink1 et DJ-1 chez la souris soit tout simplement due à l'importance réduite des mécanismes reliés à ces gènes dans les neurones de souris qui ont un axone modestement arborisé comparativement à ceux des neurones de du rat ou de l'humain.

7.4.3 Lésion néonatale à la 6-OHDA et son impact sur la vulnérabilité

Basée sur nos travaux en culture et en parallèle à nos projets dans le laboratoire, une étudiante à la maîtrise, Pamela Cassidy, a aussi tenté d'augmenter la taille de l'arborisation axonale des neurones dopaminergiques de la SNc à l'aide d'une lésion néonatale à la 6-OHDA, pour ensuite évaluer leur vulnérabilité chez l'adulte à l'aide de surexpression d'α-synucléine. En effet, il a été montré précédemment, dans des modèles de lésions, que les neurones dopaminergiques ont la capacité de compenser la perte de terminaisons striatales par un phénomène de bourgeonnement compensatoire [208, 209]. Ces mécanismes semblent aussi plus actifs chez les souris plus jeunes [208]. Pamela Cassidy a donc induit ses lésions chez les souris néonatales et a observé une taille d'arborisation axonale deux fois plus importante des neurones dopaminergiques survivants dans la SNc de ces mêmes souris à l'âge adulte (Annexe I A). Lorsqu'elle a par la suite évalué la vulnérabilité de ces mêmes neurones à l'aide du modèle de surexpression d'α-synucléine chez l'adulte, elle a observé une vulnérabilité plus de deux fois plus importante chez ceux-ci, en comparaison à des neurones dont l'arborisation n'avait pas changé (sans lésion néonatale à la 6-OHDA) (Annexe I B,C).

Ces résultats renforcent d'autant plus notre hypothèse postulant que la taille de l'arborisation axonale est un facteur majeur dans la vulnérabilité des neurones dopaminergiques de la SNc dans le contexte de la MP. Pour plus de détails, j'invite le lecteur à se référer au mémoire de maîtrise de Pamela Cassidy intitulé : « Augmenter la taille de l'arborisation axonale des neurones dopaminergiques afin de produire un meilleur modèle animal de la Maladie de

Parkinson », qui sera disponible en 2019 sur le site web de l'Université de Montréal, dans l'outil de dépôt institutionnel « Papyrus ».

7.5 Vers un consensus des hypothèses de vulnérabilité sélective

Bien que nos résultats appuient l'hypothèse selon laquelle la taille de l'arborisation axonale serait un facteur déterminant dans la vulnérabilité sélective des neurones dopaminergiques de la SNc, il serait réducteur de penser que seule cette caractéristique soit impliquée dans la MP. L'article I de cette thèse propose un tour d'horizon des différentes hypothèses de vulnérabilité et pave la voie vers un consensus entre celles-ci [143]. Pour rappel, le patron de décharge autonome et constant de ces neurones, tout comme leur expression de canaux calciques CAV1.3, leur contenu élevé en fer, leur arborisation axonale de taille particulièrement importante et le potentiel toxique de la dopamine sont toutes des caractéristiques qui induisent de grandes demandes bioénergétiques/mitochondriales avec de hauts niveaux de stress oxydatif. Nous proposons alors que tout stress supplémentaire, comme les diverses dysfonctions cellulaires causées par les mutations impliquées dans les formes familiales de la MP, l'exposition à des toxines environnementales et même le vieillissement, pourraient sélectivement mener ces neurones à une situation où leurs systèmes de défense antioxydante ne sont plus suffisants pour contrer ce stress. Des travaux précédents ont en effet démontré que les niveaux d'antioxydants tels que le glutathion sont particulièrement bas dans les cerveaux de patients parkinsoniens [210–212].

À terme, il est aussi possible que ce stress oxydatif affecte la capacité des neurones à produire de l'énergie à un point tel que certaines fonctions cellulaires de base, telles que la dégradation de protéines endommagées, soient compromises [147]. Puisque près de la moitié de l'énergie produite par les mitochondries est utilisée par des mécanismes majoritairement axonaux, tels que la relâche de neurotransmetteurs et la propagation de potentiels d'action [158], ce manque d'énergie pourrait préférentiellement affecter les terminaisons axonales et

déclencher une cascade de mort rétrograde, phénomène effectivement observé dans la MP et à la base de l'hypothèse appelée "dying-back" [213, 112, 214]. Même si cette dégénérescence axonale pourrait avoir comme conséquence initiale de réduire les besoins énergétiques des neurones affectés, elle mènerait du même coup à une augmentation du nombre de protéines axonales à dégrader. Les mécanismes de dégradation étant eux aussi énergivores et donc potentiellement au ralenti dans un contexte énergétique limité [215, 216], les protéines en attente de dégradation pourraient alors avoir tendance à s'agréger et à former des inclusions intracellulaires toxiques. Dans la MP, ces inclusions sont observables et sont majoritairement formées d'α-synucléine mal-repliées, une protéine normalement très concentrée dans les terminaisons axonales.

De manière intéressante, des déficits lysosomiaux causés par des mutations dans la glucocérébrosidase [217–221, 91, 92], une enzyme importante pour la dégradation de protéines, tout comme des mutations dans des protéines importantes pour la dégradation et la présentation antigénique mitochondriale (PARK2 ou Parkin, Pink1) [87, 120], la réponse au stress oxydatif (PARK7 ou DJ-1) [89, 90], le trafic de vésicules (LRRK2) [88, 222] ou dans l'α-synucléine elle-même, augmentant son potentiel toxique, sont présentes dans près de 15% des cas de MP. En théorie, les effets néfastes de ces mutations pourraient avoir un impact plus important chez les cellules aux besoins énergétiques particulièrement élevés, telles que les neurones dopaminergiques de la SNc.

7.6 Critique des données sur la mort neuronale dans la MP chez l'humain

Bien que nos travaux se soient concentrés principalement sur les neurones dopaminergiques de la SNc, il est probable que les autres populations neuronales atteintes dans la MP aient elles aussi un assemblage de caractéristiques, dont une arborisation axonale de taille massive, qui les pousse à la limite de leurs capacités énergétiques. Toutefois, les données sur

l'identification de ces populations, mais surtout sur leur niveau d'atteinte les unes par rapport aux autres à différents stades de la maladie restent à ce jour limitées. Un résumé critique de ces données est présenté dans le premier article de cette thèse [143].

Brièvement, il semble clair qu'un certain niveau de neurodégénérescence soit présent dans quelques populations neuronales spécifiques, telles que les neurones dopaminergiques de la SNc et moindrement de la VTA, les neurones noradrénergiques du locus coeruleus et les neurones cholinergiques du noyau basal de Meinert, du noyau pédonculopontin et du noyau dorsal du nerf vague. Toutefois, le manque de données pour certaines régions, la disparité des techniques utilisées, le manque d'information sur les considérations anatomiques des structures ajacentes, telles que la SNc et la VTA, et les multiples sources potentielles de biais dues au manque d'uniformité dans les critères de sélection des cerveaux des différentes études, nous empêchent de tirer des conclusions claires en ce qui concerne le niveau relatif d'atteinte de chaque région. La poursuite du développement des hypothèses de vulnérabilité sélective souffre donc grandement de ces lacunes et une étude rigoureuse comparant le niveau de mort neuronale dans chacune de ces régions à différents stades de la maladie y serait grandement bénéfique.

Il faut tout de même souligner les efforts importants sur le sujet effectués au début des années 2000 par Heiko Braak et ses collègues. Dans leurs travaux réunissant plusieurs cerveaux parkinsoniens à différents temps post-diagnostiques, la présence de corps de Lewy, marqueurs caractéristiques de la pathologie, a été évaluée dans une multitude de régions cérébrales et a été corrélée aux différentes phases symptomatiques de la maladie [223, 100, 224]. Par contre, ces travaux n'ont en aucun cas évalué la présence ou l'absence de mort neuronale dans ces mêmes régions. Les corps de Lewy ont longtemps été considérés comme marqueurs de la pathologie et de la mort neuronale dans la MP, mais des données récentes tendent à mettre en doute cette relation [225]. En effet, ces corps de Lewy ne sont pas toujours présents dans les cerveaux parkinsoniens, y compris dans certaines formes génétiques précoces de la maladie [226–228] et ils sont parfois observés dans des cerveaux sains [229]. Serait-il alors possible que ces corps de Lewy fassent plutôt partie d'un processus sain de gestion des protéines agrégées difficiles à dégrader normalement? Processus qui serait exacerbé dans des conditions pathologiques comme la MP? D'ici à ce que ces questions trouvent réponse, il serait plus judicieux de s'appuyer sur

la mort neuronale pour élaborer et évaluer les hypothèses de vulnérabilité sélective des populations neuronales dans la MP.

Chapitre 8 : Perspectives

En plus de l'évaluation de la mort neuronale dans différentes régions à différents stades de la MP, plusieurs travaux seront nécessaires pour étendre notre compréhension de la vulnérabilité sélective des différentes populations neuronales et pour ultimement proposer de meilleurs traitements.

Du côté de la croissance axonale, il serait très utile de connaître les gènes exprimés par les neurones dopaminergiques de la SNc qui les poussent à former une arborisation axonale aussi élaborée et de déterminer si ce profil génétique est aussi présent chez les autres populations neuronales affectées dans la MP. Il serait aussi intéressant d'évaluer si ces mêmes gènes sont impliqués dans le bourgeonnement compensatoire observé dans les modèles de lésions [208, 209] et si cette compensation est bel et bien présente dans les phases présymptomatiques de la MP chez l'humain. Si tel est le cas, elle pourrait retarder initialement l'apparition des symptômes moteurs, tout en exacerbant le stress subit par les neurones survivants. À terme, en tentant de compenser la perte des terminaisons formées par les premiers neurones qui dégénèrent, les neurones survivants pourraient avoir à augmenter encore plus la taille de leur arborisation axonale et du même coup les besoins énergétiques nécessaires au maintien de cet axone. Cette pression augmentée pourrait alors accélérer la pathologie, jusqu'à ce que le nombre de terminaisons à remplacer soit trop grand pour le nombre de neurones restants et qu'apparaissent les premiers symptômes moteurs. Une meilleure connaissance des mécanismes impliqués dans ce bourgeonnement compensatoire pourrait alors être utile à l'élaboration de meilleurs traitements. Par exemple, serait-il possible de sauvegarder les neurones survivants tôt dans la maladie en inhibant ce bourgeonnement tout en administrant la L-DOPA pour pallier au manque de dopamine? Dans ce contexte, l'utilisation de la Sema7A pourrait s'avérer efficace, bien que nos résultats sur l'influence du KO de la Sema7A sur la croissance axonale chez la souris adulte se soient avérés négatifs. Par exemple, il est possible que l'inhibition de la voie de signalisation du récepteur β1-intégrine par celle du récepteur plexine C1 soit plus forte chez l'adulte. On pourrait alors espérer inhiber la croissance compensatoire observée dans les modèles de la MP

en administrant de la Sema7A, mais aussi en inhibant le récepteur plexine C1 pour potentialiser l'effet de l'activation de la voie β1-intégrine. Des expériences d'administration de Sema7A dans des modèles de lésions, avec ou sans antagonistes du récepteur plexine C1, seraient très utiles à l'évaluation de cette hypothèse.

Une autre approche pour tenter de réduire la croissance compensatoire des neurones dopaminergiques pourrait être l'administration d'agonistes du récepteur D2. En effet, puisque nos travaux ont montré une augmentation de la croissance axonale suite au KO de ce récepteur et que d'autres travaux ont montré que son activation inhibait cette croissance [230], cette approche pourrait s'avérer efficace pour réduire la croissance compensatoire des neurones survivant dans la MP. Serait-il possible que le récepteur D2 agisse comme senseur des niveaux de dopamine au niveau des terminaisons axonales, laissant la croissance axonale se produire en absence de dopamine, mais inhibant celle-ci lorsque les niveaux physiologiques sont atteints? De manière intéressante, l'administration d'agonistes de ce récepteur est déjà utilisée pour réduire les symptômes de la MP [231–233] et serait potentiellement associée à une diminution de la progression de la maladie [234, 235].

En parallèle à la réduction de la croissance compensatoire axonale, une approche complémentaire pourrait être de réduire l'impact de la taille de cette arborisation axonale au niveau bioénergétique en optimisant la fonction mitochondriale pour fournir plus d'énergie lorsque nécessaire, tout en réduisant les niveaux de stress oxydatif. En ce sens, nous avons récemment collaboré avec le laboratoire du Dre Joanne E. Nash de l'université de Toronto dans un article où nous avons conjointement démontré que la surexpression de sirtuine 3 (SIRT3) stabilisait la fonction mitochondriale des neurones dopaminergiques de la SNc et était neuroprotectrice dans un modèle de surexpression d'α-synucléine [236]. Les sirtuines sont des désacétylases et des ADP ribosylases qui régulent une multitude de processus physiologiques. De manière intéressante, dans la mitochondrie, il existe plus de 2200 sites d'acétylation [237] et cette acétylation est associée à une diminution de l'activité de la chaîne de transport d'électron et de la production d'ATP et à une augmentation du stress oxydatif [238, 239]. SIRT3, 4 et 5 y sont alors requis pour réguler ces processus par désacétylation [240]. En particulier, l'expression de SIRT3 a été montrée comme bénéfique pour l'efficacité bioénergétique mitochondriale et

pour la régulation du stress oxydatif chez des modèles non neuronaux [241, 238, 239]. De plus, sa délétion augmenterait la vulnérabilité des neurones dopaminergiques au MPP+ et au KO de DJ-1 [242, 243]. Nous étions donc intéressés au potentiel effet neuroprotecteur de sa surexpression chez les neurones dopaminergiques. Dans nos cultures de neurones de la SNc, cette surexpression a en effet démontré une réduction de la consommation mitochondriale d'oxygène nécessaire aux fonctions des neurones, suggérant une augmentation de l'efficacité mitochondriale qui pourrait expliquer l'effet neuroprotecteur observé *in vivo* lors de la surexpression d'α-synucléine. D'autres travaux seront toutefois nécessaires à l'élaboration de traitements pharmacologiques permettant d'optimiser la production d'énergie neuronale, que ce soit en rendant plus efficace la chaîne de transport des électrons et/ou en améliorant la défense antioxydante.

Ces approches pourraient permettre de protéger un nombre non-négligeable de neurones dopaminergiques chez les patients symptomatiques, puisqu'il est en effet estimé que 40 à 50% des neurones dopaminergiques sont encore présents lors du diagnostic initial [244]. Toutefois, puisque près de 20 ans peuvent s'écouler entre le début des processus pathologiques et l'apparition des premiers symptômes moteurs, il est fort probable que la plupart des traitements potentiels découlant de l'étude des mécanismes de croissance et d'optimisation métabolique décrits ci-haut n'atteignent pas leur potentiel thérapeutique maximal si utilisés durant les stades symptomatiques de la maladie. Idéalement, il faudrait utiliser ces approches le plus tôt possible dans la maladie, bien avant l'apparition des premiers symptômes moteurs. Le développement de biomarqueurs précoces sera alors fort utile pour maximiser l'effet des traitements visant la protection neuronale. Par exemple, des dysfonctions du microbiote intestinal avec accumulation d'α-synucléine sont souvent observées plusieurs années avant l'apparition des symptômes chez les patients parkinsoniens [245] tout comme des dysfonctions olfactives et des troubles du sommeil [94]. Ces indicateurs précoces de la maladie, couplés à de nouvelles approches d'imagerie [246] ou de profilage de métabolites (sanguins ou du liquide céphalorachidien) [247], pourraient éventuellement permettre une détection précoce de la maladie et son traitement avant que la neurodégénérescence ne soit trop avancée.

Chapitre 9 : Conclusions

En conclusion, cette thèse nous a permis de statuer que la taille de l'arborisation axonale des neurones dopaminergiques de la SNc est un facteur majeur déterminant leurs besoins bioénergétiques et leur vulnérabilité dans le contexte de la MP et que la modulation du niveau de développement de cette arborisation, *in vitro* comme *in vivo*, peut avoir un grand impact sur cette vulnérabilité. Nous apportons aussi de nouvelles pistes quant à la compréhension de certaines formes familiales de la maladie et mettons de l'avant l'hypothèse que la taille de l'arborisation axonale est potentiellement une caractéristique commune aux populations neuronales affectées dans la maladie, bien que l'état des connaissances sur ces neurones mérite d'être développé davantage. Nous suggérons que l'étude de la vulnérabilité sélective dans la MP à de fortes chances de mener à l'élaboration de traitements qui pour la première fois pourraient réduire la progression de la pathologie, pourvu qu'ils soient utilisés le plus tôt possible dans la maladie, idéalement avant même l'apparition des premiers symptômes moteurs.

En plus des éléments couverts dans cette thèse, l'implication de plusieurs autres caractéristiques particulières des neurones dopaminergiques dans la MP reste à explorer. Par exemple, certains de ces neurones sont connus pour avoir la capacité de relâcher à la fois de la dopamine, du glutamate et/ou du GABA [54, 248]. En ce sens, des travaux récents du laboratoire ont démontré que la capacité de libérer du glutamate était importante pour leur survie et donc pourrait être une cible thérapeutique intéressante dans le contexte de la MP [249]. Une autre caractéristique particulière de l'axone de ces neurones est que la majorité de leurs terminaisons axonales sont formées en l'absence compartiments post-synaptiques [250, 251]. Le manque de signaux post-synaptiques, ayant normalement des effets prosurvie [252], pourrait donc aussi jouer un rôle dans leur vulnérabilité. En définitive, malgré tout le travail des 100 dernières années passées à tenter de comprendre les multiples fonctions du système dopaminergique, plus particulièrement l'implication des neurones de la SNc dans les contextes pathologiques, il est clair que cette petite population neuronale aux axones ambitieux nous réserve encore plusieurs surprises.

Bibliographie

1. Holtz P (1939) Dopadecarboxylase. Naturwissenschaften 27:724–725

2. Blaschko H (1939) The specific action of L-dopa decarboxylase. J. Physiol. 96:

3. Nagatsu T, Levitt M, Udenfriend S (1964) Tyrosine hydroxylase. The initial step in norepinephrine biosynthesis. J Biol Chem 239:2910–2917

4. Hornykiewicz O (2002) Dopamine miracle: from brain homogenate to dopamine replacement. Mov Disord 17:501–508

5. Montagu KA (1957) Catechol compounds in rat tissues and in brains of different animals. Nature 180:244–245

6. Sano I, Gamo T, Kakimoto Y, Taniguchi K, Takesada M, Nishinuma K (1959) Distribution of catechol compounds in human brain. Biochim Biophys Acta 32:586–587

7. Bertler A, Rosengren E (1959) Occurrence and distribution of dopamine in brain and other tissues. Experientia 15:10–11

8. Carlsson A, Lindqvist M, Magnusson T, Waldeck B (1958) On the presence of 3-hydroxytyramine in brain. Science 127:471

9. Rosengren E (1960) On the Role of Monoamine Oxidase for the Inactivation of Dopamine in Brain. Acta Physiol Scand 49:370–375

10. Hare ML (1928) Tyramine oxidase: A new enzyme system in liver. Biochem J 22:968–979

11. Zeller E. Albert (2004) Über den enzymatischen Abbau von Histamin und Diaminen. 2. Mitteilung. Helv Chim Acta 21:880–890

12. Corrodi A, Jonsson G (1967) The formaldehyde fluorescence method for the histochemical demonstration of biogenic monoamines a review on the methodology. J Histochem Cytochem 15:65–78

13. Dahlstroem A, Fuxe K (1964) Evidence for the existence of monoamine-containing neurons in the central nervous system. I. Demonstration of monoamines in the cell bodies of brain stem neurons. Acta Physiol Scand Suppl SUPPL 232:1-55

14. Fuxe K (1965) Evidence for the existence of monoamine neurons in the central nervous system. Iv. Distribution of monoamine nerve terminals in the central nervous system. Acta Physiol Scand Suppl SUPPL 247:37+

15. Andén N.-E., Dahlström A., Fuxe K., Larsson K., Olson L., Ungerstedt U. (1966) Ascending monoamine neurons to the telencephalon and diencephalon. Acta Physiol Scand 67:313–326

16. Björklund A, Dunnett SB (2007) Dopamine neuron systems in the brain: an update. Trends Neurosci 30:194–202

17. Ryczko D, Cone JJ, Alpert MH, Goetz L, Auclair F, Dubé C, Parent M, Roitman MF, Alford S, Dubuc R (2016) A descending dopamine pathway conserved from basal vertebrates to mammals. Proc Natl Acad Sci U S A 113:E2440-2449

18. Poulin J-F, Caronia G, Hofer C, Cui Q, Helm B, Ramakrishnan C, Chan CS, Dombeck DA, Deisseroth K, Awatramani R (2018) Mapping projections of molecularly defined dopamine neuron subtypes using intersectional genetic approaches. Nat Neurosci 21:1260–1271

19. Bolam JP, Pissadaki EK (2012) Living on the edge with too many mouths to feed: why dopamine neurons die. Mov Disord 27:1478–1483

20. Brignani S, Pasterkamp RJ (2017) Neuronal subset-specific migration and axonal wiring mechanisms in the developing midbrain dopamine system. Front Neuroanat.

21. Yamauchi K, Mizushima S, Tamada A, Yamamoto N, Takashima S, Murakami F (2009) FGF8 signaling regulates growth of midbrain dopaminergic axons by inducing semaphorin 3F. J Neurosci 29:4044–4055

22. Fenstermaker AG, Prasad AA, Bechara A, Adolfs Y, Tissir F, Goffinet A, Zou Y, Pasterkamp RJ (2010) Wnt/planar cell polarity signaling controls the anterior-posterior organization of monoaminergic axons in the brainstem. J Neurosci 30:16053–16064

23. Li J, Duarte T, Kocabas A, Works M, McConnell SK, Hynes MA (2014) Evidence for topographic guidance of dopaminergic axons by differential Netrin-1 expression in the striatum. Mol Cell Neurosci 61:85–96

24. Van den Heuvel DMA, Pasterkamp RJ (2008) Getting connected in the dopamine system. Prog Neurobiol 85:75–93

25. Prestoz L, Jaber M, Gaillard A (2012) Dopaminergic axon guidance: which makes what? Front Cell Neurosci.

26. Xiao D, Miller GM, Jassen A, Westmoreland SV, Pauley D, Madras BK (2006) Ephrin/Eph receptor expression in brain of adult nonhuman primates: implications for neuroadaptation. Brain Res 1067:67–77

27. Mufson EJ, Kroin JS, Sobreviela T, Burke MA, Kordower JH, Penn RD, Miller JA (1994) Intrastriatal infusions of brain-derived neurotrophic factor: retrograde transport and

colocalization with dopamine containing substantia nigra neurons in rat. Exp Neurol 129:15–26

28. Reuss B, Unsicker K (2000) Survival and differentiation of dopaminergic mesencephalic neurons are promoted by dopamine-mediated induction of FGF-2 in striatal astroglial cells. Mol Cell Neurosci 16:781–792

29. Dluzen DE, Gao X, Story GM, Anderson LI, Kucera J, Walro JM (2001) Evaluation of nigrostriatal dopaminergic function in adult +/+ and +/- BDNF mutant mice. Exp Neurol 170:121–128

30. Barroso-Chinea P, Cruz-Muros I, Aymerich MS, Rodríguez-Díaz M, Afonso-Oramas D, Lanciego JL, González-Hernández T (2005) Striatal expression of GDNF and differential vulnerability of midbrain dopaminergic cells. Eur J Neurosci 21:1815–1827

31. Grothe C, Timmer M (2007) The physiological and pharmacological role of basic fibroblast growth factor in the dopaminergic nigrostriatal system. Brain Res Rev 54:80–91

32. Wang J, Carnicella S, Ahmadiantehrani S, He D-Y, Barak S, Kharazia V, Ben Hamida S, Zapata A, Shippenberg TS, Ron D (2010) Nucleus accumbens-derived GDNF is a retrograde enhancer of dopaminergic tone in the mesocorticolimbic system. J Neurosci 30:14502–14512

33. Kebabian JW, Petzold GL, Greengard P (1972) Dopamine-sensitive adenylate cyclase in caudate nucleus of rat brain, and its similarity to the “dopamine receptor.” Proc Natl Acad Sci U S A 69:2145–2149

34. Seeman P, Lee T, Chau-Wong M, Wong K (1976) Antipsychotic drug doses and neuroleptic/dopamine receptors. Nature 261:717–719

35. Kebabian JW, Calne DB (1979) Multiple receptors for dopamine. Nature 277:93–96

36. Beaulieu J-M, Gainetdinov RR (2011) The physiology, signaling, and pharmacology of dopamine receptors. Pharmacol Rev 63:182–217

37. Ford CP (2014) The role of D2-autoreceptors in regulating dopamine neuron activity and transmission. Neuroscience 282:13–22

38. Barton AC, Black LE, Sibley DR (1991) Agonist-induced desensitization of D2 dopamine receptors in human Y-79 retinoblastoma cells. Mol Pharmacol 39:650–658

39. Vickery RG, von Zastrow M (1999) Distinct dynamin-dependent and -independent mechanisms target structurally homologous dopamine receptors to different endocytic membranes. J Cell Biol 144:31–43

40. Ito K, Haga T, Lameh J, Sadée W (1999) Sequestration of dopamine D2 receptors depends on coexpression of G-protein-coupled receptor kinases 2 or 5. Eur J Biochem 260:112–119

41. Hasbi A, O'Dowd BF, George SR (2011) Dopamine D1-D2 receptor heteromer signaling pathway in the brain: emerging physiological relevance. Mol Brain 4:26

42. Albin RL, Young AB, Penney JB (1989) The functional anatomy of basal ganglia disorders. Trends Neurosci 12:366–375

43. Bolam JP, Hanley JJ, Booth PA, Bevan MD (2000) Synaptic organisation of the basal ganglia. J Anat 196 (Pt 4):527–42

44. Keeler JF, Pretsell DO, Robbins TW (2014) Functional implications of dopamine D1 vs. D2 receptors: A "prepare and select" model of the striatal direct vs. indirect pathways. Neuroscience 282:156–175

45. Macpherson T, Morita M, Hikida T (2014) Striatal direct and indirect pathways control decision-making behavior. Front Psychol 5:1301

46. Calabresi P, Picconi B, Tozzi A, Ghiglieri V, Filippo MD (2014) Direct and indirect pathways of basal ganglia: a critical reappraisal. Nat Neurosci 17:1022–1030

47. Usdin TB, Mezey E, Chen C, Brownstein MJ, Hoffman BJ (1991) Cloning of the cocaine-sensitive bovine dopamine transporter. Proc Natl Acad Sci U S A 88:11168–11171

48. Shimada S, Kitayama S, Lin CL, Patel A, Nanthakumar E, Gregor P, Kuhar M, Uhl G (1991) Cloning and expression of a cocaine-sensitive dopamine transporter complementary DNA. Science 254:576–578

49. Kilty JE, Lorang D, Amara SG (1991) Cloning and expression of a cocaine-sensitive rat dopamine transporter. Science 254:578–579

50. Erickson JD, Eiden LE, Hoffman BJ (1992) Expression cloning of a reserpine-sensitive vesicular monoamine transporter. Proc Natl Acad Sci U S A 89:10993–10997

51. Giros B, el Mestikawy S, Godinot N, Zheng K, Han H, Yang-Feng T, Caron MG (1992) Cloning, pharmacological characterization, and chromosome assignment of the human dopamine transporter. Mol Pharmacol 42:383–390

52. Liu Y, Peter D, Roghani A, Schuldiner S, Privé GG, Eisenberg D, Brecha N, Edwards RH (1992) A cDNA that suppresses MPP+ toxicity encodes a vesicular amine transporter. Cell 70:539–551

53. Ciccarone D (2011) Stimulant abuse: pharmacology, cocaine, methamphetamine, treatment, attempts at pharmacotherapy. Prim Care 38:41–58

54. El Mestikawy S, Wallen-Mackenzie A, Fortin GM, Descarries L, Trudeau LE (2011) From glutamate co-release to vesicular synergy: vesicular glutamate transporters. Nat Rev Neurosci 12:204–16

55. Takada M, Kang Y, Imanishi M (2001) Immunohistochemical localization of voltage-gated calcium channels in substantia nigra dopamine neurons. Eur J Neurosci 13:757–762

56. Bell DC, Butcher AJ, Berrow NS, Page KM, Brust PF, Nesterova A, Stauderman KA, Seabrook GR, Nürnberg B, Dolphin AC (2001) Biophysical properties, pharmacology, and modulation of human, neuronal L-type (alpha(1D), Ca(V)1.3) voltage-dependent calcium currents. J Neurophysiol 85:816–827

57. Lavoie B, Parent A (1991) Dopaminergic neurons expressing calbindin in normal and parkinsonian monkeys. Neuroreport 2:601–604

58. Isaacs KR, Jacobowitz DM (1994) Mapping of the colocalization of calretinin and tyrosine hydroxylase in the rat substantia nigra and ventral tegmental area. Exp Brain Res 99:34–42

59. Blanchard V, Raisman-Vozari R, Vyas S, Michel PP, Javoy-Agid F, Uhl G, Agid Y (1994) Differential expression of tyrosine hydroxylase and membrane dopamine transporter genes in subpopulations of dopaminergic neurons of the rat mesencephalon. Brain Res Mol Brain Res 22:29–38

60. Hurd YL, Pristupa ZB, Herman MM, Niznik HB, Kleinman JE (1994) The dopamine transporter and dopamine D2 receptor messenger RNAs are differentially expressed in limbic- and motor-related subpopulations of human mesencephalic neurons. Neuroscience 63:357–362

61. Parent M, Parent A (2006) Relationship between axonal collateralization and neuronal degeneration in basal ganglia. J Neural Transm Suppl 85–8

62. Matsuda W, Furuta T, Nakamura KC, Hioki H, Fujiyama F, Arai R, Kaneko T (2009) Single nigrostriatal dopaminergic neurons form widely spread and highly dense axonal arborizations in the neostriatum. J Neurosci 29:444–453

63. Watabe-Uchida M, Zhu L, Ogawa SK, Vamanrao A, Uchida N (2012) Whole-brain mapping of direct inputs to midbrain dopamine neurons. Neuron 74:858–873

64. Pérez-Fernández J, Stephenson-Jones M, Suryanarayana SM, Robertson B, Grillner S (2014) Evolutionarily conserved organization of the dopaminergic system in lamprey: SNc/VTA afferent and efferent connectivity and D2 receptor expression. J Comp Neurol 522:3775–3794

65. Beier KT, Steinberg EE, DeLoach KE, Xie S, Miyamichi K, Schwarz L, Gao XJ, Kremer EJ, Malenka RC, Luo L (2015) Circuit architecture of VTA dopamine neurons revealed by systematic input–output mapping. Cell 162:622–634

66. Faget L, Osakada F, Duan J, Ressler R, Johnson AB, Proudfoot JA, Yoo JH, Callaway EM, Hnasko TS (2016) Afferent inputs to neurotransmitter-defined cell types in the ventral tegmental area. Cell Rep 15:2796–2808

67. Morales M, Margolis EB (2017) Ventral tegmental area: cellular heterogeneity, connectivity and behaviour. Nat Rev Neurosci 18:73–85

68. Hegarty SV, Sullivan AM, O'Keeffe GW (2013) Midbrain dopaminergic neurons: a review of the molecular circuitry that regulates their development. Dev Biol 379:123–138

69. Doucet-Beaupré H, Gilbert C, Profes MS, et al (2016) Lmx1a and Lmx1b regulate mitochondrial functions and survival of adult midbrain dopaminergic neurons. Proc Natl Acad Sci U S A 113:E4387-4396

70. Smidt MP, Asbreuk CH, Cox JJ, Chen H, Johnson RL, Burbach JP (2000) A second independent pathway for development of mesencephalic dopaminergic neurons requires Lmx1b. Nat Neurosci 3:337–341

71. Peng C, Aron L, Klein R, Li M, Wurst W, Prakash N, Le W (2011) Pitx3 is a critical mediator of GDNF-induced BDNF expression in nigrostriatal dopaminergic neurons. J Neurosci 31:12802–12815

72. Jacobs FMJ, Smits SM, Noorlander CW, von Oerthel L, van der Linden AJA, Burbach JPH, Smidt MP (2007) Retinoic acid counteracts developmental defects in the substantia nigra caused by Pitx3 deficiency. Dev Camb Engl 134:2673–2684

73. Bissonette GB, Roesch MR (2016) Development and function of the midbrain dopamine system: what we know and what we need to. Genes Brain Behav 15:62–73

74. Dean L (2012) Schizophrenia. Med. Genet. Summ.

75. Birnbaum R, Weinberger DR (2017) Genetic insights into the neurodevelopmental origins of schizophrenia. Nat Rev Neurosci 18:727–740

76. Kesby JP, Eyles DW, McGrath JJ, Scott JG (2018) Dopamine, psychosis and schizophrenia: the widening gap between basic and clinical neuroscience. Transl Psychiatry 8:30

77. Volkow ND, Wise RA, Baler R (2017) The dopamine motive system: implications for drug and food addiction. Nat Rev Neurosci 18:741–752

78. Egervari G, Ciccocioppo R, Jentsch JD, Hurd YL (2018) Shaping vulnerability to addiction - the contribution of behavior, neural circuits and molecular mechanisms. Neurosci Biobehav Rev 85:117–125

79. Gallo EF, Posner J (2016) Moving towards causality in attention-deficit hyperactivity disorder: overview of neural and genetic mechanisms. Lancet Psychiatry 3:555–567

80. Gonon F (2009) The dopaminergic hypothesis of attention-deficit/hyperactivity disorder needs re-examining. Trends Neurosci 32:2–8

81. (1993) A novel gene containing a trinucleotide repeat that is expanded and unstable on Huntington's disease chromosomes. The Huntington's Disease Collaborative Research Group. Cell 72:971–983

82. Vonsattel JP, DiFiglia M (1998) Huntington disease. J Neuropathol Exp Neurol 57:369–384

83. Rosas HD, Tuch DS, Hevelone ND, Zaleta AK, Vangel M, Hersch SM, Salat DH (2006) Diffusion tensor imaging in presymptomatic and early Huntington's disease: Selective white matter pathology and its relationship to clinical measures. Mov Disord 21:1317–1325

84. Chen JY, Wang EA, Cepeda C, Levine MS (2013) Dopamine imbalance in Huntington's disease: a mechanism for the lack of behavioral flexibility. Front Neurosci 7:114

85. Government of Canada SC (2014) Parkinson's disease: Prevalence, diagnosis and impact. https://www150.statcan.gc.ca/n1/pub/82-003-x/2014011/article/14112-eng.htm. Accessed 12 Jun 2018

86. Ascherio A, Schwarzschild MA (2016) The epidemiology of Parkinson's disease: risk factors and prevention. Lancet Neurol 15:1257–1272

87. Ashrafi G, Schwarz TL (2015) Pink1- and PARK2-mediated local mitophagy in distal neuronal axons. Autophagy 11:187–9

88. MacLeod D, Dowman J, Hammond R, Leete T, Inoue K, Abeliovich A (2006) The familial Parkinsonism gene LRRK2 regulates neurite process morphology. Neuron 52:587–93

89. Sheng C, Heng X, Zhang G, Xiong R, Li H, Zhang S, Chen S (2013) DJ-1 deficiency perturbs microtubule dynamics and impairs striatal neurite outgrowth. Neurobiol Aging 34:489–98

90. Di Nottia M, Masciullo M, Verrigni D, et al (2017) DJ-1 modulates mitochondrial response to oxidative stress: clues from a novel diagnosis of PARK7. Clin Genet 92:18–25

91. Wong YC, Krainc D (2016) Lysosomal trafficking defects link Parkinson's disease with Gaucher's disease. Mov Disord 31:1610–1618

92. Kinghorn KJ, Asghari AM, Castillo-Quan JI (2017) The emerging role of autophagic-lysosomal dysfunction in Gaucher disease and Parkinson's disease. Neural Regen Res 12:380–384

93. Parkinson J (2002) An essay on the shaking palsy. 1817. J Neuropsychiatry Clin Neurosci 14:223–236; discussion 222

94. Postuma RB, Berg D, Stern M, et al (2015) MDS clinical diagnostic criteria for Parkinson's disease. Mov Disord 30:1591–1601

95. Birkmayer W, Hornykiewicz O (1961) [The L-3,4-dioxyphenylalanine (DOPA)-effect in Parkinson-akinesia]. Wien Klin Wochenschr 73:787–788

96. Hoehn MM, Yahr MD (1967) Parkinsonism: onset, progression and mortality. Neurology 17:427–442

97. Thanvi B, Lo N, Robinson T (2007) Levodopa-induced dyskinesia in Parkinson's disease: clinical features, pathogenesis, prevention and treatment. Postgrad Med J 83:384–388

98. Engelhardt E, Gomes M da M (2017) Lewy and his inclusion bodies: Discovery and rejection. Dement Neuropsychol 11:198–201

99. Emamzadeh FN (2016) Alpha-synuclein structure, functions, and interactions. J Res Med Sci Off J Isfahan Univ Med Sci 21:29

100. Braak H, Del Tredici K, Rüb U, De Vos RA, Steur ENJ, Braak E (2003) Staging of brain pathology related to sporadic Parkinson's disease. Neurobiol Aging 24:197–211

101. Langston JW (2017) The MPTP Story. J Park Dis 7:S11–S19

102. Trotta AP, Gelles JD, Serasinghe MN, Loi P, Arbiser JL, Chipuk JE (2017) Disruption of mitochondrial electron transport chain function potentiates the pro-apoptotic effects of MAPK inhibition. J Biol Chem 292:11727–11739

103. Glinka Y, Gassen M, Youdim MB (1997) Mechanism of 6-hydroxydopamine neurotoxicity. J Neural Transm Suppl 50:55–66

104. Bélanger M, Allaman I, Magistretti PJ (2011) Brain energy metabolism: Focus on astrocyte-neuron metabolic cooperation. Cell Metab 14:724–738

105. Larsen SB, Hanss Z, Krüger R (2018) The genetic architecture of mitochondrial dysfunction in Parkinson's disease. Cell Tissue Res 373:21–37

106. Osellame LD, Blacker TS, Duchen MR (2012) Cellular and molecular mechanisms of mitochondrial function. Best Pract Res Clin Endocrinol Metab 26:711–723

107. Bové J, Perier C (2012) Neurotoxin-based models of Parkinson's disease. Neuroscience 211:51–76

108. Duprez L, Wirawan E, Berghe TV, Vandenabeele P (2009) Major cell death pathways at a glance. Microbes Infect 11:1050–1062

109. Venderova K, Park DS (2012) Programmed cell death in Parkinson's disease. Cold Spring Harb Perspect Med.

110. Kostrzewa RM (2000) Review of apoptosis vs. necrosis of substantia nigra pars compacta in Parkinson's disease. Neurotox Res 2:239–250

111. Yonekawa T, Thorburn A (2013) Autophagy and cell death. Essays Biochem 55:105–117

112. Burke RE, O'Malley K (2013) Axon degeneration in Parkinson's disease. Exp Neurol 246:72–83

113. Baker MJ, Tatsuta T, Langer T (2011) Quality control of mitochondrial proteostasis. Cold Spring Harb Perspect Biol 3:a007559

114. Narendra DP, Jin SM, Tanaka A, Suen D-F, Gautier CA, Shen J, Cookson MR, Youle RJ (2010) Pink1 is selectively stabilized on impaired mitochondria to activate Parkin. PLOS Biol 8:e1000298

115. Okatsu K, Saisho K, Shimanuki M, et al (2010) p62/SQSTM1 cooperates with Parkin for perinuclear clustering of depolarized mitochondria. Genes Cells 15:887–900

116. Neuspiel M, Schauss AC, Braschi E, Zunino R, Rippstein P, Rachubinski RA, Andrade-Navarro MA, McBride HM (2008) Cargo-selected transport from the mitochondria to peroxisomes is mediated by vesicular carriers. Curr Biol 18:102–108

117. McLelland G-L, Soubannier V, Chen CX, McBride HM, Fon EA (2014) Parkin and Pink1 function in a vesicular trafficking pathway regulating mitochondrial quality control. EMBO J 33:282–295

118. Chen H, McCaffery JM, Chan DC (2007) Mitochondrial fusion protects against neurodegeneration in the cerebellum. Cell 130:548–562

119. Chen Y, Dorn GW (2013) Pink1-phosphorylated Mitofusin 2 is a Parkin receptor for culling damaged mitochondria. Science 340:471–475

120. Matheoud D, Sugiura A, Bellemare-Pelletier A, et al (2016) Parkinson's disease-related proteins Pink1 and Parkin repress mitochondrial antigen presentation. Cell 166:314–327

121. Trempe J-F, Fon EA (2013) Structure and function of Parkin, Pink1, and DJ-1, the three musketeers of neuroprotection. Front Neurol 4:38

122. Goldberg MS, Fleming SM, Palacino JJ, et al (2003) Parkin-deficient mice exhibit nigrostriatal deficits but not loss of dopaminergic neurons. J Biol Chem 278:43628–43635

123. Chandran JS, Lin X, Zapata A, et al (2008) Progressive behavioral deficits in DJ-1 deficient mice are associated with normal nigrostriatal function. Neurobiol Dis 29:505–514

124. Ramsey CP, Tsika E, Ischiropoulos H, Giasson BI (2010) DJ-1 deficient mice demonstrate similar vulnerability to pathogenic Ala53Thr human α-syn toxicity. Hum Mol Genet 19:1425–1437

125. Aguiar AS, Tristão FSM, Amar M, Chevarin C, Lanfumey L, Mongeau R, Corti O, Prediger RD, Raisman-Vozari R (2013) Parkin-knockout mice did not display increased vulnerability to intranasal administration of 1-methyl-4-phenyl-1,2,3,6-tetrahydropyridine (MPTP). Neurotox Res 24:280–287

126. Moisoi N, Fedele V, Edwards J, Martins LM (2014) Loss of Pink1 enhances neurodegeneration in a mouse model of Parkinson's disease triggered by mitochondrial stress. Neuropharmacology 77:350–357

127. Schapira AHV (2015) Glucocerebrosidase and Parkinson disease: Recent advances. Mol Cell Neurosci 66:37–42

128. Mazzulli JR, Xu Y-H, Sun Y, Knight AL, McLean PJ, Caldwell GA, Sidransky E, Grabowski GA, Krainc D (2011) Gaucher disease glucocerebrosidase and α-synuclein form a bidirectional pathogenic loop in synucleinopathies. Cell 146:37–52

129. Stefanis L (2012) α-synuclein in Parkinson's disease. Cold Spring Harb Perspect Med.

130. Wong YC, Krainc D (2017) α-synuclein toxicity in neurodegeneration: mechanism and therapeutic strategies. Nat Med 23:1–13

131. Fornai F, Schlüter OM, Lenzi P, et al (2005) Parkinson-like syndrome induced by continuous MPTP infusion: Convergent roles of the ubiquitin-proteasome system and α-synuclein. Proc Natl Acad Sci U S A 102:3413–3418

132. Nisticò R, Mehdawy B, Piccirilli S, Mercuri N (2011) Paraquat- and rotenone-induced models of Parkinson's disease. Int J Immunopathol Pharmacol 24:313–322

133. Lesage S, Brice A (2009) Parkinson's disease: from monogenic forms to genetic susceptibility factors. Hum Mol Genet 18:R48–R59

134. Wallings R, Manzoni C, Bandopadhyay R (2015) Cellular processes associated with LRRK2 function and dysfunction. Febs J 282:2806–2826

135. Godena VK, Brookes-Hocking N, Moller A, Shaw G, Oswald M, Sancho RM, Miller CCJ, Whitworth AJ, De Vos KJ (2014) Increasing microtubule acetylation rescues axonal transport and locomotor deficits caused by LRRK2 Roc-COR domain mutations. Nat Commun 5:5245

136. Carrion MDP, Marsicano S, Daniele F, et al (2017) The LRRK2 G2385R variant is a partial loss-of-function mutation that affects synaptic vesicle trafficking through altered protein interactions. Sci Rep 7:5377

137. Singh A, Zhi L, Zhang H (2019) LRRK2 and mitochondria: Recent advances and current views. Brain Res 1702:96–104

138. Anderson DW, Schray RC, Duester G, Schneider JS (2011) Functional significance of aldehyde dehydrogenase ALDH1A1 to the nigrostriatal dopamine system. Brain Res 1408:81–87

139. Liu G, Yu J, Ding J, et al (2014) Aldehyde dehydrogenase 1 defines and protects a nigrostriatal dopaminergic neuron subpopulation. J Clin Invest 124:3032–3046

140. Nemoto C, Hida T, Arai R (1999) Calretinin and calbindin-D28k in dopaminergic neurons of the rat midbrain: a triple-labeling immunohistochemical study. Brain Res 846:129–136

141. Dopeso-Reyes IG, Rico AJ, Roda E, Sierra S, Pignataro D, Lanz M, Sucunza D, Chang-Azancot L, Lanciego JL (2014) Calbindin content and differential vulnerability of midbrain efferent dopaminergic neurons in macaques. Front Neuroanat 8:146

142. Double KL, Reyes S, Werry EL, Halliday GM (2010) Selective cell death in neurodegeneration: Why are some neurons spared in vulnerable regions? Prog Neurobiol 92:316–329

143. Giguère N, Burke Nanni S, Trudeau L-E (2018) On cell loss and selective vulnerability of neuronal populations in Parkinson's disease. Front Neurol 9:455

144. Segura-Aguilar J, Paris I, Muñoz P, Ferrari E, Zecca L, Zucca FA (2014) Protective and toxic roles of dopamine in Parkinson's disease. J Neurochem 129:898–915

145. Fahn S, Parkinson Study Group (2005) Does levodopa slow or hasten the rate of progression of Parkinson's disease? J Neurol 252 Suppl 4:IV37–IV42

146. Lipski J, Nistico R, Berretta N, Guatteo E, Bernardi G, Mercuri NB (2011) L-DOPA: a scapegoat for accelerated neurodegeneration in Parkinson's disease? Prog Neurobiol 94:389–407

147. Surmeier DJ, Schumacker PT, Guzman JD, Ilijic E, Yang B, Zampese E (2017) Calcium and Parkinson's disease. Biochem Biophys Res Commun 483:1013–1019

148. Guzman JN, Sanchez-Padilla J, Wokosin D, Kondapalli J, Ilijic E, Schumacker PT, Surmeier DJ (2010) Oxidant stress evoked by pacemaking in dopaminergic neurons is attenuated by DJ-1. Nature 468:696–700

149. Goldberg JA, Guzman JN, Estep CM, Ilijic E, Kondapalli J, Sanchez-Padilla J, Surmeier DJ (2012) Calcium entry induces mitochondrial oxidant stress in vagal neurons at risk in Parkinson's disease. Nat Neurosci 15:1414–1421

150. Sanchez-Padilla J, Guzman JN, Ilijic E, et al (2014) Mitochondrial oxidant stress in locus coeruleus is regulated by activity and nitric oxide synthase. Nat Neurosci 17:832–840

151. Hell JW, Westenbroek RE, Warner C, Ahlijanian MK, Prystay W, Gilbert MM, Snutch TP, Catterall WA (1993) Identification and differential subcellular localization of the neuronal class C and class D L-type calcium channel alpha 1 subunits. J Cell Biol 123:949–962

152. Hurley MJ, Gentleman SM, Dexter DT (2015) Calcium CaV1 channel subtype mRNA expression in Parkinson's disease examined by in situ hybridization. J Mol Neurosci MN 55:715–724

153. Choi W-S, Palmiter RD, Xia Z (2011) Loss of mitochondrial complex I activity potentiates dopamine neuron death induced by microtubule dysfunction in a Parkinson's disease model. J Cell Biol 192:873–882

154. Gauthier J, Parent M, Lévesque M, Parent A (1999) The axonal arborization of single nigrostriatal neurons in rats. Brain Res 834:228–232

155. Prensa L, Parent A (2001) The nigrostriatal pathway in the rat: A single-axon study of the relationship between dorsal and ventral tier nigral neurons and the striosome/matrix striatal compartments. J Neurosci 21:7247–60

156. Aransay A, Rodríguez-López C, García-Amado M, Clascá F, Prensa L (2015) Long-range projection neurons of the mouse ventral tegmental area: a single-cell axon tracing analysis. Front Neuroanat.

157. Pissadaki EK, Bolam JP (2013) The energy cost of action potential propagation in dopamine neurons: clues to susceptibility in Parkinson's disease. Front Comput Neurosci 7:13

158. Pacelli C, Giguère N, Bourque M-J, Lévesque M, Slack RS, Trudeau L-É (2015) Elevated mitochondrial bioenergetics and axonal arborization size are key contributors to the vulnerability of dopamine neurons. Curr Biol CB 25:2349–2360

159. Chabrat A, Brisson G, Doucet-Beaupré H, et al (2017) Transcriptional repression of Plxnc1 by Lmx1a and Lmx1b directs topographic dopaminergic circuit formation. Nat Commun 8:933

160. Pasterkamp RJ (2012) Getting neural circuits into shape with semaphorins. Nat Rev Neurosci 13:605–618

161. Pasterkamp RJ, Peschon JJ, Spriggs MK, Kolodkin AL (2003) Semaphorin 7A promotes axon outgrowth through integrins and MAPKs. Nature 424:398–405

162. Scott GA, McClelland LA, Fricke AF (2008) Semaphorin 7a promotes spreading and dendricity in human melanocytes through beta1-integrins. J Invest Dermatol 128:151–161

163. Scott GA, McClelland LA, Fricke AF, Fender A (2009) Plexin C1, a receptor for semaphorin 7a, inactivates cofilin and is a potential tumor suppressor for melanoma progression. J Invest Dermatol 129:954–963

164. Chan CS, Guzman JN, Ilijic E, Mercer JN, Rick C, Tkatch T, Meredith GE, Surmeier DJ (2007) "Rejuvenation" protects neurons in mouse models of Parkinson's disease. Nature 447:1081–6

165. van Duijn CM, Dekker MC, Bonifati V, et al (2001) Park7, a novel locus for autosomal recessive early-onset parkinsonism, on chromosome 1p36. Am J Hum Genet 69:629–634

166. Bonifati V, Dekker MCJ, Vanacore N, et al (2002) Autosomal recessive early onset parkinsonism is linked to three loci: PARK2, PARK6, and PARK7. Neurol Sci 23 Suppl 2:S59-60

167. Tan E-K, Yew K, Chua E, et al (2006) Pink1 mutations in sporadic early-onset Parkinson's disease. Mov Disord 21:789–793

168. Ben-Shachar S, Afawi Z, Masalha R, Badarny S, Neiman T, Pavzner D, Bar-Shira A, Orr-Urtreger A (2017) Variable PARK2 mutations cause early-onset Parkinson's disease in a small restricted population. J Mol Neurosci MN 63:216–222

169. Giguère N, Pacelli C, Saumure C, Bourque M-J, Matheoud D, Levesque D, Slack RS, Park DS, Trudeau L-É (2018) Comparative analysis of Parkinson's disease-associated genes in mice reveals altered survival and bioenergetics of Parkin-deficient dopamine neurons. J Biol Chem 293:9580–9593

170. Booth HDE, Hirst WD, Wade-Martins R (2017) The role of astrocyte dysfunction in Parkinson's disease pathogenesis. Trends Neurosci 40:358–370

171. Solano RM, Menéndez J, Casarejos MJ, Rodríguez-Navarro JA, García de Yébenes J, Mena MA (2006) Midbrain neuronal cultures from parkin mutant mice are resistant to nitric oxide-induced toxicity. Neuropharmacology 51:327–340

172. Solano RM, Casarejos MJ, Menéndez-Cuervo J, Rodriguez-Navarro JA, García de Yébenes J, Mena MA (2008) Glial dysfunction in parkin null mice: effects of aging. J Neurosci 28:598–611

173. Khasnavis S, Pahan K (2014) Cinnamon treatment upregulates neuroprotective proteins Parkin and DJ-1 and protects dopaminergic neurons in a mouse model of Parkinson's disease. J Neuroimmune Pharmacol 9:569–581

174. Barnum CJ, Chen X, Chung J, Chang J, Williams M, Grigoryan N, Tesi RJ, Tansey MG (2014) Peripheral administration of the selective inhibitor of soluble tumor necrosis factor (TNF) XPro®1595 attenuates nigral cell loss and glial activation in 6-OHDA hemiparkinsonian rats. J Park Dis 4:349–360

175. Joers V, Tansey MG, Mulas G, Carta AR (2017) Microglial phenotypes in Parkinson's disease and animal models of the disease. Prog Neurobiol 155:57–75

176. Sun L, Shen R, Agnihotri SK, Chen Y, Huang Z, Büeler H (2018) Lack of Pink1 alters glia innate immune responses and enhances inflammation-induced, nitric oxide-mediated neuron death. Sci Rep 8:383

177. McWilliams TG, Prescott AR, Montava-Garriga L, Ball G, Singh F, Barini E, Muqit MMK, Brooks SP, Ganley IG (2018) Basal mitophagy occurs independently of Pink1 in mouse tissues of high metabolic demand. Cell Metab 27:439-449.e5

178. Villa E, Proïcs E, Rubio-Patiño C, et al (2017) Parkin-independent mitophagy controls chemotherapeutic response in cancer cells. Cell Rep 20:2846–2859

179. Lim GG, Lim K-L (2017) Parkin-independent mitophagy-FKBP8 takes the stage. EMBO Rep 18:864–865

180. Koentjoro B, Park J-S, Sue CM (2017) Nix restores mitophagy and mitochondrial function to protect against Pink1/Parkin-related Parkinson's disease. Sci Rep 7:44373

181. Chen Z, Liu L, Cheng Q, et al (2017) Mitochondrial E3 ligase MARCH5 regulates FUNDC1 to fine-tune hypoxic mitophagy. EMBO Rep 18:495–509

182. Murakawa T, Yamaguchi O, Hashimoto A, et al (2015) Bcl-2-like protein 13 is a mammalian Atg32 homologue that mediates mitophagy and mitochondrial fragmentation. Nat Commun 6:7527

183. Vercammen L, Van der Perren A, Vaudano E, Gijsbers R, Debyser Z, Van den Haute C, Baekelandt V (2006) Parkin protects against neurotoxicity in the 6-hydroxydopamine rat model for Parkinson's disease. Mol Ther 14:716–723

184. Dave KD, De Silva S, Sheth NP, et al (2014) Phenotypic characterization of recessive gene knockout rat models of Parkinson's disease. Neurobiol Dis 70:190–203

185. Kovacević N, Henderson JT, Chan E, Lifshitz N, Bishop J, Evans AC, Henkelman RM, Chen XJ (2005) A three-dimensional MRI atlas of the mouse brain with estimates of the average and variability. Cereb Cortex N Y N 1991 15:639–645

186. Hamezah HS, Durani LW, Ibrahim NF, Yanagisawa D, Kato T, Shiino A, Tanaka S, Damanhuri HA, Ngah WZW, Tooyama I (2017) Volumetric changes in the aging rat brain and its impact on cognitive and locomotor functions. Exp Gerontol 99:69–79

187. Nair-Roberts RG, Chatelain-Badie SD, Benson E, White-Cooper H, Bolam JP, Ungless MA (2008) Stereological estimates of dopaminergic, GABAergic and glutamatergic neurons in the ventral tegmental area, substantia nigra and retrorubral field in the rat. Neuroscience 152:1024–1031

188. Fabricius K, Barkholt P, Jelsing J, Hansen HH (2017) Application of the physical disector principle for quantification of dopaminergic neuronal loss in a Rat 6-hydroxydopamine nigral lesion model of Parkinson's disease. Front Neuroanat 11:109

189. Parish CL, Nunan J, Finkelstein DI, McNamara FN, Wong JY, Waddington JL, Brown RM, Lawrence AJ, Horne MK, Drago J (2005) Mice lacking the alpha4 nicotinic receptor subunit fail to modulate dopaminergic neuronal arbors and possess impaired dopamine transporter function. Mol Pharmacol 68:1376–1386

190. Lee J, Parish CL, Tomas D, Horne MK (2011) Chronic cocaine administration reduces striatal dopamine terminal density and striatal dopamine release which leads to drug-seeking behaviour. Neuroscience 174:143–150

191. Pasterkamp RJ, Kolk SM, Hellemons AJ, Kolodkin AL (2007) Expression patterns of semaphorin7A and plexinC1 during rat neural development suggest roles in axon guidance and neuronal migration. BMC Dev Biol 7:98

192. Parish CL, Stanic D, Drago J, Borrelli E, Finkelstein DI, Horne MK (2002) Effects of long-term treatment with dopamine receptor agonists and antagonists on terminal arbor size. Eur J Neurosci 16:787–794

193. Tripanichkul W, Stanic D, Drago J, Finkelstein DI, Horne MK (2003) D2 Dopamine receptor blockade results in sprouting of DA axons in the intact animal but prevents sprouting following nigral lesions. Eur J Neurosci 17:1033–1045

194. Parish CL, Finkelstein DI, Drago J, Borrelli E, Horne MK (2001) The role of dopamine receptors in regulating the size of axonal arbors. J Neurosci 21:5147–5157

195. Hare DJ, Double KL (2016) Iron and dopamine: a toxic couple. Brain J Neurol 139:1026–1035

196. Elkon H, Melamed E, Offen D (2004) Oxidative stress, induced by 6-hydroxydopamine, reduces proteasome activities in PC12 cells: implications for the pathogenesis of Parkinson's disease. J Mol Neurosci MN 24:387–400

197. Hanrott K, Gudmunsen L, O'Neill MJ, Wonnacott S (2006) 6-hydroxydopamine-induced apoptosis is mediated via extracellular auto-oxidation and caspase 3-dependent activation of protein kinase Cδ. J Biol Chem 281:5373–5382

198. Latchoumycandane C, Anantharam V, Jin H, Kanthasamy A, Kanthasamy A (2011) Dopaminergic neurotoxicant 6-OHDA induces oxidative damage through proteolytic activation of PKCδ in cell culture and animal models of Parkinson's disease. Toxicol Appl Pharmacol 256:314–323

199. Lu X, Kim-Han JS, Harmon S, Sakiyama-Elbert SE, O'Malley KL (2014) The Parkinsonian mimetic, 6-OHDA, impairs axonal transport in dopaminergic axons. Mol Neurodegener 9:17

200. Tirmenstein MA, Hu CX, Scicchitano MS, Narayanan PK, McFarland DC, Thomas HC, Schwartz LW (2005) Effects of 6-hydroxydopamine on mitochondrial function and glutathione status in SH-SY5Y human neuroblastoma cells. Toxicol Vitro 19:471–479

201. Chesselet M-F (2008) In vivo alpha-synuclein overexpression in rodents: a useful model of Parkinson's disease? Exp Neurol 209:22–27

202. Ebrahimi-Fakhari D, Cantuti-Castelvetri I, Fan Z, Rockenstein E, Masliah E, Hyman BT, McLean PJ, Unni VK (2011) Distinct roles in vivo for the ubiquitin-proteasome system and the autophagy-lysosomal pathway in the degradation of α-synuclein. J Neurosci 31:14508–14520

203. Bourdenx M, Bezard E, Dehay B (2014) Lysosomes and α-synuclein form a dangerous duet leading to neuronal cell death. Front Neuroanat 8:83

204. Mazzulli JR, Zunke F, Isacson O, Studer L, Krainc D (2016) α-Synuclein–induced lysosomal dysfunction occurs through disruptions in protein trafficking in human midbrain synucleinopathy models. Proc Natl Acad Sci 113:1931–1936

205. Glinka YY, Youdim MBH (1995) Inhibition of mitochondrial complexes I and IV by 6-hydroxydopamine. Eur J Pharmacol Environ Toxicol Pharmacol 292:329–332

206. Smith MP, Cass WA (2007) Oxidative stress and dopamine depletion in an intrastriatal 6-hydroxydopamine model of Parkinson's disease. Neuroscience 144:1057–1066

207. Tinsley RB, Bye CR, Parish CL, Tziotis-Vais A, George S, Culvenor JG, Li Q-X, Masters CL, Finkelstein DI, Horne MK (2009) Dopamine D2 receptor knockout mice develop features of Parkinson disease. Ann Neurol 66:472–484

208. Ho A, Blum M (1998) Induction of interleukin-1 associated with compensatory dopaminergic sprouting in the denervated striatum of young mice: model of aging and neurodegenerative disease. J Neurosci 18:5614–5629

209. Finkelstein DI, Stanic D, Parish CL, Tomas D, Dickson K, Horne MK (2000) Axonal sprouting following lesions of the rat substantia nigra. Neuroscience 97:99–112

210. Sofic E, Lange KW, Jellinger K, Riederer P (1992) Reduced and oxidized glutathione in the substantia nigra of patients with Parkinson's disease. Neurosci Lett 142:128–30

211. Sian J, Dexter DT, Lees AJ, Daniel S, Agid Y, Javoy-Agid F, Jenner P, Marsden CD (1994) Alterations in glutathione levels in Parkinson's disease and other neurodegenerative disorders affecting basal ganglia. Ann Neurol 36:348–55

212. Pearce RK, Owen A, Daniel S, Jenner P, Marsden CD (1997) Alterations in the distribution of glutathione in the substantia nigra in Parkinson's disease. J Neural Transm Vienna 104:661–77

213. O'Malley KL (2010) The role of axonopathy in Parkinson's disease. Exp Neurobiol 19:115–9

214. Tagliaferro P, Burke RE (2016) Retrograde axonal degeneration in Parkinson disease. J Park Dis 6:1–15

215. Pukaß K, Goldbaum O, Richter-Landsberg C (2015) Mitochondrial impairment and oxidative stress compromise autophagosomal degradation of α-synuclein in oligodendroglial cells. J Neurochem 135:194–205

216. Demers-Lamarche J, Guillebaud G, Tlili M, Todkar K, Bélanger N, Grondin M, Nguyen AP, Michel J, Germain M (2016) Loss of mitochondrial function impairs lysosomes. J Biol Chem 291:10263–10276

217. Sidransky E, Nalls MA, Aasly JO, et al (2009) Multicenter analysis of glucocerebrosidase mutations in Parkinson's disease. N Engl J Med 361:1651–61

218. Gegg ME, Burke D, Heales SJ, Cooper JM, Hardy J, Wood NW, Schapira AH (2012) Glucocerebrosidase deficiency in substantia nigra of Parkinson disease brains. Ann Neurol 72:455–63

219. Dehay B, Martinez-Vicente M, Caldwell GA, Caldwell KA, Yue Z, Cookson MR, Klein C, Vila M, Bezard E (2013) Lysosomal impairment in Parkinson's disease. Mov Disord 28:725–32

220. Murphy KE, Halliday GM (2014) Glucocerebrosidase deficits in sporadic Parkinson disease. Autophagy 10:1350–1

221. Migdalska-Richards A, Schapira AH (2016) The relationship between glucocerebrosidase mutations and Parkinson disease. J Neurochem 139 Suppl 1:77–90

222. Yue M, Hinkle KM, Davies P, et al (2015) Progressive dopaminergic alterations and mitochondrial abnormalities in LRRK2 G2019S knock-in mice. Neurobiol Dis 78:172–95

223. Braak H, Del Tredici K, Bratzke H, Hamm-Clement J, Sandmann-Keil D, Rub U (2002) Staging of the intracerebral inclusion body pathology associated with idiopathic Parkinson's disease (preclinical and clinical stages). J Neurol 249 Suppl 3:III/1-5

224. Braak H, Ghebremedhin E, Rüb U, Bratzke H, Del Tredici K (2004) Stages in the development of Parkinson's disease-related pathology. Cell Tissue Res 318:121–134

225. Surmeier DJ, Obeso JA, Halliday GM (2017) Selective neuronal vulnerability in Parkinson disease. Nat Rev Neurosci 18:101–113

226. Hayashi S, Wakabayashi K, Ishikawa A, Nagai H, Saito M, Maruyama M, Takahashi T, Ozawa T, Tsuji S, Takahashi H (2000) An autopsy case of autosomal-recessive juvenile parkinsonism with a homozygous exon 4 deletion in the parkin gene. Mov Disord 15:884–8

227. Sasaki S, Shirata A, Yamane K, Iwata M (2004) Parkin-positive autosomal recessive juvenile Parkinsonism with alpha-synuclein-positive inclusions. Neurology 63:678–82

228. Schneider SA, Alcalay RN (2017) Neuropathology of genetic synucleinopathies with parkinsonism: Review of the literature. Mov Disord 32:1504–1523

229. Markesbery WR, Jicha GA, Liu H, Schmitt FA (2009) Lewy body pathology in normal elderly subjects. J Neuropathol Exp Neurol 68:816–22

230. Fasano C, Poirier A, DesGroseillers L, Trudeau LE (2008) Chronic activation of the D2 dopamine autoreceptor inhibits synaptogenesis in mesencephalic dopaminergic neurons in vitro. Eur J Neurosci 28:1480–90

231. Shill HA, Stacy M (2009) Update on ropinirole in the treatment of Parkinson's disease. Neuropsychiatr Dis Treat 5:33–36

232. Antonini A, Barone P, Ceravolo R, Fabbrini G, Tinazzi M, Abbruzzese G (2010) Role of pramipexole in the management of Parkinson's disease. CNS Drugs 24:829–841

233. Boyle A, Ondo W (2015) Role of apomorphine in the treatment of Parkinson's disease. CNS Drugs 29:83–89

234. Ahlskog JE (2003) Slowing Parkinson's disease progression: recent dopamine agonist trials. Neurology 60:381–389

235. Whone AL, Watts RL, Stoessl AJ, et al (2003) Slower progression of Parkinson's disease with ropinirole versus levodopa: The REAL-PET study. Ann Neurol 54:93–101

236. Gleave JA, Arathoon LR, Trinh D, et al (2017) Sirtuin 3 rescues neurons through the stabilisation of mitochondrial biogenetics in the virally-expressing mutant alpha-synuclein rat model of parkinsonism. Neurobiol Dis 106:133–146

237. Hebert AS, Dittenhafer-Reed KE, Yu W, et al (2013) Calorie restriction and SIRT3 trigger global reprogramming of the mitochondrial protein acetylome. Mol Cell 49:186–199

238. Ahn B-H, Kim H-S, Song S, Lee IH, Liu J, Vassilopoulos A, Deng C-X, Finkel T (2008) A role for the mitochondrial deacetylase Sirt3 in regulating energy homeostasis. Proc Natl Acad Sci U S A 105:14447–14452

239. Someya S, Yu W, Hallows WC, Xu J, Vann JM, Leeuwenburgh C, Tanokura M, Denu JM, Prolla TA (2010) Sirt3 mediates reduction of oxidative damage and prevention of age-related hearing loss under caloric restriction. Cell 143:802–812

240. Herskovits AZ, Guarente L (2013) Sirtuin deacetylases in neurodegenerative diseases of aging. Cell Res 23:746–758

241. Lombard DB, Alt FW, Cheng H-L, et al (2007) Mammalian Sir2 homolog SIRT3 regulates global mitochondrial lysine acetylation. Mol Cell Biol 27:8807–8814

242. Liu L, Peritore C, Ginsberg J, Kayhan M, Donmez G (2015) SIRT3 attenuates MPTP-induced nigrostriatal degeneration via enhancing mitochondrial antioxidant capacity. Neurochem Res 40:600–608

243. Shi H, Deng H-X, Gius D, Schumacker PT, Surmeier DJ, Ma Y-C (2017) Sirt3 protects dopaminergic neurons from mitochondrial oxidative stress. Hum Mol Genet 26:1915–1926

244. Cheng HC, Ulane CM, Burke RE (2010) Clinical progression in Parkinson disease and the neurobiology of axons. Ann Neurol 67:715–25

245. Nair AT, Ramachandran V, Joghee NM, Antony S, Ramalingam G (2018) Gut microbiota dysfunction as reliable non-invasive early diagnostic biomarkers in the pathophysiology of Parkinson's disease: A Critical Review. J Neurogastroenterol Motil 24:30–42

246. Saeed U, Compagnone J, Aviv RI, Strafella AP, Black SE, Lang AE, Masellis M (2017) Imaging biomarkers in Parkinson's disease and Parkinsonian syndromes: current and emerging concepts. Transl Neurodegener 6:8

247. Havelund JF, Heegaard NHH, Færgeman NJK, Gramsbergen JB (2017) Biomarker research in Parkinson's disease using metabolite profiling. Metabolites.

248. Yoo JH, Zell V, Gutierrez-Reed N, Wu J, Ressler R, Shenasa MA, Johnson AB, Fife KH, Faget L, Hnasko TS (2016) Ventral tegmental area glutamate neurons co-release GABA and promote positive reinforcement. Nat Commun 7:13697

249. Fortin GM, Bourque MJ, Mendez JA, et al (2012) Glutamate corelease promotes growth and survival of midbrain dopamine neurons. J Neurosci 32:17477–91

250. Descarries L, Watkins KC, Garcia S, Bosler O, Doucet G (1996) Dual character, asynaptic and synaptic, of the dopamine innervation in adult rat neostriatum: A quantitative autoradiographic and immunocytochemical analysis. J Comp Neurol 375:167–186

251. Liu C, Kershberg L, Wang J, Schneeberger S, Kaeser PS (2018) Dopamine secretion is mediated by sparse active zone-like release sites. Cell 172:706-718.e15

252. Hardingham GE (2006) Pro-survival signalling from the NMDA receptor. Biochem Soc Trans 34:936–938

Annexe I : Sémaphorine 7A, données supplémentaires

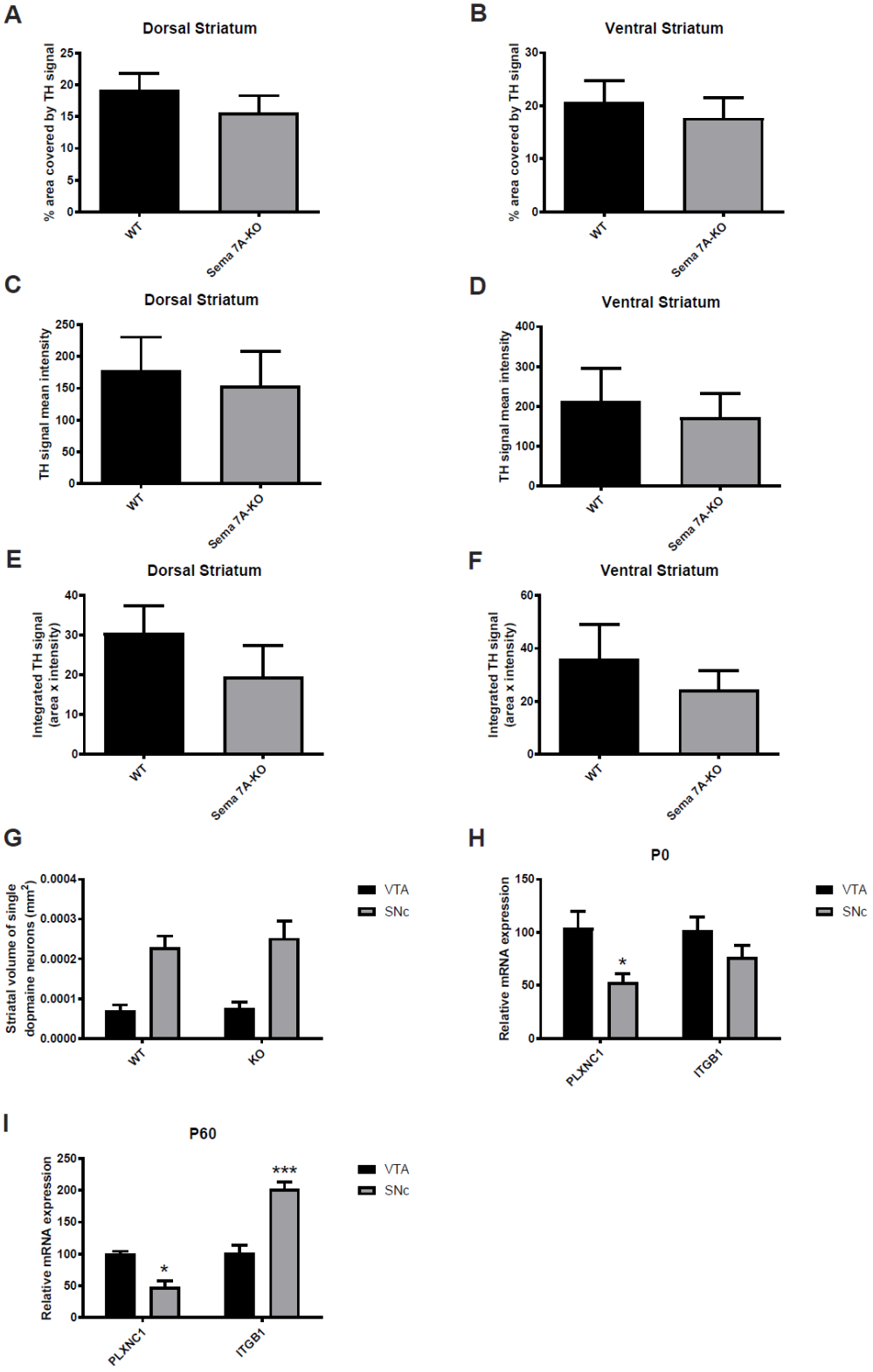

Effet du KO de la Sema7A sur la taille de l'arborisation axonale des neurones dopaminergiques *in vivo*. Surface du signal TH (A,B), de son intensité (C,D) et du signal intégré (E,F) dans le striatum dorsal (A,C,E) et ventral (B,D,F) des souris KO pour la Sema7A. Les valeurs représentent la moyenne ± SEM, n = 4-11 souris. G. Volume axonal pour les neurones dopaminergiques de la SNc et de la VTA chez les souris Sema7A KO et WT. Les valeurs représentent la moyenne ± SEM, n = 5-7 souris. Expression par RT-qPCR du récepteur β1-intégrine et plexine C1 chez les neurones dopaminergiques de la SNc et de la VTA à P0 (H) et à P60 (I). Les valeurs représentent la moyenne ± SEM, n = 3-4 souris. *$p < 0.05$, ***$p < 0.001$.

*J'aimerais souligner la contribution de Chloé Buj, une stagiaire à l'été 2016 en échange dans le cadre de son Master de Neurosciences de l'Université de Marseille, pour le panneau G de cette annexe.

Annexe II : Lésion partielle néonatale à la 6-OHDA

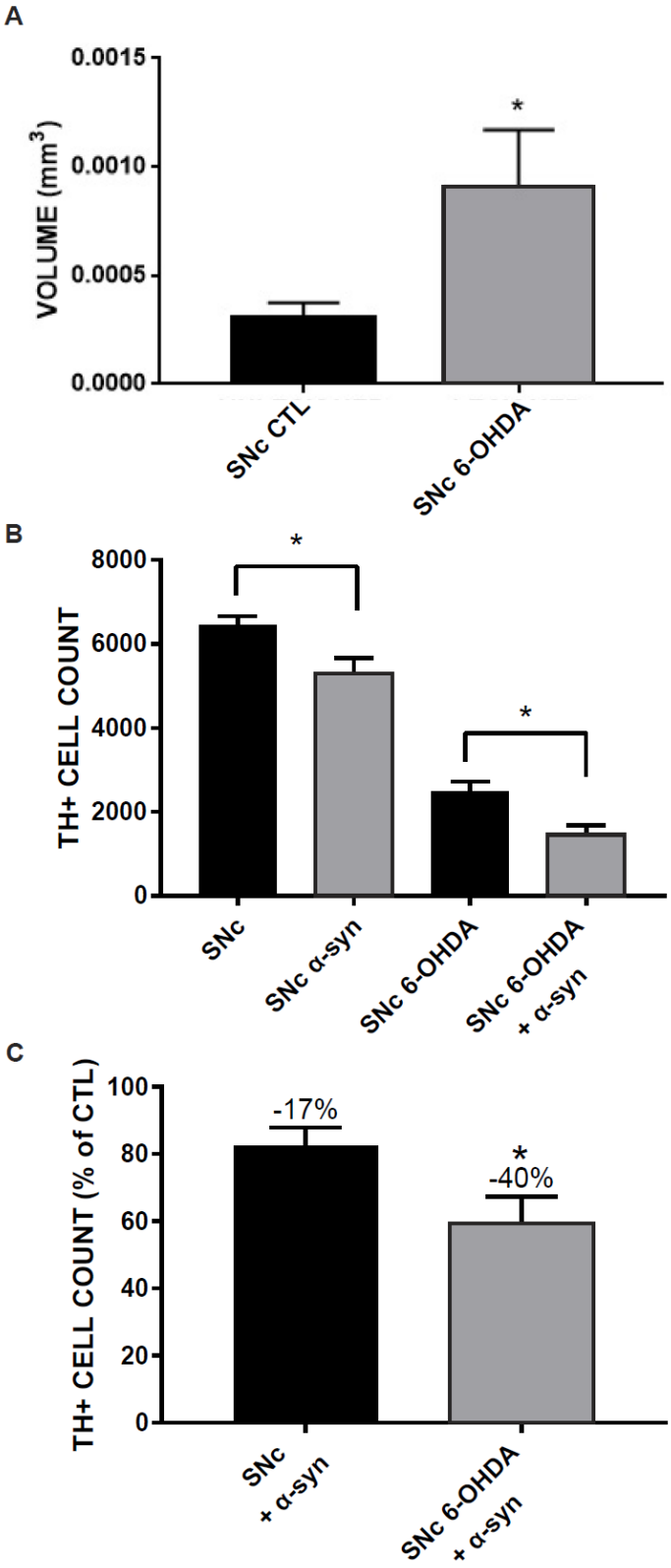

Extrait modifié de la thèse de maîtrise de Pamela Cassidy intitulée : « Augmenter la taille de l'arborisation axonale des neurones dopaminergiques afin de produire un meilleur modèle animal de la Maladie de Parkinson ». (A) Volume de l'arborisation axonale des neurones dopaminergiques de la SNc dans le striatum dorsal adulte suite à une lésion partielle unilatérale néonatale à la 6-OHDA. Les valeurs représentent la moyenne ± SEM, n = 15 souris. *$p < 0.05$ (B) Nombre de neurones dopaminergiques dans la SNc suite à une lésion néonatale à la 6-OHDA, à une surexpression chez l'adulte d'α-synucléine ou à la combinaison des deux. (C) Nombre de neurones dopaminergiques de la SNc survivants à la surexpression chez l'adulte d'α-synucléine en % de l'hémisphère sans surexpression, chez les souris contrôles et les souris ayant subie une lésion partielle néonatale à la 6-OHDA. Les valeurs représentent la moyenne ± SEM, n = 16 souris. *$p < 0.05$